EXPLORING SIGNAL TRANSDUCTION MECHANISMS IN MOLECULARLY IMPRINTED POLYMERS FOR FORENSIC APPLICATIONS

TIMOTHY KIRKMAN

Bachelor of Science (Forensic) (Hons)

Submitted to the Faculty of Science and Information Technology of
The University of Newcastle for the degree of
Doctor of Philosophy (Chemistry)
October 2014

DECLARATION

The thesis contains no material which has been accepted for the award of any other degree or diploma in any university or other tertiary institution and, to the best of my knowledge and belief, contains no material previously published or written by another person, except where due reference has been made in the text. I give consent to the final version of my thesis being made available worldwide when deposited in the University's Digital Repository, subject to the provisions of the Copyright Act 1968.

……

Timothy Kirkman

ACKNOWLEDGMENTS

Firstly, to Clovia, Mike and Adam, I greatly appreciate the assisting, prodding, suggesting, encouraging, rebuking and guiding you have done over the last few years. I could not have done it without all the time and effort you have given me.

To the University of Newcastle for awarding me a scholarship, allowing me to undertake this research in the first place.

A big thanks to all the friends, groupmates and colleagues that I have had over the past few years. Thank you to Carrie, Kate B, Kate W, Sun, Azrin, Anang, Delfin, Edwin, Jenny, Andy, Samala, Ryan, Nolene, Nat, and anyone I may have forgotten. Thank you to all the academic, technical and clerical staff. You made the Chemistry building a pretty good place to work. I'm going to miss you all.

And finally to my parents, family and friends, thank you for encouraging me to do my PhD in the first place, and all the support you have given me in the years since, particularly when the end seemed always just out of reach. I would never have gotten through this without you.

TABLE OF CONTENTS

LIST OF ABBREVIATIONS

(+)-PSEPD	(*1S,2S*)-(+)-pseudoephedrine
(-)-PSEPD	(*1R,2R*)-(-)-pseudoephedrine
^{13}C NMR	Carbon nuclear magnetic resonance
^{1}H NMR	Carbon nuclear magnetic resonance
1D9T	1-Decene-9-thiol
AA	Acrylic acid
ADR	(±)-Adrenaline (epinephrine)
AIBN	Azobisisobutyronitrile
AM	Allyl mercaptan
AN	Acrylonitrile
Au_{1D9T}	Gold nanoparticles stabilised with 1-decene-9-thiol
Au_{AM}	Gold nanoparticles stabilised with allyl mercaptan
Au_{MUA}	Gold nanoparticles stabilised with 11-mercaptoundecanoic acid
Au_{NDT}	Gold nanoparticles stabilised with n-decanethiol
B	Binding
CAFF	Caffeine
$CDCl_3$	Deuterated chloroform
CP	Conductive polymer
D_2O	Deuterium oxide
D_6-DMSO	Deuterated dimethyl sulfoxide
DMSO	Dimethyl sulfoxide
EDOT	3,4-Ethylenedioxythiophene
$E_{Interaction}$	Energy of Interaction
EPD	(*1R,2S*)-(-)-Ephedrine
EPDHCL	(*1S,2R*)-(+)-ephedrine hydrochloride
Ex	Extracted
FTIR	Fourier transform infrared spectroscopy
GPC	Gel permeation chromatography
H_f	Heat of formation
HPLC	High pressure liquid chromatography
I	Imprinted factor

IPA	N-Isopropylacrylamide
M	Monomer
MBA	N,N'-Methylenebisacrylamide
MeOH	Methanol
MIP	Molecularly imprinted polymer
MIPf	Molecularly imprinted polymeric film
MIPp	Molecularly imprinted polymeric particle
MMA	Methyl Methacrylate
MTMA	3-Methylthienyl Methacrylate
MUA	11-Mercaptoundecanoic Acid
NDT	N-Decanethiol
NIP	Non-imprinted polymer
NIPf	Non-imprinted polymeric film
NIPp	Non-imprinted polymeric particle
p/P	Polymer
PEDOT:PSS	Poly(3,4-ethylenedioxythiophene):Poly(styrenesulfonic acid)
PSS	Poly(styrenesulfonic acid)
Rb	Rebound
SEM	Scanning electron microscope
SPR	Surface plasmon resonance
SS	Styrenesulfonic acid
T	Template
THEO	Theophylline
TOAB	Tetraoctylammonium bromide
UV-Vis	Ultraviolet visible spectroscopy
V	Virgin

LIST OF TABLES AND FIGURES

TABLES

FIGURES - CHAPTER 1

FIGURES - CHAPTER 2

FIGURES - CHAPTER 3

FIGURES - CHAPTER 4

ABSTRACT

This work explores the potential of two signal transduction mechanisms for molecularly imprinted polymers (MIPs) primarily for the detection of (-)-ephedrine (EPD).

Firstly, gold nanoparticles were utilised resulting in a surface plasmon resonance based detection mechanism. Poly(acrylic acid-*co*-N'-isopropylacrylamide-*co*-N,N'-methylenebisacrylamide) (PAA-IPA-MBA), a conventional cross-linked MIP film, and poly(acrylic acid-*co*-acrylonitrile-*co*-methyl methacrylate) (PAA-AN-MMA), a phase-inversed 2D MIP film, were investigated. Gold nanoparticles were prepared and embedded into these polymers, with the resulting MIP systems demonstrating good selectivity and specificity for EPD. Spectroscopic detection studies based on hypsochromic shift in the wavelength of maximum absorbance in the surface plasmon resonance (SPR) of the embedded gold nanoparticles were performed. While SPR response was not observed for PAA-IPA-MBA, PAA-AN-MMA MIP films exhibited prominent shifts of up to 15nm after as little as 10 minutes of EPD sorption. Wavelengths shift observed in the non-imprinted PAA-AN-MMA after EPD sorption was minimal (≤8 nm) signifying MIP selectivity and significantly reduced (≤5 nm) in the presence of template analogues signifying MIP specificity. To the best of our knowledge, this is the first time SPR signal has been observed in 2D MIP films.

Secondly, a composite of molecularly imprinted and poly(3,4-ethylenedioxythiophene): polystyrenesulfonic acid (PEDOT:PSS) conductive polymer (CP) was developed for the detection of EPD. 3-Methylthienyl methacrylate (MTMA) was successfully used as a dual purpose monomer to link between the CP (via its thiophene moiety) and MIP (via its vinylic group) components of the composite. Composite particles of PEDOT:PSS and cross-linked MIP of acrylic acid and methylenebisacrylamide afforded the highest level of MIP binding (0.91μmol/mg after 2 hours) and selectivity (imprinting factor of 27 obtained after 10 minutes stabilising to 11 after 2 hours). While this CP-MIP composite particles lost its selectivity when embedded into a PEDOT:PSS conductive matrix (to allow electrochemical detection) due to significant non-selective interaction between EPD and the PSS in excess, we have demonstrated, for the first time, the potential of a CP-MIP composite for electrochemical sensing given the right conditions and matrix.

The design and formulation of all MIPs investigated in this study are supported by interaction studies between monomers and analytes (template and competing analogues) using semi-empirical molecular modelling and NMR spectroscopy.

CHAPTER 1 - INTRODUCTION

1.1 Illicit Drug Detection

Illicit drugs are a serious world problem costing thousands of lives and millions of dollars[1]. The majority of these illicit drugs fall into 4 main categories – cannabis, cocaine, opiates (including heroin) and amphetamine-type substances (ATS) (including ice and ecstasy). Between 1997 and 2010, over 100 tonne of drugs from these 4 main categories have been seized by law enforcement in Australia (Figure 1.1).

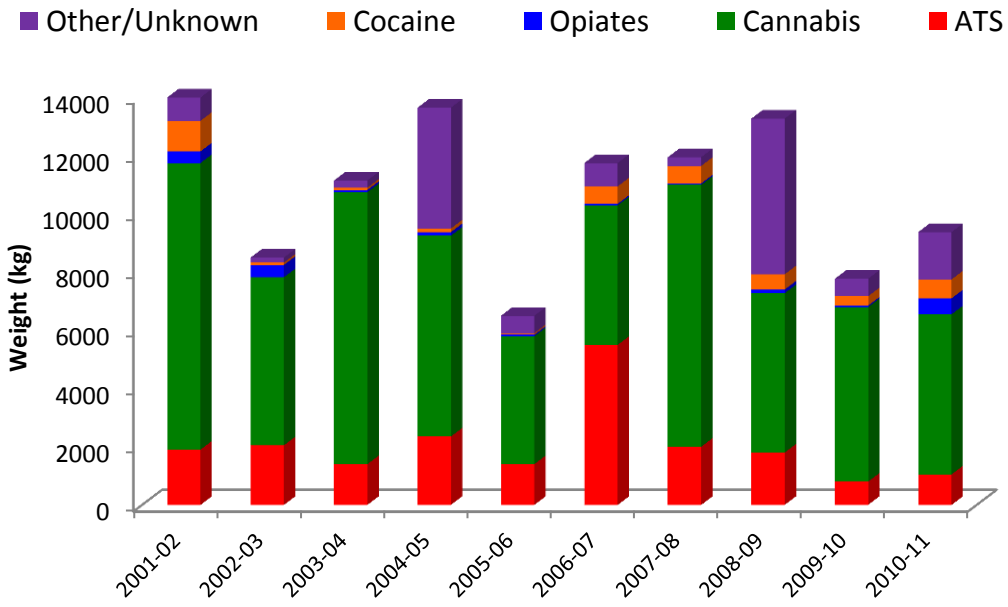

Figure 1.1 Australian seizures of Cannabis, Amphetamine-type substances (ATS), Cocaine and Opiates[2].

Research by the National Drug Research Institute estimates that in 2010, illicit drugs were responsible for up to 253,000 deaths worldwide[1a]. Reducing the supply of drugs to the consumer market is a vital step in the elimination of the drug problem that plagues the world community. The scientific analysis of drugs is a vital component in the 'war on drugs' which makes it necessary to reliably identify a huge variety of drugs often in remote locations[1a, 3].

Methods of drug detection are varied but often limited with respect to accuracy, specificity or the types of drugs which can be detected. Using cocaine as an example, current methods[4] used for detection include a variety of lab based instrumental techniques including thermal analysis[5], gas chromatography[6], infrared spectroscopy[7], mass spectrometry[6b, 8] and thin layer chromatography[9]. Other detection methods also include in-field colour and smell tests[10] as well as combinatorial approaches[11] involving several techniques.

Canine detection of narcotics is also possible however this relies on the olfactory system of highly trained dogs. As such it is limited by the attention span of the dog and the amount of reliable scientific information they can provide. In addition, the care, training and handling of the dogs can become expensive. As a result, this form of detection is primarily limited to border entry points such as airports and wharfs[12]. Detection methods such as chromatography and spectroscopy, while being both very specific and accurate, often require the use of large and expensive equipment that are almost exclusively used in the laboratory environment. This makes them incompatible for use with in-field testing. Mobile or in-field analysis is primarily limited to colour tests, which have varying degrees of sensitivity and specificity and may not react with all drug derivatives. In addition, these colour test may react positively to licit substances. This makes false positives and false negatives a possibility, making them less than ideal as they are only used as presumptive tests and subsequent laboratory analysis is necessary. When dealing with large numbers of samples, these tests can become time-consuming and expensive and may necessitate the need for large amounts of the reagent. The solvents used in these tests are often dangerous and require specific handling making them less than ideal for transportation to remote locations[13]. In-field detection allows evidence to be collected quickly to be used in both ongoing police investigations and eventual prosecutions of drug users and particularly drug traffickers.

The focus of this project is the detection of amphetamine-type substances (ATS). ATS refer to a group of synthetic substances which include amphetamine and ecstasy and their analogues as shown in Figures 1.2 and 1.3, respectively. The compounds shown in these two figures are the more common analogues available, however, even with only

simple substitutions and structural variations the number of compounds that can fall within this grouping is extremely large.

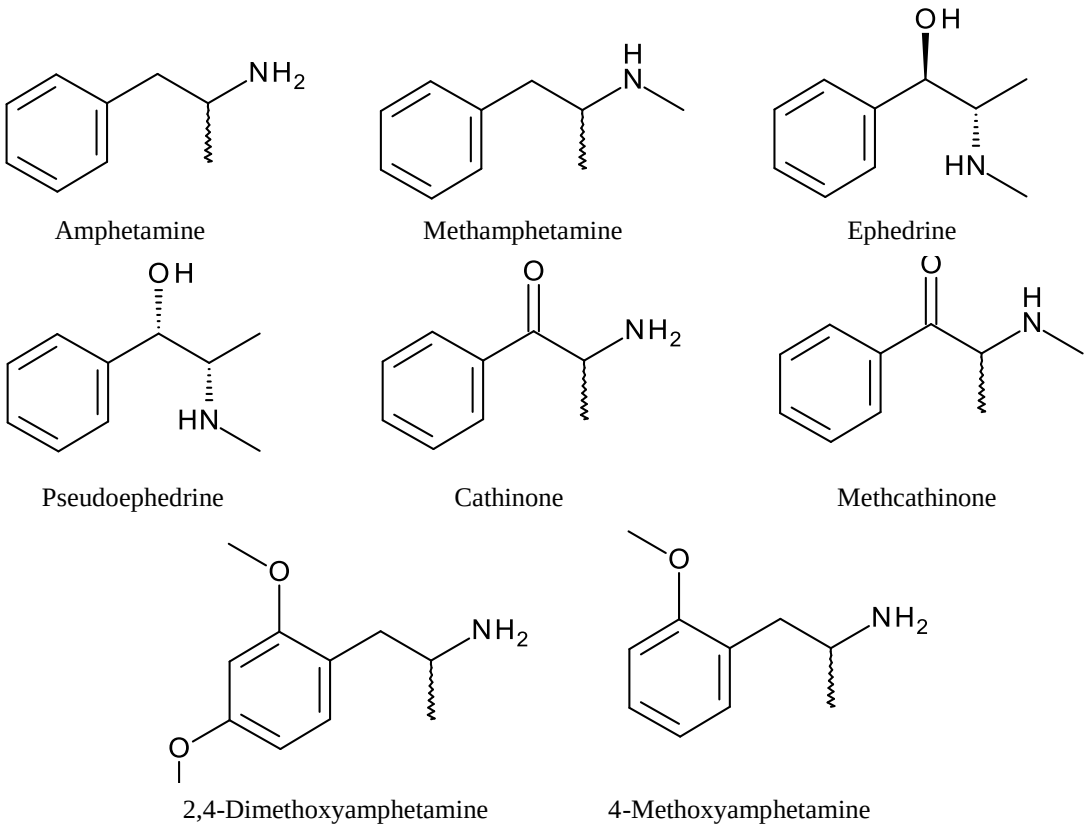

Figure 1.2 Amphetamine and some common analogues.

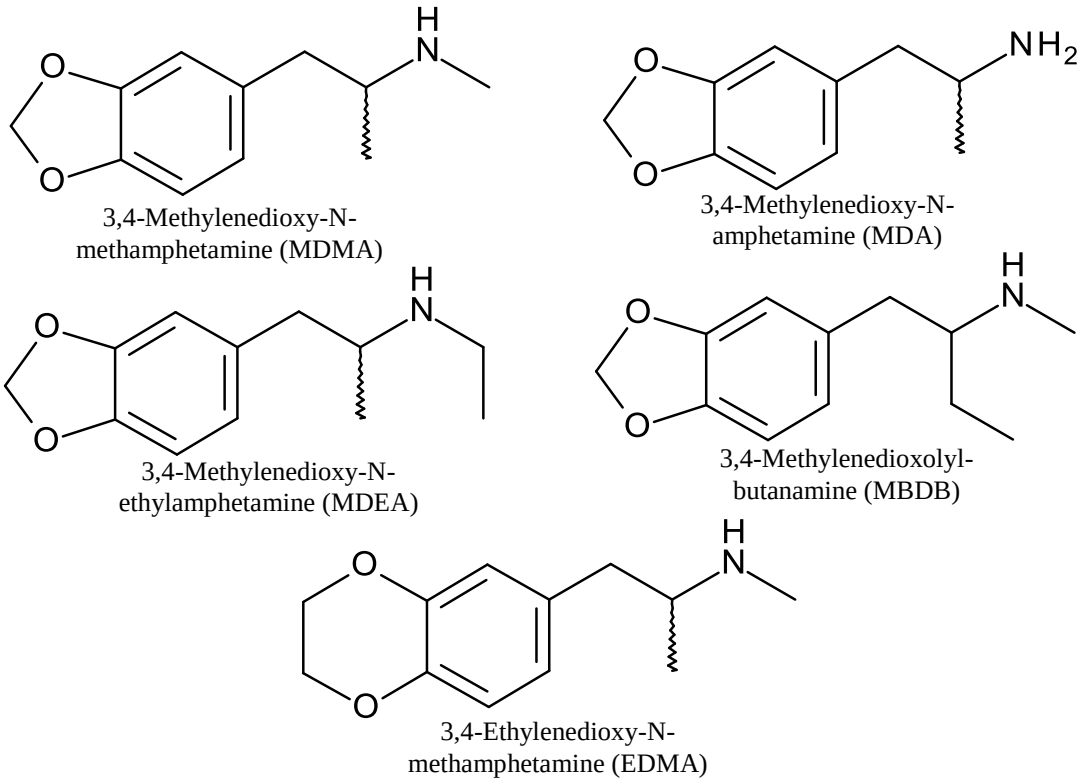

Figure 1.3 Ecstasy (MDMA) and some common analogues.

The first of the amphetamine group of substances date back to the late nineteenth century and were used (as they still are today) as nasal decongestants. The uncontrolled use of amphetamines led to widespread misuse and by the 1970s national and international control measures were introduced and licit pharmaceutical manufacture was greatly reduced. As a result, clandestine manufacture of these substances became the primary source for their supply. The ecstasy group of substances were first synthesised in the early twentieth century but were found to have little therapeutic use. During the 1990s however its recreational use increased considerably.[14]

All ATS are available in diverse forms including powder, tablet, paste or crystalline form and vary in purity. ATS do not require crop cultivation such as coca leaf or opium poppy required for the synthesis of cocaine and opiates, respectively. As such they are not limited to specific geographic locations, thus clandestine laboratories can operate anywhere and can are often placed close to consumer markets. This makes the number

of laboratories and amount of ATS being manufactured difficult to determine accurately.

Total worldwide seizures of ATS reached over 67 tonne in 2010. Figure 1.1 shows a steady rate of ATS seizures in Australia since 2001-02 of approximately 1-2 tons annually, with the exception of 2006-07 which saw a significant increase in ATS seizures to over 5 tons. Australian ATS seizures since 2001-02 have been greater than cocaine and opiates combined. An estimated 2.4% and 3.0% of the Australian population used ATS and ecstasy, respectively, at least once in 2010 compared with 10.3%, 2.1%, and 3.4% for cannabis, cocaine and opiates, respectively.[1a, 2, 15]

ATS can be synthesised from a variety of starting materials using a range of methods. This means that a large number of precursor chemicals must be monitored. Since many of these precursors are relatively common chemicals with benign and licit uses, this makes precursor control difficult. For methamphetamine, the most common precursor compounds are ephedrine and pseudoephedrine due to their availability in cold and flu medications. This makes ATS a high profit, low risk drug from a manufacturing standpoint, resulting in a greatly increased availability.[2]

This study aims to explore detection mechanisms for forensic applications by using (-)-ephedrine, an ATS, as a model analyte.

1.2 Molecular Imprinting

1.2.1 Background to Molecular Imprinting

Molecularly imprinting is a relatively new approach to molecular recognition that mimics biological recognition such as that involved in proteins, enzymes and nucleic acid activity. The process of molecular imprinting was developed to allow molecular recognition for specific target molecules with more stability and longer shelf lives.

In molecular imprinting, the detection target is used as a template around which functional monomers arrange themselves such that their functional groups are complementary to the template. This complex then undergoes polymerisation, usually with a second crosslinking monomer, causing the functional monomers to be immobilised. By subsequently removing the template from the system, a cavity or hollow is left which is specific to the size, shape and functionality of the template. This molecularly imprinted polymer (MIP) is then capable of molecular recognition when the template is reintroduced. Figure 1.4 below depicts a graphical representation of the molecular imprinting process.

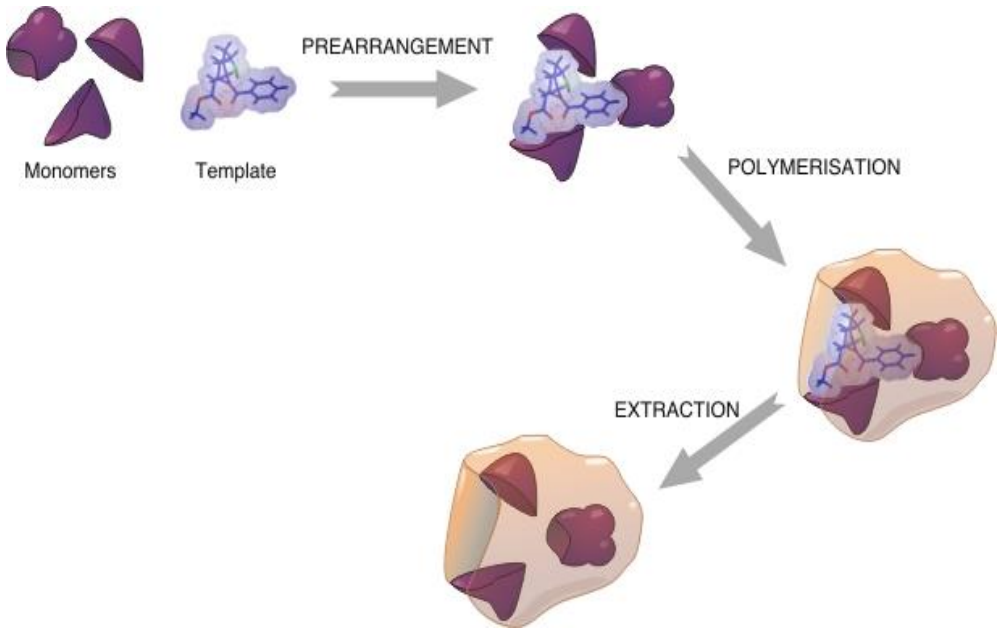

Figure 1.4 Overview of molecular imprinting. Reproduced from Mizaikoff (2001)[16].

In order to properly assess the performance of a MIP and the efficiency of the imprinting process, it is necessary to produce a non-imprinted polymer (NIP) to act as a control. NIPs are produced in an identical way to a MIP but with the absence of the template molecule.

Polymerisation is achieved primarily through free-radical or ionic initiation, although ionic initiation is limited with respect to the monomers that can be used. Free radicals are less selective due to their electrical neutrality and are generally a more useful initiator for molecular imprinting. Initiation of free radical polymerisation can occur via high-energy radiation or more commonly through addition of initiator molecules. These initiator molecules are then activated thermally, photochemically, or via a separate reaction. A chain carrier, or propagation radical, is then formed by the reaction a free radical with a monomer unit, propagation then occurs quickly through addition of monomer units to form linear polymer chains[17]. The most commonly used free radical initiators are 2,2'-azobis(isobutyronitrile) (AIBN) and 2,2'-azobis(2,4-dimethylvaleronitrile) (ADVN).

1.2.2 Covalent vs. Non-Covalent Imprinting

The template-functional monomer complex is traditionally formed by either covalent or non-covalent binding. A hybrid of these two methods known as semi-covalent imprinting has also been reported. Following successful formation of a MIP, it is necessary to completely remove any bound template molecules. This leaves behind a template specific cavity which can be used for subsequent detection of the template. [18]

The first covalent imprinting was reported by Wulff, G. et al. in 1977 with a 4-nitrophenyl-α-D-mannopyranoside template[19]. Recent covalent imprinting has included templates such as cholesteryl (4-vinyl)phenyl carbonate[20]; nortriptyline[21]; allyl phenyl disulfide[22]; propazine methacrylate[23]; and organotin species[24].

In covalent imprinting the functional monomers are initially bound by a covalent linkage before this covalent conjugate is polymerised such that the covalent linkage remains intact. After polymerisation the covalent linkage is then cleaved in order to remove the template leaving the template specific cavity. Upon reintroduction the template reforms these covalent bonds. Since the functional monomer and template are covalently linked, less non-specific binding cavities are formed resulting in improved binding.

Covalent imprinting is not as popular as non-covalent imprinting because of the limited monomers capable of forming covalent linkages to specific templates, often resulting in the need for expensive and time consuming custom monomer synthesis. Harsh conditions are also often required to cleave the template from the cavity which can damage the polymer. Covalent imprinting also suffers from poor binding kinetics, which results in slow rebinding times.

Non-covalent imprinting had its birth when in 1981 Arshady, R. and Mosbach, K. successfully imprinted Rhodaline blue, Safranine O and 4-amino-benzeneethanamine using non-covalent interactions[25]. Recent non-covalent imprinting has included templates such as Nylon-6[26]; Dibenzofuran[27]; Caffeine[28]; Naringin[29]; Cyclobarbital[30]; Theophylline[31]; Rhodamine B[32]; and Phenylalanine[33].

In non-covalent imprinting the functional monomer connects to the template via non-covalent interactions (e.g. hydrogen bonding, electrostatic interactions, and co-ordination bond formation). Thus polymerisation can occur after simply mixing the components and removal of the template is achieved through washing with an appropriate solvent. Non-covalent imprinting is significantly easier to achieve than covalent imprinting and is applicable to a far wider range of templates. Multiple non-covalent interactions can be just as strong as a single covalent interaction and provide greater interactions with the template, thus providing greater specificity.

The main disadvantage of non-covalent imprinting is the formation of binding sites with varying specificity. The formation of the template functional monomer complex used in non-covalent imprinting is an equilibrium driven process which relies typically relies on an excess of the functional monomer. This results in a range of stoichiometries of the

functional monomer to the template in the binding cavities as wells as functional monomers unassociated with the template. The non-specific binding cavities formed as a result can be minimised through optimisation of the functional monomer to template ratio used in the polymerisation.

Because non-covalent imprinting is useful for a broader range of templates and it is easier to achieve, it is the most suitable for the molecular recognition of illicit substance such as drugs and explosives. Molecular imprinting has been used successfully in the past for the recognition of illicit drugs including morphine[34], ephedrine[35] and cocaine [36; 37; 38], and explosives such as TNT[39].

In semi-covalent imprinting the functional monomer is covalently bound to the template and polymerised in the same way as covalent imprinting. This limits the formation of non-specific binding sites, the main disadvantage seen in non-covalent imprinting. Following polymerisation the template is again cleaved from the binding cavity, however these covalent bonds do not reform upon re-introduction of the template. Instead template rebinding relies on non-covalent interactions which improves binding kinetics, resulting in faster rebinding times. Whilst semi-covalent imprinting has advantages over both covalent and non-covalent imprinting, it is still limited by the monomers capable of forming covalent linkages to specific templates.

1.2.3 MIP Design

Whatever type of molecular imprinting is used, whether covalent or non-covalent, the template-monomer interaction is vital to successful recognition. In designing a MIP, the most important aspect is the choice of functional monomer/s and cross-linking monomer. The functional monomer/s (see Table 1.1 for examples) must have favourable interactions with the target template so that a cavity with complimentary functionality can be formed. This is most commonly achieved through hydrogen-bonding and ion-pairing. The crosslinking monomer (See Table 1.2 for examples) provides support and rigidity to the polymer allowing the functional monomers to remain stationary. A large variety of monomers and cross-linkers exist which are both cheap and commercially available.

Table 1.1 Examples of functional monomers[40].

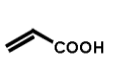 acrylic acid	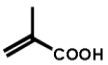 methacrylic acid	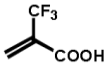 trifluoro-methacrylic acid
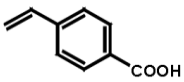 4-vinylbenzoic acid	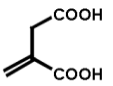 itaconic acid	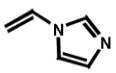 1-vinylimidazole
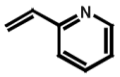 2-vinylpyridine	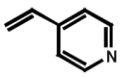 4-vinylpyridine	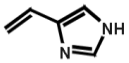 4(5)-vinylimidazole
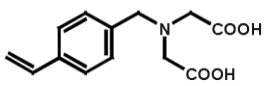 4-vinylbenzyl-iminodiacetic acid	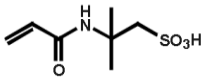 2-acrylamido-2-methyl-1-propane sulphonic acid	

Table 1.2 Example of cross-linking monomers[40].

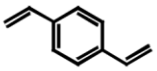 4-divinylbenzene	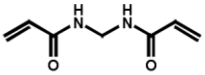 N,N'-methylene-bisacrylamide
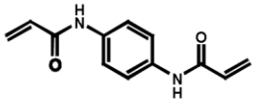 N,N'-phenylene-bisacrylamide	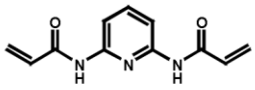 2,6-bisacrylamidopyridine
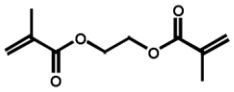 ethylene glycol dimethacrylate	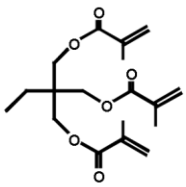 trimethylolpropane trimethacrylate

After an appropriate functional monomer has been chosen, it is necessary to determine the number of functional monomer units per template molecule that will produce the greatest template-monomer interactions. A sufficient template-monomer ratio is vital to producing a MIP with the greatest possible selectivity to the template molecule. Initially, this ideal template-monomer ratio was determined by trial and error. This meant that MIPs having a huge range of template-monomer ratios needed to be

produced in order to determine which had the best binding and specificity. This can be extremely tedious, time-consuming and expensive. Molecular modelling and nuclear magnetic resonance (NMR) titrations can be used to predict the performance of any given template-monomer ratio drastically reducing the time and money previously used during trial and error production.

1.2.4 Interaction Studies: Molecular Modelling and NMR Titrations

Molecular modelling using commercially available software (e.g. Spartan®, Wavefunction Inc.) has been used previously to investigate template-monomer interactions. This is of particular importance when developing systems based on non-covalent interactions in order to assess the number and relative strength of the interactions. Using molecular modelling software libraries of different functional monomers can be screened in a fraction of the time previously required to synthesise and then test the same number of polymers[35].

Molecular modelling involves the creation of template-monomer cluster within the software by placing two sets of virtual molecules together. Computational algorithms within the software are then used to calculate valuable information from these clusters, including enthalpy of formations and intermolecular distances. Energies of interaction for each template-monomer ratio are then able to be calculated using (Equation 1)[37].

$$\Delta E_{Interaction} = \Delta H_{f\ template\text{-}monomer\ complex} - (\Delta H_{f\ monomer\ cluster} + \Delta H_{f\ template}) \qquad \textbf{(Equation 1)}$$

When using Equation 1 to calculate the ideal template-monomer ratio it is important to take into account monomer-monomer interactions within the cluster. These interactions will often appear to favourably influence the energy within the template-monomer cluster, but if they are not associating with the template then they are not contributing to the stability of the imprints and must be ignored. Molecular modelling is useful in this regard as inter- and intra-molecular distances can be calculated which allows the determination of whether a given interaction is valuable to the imprinting process. Distances of approximately 1-3Å for example are within the limits of the hydrogen

bonding[41] required for template-monomer interactions. As with all computation methods, molecular modelling is used only as estimation and must be confirmed experimentally.

NMR titrations have also been used previously to investigate monomer template interactions. NMR titrations can be used as a means to predict MIP performance for a given template-monomer ratio[42] and to select the predicted ideal template-monomer ratio[43]. NMR titrations are carried out by adding increasing molar equivalents of the monomer to a solution containing the template and monitoring chemical shift changes. The chemical shifts of the functional groups within the system are sensitive to changes in their surrounding chemical environment. By observing changes in chemical shifts of individual atoms over incremental changes in monomer concentration, the optimal template-monomer ratio can be predicted. When changes in chemical shift cease, it indicates that the monomer has reached an excess and is no longer impacting on the chemical shifts of the template.

The combination of NMR and Molecular modeling as predictive tools has been successfully used in the design of a range of MIP systems, allowing the time and energy normally wasted on trial and error MIP production to be bypassed. Examples of templates successfully imprinted using this combinatorial approach include cocaine[37], ibuprofen[44], theophylline[45], acetochlor[46] and N-boc-L-phenylalanine[47].

1.2.5 MIP Configuration and Application

MIPS can be synthesised in an ever increasing range of application-minded formats. Because the basic principle of MIP construction is so simple – self arrangement of a template-monomer complex followed by polymerisation – the process can be applied to a vast number of potential roles. MIP design and production is extremely flexible and different configurations have been produced to suit a variety of situations and functions. With intelligent design and the selection of an appropriate configuration MIPs can be customised to suit nearly any purpose.

One of the largest applications of MIPs is in the field of separation science. MIPs have been used to coat fibres to act as selective sorbents for extraction purposes[48], incorporated into gels for use in chromatographic columns[49], and as coatings for capillary electrochromatography. Due to their ability to be selective to almost any given compound, they are capable of separating compounds based on their selectivity to the particular MIP used in the technique.

An emerging field of MIP design is in the field of drug delivery. Incorporation of a MIP into a delivery medium capable of crossing the necessary cell barriers, such as a hydrogel[50], allows the bound drug molecule to be released directly into the target area. This has huge advantages over previous less efficient drug delivery systems that may have been incapable of delivery the drug to the desired region.

The first MIPs were produced in a method now known as bulk imprinting, which produced bulk monoliths by undertaking polymerisation is a relatively small amount of solvent and a large proportion of crosslinker. This method is very simple and easy to achieve but results in large and irregular particles. It is then necessary to grind the polymer to produce particles small enough to allow the analyte access to the binding sites throughout the bulk polymer. Small particles are also desirable to increase the surface area of the polymer and thereby enhance mass transfer of the template. Grinding does however lead to the mechanical destruction or damage of some of the binding sites, which can lead to non-selective binding. Additionally, grinding can result in non-uniform particle sizes resulting in reduced polymer performance.
Two of the most versatile and common MIP configurations currently used are films and particles. Both of these formats are used in this work and are discussed in more detail below. Other MIP forms include microspheres[51], nanoparticles[52], core-shell particles[53], polymer beads[54], rods[55], and nanowires[56]. As well as altering the configuration of the MIP itself, it is possible to coat a material with a MIP or graft the MIP onto a surface making MIPs even more versatile and valuable. Materials that have been coated with, or had MIPs grafted to include electrodes[57], quartz crystals microbalances[58], silica supports[59], microplates[60] and fibres[61].

1.2.6 MIP Films

An interesting MIP configuration that is becoming increasingly popular is that of the Molecularly Imprinted Polymer Film (MIPf). MIPfs are particularly useful in the field of sensor technology having been used successfully for the detection of a range of analytes including proteins[62], drugs[63], pesticides[18], and explosives[39b, 64].

MIPfs can be prepared in a variety of ways such as by immobilising previously prepared MIP particles using a binding agent or plasticiser, although this method has been associated with problems due to film thickness and low homogeneity of the immobilised particles[65]. An alternative technique involves formation of a MIP onto a previously prepared membrane, typically through electropolymerisation[66] or grafting[59, 67]. MIPfs can also be produced by cutting thin slices of bulk polymers, typically aero- or hydrogels[68]. Another route to obtaining MIPfs sees the imprinting and film formation processes occurring simultaneously in a process known as phase inversion.

1.2.7 Phase Inversed MIP Films

Phase inversed MIPf are made differently to more traditional MIP systems, although the basic imprinting principles remain the same. The main point of difference in phase inversed MIPf is that a crosslinker is not used. The crosslinker provides traditional MIPs with rigidity and support and typically makes up the majority of the MIPs composition, however in the form of a MIPf a crosslinker makes the film brittle and difficult to use. In phase inversed MIPf the cross-linker is replaced with a matrix monomer, which is copolymerised with the functional monomer, to provide the necessary support without making the film fragile. Matrix monomers, such as acrylonitrile[31b], provide support through intermolecular hydrogen bonding to interconnect the polymer chain.

The properties of the functional and matrix monomers used directly influence the properties of the films. While this necessitates experimentation to investigate the effect of the choice and monomer and their composition, it also allows intelligent design of the MIPf to impart the desired characteristics such as sturdiness, flexibility or transparency.

Two methods are commonly used in the making of MIPf: wet and dry phase inversion. Dry phase inversion is usually achieved though spin casting, whereby a small volume of concentrated and viscous polymer solution is placed on a flat substrate such as glass. The substrate is then rotated at high speed by a casting instrument, with the resulting centripetal force spreading the solution over the surface of the substrate resulting in a uniform thin layer. Subsequent solvent evaporation leaves behind a solid polymer film, thereby restricting the technique to use with volatile solvents. Spin-casting produces extremely uniform and reproducible films and the speed, acceleration and length of rotation can be varied to produce films of desired size and thickness[63b]. Examples of templates successfully imprinted utilising the dry phase inversion technique include N-boc-L-phenylalanine[47], atrazine[69] and propranolol[70].

Wet phase inversion involves transferring the polymer from a solvent to a non-solvent thereby causing the polymer to solidify. By initially placing the polymer solution upon a substrate before placing it within the non-solvent it solidifies in the shape of the substrate. By using a flat substrate such as a glass slide a film or membrane can be formed. Solidification of the polymer occurs rapidly where there is direct exposure to the non-solvent causing the formation of a dense 'skin'. This skin hinders solvent diffusion from the remaining polymer causing the remaining polymer to precipitate more slowly and porously. The process continues until the solvent is completely removed. Films produced via phase inversion are not as uniform as those formed using spin casting and there is less control over the films thickness. These films also exhibit 'rough' morphologies, and although not uniform improve template extraction and re-binding by providing better access to the template bound cavities. The phase-inversion technique has successfully been used to produce MIPf for several templates including albumin[62], tocopherol[71] and 2,4-dinitrotoluene[72]

In both methodologies temperature plays an important role, with increased temperature allowing films to form more quickly but lower temperatures exhibiting better binding.

1.2.8 MIP Particles

Particulate polymers can be produced using a range of methods, the most common being emulsion and precipitation polymerisation. Polymeric particles can be produced in a range of sizes by varying the composition and polymerisation conditions. The uniform size and high surface to volume ratio of particulate MIPs results in very favourable binding kinetics making them ideally suited to chromatographic applications.

Emulsion polymerisation involves the formation of colloidal dispersions of monomer prior to polymerisation. A stirring mechanism is typically used to produce this emulsion with the resulting droplets stabilised through the use of a surfactant resulting in the formation of spherical structures called micelles. Initiation typically starts in the aqueous phase and the resulting oligomeric radicals can enter pre-existing micelles or form new micelles by aggregation with surfactant molecules. The monomer concentration in the micelle is much higher than the aqueous phase allowing for rapid propagation. Eventually virtually all the monomer is consumed and polymerisation effectively ceases. A surfactant stabilised polymeric particle (or latex) is the final product[73].

Precipitation polymerisation can be used to synthesise uniform spherical beads that don't require grinding before template extraction and rebinding. The formulation of particulate polymers by the precipitation method is achieved by undertaking polymerisation in a solvent where the resulting polymer is insoluble. Once the polymer chain is of sufficient length to precipitate from solution, polymerisation continues by adsorption of monomer and initiator onto the polymer particle. By using relatively large volumes of solvent the particles are prevented from aggregating and particles of uniform size can be produced[25, 74].

The precipitation method for the production of polymeric particles was chosen for the synthesis of MIP particles due to the less complicated polymerisation mixture. The addition of the surfactant required for emulsion polymerisation can result in an additional interference to the molecular imprinting process.

1.2.9 MIP Characterisation

The purpose of MIPs is to provide a substance capable of selectively separating a particular target molecule which can be attributed to the template specific cavities produced during the imprinting process. The non-imprinted polymer (NIP) is therefore used comparatively to demonstrate the selective binding of the template to the MIP.

The most common performance characterisation used to assess MIP performance is through batch rebinding. This involves placing the MIP or NIP into a stock solution of the analyte and allowing rebinding to occur over various times. The polymer is then removed and allowed to dry. Detection of the template within the polymer can be achieved through identification of template fingerprints within the infrared, visible or ultraviolet spectrum. In addition quantification of the rebinding is done by measuring the change in concentration of the stock solution before and after rebinding. This change in concentration of stock solution equates to amount of template adsorbed to the MIP or NIP (B_{MIP} and B_{NIP} respectively) as shown in Equation 2.

$$B = [\text{Template}]_{initial} - [\text{Template}]_{final} \qquad \textbf{(Equation 2)}$$

By then dividing the template adsorption of the MIP (B_{MIP}) by the absorption of NIP (B_{NIP}) an imprinting factor (*I*) (Equation 3) is produced which represents the binding directly attributable to the imprinting effect.

$$I = B_{MIP} / B_{NIP} \qquad \textbf{(Equation 3)}$$

The selectivity offered by a MIP system is typically summarised using this imprinting factor, however these factors allow only for qualitative comparison between MIP systems as it is highly dependent on the experimental conditions used during rebinding.

The level of specificity of the MIP system is determined by comparing the imprinting factor of the template with that of the analyte. The level of specificity is primarily determined by the structural similarity of the analyte to the template. This makes achieving high levels of specify more difficult if trying to differentiate enantiomers and structural isomers of the template. This can however be beneficial when using MIPs in

sensing applications as it allows detection of a class of compounds (e.g. amphetamine type substances) rather than a single target within the class.

In addition to selectivity described above, the ability of the MIP to rebind the template in preference to other analytes is an important performance characterisation used to assess MIP performance. This characterisation is known as specificity and can be determined through either cross-reactive or competitive binding. In cross-reactive binding the imprinting factor of each analyte is determinedly independently through separate batch binding. In competitive binding the binding solution contains the template and one or more competing analytes simultaneously. In both methods the concentration of each analyte is kept constant.

1.2.10 Signal Transduction

Most current methods of detection using molecularly imprinted polymers would typically require subsequent laboratory based analysis of the imprinted polymer to positively determine the identity of any substance rebound to the polymer. As such, although MIPs are far more selective and specific than current forensic in-field chemical testing, they offer no practical advantage over current methods.

The incorporation of a method of template detection directly into the imprinted polymer would remove this limitation. This may be done by incorporating a transducer into the polymer, which converts phenomenological changes such as mass differences or reaction heats to detectable signals such as by optical or electrochemical means. Methods of detection which have recently been investigated include the use of fluorescent functionalised polymers allowing fluorescence based detection[72, 75], colourimetric detection as a result of displacement of non-specific dyes from the binding cavity[76], thermometric detection based on binding event reaction heats[77], and the use of quartz crystal microbalance based sensors to allow mass based detection[18, 78].

Of particular interest for this work is the use surface plasmon resonance (SPR) sensing on metal (typically gold or silver) surfaces. SPR refers to the collective oscillations of

the valence electrons in response to light. A resonant, collective oscillation is established when the light matches the natural frequency of the surface electrons oscillating against the force of the positive nuclei. Electromagnetic waves known as surface plasmons propagate parallel to the metal surface and are very sensitive to any changes at this boundary. This effect has been utilised for the direct sensing of large molecules such as proteins and DNA[79] and in combination with MIPs for the sensing of a wide variety of analytes[80].

This work investigates the use of nanotechnology, specifically gold nanoparticles, which have been demonstrated to allow SPR based detection in MIPs[68]. This will be introduced in more detail in Chapter 1.3 and results and discussion are shown in Chapter 3.

Also of interest for this work are MIP sensors which utilise electrochemical based methods of detection. The most common types of these sensors use a MIP as a recognition element attached to, or incorporated into an electrode which will selectively bind the target molecule. Once bound the target may be electrochemically oxidised or reduced resulting in a detectable signal from the modified electrode[67a, 81]. Signal transduction is usually achieved through voltammetry[81a, 82] or amperometry[83], however conductometric[84], impedance[85] and capacitance[86] have also been used.

A number of substances have been utilised as electrodes materials for MIP based sensors including gold[81a, 83], mercury[82b], graphite[67a], and carbon paste[82a, 87]. Of particular interest for this work is the use of conductive polymer based electrodes in MIP sensors as the basis for electrochemical based detection. This will be introduced in more detail in Chapter 1.4 and results and discussion are shown in Chapter 4.

1.3 Gold Nanoparticles

1.3.1 Background to Nanotechnology

The field of nanotechnology is the study and manipulation of matter in the atomic and molecular scale. This field of study is of particular interest owing to the unique properties which can be engineered as a result of the nanoscale dimensions. In the field of sensors the most common influence of nanotechnology is as a transducer. In some cases, nanotechnology enhances transducer systems by improving input and output from the transducer component[88]. In other cases, nanoparticles have been able to completely remove the need for a transducer by imparting an electrical or visible characteristic onto the sensor itself, thereby providing a direct signal[89]. Embedded gold nanoparticles are one possible method of directly imparting signalling capability into a chemical sensor such as a MIPf.

Nanotechnology is becoming increasingly important in a variety of research fields including chemical sensor technology. The field of chemical sensing and molecular recognition is continually attempting to miniaturise the total sensor system through the integration of sensors and signal processing componentry. Particular importance is paid to technologies that permit low-cost manufacture of both sensors and their associated electronics. Interest in nanotechnology is based on the unique physical and chemical properties that nanostructures deliver. Their small size allows for their incorporation into in-field sensors and their large surface-to-volume ratio enhances surface interactions such as catalysis and therefore reaction kinetics. It has also been demonstrated that it is possible to synthesize nanoparticles - specifically metal colloids, in desired sizes, and to incorporate them into tailored matrices such as glass, ceramics and polymeric type substances that are capable of being utilized in chemical sensors[90].

Nanoparticles and other nanostructures of metals and semi-conductors are of particular importance in the field of sensors because of their size-dependent electrical, chemical and optical properties. They also efficiently utilise expensive metals that would otherwise be too expensive to use on a bulk scale. The catalytic and electrochemical

characteristics of dispersed metal nanoparticles makes them ideal in the fabrication of electrochemical sensors[91].

Gold nanoparticles, also known as gold monolayer-protected clusters (MPCs), are drawing increasing attention due their unique properties mentioned above. Generally, gold nanoparticles are produced in a solution by reduction of hydrogen tetrachloroaurate ($HAuCl_4$) as seen in Figure 2.2. Upon dissolution, the $HAuCl_4$ solution is rapidly stirred while a reducing agent is added. This causes Au^{3+} ions to reduce to neutral gold atoms. As more gold atoms form, the solution becomes supersaturated, and gold gradually starts to precipitate in the form of sub-nanometre particles. The remaining gold atoms that precipitate adhere to the existing suspended particles, forming spheres of uniform size if vigorous agitation is maintained throughout the process. To prevent over-aggregation, a stabilising agent, typically an aliphatic thiol is usually added which binds to the nanoparticle surface.

A method for the production of aqueous gold nanoparticles was first achieved in 1951 by Turkevitch J. et al[92], while a method for the creation of organically soluble gold nanoparticles was achieved by Brust and Schiffrin in 1994[93].

Gold nanoparticles themselves exhibit poor solubility caused by oxidation, aggregation and other changes in properties over time. The application of a stabilising agent forms a monolayer on the surface of the gold nanoparticle, creating a monolayer-protected cluster (MPC). The monolayer usually consists of a thiol-functionalised organic compound where the sulphur atom bonds covalently to the gold nanoparticle surface. The advantages of MPCs, apart from increased stability, include allowing the design of specific properties by altering the stabilizing agent used. Use of alkanethiols, arenethiols, and the incorporation of other functional groups such as amines, carboxylic acids and alcohols, demonstrate the versatility of MPCs[94].

1.3.2 Nanoparticles and Sensors

An area that has received particular attention in gold nanoparticle research is the detection and monitoring of biological reactions. Successful detection of polynucleotides with specific sequences has been accomplished with gold nanoparticles hybridised with complimentary nucleotides[95]. Similar hybridisation of gold nanoparticles with antibodies have been used for immunoassays[96].

Gold nanoparticles have also demonstrated usefulness as catalysts, for example the electro-catalytic oxidation of carbon monoxide and methanol[97].

Of particular interest is the use of nanoparticles in molecular recognition and chemical sensors. Their effectiveness has been demonstrated in a colorimetric heavy metal sensor[98], gaseous ozone sensor[99], and hybridised with haemoglobin for sensing of nitrites[100].

1.3.3 Gold Nanoparticles and Molecularly Imprinted Polymers

The incorporation of gold nanoparticles into MIPs can be achieved by simply including them in the pre-polymerisation mixture. Upon polymerisation, the nanoparticles are immobilised within the polymer matrix. Embedding nanoparticles by this method is straightforward and has been successfully used for sensing purposes[68].

An alternative to immobilisation within the polymer is to include the gold nanoparticle within the polymer itself. This is achieved by using a polymerisable stabilising agent. In this way, the gold nanoparticle may also serve in a cross-linking capacity or may contribute to the template rebinding[101].

Following incorporation of the gold nanoparticle into the MIP, a detection method must be available that is capable of discriminating the presence or absence of the template molecule. Demonstrated detection methods rely on matrix swelling which accompanies rebinding. When a MIP is synthesised, the template and functional monomers form a

complex, which is 'frozen' in place during polymerisation. Post-polymerisation removal of the template leaves a cavity within the polymer that is complementary in size, shape and functionality to the original template. Template removal from the resultant polymer is accompanied by a slight shrinking of the remnant cavity, which is reversed when the template is re-introduced (rebinding). The swelling effect during rebinding increases the inter-particle distance of the immobilised gold nanoparticles (Figure 1.5), producing a detectible event.

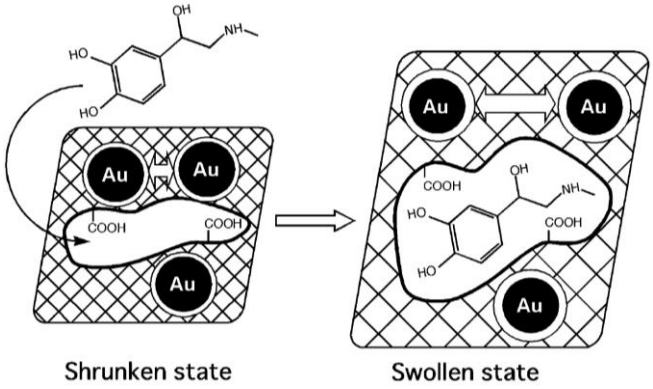

Figure 1.5 Effect of rebinding on polymer swelling and inter-particle distance of gold nanoparticles. Reproduced from Matsui (2004)[1].

One method of detection is achieved though changes in the electrical properties of the nanoparticles and therefore the MIP. Increases in inter-particle distances leads to increased resistance of the polymer, making potentiometric sensing possible. This has been achieved with nanoparticle embedded MIPs grafted onto electrode surfaces[102].

Alternatively, detection relates to a shift in the SPR absorption band of the immobilised gold nanoparticles. Previous work by Matsui et al.[68, 102] utilised this property and demonstrated that a signal could be produced upon template re-binding in a molecularly imprinted polymer. This work utilized adrenaline as a template and produced a shift up to 22nm in the plasmon absorption band of the gold nanoparticles during rebinding of adrenaline. A similar system which also utilised a gold substrate in additional to gold nanoparticles was used with a cholesterol imprinted MIP and resulted into a shift of up to 56nm in the plasmon absorbance band[103].

1.4 Conductive Polymers

1.4.1 Background to Conductive Polymers

An alternative method of signal transduction for sensors involves the combination of the detecting element of the sensor with a conductive element which will directly respond to any changes caused by the detection of the target. Possible conductive elements capable of being used in this function are conductive polymers.

Traditional synthetic polymers used in the 'plastics' industry are generally non-conjugated polymers they are therefore insulators, and as such were of little interest as an electronic material. The discovery and development of conductive polymer has only occurred in the last fifty years but they have increasingly attracted the interest of scientists and industry, demonstrated by the increasing output of journal articles observed in Figure 1.6.

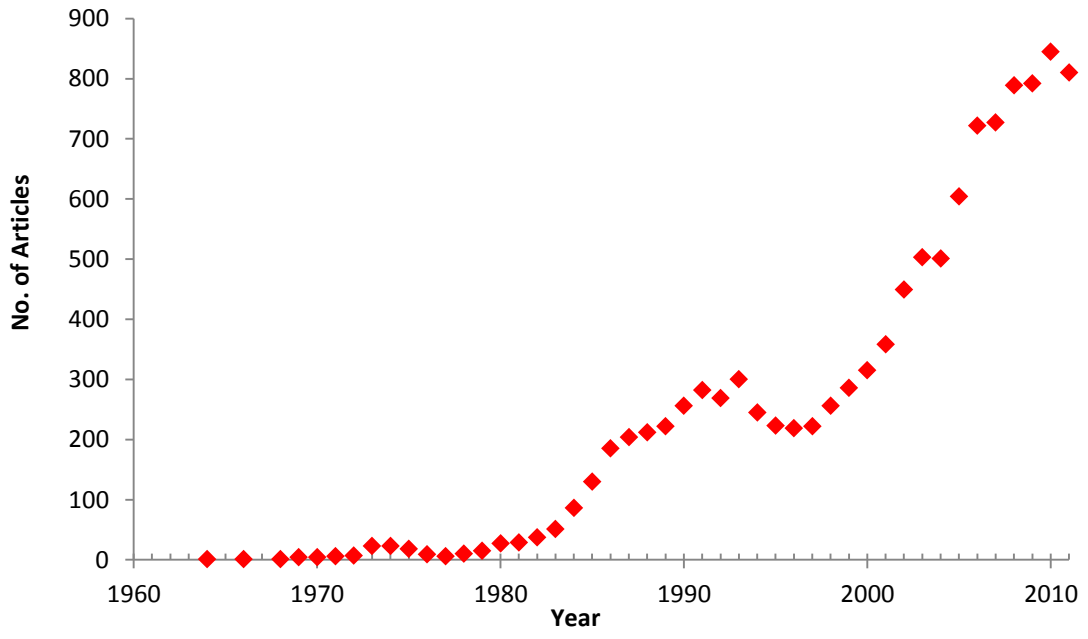

Figure 1.6 Growth of research into conductive polymers indicated by increasing number of journal articles.

The insulating properties of non-conjugated polymers results from the electronic configuration of the four valence electrons which are all used in covalent bonds. Conjugated polymers, however, have a different electronic configuration, whereby one electron is unpaired per carbon atom – the π-electron. In addition, π-bonding, whereby orbitals of successive carbon atoms along the polymer backbone overlap, leads to a delocalisation of electrons. This delocalisation allows charge mobility along the polymer chain.

Amongst the first works into the field of conductive polymers was the work of DE Weiss *et al*. in 1963 which reported, in a series of papers, the synthesis of iodine-doped polypyrrole with conductivities as high as 1 S/m[104]. Later work by the same group in 1965 achieved conductivities as high as 3 S/m[105]. This is comparable to the conductivity of semiconductors such as silicon and germanium 1.56×10^{-3} and 2.17 S/m respectively, but still far below that of metals such as silver which possesses the highest conductivity of all metals at 6.3×10^{7} S/m[106].

Most conductive polymers, by themselves, exhibit relatively low conductivities when compared to traditional conductors and semiconductors, but, by doping the polymer, a far greater range of conductivities can be achieved[107], as observed in Figure 1.7. When doping levels are sufficiently high, the electronic structure evolves to that of a metal[108].

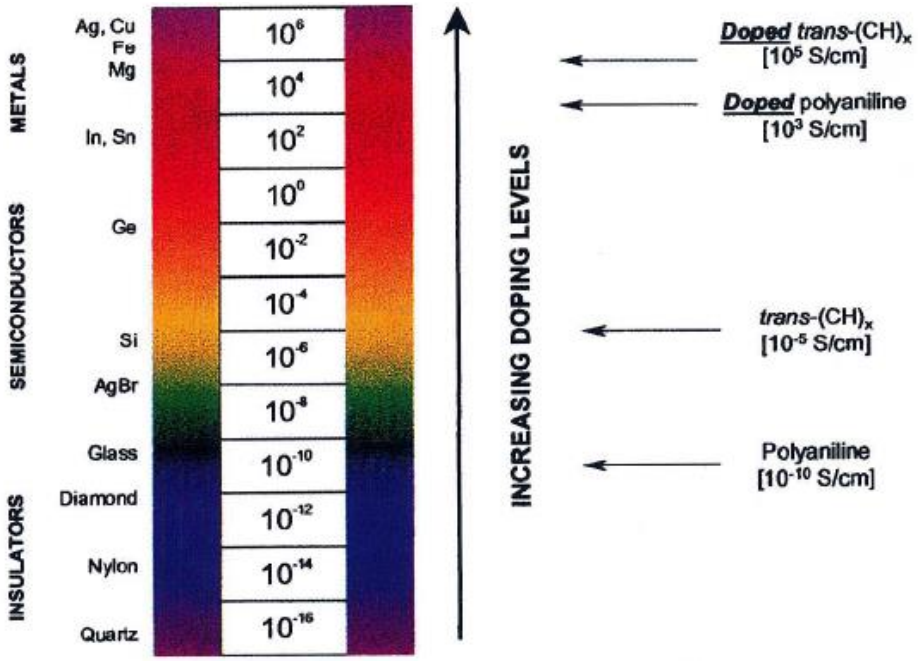

Figure 1.7 Relative conductivity of various electroactive polymers. Reproduced from MacDiarmid (2000)[109].

During the doping process, controlled additions of non-stoichiometric quantities of chemical species results in the production of 'charge-carriers' and the ability of these carriers to move along the conjugated polymer backbone results in the observed conductivity. Doping is typically reversible and may be carried out in a number of ways, including chemically or electrochemically (Figure 1.8). By adjusting the doping level, conductivities ranging from insulating to highly conducting materials may be produced. Doping levels of up to 40% can be used for conductive polymers compared with less than 1% for more traditional silicon based semi-conductors[108-109].

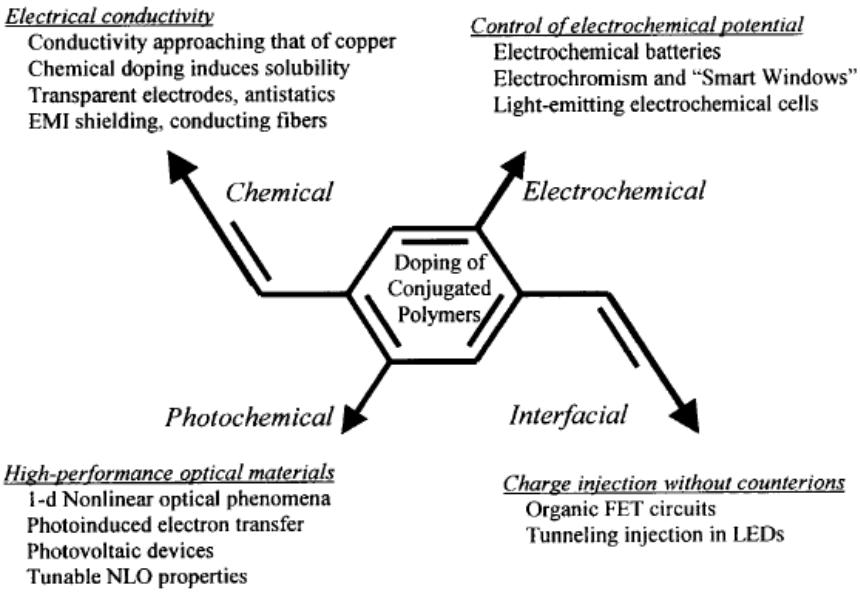

Figure 1.8 Doping Mechanisms and Related Applications. Reproduced from Heeger (2000)[108].

n-Doping is achieved through chemical reduction (addition of an electron) to the π-system of the polymer backbone and typically uses cationic dopants. The most common form of doping however, is p-doping, achieved through chemical oxidation (removal of an electron) using a range of anionic dopants. A wide range of chemical dopants can be used and typically depend on the type of conductive polymer involved and the desired conductivity. Table 1.3 shows some examples of chemical dopants for a range of conductive polymers as well as the resulting conductivities[110].

Table 1.3 Conductivities of conductive polymers with selected dopants. Reproduced from Kumar (1998)[111].

Polymer	Doping Material	Conductivity
Polyacetylene	I_2, Br_2Li, Na,	10^4
Polypyrrole	BF_4^-, ClO_4^-,	500 - $7.5x10^3$
Polythiophene	BF_4^-, ClO_4^-,	10^3
Poly(3-alkylthiophene)	BF_4^-, ClO_4^-,	10^3 - 10^4
Polyphenylenesulphide	AsF_5	500
Polyphenylene-vinylene	AsF_5	10^4
Polythienylene-vinylene	AsF_5	$2.7x10^3$
Polyphenylene	AsF_5, Li, K	10^3
Polyisothi-anaphthene	BF_4^-, ClO_4^-	50
Polyazulene	BF_4^-, ClO_4^-	1
Polyfuran	BF_4^-, ClO_4^-	100
Polyaniline	HCl	200

Perhaps the greatest difficulty associated with conductive polymer relates not to their conductivity, but rather their processability. Many conductive polymers become both insoluble and infusible particularly with increasing molecular weight. This makes them unsuitable for use in virtually all conceivable devices for which they might be employed.

One major avenue of research in the field of conductive polymers involves the development of conductive polymers capable of being more easily processed for use in devices and other applications. The introduction of functionalised side chains onto the conjugated polymer backbone to improve the properties of the polymer, including processability, has been used successfully for a variety of conductive polymers. For example 3-alkyl substituted polythiophenes can be processed from solution whereas unsubstituted polythiophene is insoluble[112].

The use of a soluble co-polymer which can also act as the dopant for the conductive polymer component may be used. The most prominent example of this is poly(3,4-ethylenedioxythiophene):poly(styrene sulfonate) or PEDOT:PSS as seen in Figure 1.9. In this conductive polymer system, the PEDOT and PSS act as co-ionomers, with the

PSS carrying the negative charge and the PEDOT carrying the positive charge, resulting in a neutral macromolecular salt[113].

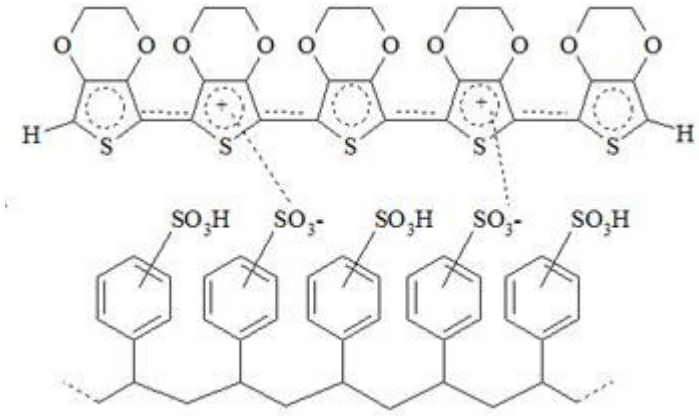

Figure 1.9 Structure of poly(3,4-ethylenedioxythiophene):poly(styrene sulfonate).

The optimisation of desired physical properties of conductive polymers including solubility, stability and optical properties can be achieved by small changes at the molecular level to the polymer. Since even the smallest changes at the molecular level can cause changes to inter- and intra-molecular forces within the polymer chains, the resulting changes to the physical properties can be drastic. However changes to the polymer chain, such as through the steric interaction of side chains, can cause a reduction in the degree of conjugation of the polymer backbone. This will have a consequential reduction in the conductivity of the polymer. Conversely, changes which increase the degree of conjugation, such as through the introduction of fused rings to the system, may produce an increase in conductivity[114].

The design of conductive polymers has thus become a trade-off between conductivity and desirable physical properties including processability. The ultimate goal of an ideal synthetic metal - a conductive polymer with the conductivity of a metal capable of being easily and inexpensively processed for broad use in industrial products - has yet to be fully realised[108].

1.4.2 Applications of Conductive Polymers

Since their discovery, conductive polymers have been used across increasingly diverse fields and in a wide range of applications. Figure 1.10 divides conductive polymer research, based on scientific papers from 1993-2011, into various uses with batteries and sensors noted as being the most prolific applications.

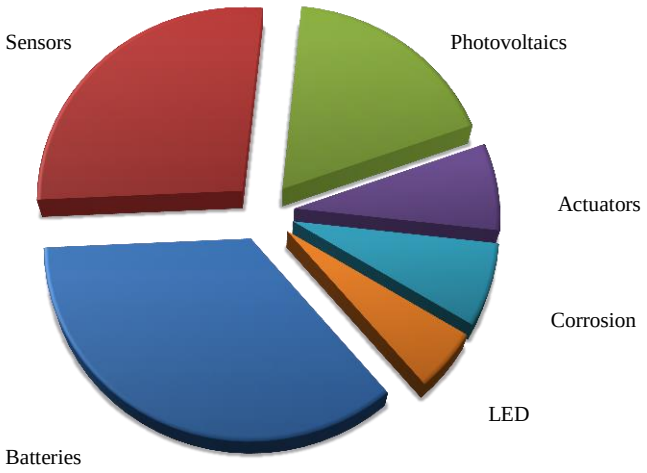

Figure 1.10 Scientific papers published on conducting polymers from 2000-2011 categorized into various topics.

Among the most promising application of conductive polymers is in the field of electronics. The advantage of 'plastic' electronics such as transistors and integrated circuits over much faster traditional silicon-based devices is the extremely low-cost and flexibility[115]. In addition conductive polymers have shown to be particularly useful in micro- and nano-electronic devices[109, 116]. Devices of these sizes may revolutionize electronic devices worldwide allowing for miniaturisation beyond that which has been achieved in the last decade.

Conducting polymers, such as polypyrrole, also show promise as rechargeable battery materials since they are capable of being readily oxidised and reduced. When combined with traditional electrodes such as lithium, usable voltages are obtained with energy densities several times that of traditional nickel-cadmium or lead-acid batteries[117]. Conductive polymer super-capacitors (capable of storing 50 F/g) have also been

reported, and have attracted interest for use in electric powered-vehicles and alternative energy production[118].

Polymer photovoltaics using conductive polymers have also been developed. These devices have very low efficiencies compared to silicon based solar cells, however due to their low cost they can be applied to very large areas such as rooftops as building walls[119]. The process involved in these photovoltaic devices can also be reversed to produce light emitting diodes with the colour of light produced depending on the band gap between the valence and conduction band of the polymer.

Electrochromic devices capable of transcending a spectrum of colours based on the current applied to them may also be produced using conductive polymers. Devices based on this type of technology may be used as memory storage or as 'smart windows'[120].

1.4.3 Conductive Polymers in Sensors

One of the largest applications of conductive polymers relates to their use as or in sensors based on the effect a desired target will have on the polymer itself. Changes in the environment around a conductive polymer such as those caused by presence of another chemical species can cause changes in the shape, orientation and degree of conjugation along the polymer backbone. These changes cause a subsequent change in the electrical properties of the polymer which are capable of being analysed[121]. Devices based on this principle have been developed capable of interacting with simple anions[122], metal ions[123], small organic molecules[124] and proteins[125].

pH sensors, based on the protonation/deprotonation of certain conductive polymers which possess acidic or basic groups have also been developed. Deprotonisation results in the removal of charge carriers for the conjugated backbone, and is accompanied by changes to the electrical properties. For polypyrrole for example protonation increases conductivity (21 S/cm at pH 3) while deprotonation results in lower conductivity ($5x10^{-3}$ S/cm at pH 13)[126].

In these cases, target recognition of the analytes is limited to those which have a direct interaction with the conductive polymer. For example the ability of poly(3-aminophenolboronic acid) to bind diols has be utilised to produce a potentiometric sensor for sugars[127]. This severely limits the number and type of analytes which may be directly detected using conductive polymers alone.

1.4.4 Conductive Polymers and Molecularly Imprinted Polymers

As mentioned previously, MIP-based electrochemical sensors utilise molecular imprinting for target recognition to selectively bind the target molecule. The MIP component is typically grafted onto an electrodes surface[67a, 81] or incorporated as particles into the electrode itself[82a, 87]. Conductive polymer based electrodes have also been used in this manner by embedding MIP particles into the conductive polymer during electropolymerisation.

The first study to describe this technique was reported in 2005 by Ho et al. for the amperometric detection of morphine[128] as seen in Figure 1.11. Sensors for both nicotine[129] and (-)-ephedrine[130] have also been successfully prepared using similar formats. Detection limits as low as 10nM have been reported in addition to high specificity when compared to compounds with similar molecular structures[129].

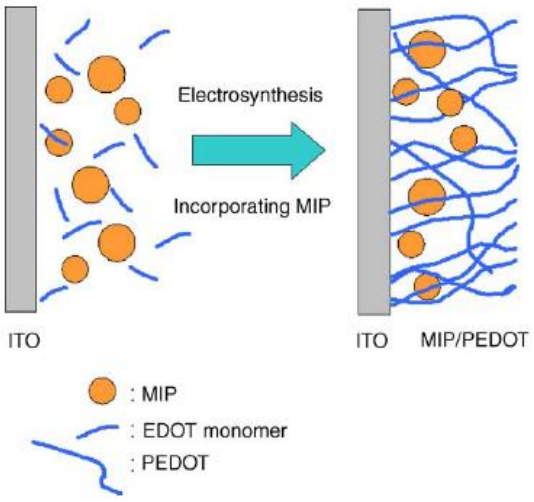

Figure 1.11 Preparation of a PEDOT electrode with embedded MIP particles. Reproduced from K.C. Ho et al.[128].

The use of conductive polymers also allows the electrode itself to be molecularly imprinted with the target molecule. By electrosynthesising a conductive polymer in the presence of the desired template, an imprinted conductive polymer can be produced which contains template specific cavities in much the same way as traditional MIP systems.

Several conductive polymers have been imprinted this way including polypyrroles[131], polyphenylenediamines[132], polyphenols[133], and polythiophenes[66a, 134] including PEDOT imprinted with a morphine template as seen in Figure 1.12[135]. Subsequent detection was achieved amperometrically by selective electrocatalysis of morphine oxidation. The detection limit for this system was calculated as 0.2mM and also showed high selectivity in comparison to structurally similar compounds[135].

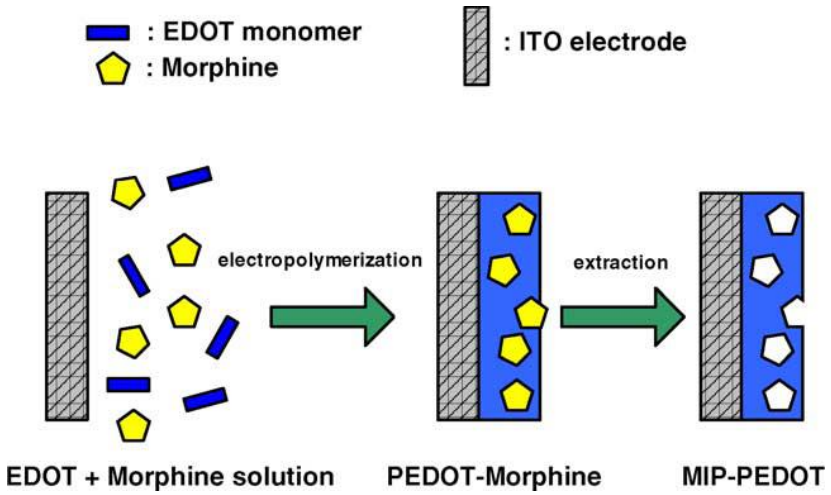

Figure 1.12 Preparation of an imprinted PEDOT electrode. Reproduced from W.M. Yeh et al.[135]

By using conductive polymers in MIPs, imprinting and signal transduction can be achieved simultaneously. Whilst this offers a significant advantage over traditional MIP formats for use in sensors there are some disadvantages such as binding site heterogeneity, slow diffusion kinetics resulting in high response times and the need for a trial-and-error approach to monomer selection and electropolymerisation conditions[130, 136].

1.5 Aims of the Study

In this study, signal transduction mechanisms for molecularly imprinted polymeric systems have been explored using *(-)-ephedrine* as the model template. This study has two parts:

Firstly, the capability of gold nanoparticles for signal transduction when incorporated in MIP systems has been examined. This involves the development a 2-dimensional phase-inversed MIP film format for the detection of (-)-ephedrine. The results for this study are discussed in Chapter 3.

Secondly, the potential of conductive polymers as a signal transducer for MIPs has been explored. Composite particles of conductive polymer PEDOT:PSS and (-)-ephedrine selective MIP have been developed. The results for this study are discussed in Chapter 4.

In all cases, interaction studies between monomers and analytes (template and competing analogues) have been conducted using semi-empirical molecular modelling and NMR spectroscopy.

CHAPTER 2 - EXPERIMENTAL

2.1 Reagents

Azobisisobutyronitrile (AIBN, 99.9%) was purchased from Dulux and recrystallised in acetone prior to use.

Acrylic Acid (AA, **1)**, acrylonitrile (AN, **2**) and methyl methacrylate (MMA, **3**), were purchased from Sigma-Aldrich Australia (≥ 98%) and were distilled under reduced pressure prior to use. N-isopropylacrylamide (IPA, 99.5%, **4**) was also purchased from Sigma-Aldrich Australia and recrystallised in hexane prior to use. N,N'-methylenebisacrylamide (MBA, 98%, **5**) was purchased from Sigma-Aldrich Australia and recrystallised in acetone prior to use.

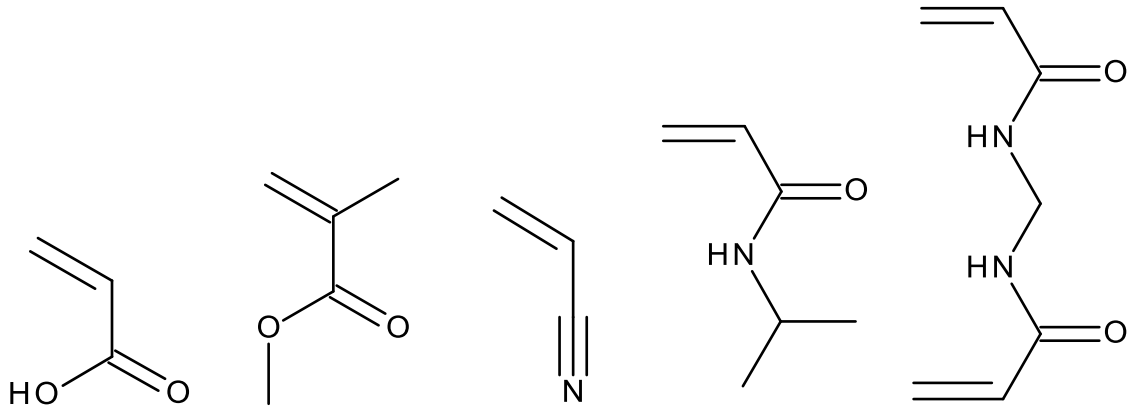

(1) **(2)** **(3)** **(4)** **(5)**

(*1R,2S*)-(-)-Ephedrine (EPD, **6**), (*1S,2R*)-(+)-ephedrine hydrochloride, (EPDHCl,**7**), (*1S,2S*)-(+)-pseudoephedrine (+PSEPD, **8**), (*1R,2R*)-(-)-pseudoephedrine (-PSEPD, **9**), (±)-adrenaline (or epinephrine) (ADR, **10**), caffeine (CAFF, **11**) and theophylline (THEO, **12**), were purchased from Sigma-Aldrich Australia (≥98%) and used as received.

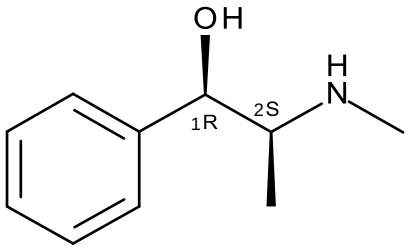

(6)

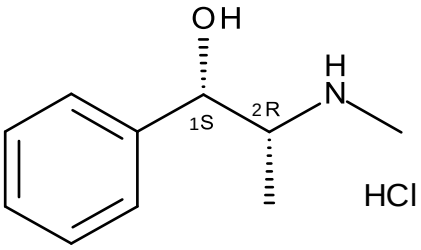

(7)

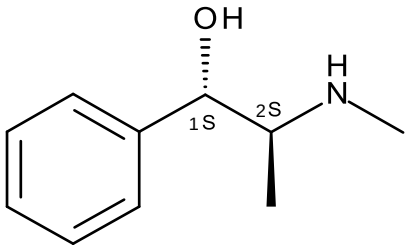

(8)

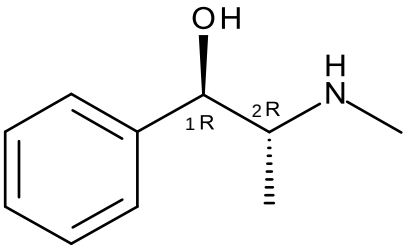

(9)

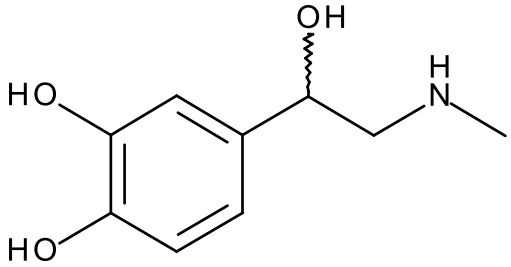

(10)

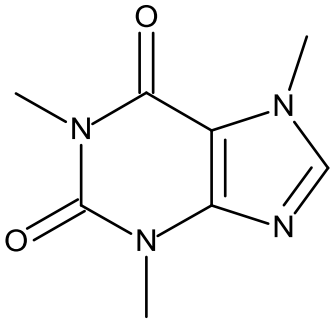

(11)

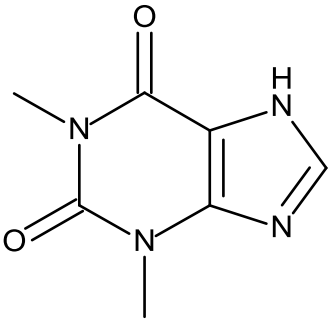

(12)

Allyl mercaptan (AM, Fluka, 99%, **13**) was distilled under reduced pressure prior to use. N-Decanethiol (NDT, **14**) and 11-mercaptoundecanoic Acid (MUA, **15**) were purchased from Sigma-Aldrich Australia (≥99%) and used as received.

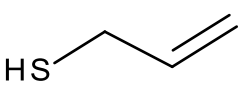

(13)

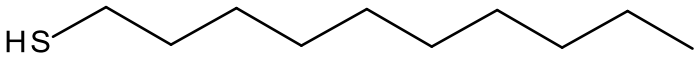

(14)

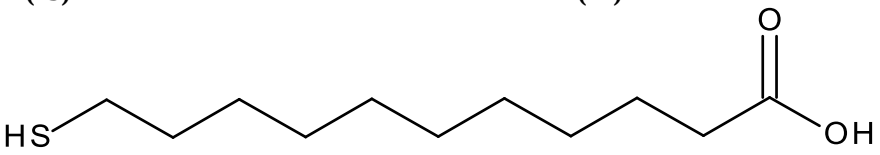

(15)

Methacryloyl chloride (**16)** was purchased from Sigma-Aldrich Australia (≥99%) and was distilled under reduced pressure prior to use. Pyrrole (99%,**17**), thiophene (99.5%,**18**) and poly(4-styrenesulfonic acid) (PSS, 99.5%, **19**)were purchased from Sigma-Aldrich Australia and used as received. 3-Thiophenemethanol (98%, **20**) and 3,4-ethylenedioxythiophene (EDOT, 99%, **21**) were purchased from International Laboratories and Bosche Scientific respectively and used as received.

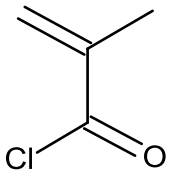

(16)

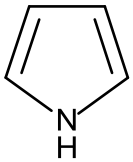

(17)

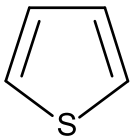

(18)

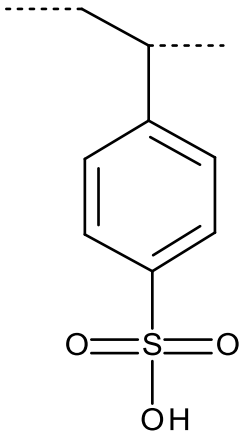

(19)

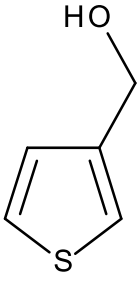

(20)

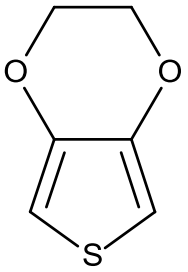

(21)

Lewattit ion exchange resins M-500 and SP-112 were purchased from Sigma-Aldrich and used as received.

AR grade solvents – methanol, ethanol and tetrahydrofuran were used as received.

HPLC grade solvents - acetonitrile and methanol - were purchased from Merck and used as received.

Glacial acetic acid (Sigma-Aldrich), ammonia gas (BOC Gases), ammonium chloride (Ajax), copper (I) chloride (Sigma-Adrich), 1,9-decadiene (Sigma-Aldrich), deuterium oxide (D_2O, Cambridge Isotope), dimethyl sulfoxide (DMSO, Fluka), dimethyl Sulfoxide-d_6 (Cambridge Isotope), hydrochloric acid (Sigma-Aldrich), hydrogen tetrachloroaurate (Sigma Aldrich), iron (III) sulphate (Sigma-Aldrich), potassium dihydrogen phosphate (KH_2PO_4,Fluka), potassium hydrogen phosphate (K_2HPO_4,Fluka), sodium borohydride (Sigma-Aldrich), sodium hydroxide (NaOH, Sigma-Aldrich), tetraoctylammonium bromide (TOAB, Sigma-Aldrich), thioacetic Acid (Merck) triethylamine (Sigma-Aldrich), and trisodium citrate (Ajax) were used as received.

A commercial 1.1% in water, pH neutral poly(3,4-ethylenedioxthhiophene)-poly(styrenesulfonate) (Sigma-Aldrich) solution was used as a reference conductive polymer solution.

2.2 Template Monomer Interaction Studies

2.2.1 Molecular Modelling

Spartan® '04 software was used to carry out molecular modelling studies. Geometric optimisation was performed on a semi-empirical level using AM1 force fields. Energies of interaction were calculated using Equation 1, based on the enthalpies of formation calculated by the software.

2.2.2 NMR experiments

A Bruker Ascend™ 400MHz Spectrometer was used to record ^{1}H spectra at 400.13 MHz. Titration experiments were performed by adding increasing molar equivalents of monomer to the template in a deuterated solvent (typically dimethyl sulfoxide). Spectra were obtained for monomer to template ratios up to 10:1.

2.3 Synthetic Methods: MIP-Gold Nanoparticulate Systems (Chapter 3)

2.3.1 Synthesis of 9-Decen-1-thiol (9D1T)

9-Decene-1-thiol was synthesised using a previously reported method[137]. An equimolar mixture of 1,9-decadiene (5mL; 27.125mmol) and thioacetic acid (1.939mL; 27.125mmol) was stirred and irradiated with ultraviolet light at 55°C for 1.5 hours. Distillation afforded 9-decenyl thioacetate. Dry ammonia was passed through a solution of the 9-decenyl thioacetate in ethanol (10mL) for 1.5 hours. The reaction mixture was then washed with a 10% aqueous ammonium chloride solution and extracted with hexane. The solvent was then removed to provide liquid 9-decene-1-thiol. Crude yield 41%. ^{1}H NMR (400MHz, CDCl3) δ 1.3 (13H, m), 2.0 (2H, m), 2.5 (2H, m), 5.0 (2H, d), 5.8 (1H, m).

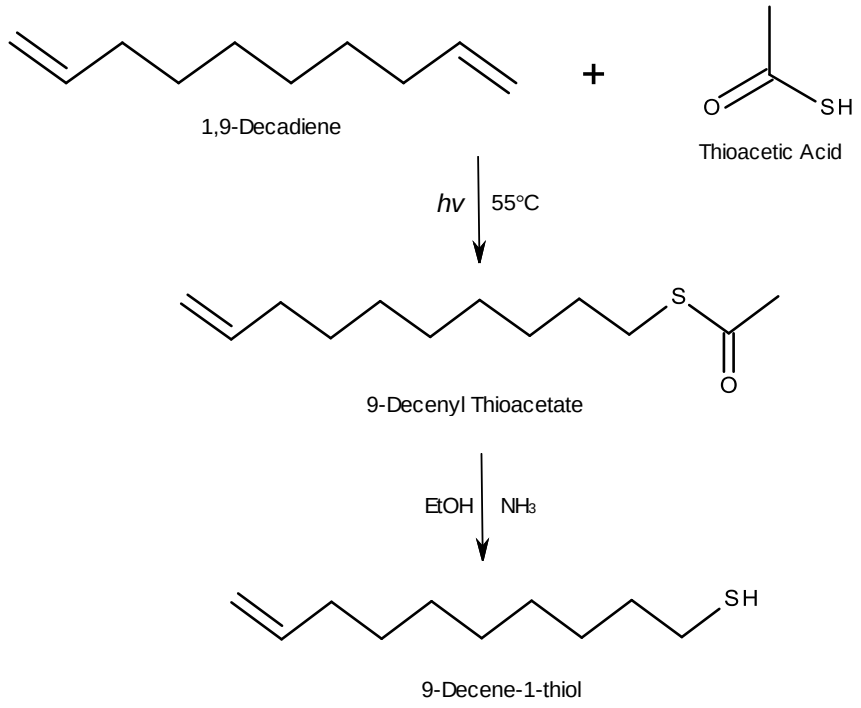

Figure 2.1 Reaction scheme for synthesised of 9-decene-1-thiol

2.3.2 Synthesis of Gold Nanoparticles

Gold nanoparticles were produced using a previously reported method[68, 102]. An aqueous solution of hydrogen tetrachloroaurate (15mM, 200mL) and TOAB (6.0mmol) in toluene (400mL) were mixed. Into the mixture was added a stabilising agent (3.0mmol) in toluene (100mL) gradually with vigorous stirring. Stabilising agents used were 11-mercaptoundecanoic acid (MUA), allyl mercaptan (AM), n-decanethiol or (NDT) 9-decene-1-thiol (9D1T). A freshly prepared aqueous solution of sodium borohydride (0.3M, 100mL) was then added dropwise. The mixture was stirred for 1 hour before the organic phase was separated and washed with distilled water. The solvent was removed using a rotary evaporator followed by high vacuum. The resulting black solid was then heat-treated using a pre-programmed Büchi® Syncore, starting at 150°C and increasing at 2°C.min^{-1} for 30 minutes to a final temperature of 210°C. The heat-treated product was then dissolved in 50mL of toluene and mixed with 400mL of chloroform to remove the TOAB and excess stabilising agent. The product was then filtered and dried under vacuum to give the gold nanoparticles.

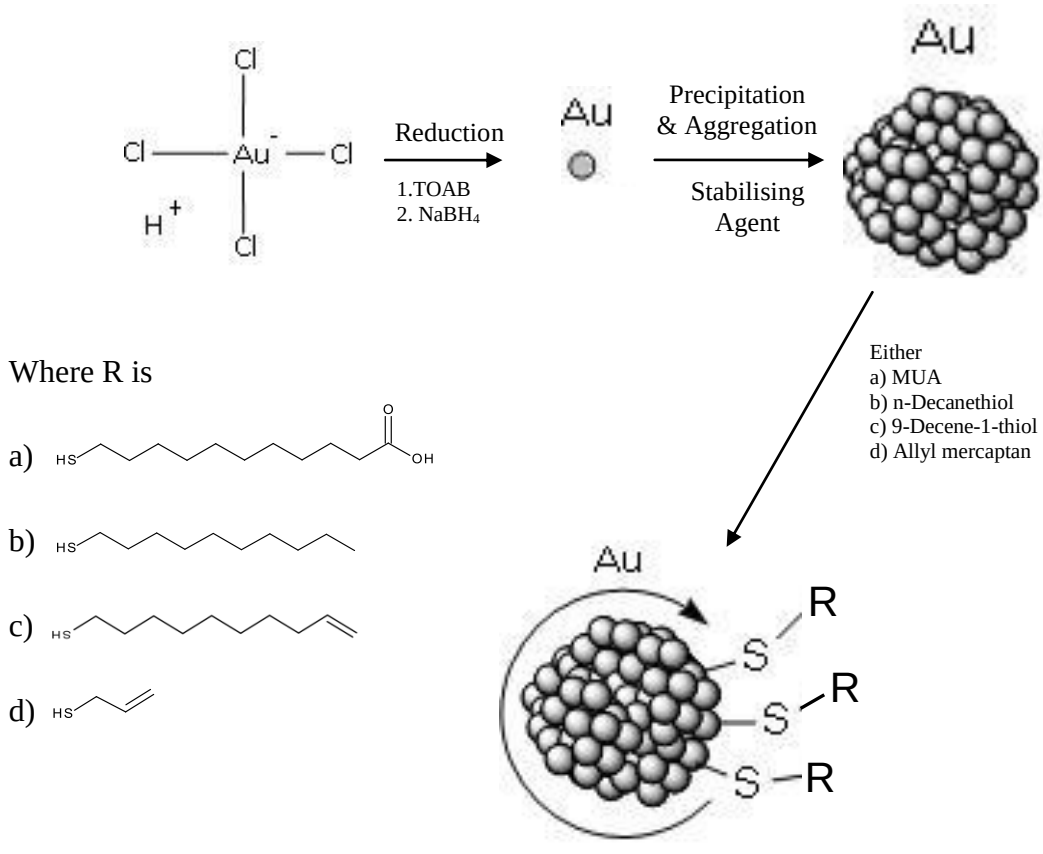

Figure 2.2. Reaction scheme for synthesised of Gold Nanoparticles

2.3.3 Synthesis of Poly(Acrylic Acid-co-N-Isopropylacrylamide-co-N,N'-Methylenebisacrylamide) MIPs – PAA-IPA-MBA

N-isopropylacrylamide (3.65mmol, 413mg), acrylic acid (0.90mmol, 61.8µL), and N,N'-methylenebisacrylamide (0.23mmol, 35.5mg) were added to 2.7mL of dimethyl sulfoxide together with azobisisobutyronitrile (10mg). Adrenaline (0.23mmol, 42.1mg) and (-)-ephedrine (0.23mmol, 38.0mg) were included for the MIP_{ADR} and MIP_{EPD} respectively. A non-imprinted control polymer, NIP, was also produced with no template included. The polymer mixture was purged with nitrogen and then heated at 60°C using a Büchi® Syncore for 24 hours. The resulting polymer was washed using methanol before being dried under vacuum.

2.3.4 Synthesis of Poly(Acrylic Acid-co-Acrylonitrile-co-Methyl Methacrylate) MIP films – PAA-AN-MMA

Polymer Synthesis: Acrylic acid (2.96mmol, 203.3µL), acrylonitrile (8.37mmol, 548.3µL), and methyl methacrylate (8.37mmol, 891.5µL) were added to 2.7mL of dimethyl sulfoxide together with azobisisobutyronitrile (20mg). The polymer mixture was purged with nitrogen and then heated at 60°C using a Büchi® Syncore for 24 hours. The resulting polymer was precipitated drop-wise into excess water (~400mL), before being filtered and dried under vacuum. The dried polymer was re-dissolved into 5mL of dimethyl sulfoxide and re-precipitated into excess methanol. The resulting purified polymer was dried under vacuum for ~4 hours. Molecular weight (M_n) was determined via gel permeation chromatography (GPC), to be 169kDa with polydispersity index (PDI) of 1.9[138].

Table 2.1 PAA-AN-MMA monomer feed ration and final polymer composition[139]

Polymer Code	AA	AN	MMA
Monomer Feed (mmol)	2.96mmol	8.37mmol	8.37mmol
Monomer Feed (%)	15%	42.5%	42.5%
Actual Polymer (%)	17%	41%	42%

Post-Polymerisation Imprinting: 75mg of dried poly(acrylic acid-*co*-acrylonitrile-*co*-methyl methacrylate) was dissolved in 1mL of dimethyl sulfoxide. For the imprinted polymer, (-)-ephedrine was added to the mixture based on the optimal 3:1 functional monomer to template ratio determined by molecular modelling and NMR studies.
Film Formation: A clean 1cm^2 glass slide was mounted on a Laurell® Spin Processor (Model WS-400E-6NPP-LITE). A drop of polymer solution was placed in the middle of the slide. The slide was then spun at 2000rpm for 10 seconds, then removed and placed in a coagulation bath containing tetrahydrofuran cooled to ~0°C for a minimum of 2 minutes. The resulting films were then removed from the slide by immersing in a water bath then laid flat on filter paper to dry.

2.3.5 Preparation of Gold Nanoparticle Embedded MIPs

PAA-IPA-MBA was prepared as described above with 230mg of synthesised gold nanoparticles included in the pre-polymerisation mixture.

PAA-AN-MMA was prepared as described above with 18, 36 or 72mg of synthesised gold nanoparticles included in the post-polymerisation solution prior to film formation.

2.4 Synthetic Methods: MIP-Conductive Polymer Composite Systems (Chapter 4)

2.4.1 Synthesis of 3-Methylthienyl Methacrylate

3-Methylthienylmethacrylate (MTMA) was synthesised using a previously reported method[140]. 3-Thiophenemethanol (50mmol, 5.7g), triethylamine (71mmol, 7.3g) and a small amount of copper (I) chloride were mixed in 35mL of dry diethyl ether. Methacryloyl chloride (51mmol, 5.35g) in 35mL of dry diethyl ether was slowly added at 0°C. The mixture was then stirred for 2 hours. The mixture was then filtered through a silica gel column to remove the triethylammonium chloride. This was followed by solvent evaporation using a rotary evaporator. The remaining mixture was then stirred overnight in a 1:1 mixture of dichloromethane and 2M sodium hydroxide aqueous solution. The organic layer was separated, washed with water and dried over calcium chloride. The solvent was removed through rotary evaporation and the residue was distilled under vacuum (1mmHg, 90°C). Yield: 64%. ^{1}H NMR (400MHz, CDCl3) δ 2.0 (3H, s), 5.2 (2H, s), 5.6 (1H, s), 6.2 (1H, s), 7.1 (1H, m), 7.3 (2H, m).

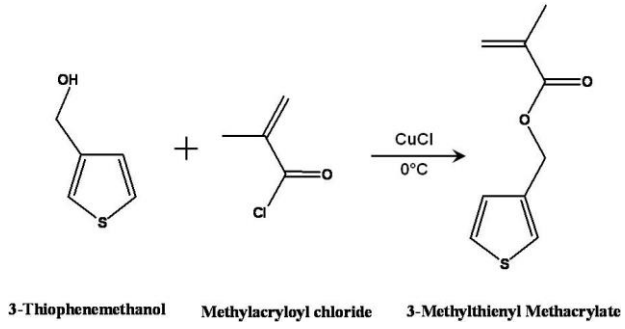

Figure 2.3 Reaction scheme for synthesis of 3-methylthienyl methacrylate

2.4.2 Synthesis of Poly(Acrylic Acid-co-Acrylonitrile-co-Methyl Methacrylate-co3-Methylthienyl Methacrylate) MIP films

Polymer Synthesis: Acrylic acid (2.96mmol, 203.3μL), Acrylonitrile (8.37mmol, 548.3μL) and Methyl Methacrylate (8.37mmol, 891.5μL) and were added to 2.7mL of dimethyl sulfoxide. The polymer mixture was purged with nitrogen and then heated at

60°C using a Büchi® Syncore for 24 hours. The resulting polymer was precipitated dropwise into excess water (~400mL), before being dried under vacuum. The resulting polymer was re-dissolved in approximately 5mL of dimethyl sulfoxide and re-precipitated into excess methanol. The resulting purified polymer was dried under vacuum for ~4 hours.

Additional copolymers were prepared by incorporating increasing amounts of 3-methylthienyl methacrylate into the feed ratio, while maintaining the ratio of the remaining co-monomers. The reaction ratios for these polymers are shown in Table 3.2.

Table 2.2 Reaction ratios of synthesised of MTMA-AA-AN-MMA copolymers

% 3-Methylthienyl Methacrylate	% Acrylic Acid	% Acrylonitrile	% Methyl Methacrylate
0	15	42.5	42.5
5	14.25	40.375	40.375
15	12.75	36.125	36.125
25	11.25	31.875	31.875
50	7.5	21.25	21.25

Post-Polymerisation Imprinting: 75mg of dried poly(acrylic acid-*co*-acrylonitrile-*co*-methyl methacrylate-*co*-3-methylthienyl methacrylate) was dissolved in 1mL of dimethyl sulfoxide. For the imprinted polymer, (-)-ephedrine was added to the mixture based on the optimal 3:1 ratio determined by molecular modelling and NMR studies.

Film Formation: A clean 1cm^2 glass slide was mounted on a Laurell® Spin Processor (Model WS-400E-6NPP-LITE). A drop of polymer solution was placed in the middle of the slide. The slide was then spun at 2000rpm for 10 seconds. The slide was then placed in a coagulation bath containing tetrahydrofuran cooled to ~0°C for at least 2 minutes. The resulting films were removed from the slide by immersing in a water bath then laid flat on filter paper to dry.

2.4.3 Synthesis of Conductive Polymers

PEDOT:PSS (Poly(3,4-ethylenedioxthiophene):Poly(styrenesulfonic acid)) was prepared using a previously reported method[113], by mixing 3,4-ethylenedioxythiophene (75mmol, 10.65g), Poly(4-styrenesulfonic acid) (26.30g) and sodium persulfate (104mmol, 21.4g) in 2475mL of water. The mixture was stirred for 10 minutes before adding iron (III) sulphate (0.47mmol, 187mg), then stirred vigorously for 24 hours. The resulting PEDOT:PSS mixture was then purified using acidic and basic ion exchange resins (Lewatitt M-500 and SP112 respectively).

Additional conductive polymers were produced as above by replacing some or all of the 3,4-ethylyenedioxythiophene with equimolar amounts of 3-methylthienyl methacrylate. Polymers were synthesised using this method are summarised in Table 3.3 below.

Table 2.3 Reaction ratios for synthesised of conductive polymers

Polymer	**EDOT**			**MTMA**			**PSS**
Code	**%**	Moles ($x10^{-3}$)	Mass (g)	%	Moles ($x10^{-3}$)	Mass (g)	Mass (g)
PEDOT:PSS	**100**	75	10.65	**0**	-	-	26.30
PEMS25	**75**	56.25	7.99	**25**	18.75	3.42	26.30
PEMS50	**50**	37.5	5.33	**50**	37.5	6.83	26.30
PMTMA:PSS	**0**	-	-	**0**	75	13.67	26.30

2.4.4 Preparation of Conductive Polymer Films

Solvent was removed from conductive polymer solutions prepared above by rotary evaporation. The resulting viscous solutions were dropped onto glass slides and then spun-cast at 1500rpm for 10 seconds using a Laurell® WS-400-6NPP-LITE spin coater. The resulting films were then annealed at 110°C. Additional films were also prepared via solvent evaporation using a vacuum oven following spin casting.

2.4.5 Synthesis of (-)-Ephedrine Imprinted Conductive Polymer Composite Particles

Imprinted particles were prepared using acrylic acid as a functional monomer. Polymerisation involved addition of up to 10mmol of acrylic acid to 6mL of as synthesised conductive polymer solution with 12.5mg of sodium persulfate as an initiator as listed in Table 2.4. (-)-ephedrine was added based on the feed ratio of acrylic acid, in the optimal 3:1 monomer-template ratio based on molecular modelling and NMR results. A non-imprinted polymer solution was also prepared with the absence of (-)-ephedrine. The polymerisation mixture was purged with nitrogen and then polymerised at 60°C for 24 hours in a Büchi® Syncore.

Table 2.4 Reaction ratios for synthesised of composite particles using an acrylic acid functional monomer

Polymer Code	Conductive Polymer	AA (mmol)	EPD (mmol)
PMTMA:PSS-AA1	PMTMA (97.2mg in 6mL H_2O)	1	0.33
PEMS25-AA1	PEMS25 (91.2mg in 6mL H_2O)	1	0.33
PEMS50-AA0.5	PEMS50 (93.0mg in 6mL H_2O)	0.5	0.17
PEMS50-AA1	PEMS50 (93.0mg in 6mL H_2O)	1	0.33
PEMS50-AA2.5	PEMS50 (93.0mg in 6mL H_2O)	2.5	0.83
PEMS50-AA10	PEMS50 (93.0mg in 6mL H_2O)	10	3.33

The resulting particles was then filtered through a 20μm polyethylene filter and rinsed with water before being dried under vacuum.

Additional particles were prepared which included N,N'-methylenebisacrylamide as a cross-linker, in addition to the acrylic acid functional monomer. These polymers are listed in Table 2.5.

Table 2.5 Reaction ratios for synthesised of composite particles using an acrylic acid functional monomer and a N,N'-methylenebisacrylamide crosslinker

Polymer Code	Conductive Polymer	AA (mmol)	MBA (mmol)	EPD (mmol)
PEMS50-MBA0.2	PEMS50 (93.0mg in 6mL H_2O)	0.8	0.2	0.27
PEMS50- MBA0.35	PEMS50 (93.0mg in 6mL H_2O)	0.65	0.35	0.22
PEMS50-MBA0.5	PEMS50 (93.0mg in 6mL H_2O)	0.5	0.5	0.17
PEMS50- MBA0.65	PEMS50 (93.0mg in 6mL H_2O)	0.35	0.65	0.12
PEMS50- MBA0.8	PEMS50 (93.0mg in 6mL H_2O)	0.2	0.8	0.07

2.4.6 Embedding Composite Particles in Conductive Matrix

50-500mg of composite particles were added to 1mL of PEDOT:PSS before being sonicated for 30 minutes. The resulting solution was dropped onto glass slides and then spun-cast at 1500rpm for 10 seconds using a Laurell® WS-400-6NPP-LITE spin coater. The resulting films were then annealed at 110°C.

2.5 Swelling Measurements

The swelling capacity of the MIP and NIP films were measured by weighing a number of films and then soaking them in water for various time periods (10min to 25h). The wet films had excess water removed from them by touch drying with filter paper before being re-weighed. The differences in weights were calculated using Equation 4[141] and recorded as a percentage change for each group of films.

$$\%\text{Swelling} = [(W_{final} - W_{initial}) / W_{initial}] \times 100 \qquad \textbf{(Equation 4)}$$

2.6 Template Extraction

Template extraction for each template in all polymer systems was performed by stirring of the polymer in a 1:99 (volume ratio) solution of acetic acid and water. This was repeated at least three times with fresh extraction solution to ensure template removal. The polymers were then rinsed in water to remove any residual acetic acid. Polymeric films were then laid flat on filter paper to dry, and polymeric particles were filtered through a 20μm polyethylene frit then dried under vacuum dried under vacuum. Successful extraction was confirmed using FTIR for (-)-ephedrine and HPLC analysis for adrenaline.

2.7 Rebinding Studies

Fresh 1.0mM aqueous stock solutions of the relevant template or cross-reactivity analyte were prepared as needed. Polymers were weighed and then 1mL aliquots of stock solution were added to each polymer sample. Poly(acrylic acid-*co*-N-isopropylacrylamide-*co*-N,N'-methylenebisacrylamide) films were allowed to rebind for 24 hours using both MIPs and NIPs, while all remaining polymer systems were allowed to rebind for various times (10min to 24h). Following rebinding, the polymeric films/particles were separated from the rebinding solution and the bound template concentration assessed quantitatively using HPLC.

Binding (B) was calculated according to Equation 2 and standardised to polymer mass. Imprinting factors (I) were then calculated according to Equation 3.

$$B = [\text{Template}]_{\text{initial}} - [\text{Template}]_{\text{final}} \qquad \textbf{(Equation 2)}$$

$$I = B_{MIP} / B_{NIP} \qquad \textbf{(Equation 3)}$$

2.8 Instrumental

2.8.1 NMR Analysis

A Bruker Ascend™ 400MHz Spectrometer was used to record ^{1}H and ^{13}C spectra at 400.13 and 100.47MHz, respectively. Inverse-gated ^{13}C NMR experiments were also performed at 100.47MHz respectively when determining polymer compositions.

2.8.2 FT-IR Analysis

Qualitative FT-IR spectroscopic studies were used to assess the success of imprinting and extraction of the (-)-ephedrine template from the polymers. A Shimadzu® FTIR-8400S spectrophotometer (16 scans, at 0.8cm^{-1} resolution, from 400 to 4000nm) was used for the analysis. Polymer films were analysed by placing them in the path of the beam. All other samples were analysed using a Pike® EasiDiff accessory after solvent evaporation where necessary and subsequent mixing/grinding with potassium bromide. The aromatic C-H out of plane bending at ~700cm^{-1} was used as the diagnostic peak for (-)-ephedrine.

2.8.3 HPLC Analysis

Template (Adrenaline and (-)-ephedrine) and cross-reactivity analyte ((-)-pseudoephedrine, (+)-pseudoephedrine, (+)-ephedrine hydrochloride, caffeine, and theophylline) rebinding was determined using a Shimadzu® High Performance Liquid Chromatograph (LC-20AD) fitted with a Grace® Econsphere™ C18, 5µm column. The mobile phase consisted of 75% aqueous buffer solution (50mM KH_2PO_4 adjusted to a pH of 3.5 with H_3PO_4) and 25% 7:3 acetonitrile:water (with 10mM triethylamine). A 10µL injection volume was used with a run time of 10 minutes at a flow rate of 1.0mL/min. Template concentration was monitored using a UV/Vis Photodiode Array Detector at a wavelength of 190nm. Quantification was conducted using an external calibration method with a curve over a concentration range from 0.1-1.5mM.

2.8.4 GPC Analysis

Polymer molecular weights were determined using a Shimadzu® High Performance Liquid Chromatograph (LC-20AD) fitted with two Waters Styragel® columns (HT 5 THF and HT 3 THF). Calibration was performed using a series of Shodex® standards with molecular weights ranging from 3950 to 3250000. 1-2mg of sample or standard was dissolved in1mL of HPLC grade THF and shaken for 12 hours. A 10μL injection volume was used with a run time of 15 minutes, with an oven set to 40°C and a flow rate of 0.7mL/min. Template concentration was monitored using a UV/Vis Photodiode Array Detector at a wavelength of 270nm.

2.8.5 UV-Vis Analysis

Gold nanoparticles and imprinted polymers containing gold nanoparticles were analysed as colloidal dispersions in water or toluene (quartz cuvette) using a Cary® UV-Vis spectrophotometer from 300-700nm. Polymers were analysed by holding the film in position inside the cuvette.

2.8.6 Particle Sizing

The sizes of gold nanoparticles were determined using a Malvern Zetasizer – Nano ZS. Nanoparticles were dispersed in toluene in a quartz cuvette prior to analysis.

2.8.7 Surface Morphology Studies - Scanning Electron Microscope

Scanning electron microscope (SEM) images were generated using a Philips XL30 SEM and Oxford ISIS EDS (1997) Software.

2.8.8 Conductivity Measurements

Conductivity measurements were conducted using a four-point probe apparatus as seen in Figure 3.8, supplied by SES Instruments Pvt. Ltd., India. Film thickness was determined using an Alpha-Step 500 Profilometer supplied by KLA Tencor, USA. Volume resistivity was calculated using Equation 5and converted to conductivity.

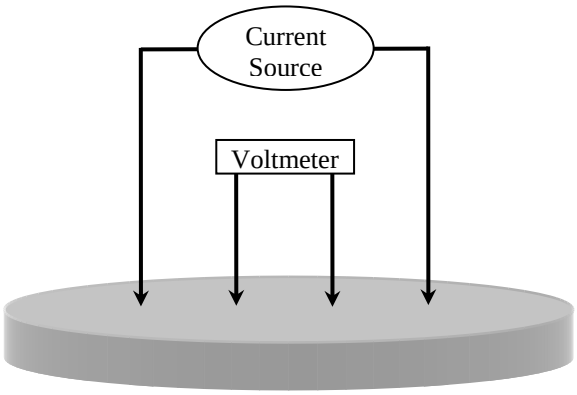

Figure 2.4 4-point probe apparatus

$$\rho = \frac{\pi}{ln2} \times \frac{V}{I} \times t \times k \qquad \textbf{(Equation 5)}$$

Where ρ = volume resistance (Ω.cm)
V = measure voltage (volts)
I = applied current (amperes)
t = sample thickness (cm)
k = correction factor based on the ratio of the probe spacing to the films diameter and thickness

CHAPTER 3- GOLD NANOPARTICLES AND MOLECULARLY IMPRINTED POLYMERS

In this chapter the use of gold nanoparticles as a signal transduction mechanism in molecularly imprinted polymers will be investigated. Previous work by Matsui et al. [68] suggests that gold nanoparticles may be used in conjunction with molecularly imprinted polymers to produce a detectable shift in the UV-Visible spectrum of the nanoparticles upon binding of the desired template molecule.

Several polymer and template system were investigated, beginning with molecular modelling and NMR studies to model and examine the interactions between the polymer and template. Molecular modelling was used as a predicative tool to assess possible interactions of the templates with a range of monomers and crosslinkers. NMR titrations were then performed to further investigate the possible template monomer interactions identified through molecular modelling. This combination of molecular modelling and NMR as predictive tools for MIP design is more time and cost efficient than traditional trial and error MIP production. Examples of templates imprinted using this combinatorial approach include creatine[142], cocaine[37], caffeine[143], ibuprofen[44], theophylline[45], acetochlor[46] and N-boc-L-phenylalanine[47].

Polymers were then synthesised based on this predictive MIP design approach. The binding performances of these polymers were then assessed including cross-reactivity studies to assess selectivity and specificity. Additional characterisations were also performed including spectroscopic analysis and surface morphology studies.

Finally gold nanoparticles were synthesised and characterised before being incorporated into these polymer systems to assess their utility as a signal transduction mechanism.

3.1 Model System – Poly(Acrylic Acid-*co*-N-Isopropylacrylamide-*co*-Methylenebisacrylamide) – Adrenaline Template

Previous work by Matsui et al. demonstrated that the poly(acrylic acid-*co*-N-isopropylacrylamide-*co*-methylenebisacrylamide) (PAA-IPA-MBA) polymer system could be successfully imprinted with an adrenaline (ADR) template with high levels of both selectivity and specificity. In addition, gold nanoparticles embedded into this system were shown to produce a detectable shift in the plasmon absorbance band following rebinding[68].

This polymer system was therefore initially chosen as the model system for this work and the ADR imprinted PAA-IPA-MBA polymer used by Matsui et al. was attempted to be reproduced for comparative purposes. Additional investigation of this polymer system, including template-monomer interaction studies, was also performed.

3.1.1 Adrenaline - Functional Monomer Molecular Modelling

Functional monomers are the primary source of interaction with the template and it is this interaction which is the source of the selectivity in the resulting polymer. For this polymer system, acrylic acid (AA) was used as the functional monomer. Molecular modelling results for acrylic acid with ADR are shown in Figure 3.1. It can be seen that the interaction energies (ΔE) for AA - ADR clusters for ratios up to 10:1 are all negative, indicating energetically favourable interactions.

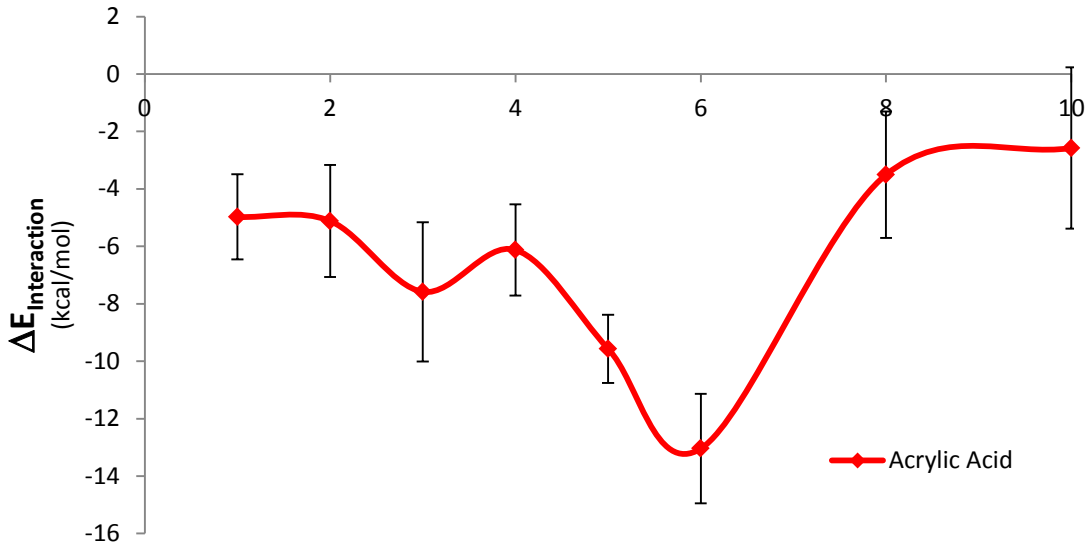

Figure 3.1 $\Delta E_{Interaction}$ of ADR with AA across a range of M-T ratios.

An AA to ADR ratio of 1:1 has an $\Delta E_{Interaction}$ of -5.0 kcal/mol indicating a favourable interaction. The modelling indicates hydrogen bonding (≤2.8Å) between the carboxylic acid moiety of the AA and secondary amine and three hydroxyl moieties of the ADR. For the 1:1 ratio, a single point interaction is observed, which would limit the specificity of the resulting MIP cavity as only one area of complimentary functionality would be present.

An AA to ADR ratio of 2:1 has an $\Delta E_{Interaction}$ of -5.1 kcal/mol, indicating a favourable interaction similar to the 1:1 ratio. This ratio however shows two areas of interaction which would improve the specificity of the MIP as there are multiple points of complimentary functionality.

The ratios of 3:1 and 4:1 both produce high $\Delta E_{Interaction}$, -7.5 and -6.1 kcal/mol, respectively, with multiple points of interaction between the monomers and the template. The 3:1 ratio, which shows the highest energy of interaction, is shown in Figure 3.2.

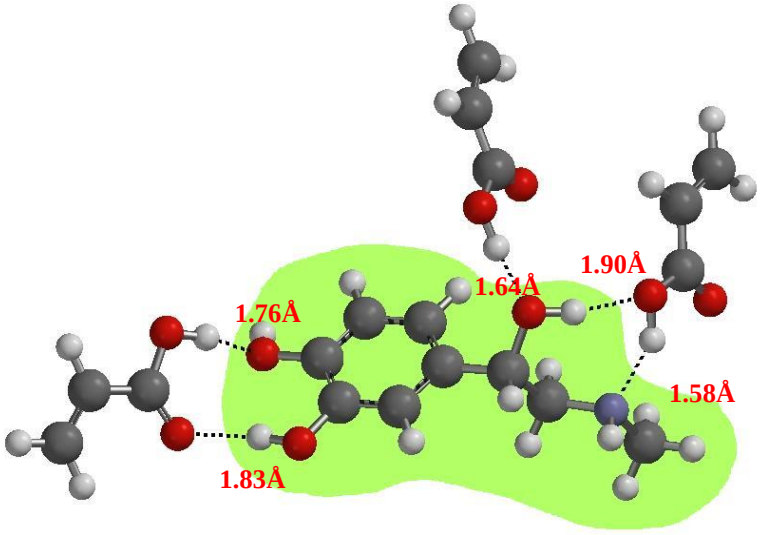

Figure 3.2 Molecular modelling of ADR with 3 AA showing multiple points of interaction. Template is shaded green and hydrogen bond distances are indicated in red.

AA to ADR ratios of 5:1 and 6:1 show the highest $\Delta E_{Interaction}$, -9.6 and -13.0 kcal/mol respectively, however, at this template to monomer ratio and above, monomer-monomer interactions become increasingly prevalent. These interactions cause the overall cluster energy to increase without an increase in template monomer interactions. Such circumstances are likely to result in the product MIP exhibiting greater levels of non-specific binding due to the presence of excess functional monomer.

As seen in Figure 3.2, the dominant interactions between the AA and ADR is hydrogen bonding between the acidic carboxyl group of the AA and the secondary amine, aliphatic hydroxyl and phenolic groups of the ADR. The modelling is performed *in silico* and suggests likely sites of interaction between the monomer and template. The limitations of the software prevent the modelling of the protonation of the secondary amine of the ADR template (pK_{a1} 8.26) by the acidic AA functional monomer (pK_a 4.26). This would lead to a stronger acid-base interaction which is not shown by the modelling. The site of this acid-base interaction is however still indicated in the modelling although as a weaker hydrogen bonding interaction.

The selection of an optimal functional monomer - template stoichiometry involves the selection of a system a high negative $\Delta E_{Interaction}$ and multipoint binding interactions. High $\Delta E_{Interaction}$ improve the selectivity of the resulting MIP whilst multiple points of

interaction improve the specificity[144]. Clusters exhibiting significant monomer-monomer self-association should be avoided to limit non-selective binding. For AA, a ratio of between 3 or 4 to 1 appears to be the most suitable imprinting ratio.

3.1.2 Adrenaline – Matrix Monomer/Crosslinker Molecular Modelling

N-isopropylacrylamide (IPA) and the cross-linker N,N'-methylenebisacrylamide (MBA) were also used in this polymer system and make up the bulk of the polymer structure. They provide the structural integrity and support for the polymer structure but ideally should have little interaction with the template molecule. The molecular modelling results for the matrix monomer N-isopropylacrylamide (IPA) and the cross-linker N,N'-methylenebisacrylamide (MBA) are compared with those for AA in Figure 3.3.

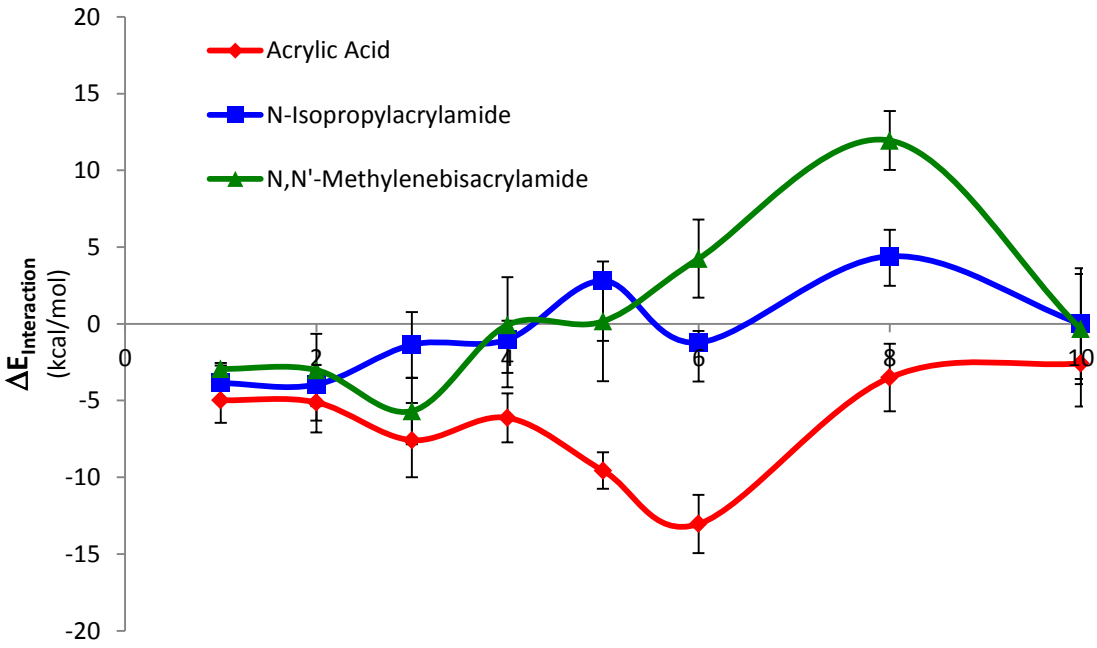

Figure 3.3 $\Delta E_{interaction}$ of ADR with AA, IPA and MBA across a range of M-T ratios.

From Figure 3.3 it can be seen that the $\Delta E_{Interaction}$ for IPA with ADR are negative for M-T ratios up 4:1, signifying a favourable interaction. These energies are significantly reduced, in absolute terms than that those produced by AA, indicating that AA interacts more strongly than IPA.

Molecular modelling indicates hydrogen bonding between the secondary amine and three hydroxyl groups of the ADR and both heteroatoms of the IPA amide unit. The 2:1 stoichiometry, which produced the greatest $\Delta E_{Interaction,}$ is shown in Figure 3.4.

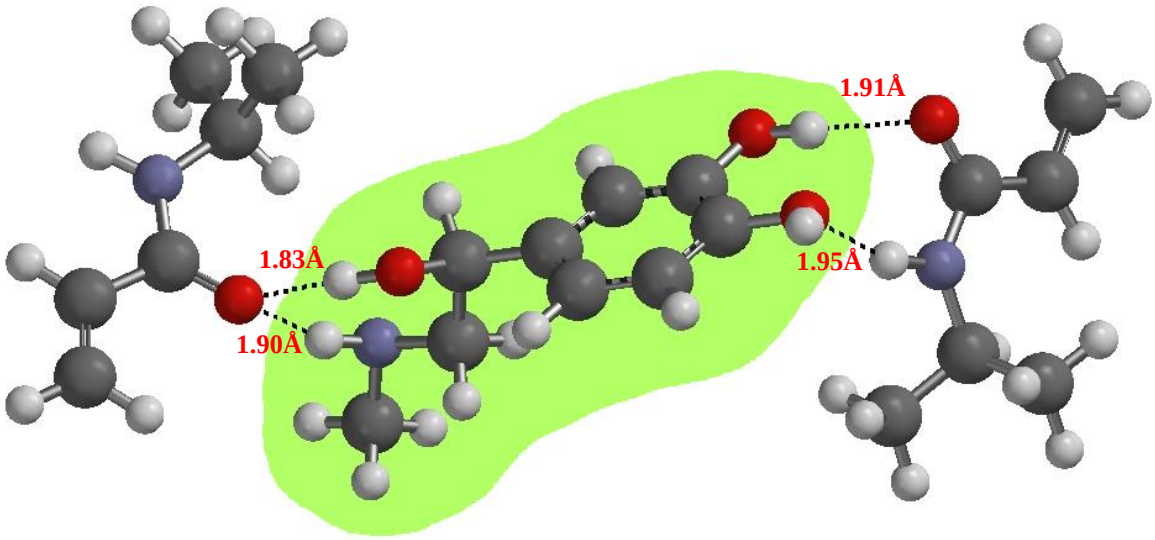

Figure 3.4 Molecular modelling of ADR with 2 IPA units showing two areas of interaction. Template is shaded green and hydrogen bond distances are indicated in red.

At ratios above 4:1, modelling indicates that the resultant clusters do not interact favourably with the template due to the dominance of monomer-monomer self-association. This is particularly evident in stoichiometries ranging between 6:1 and 10:1 which show positive or zero interaction energies.

The hydrogen bonds length for ADR with IPA, as seen in Figure 3.4, are longer than those for the corresponding hydrogen bonds for ADR with AA as seen in Figure 3.2. This suggests that the hydrogen bonds formed by IPA will not be as strong as those formed by the AA functional monomer. Additionally, the bifurcated nature of the hydrogen bonds seen at the left of Figure 3.4 results in a weaker interaction than a single hydrogen bond[145].

From Figure 3.3 it can be seen that the $\Delta E_{Interaction}$ for MBA with ADR are negative below a 3:1 ratio signifying a favourable interaction. The magnitude of the MBA interaction energies is however comparably lower than that those produced by AA, indicating that AA is a more favourable functional monomer.

Molecular modelling indicates hydrogen bonding between the ADR functional groups (secondary amine and three hydroxyl groups) and the MBA amide units. The 3:1 ratio that produced the highest energy of interaction is also shown below in Figure 3.5. At ratios of 4:1 and above modelling indicates that the additional monomer units do not interact with the template.

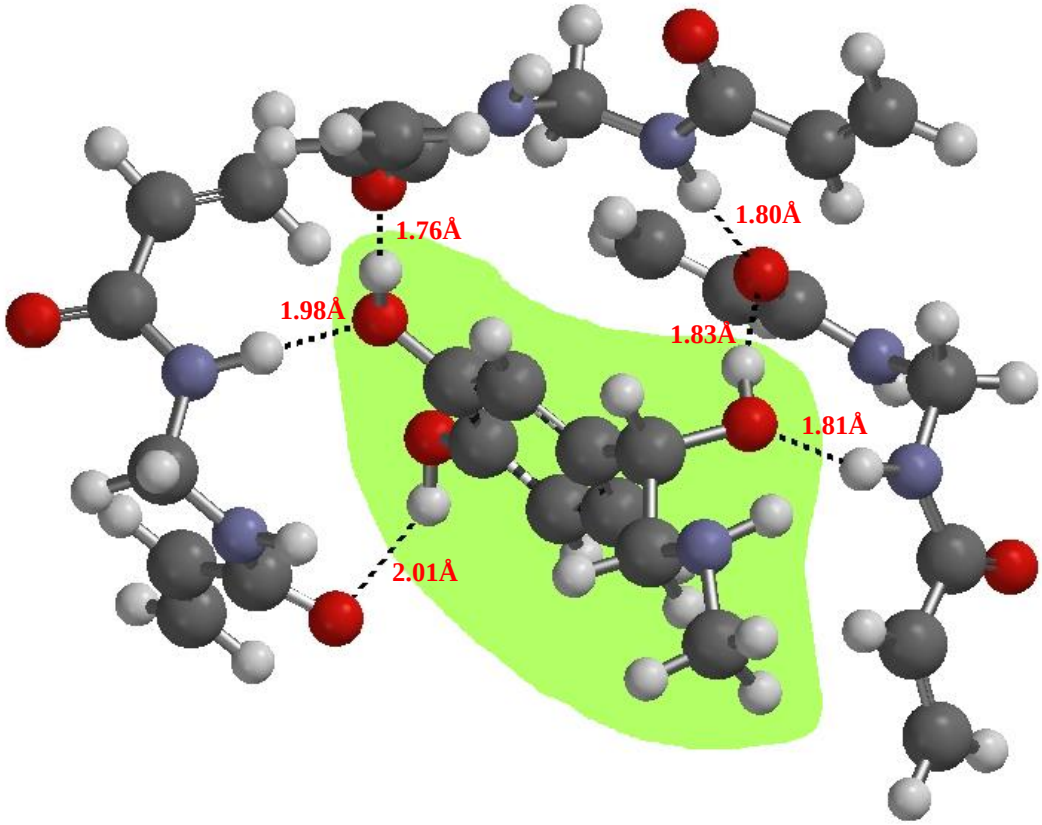

Figure 3.5 Molecular modelling of ADR with 3 MBA showing multiple points of interaction. Template is shaded green and hydrogen bond distances are indicated in red.

The hydrogen bonds distances for the ADR with MBA 3:1 cluster, are on average longer than those observed in the ADR – AA cluster, indicating reduced hydrogen bond strength. The system however exhibits multiple points of interaction suggesting that a cavity exhibiting high selectivity may result.

The molecular modelling results indicate that MBA while producing multipoint interactions with ADR generates lower interaction energies than those observed for the AA functional monomer.

3.1.3 NMR Studies

NMR titration of the AA functional monomer was performed to confirm the presence of the interactions identified using molecular modelling. Since the chemical shift (δ) of a nucleus in NMR spectroscopy is sensitive to changes in the surrounding magnetic environment, interactions such as hydrogen bonding can be observed as a function of changing concentration of the hydrogen bonding agent. Figure 3.6 shows the spectra of ADR with increasing molar equivalents of AA.

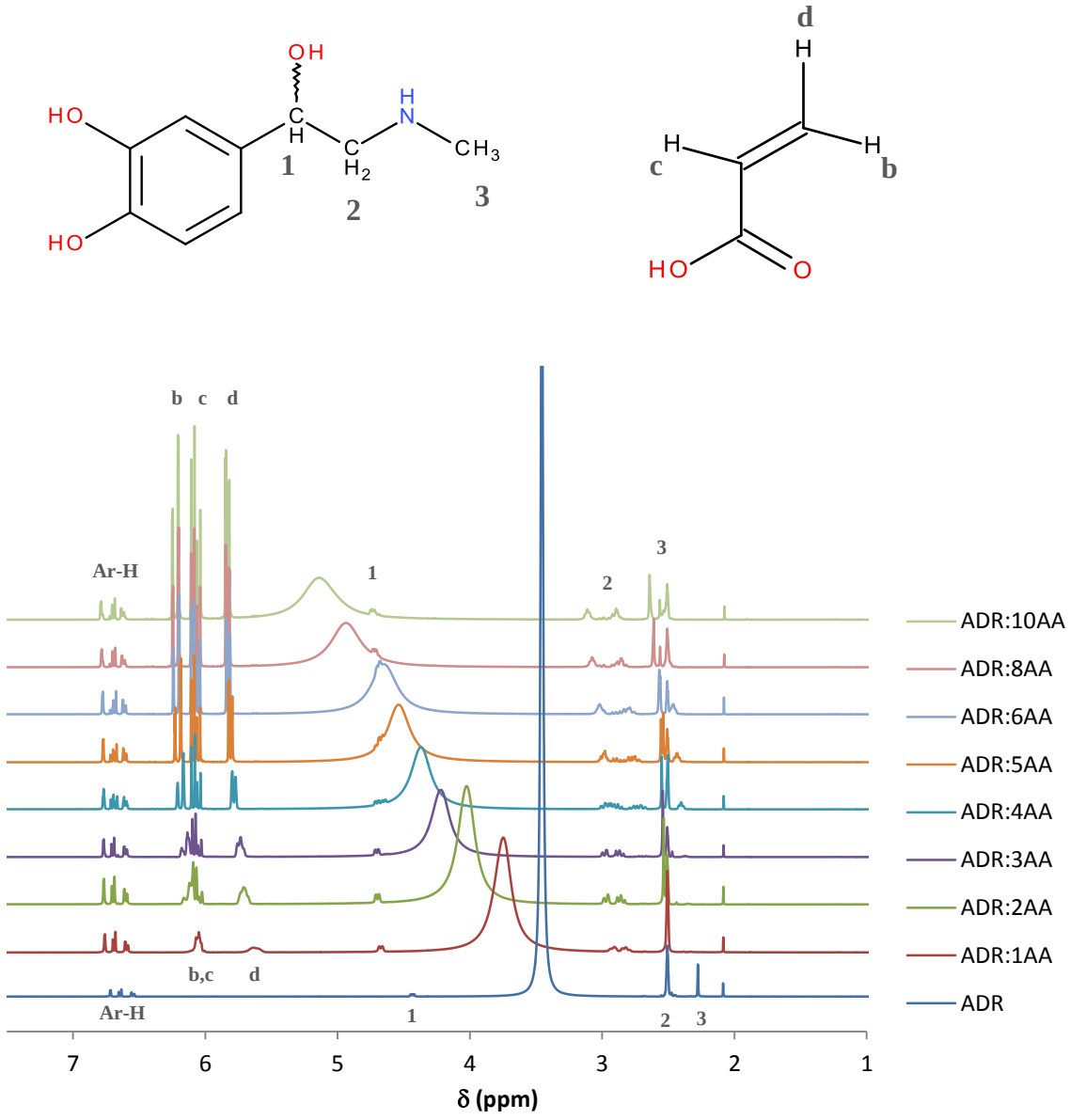

Figure 3.6 ^{1}H-NMR spectra of pure ADR and various M-T ratios (as indicated on the right) in d_6-DMSO. Structures of ADR and AA are shown above, along with corresponding proton labelling.

In the presence of AA, proton peaks associated with ADR (**1**, **2** and **3**) were seen to move downfield indicating that these nuclei were experiencing a deshielding effect. This is a result of protonation of the secondary amine in the ADR and is indicated by the large changes in chemical shifts and peak splitting observed in proton 2 of ADR. This suggests that a strong acid-base interaction will occur between the AA and ADR at this point. Figure 3.7 shows the extent of the downfield shifts as a function of the template-monomer ratio.

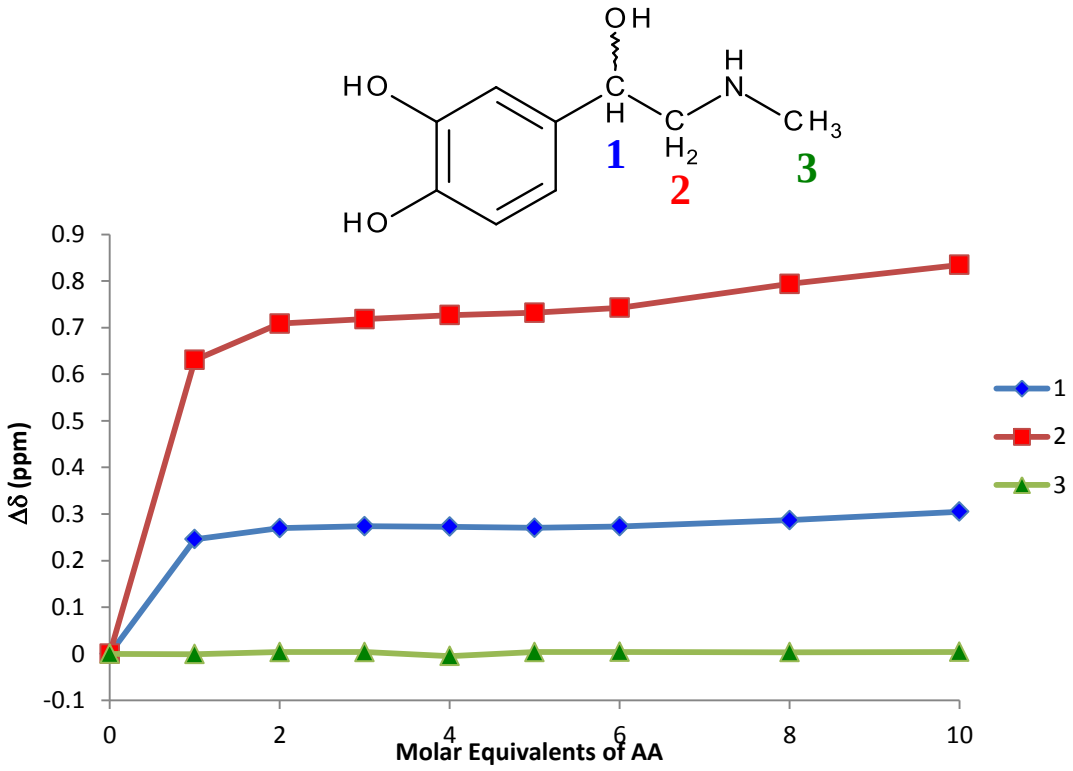

Figure 3.7 Change in chemical shift (Δδ) of different ADR protons upon titration with increasing molar equivalents of AA in d_6-DMSO. ADR structure is included above to show labelling of protons.

Figure 3.7 demonstrates that ADR protons 1 and 2 displayed the greatest shift during the titration. This is consistent with an acid-base interaction which would deshield the sites adjacent to the ADR heteroatoms in the aliphatic carbon chain. This was not observed during molecular modelling due to limitations of the modelling software in analysing this type of interaction. The modelling shown in Figure 3.2 did however suggest this secondary amine as a likely point of interaction through weaker hydrogen bonding.

The change in shift observed in Proton 1 reaches a maximum after the addition of just 1 molar equivalent of AA, indicating that the dominant changes in δ are due to formation of the 1:1 ADR-AA complex. Figure 3.7, however also shows that further AA additions can promote additional interactions, as the curve associated with Proton 2 taking slightly longer to plateau (> 2:1). , although most of the change in δ is observed following a single molar equivalent of AA. This suggests that while the acid base interaction between the AA and the secondary amine of ADR is the primary source of interaction, additional weaker interactions such as those seen in the molecular modelling in Figure 3.2, may be possible.

The NMR titration also showed significant changes in the chemical shifts of the AA protons (**b**, **c** and **d**, Figure 3.8). Chemical shift associated with increasing AA concentration in solution in the absence of ADR was undertaken to assess the significance of monomer-monomer interactions. The presence of ADR causes an upfield shift (shielding) of the AA protons which plateaus at a 3:1 M-T ratio for protons **b** and **d** and at a 2:1 M-T ratio for proton **c**. The Δδ for these protons is also greater in the presence of ADR, ~0.1ppm compared to 0.02ppm for AA alone.

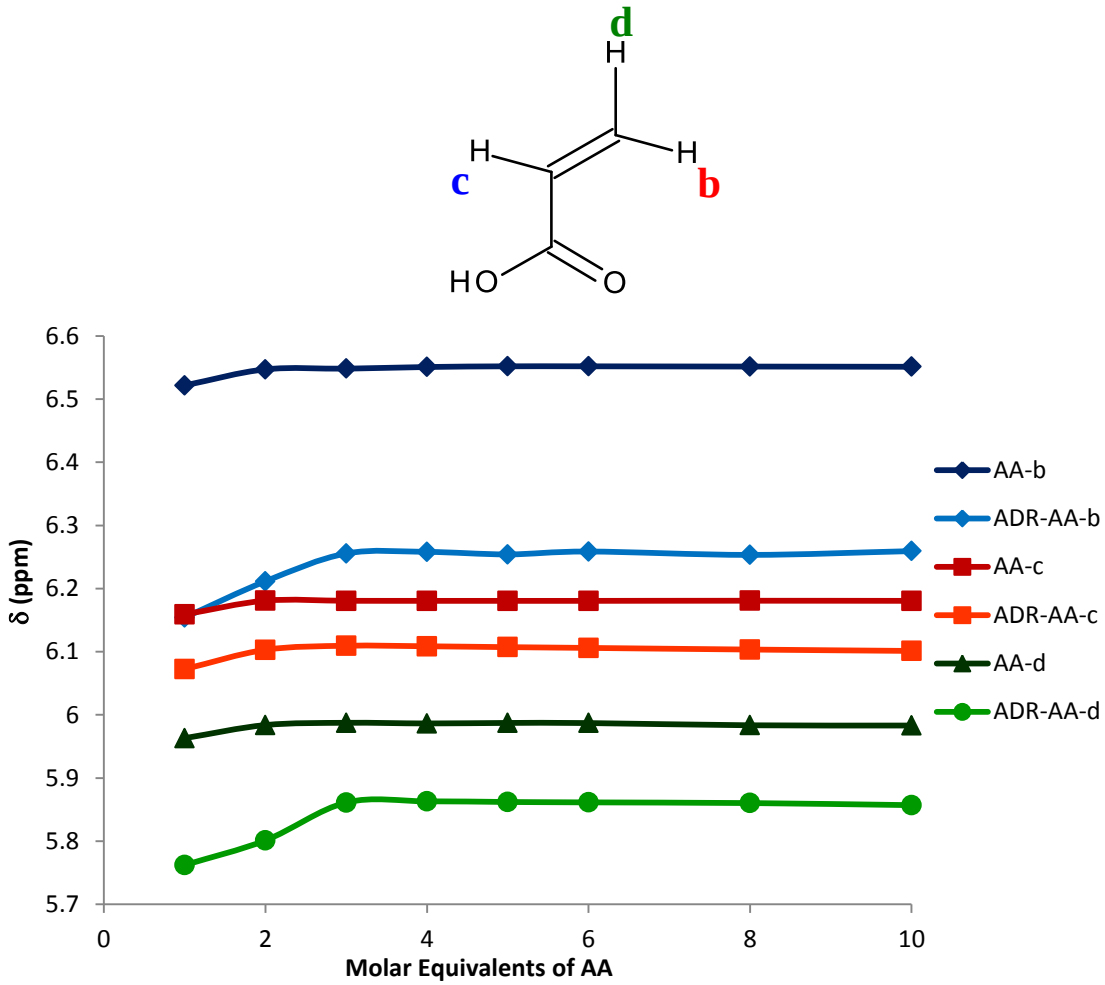

Figure 3.8 Change in chemical shift (Δδ) of different AA protons upon titration with and in the absence of ADR in d_6-DMSO. AA structure is included above to show labelling of protons.

^{1}H-NMR titrations of IPA and MBA were also performed to assess their interactions and validate the findings of the molecular modelling studies. Figures 3.9 and 3.10 show the ADR proton shifts as a function of changing template-monomer ratio (IPA and MBA, respectively).

\

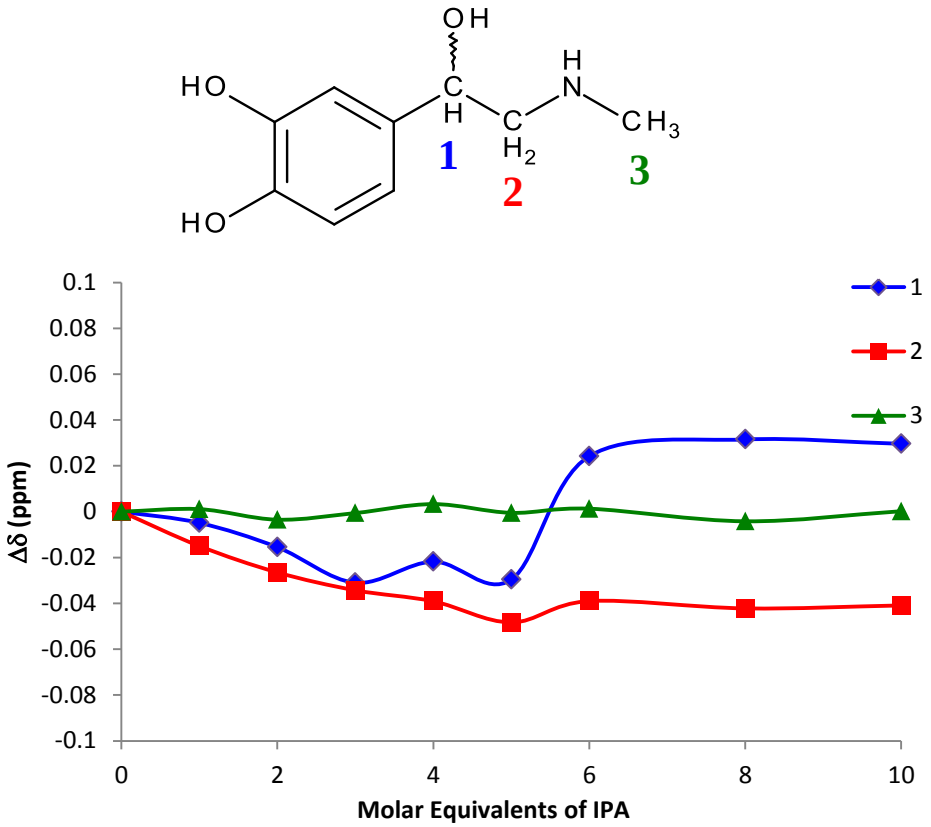

Figure 3.9 Change in chemical shift (Δδ) of different ADR protons upon titration with increasing molar equivalents of IPA in d_6-DMSO. ADR structure is included above to show labelling of protons

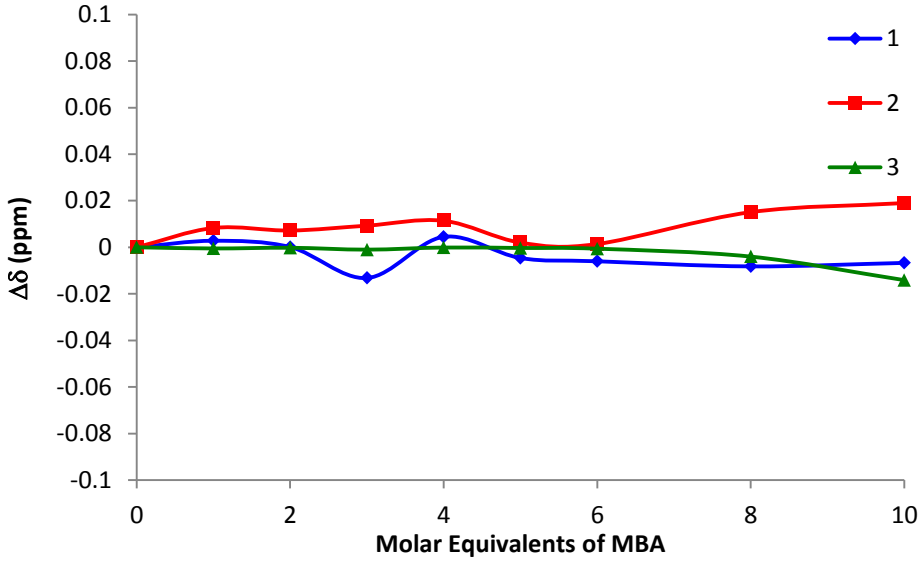

Figure 3.10 Change in chemical shift (Δδ) of different ADR protons upon titration with increasing molar equivalents of MBA in d_6-DMSO. ADR structure is included above to show labelling of protons.

These results demonstrate comparatively small (<0.05ppm) chemical shift of the ADR protons during the titration with both amide functional monomer units, suggesting little interaction with the template molecule. Monomer self-interaction studies were therefore not pursued.

The combined modelling and NMR titrations studies provided compelling evidence to warrant the use of AA as a functional monomer in the preparation of ADR imprinted polymers. A 3:1 M-T ratio with AA was identified as the preferred feed ratio from the molecular modelling as it showed a high energy of interaction, multiple points of interaction and little evidence of monomer self-association. These properties have been shown to improve the specificity and selectivity of the resulting MIP. NMR titrations however indicated that the interaction between ADR and AA will be dominated by a single acid-base interaction. This suggests that a 1:1 M-T ratio would be sufficient, however smaller increases in chemical shift were observed at M-T greater that 1:1 indicating that additional points of interaction, although weaker, may be possible as indicated by the molecular modelling.

The results also indicate that the IPA and MBA will not significantly interact with the ADR template, making them ideally suited for use as a matrix monomer and crosslinker respectively, providing structural integrity to the polymer. Low levels of interaction between the template and matrix monomer and cross-linker are desirable qualities in molecular imprinting as it improves the specificity of the resultant polymer by reducing non-specific binding interactions at the polymer surface.

3.1.4 Polymer Preparation

ADR imprinted polymers (MIP_{ADR}) and the non-imprinted control (NIP) were prepared using an AA functional monomer. The role of the functional monomer is to produce a favourable interaction with the template, resulting in a polymer that is selective for the template. From interaction studies a M-T ratio of 1:1 was identified as the sufficient for use with an AA functional monomer with an ADR template, although some evidence

did suggest that additional interactions may be also be occurring at higher M-T ratios. The M-T ratio of 3.9:1 used by Matsui et al. [68], was ultimately used for comparative purposes, with the interaction studies performed indicating that favourable interactions between the AA functional monomer and ADR template will be formed using this formulation.

The use of IPA with a MBA cross-linker also results in the formation of a hydrogel, making it easier to handle. The polymer was cut into thin sections of 2-3mm in width prior to template extraction.

The successful incorporation into, and subsequent extraction of the ADR template from the PAA-IPA-MBA polymer was initially assessed using FTIR analysis. Figure 3.11 shows the FTIR spectrum of the ADR template, a non-imprinted control polymer (NIP) and an as synthesised or virgin ADR imprinted polymer (V-MIP$_{ADR}$). No distinguishable peak was observed which did not to overlap with peaks from the polymer. Template extraction from the MIP was therefore assessed by HPLC analysis of the extraction solution.

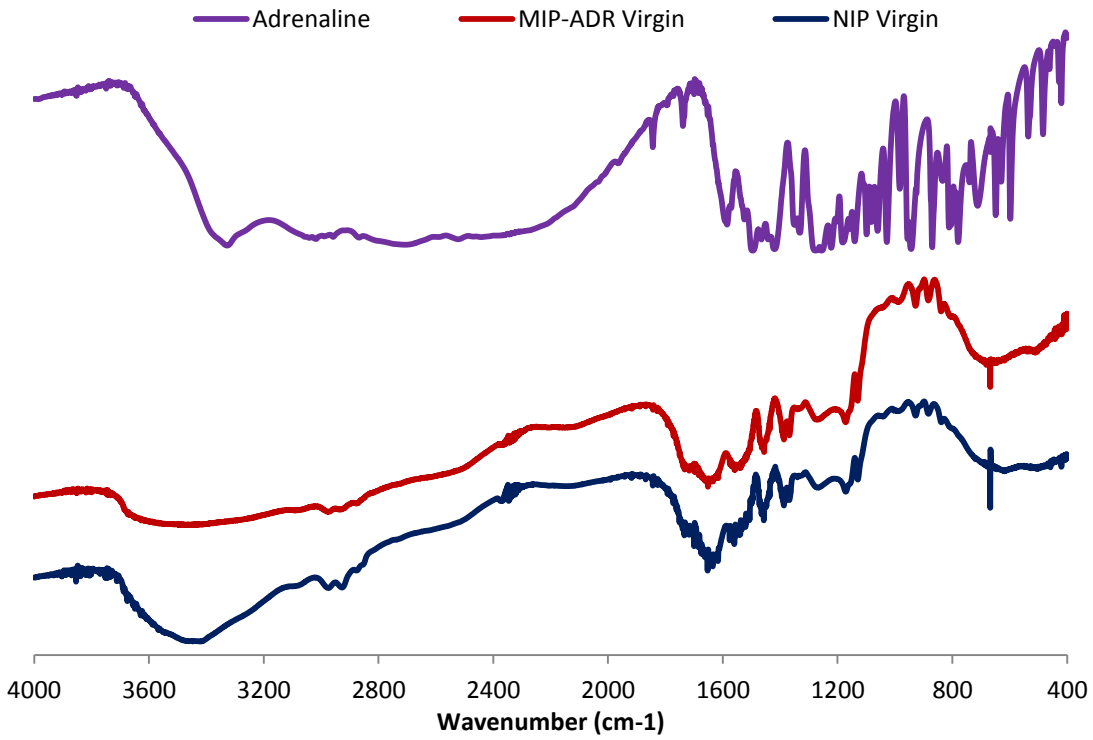

Figure 3.11 FTIR spectra of pure ADR (a) and PAA-IPA-MBA; Non-imprinted polymer (NIP) (b) and Virgin ADR imprinted polymer (V-MIP$_{ADR}$) (c).

3.1.5 Swelling Studies

The use of IPA and MBA in the polymer synthesis results in a cross-linked thermosensitive hydrogel which is hydrophilic at temperature lower than 30-35°C[146]. At temperature below this, significant swelling of the polymer in water is observed. Matsui et al.[68, 102] suggested that template rebinding for the PAA-IPA-MBA requires the polymer to be in its swollen state. The template specific cavities are formed while the polymer is swollen and following template removal, the polymer is dried, resulting in a significant loss of both volume and absorbed solvent. In its unswollen state, the internal pores and cavities of the polymer are significantly reduced, resulting in limited access to the template-specific cavities.

Swelling studies of the PAA-IPA-MBA system (Figure 3.12) indicate that complete swelling of the polymer occurs after approximately 24 hours after immersion, but that the polymer undergoes greatest swelling in the first 5 hours of exposure to solvent (water). All rebinding experiments for the PAA-IPA-MBA polymer were therefore conducted over a 24 hour period.

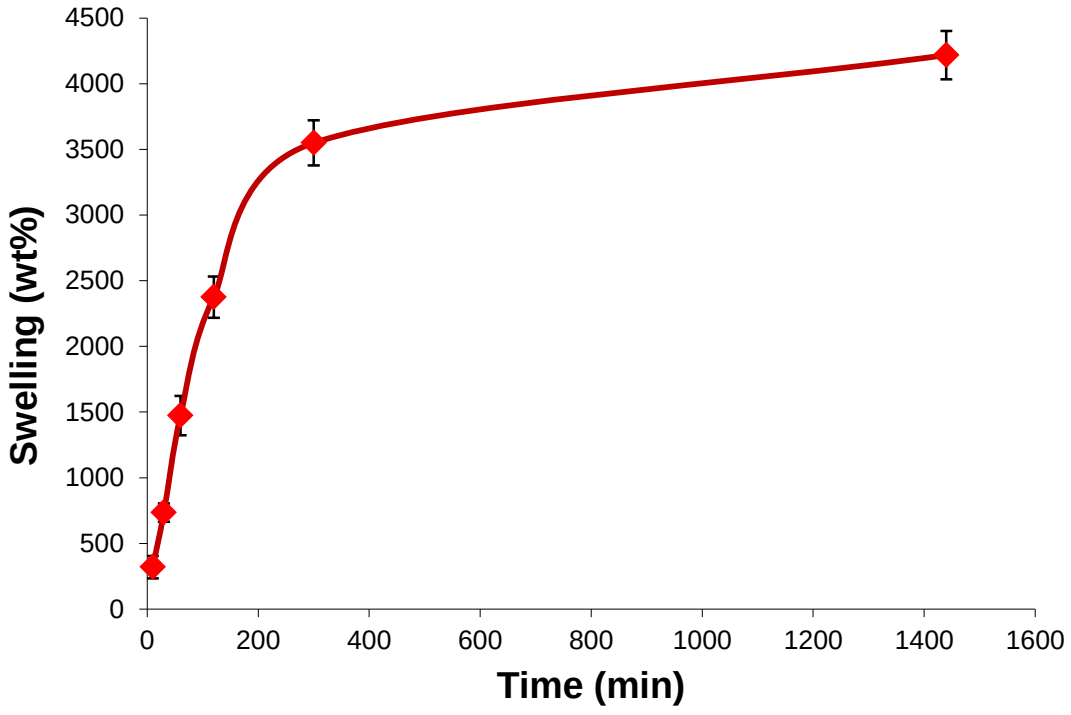

Figure 3.12 Swelling of PAA-IPA-MBA MIP_{ADR} polymers in water. Study was performed in triplicate.

3.1.6 Rebinding Studies

Quantitative rebinding results were produced using HPLC which show rebinding of ADR to the ADR imprinted polymer (MIP_{ADR}) relative to the NIP. Imprinting factors (*I*) (Equation 3) were calculated from these measurements. The MIP_{ADR} showed significantly greater selectivity for ADR compared to the NIP, resulting in an imprinting factor of 3.37 as shown in Table 3.1. The result demonstrates that the PAA-IPA-MBA system will selectively bind an ADR template.

Table 3.1 Template Rebinding and Imprinting Factors (I) for ADR imprinted PAA-IPA-MBA polymer

MIP Rebound (µmol/mg)	NIP Rebound (µmol/mg)	Imprinting Factor
33.2 ± 1.0	9.8 ± 0.5	3.4

3.1.7 Preparation and Incorporation of Gold Nanoparticles

Gold nanoparticles were successfully prepared using a using an 11-mercaptoundecanoic acid (MUA) stabilising agent. Particle sizing confirmed the formation of the gold nanoparticles with a mean diameter of 5.12nm (CV 12.6%) as shown in Figure 3.13 which was consistent with those previously produced by Matsui et al.[68]

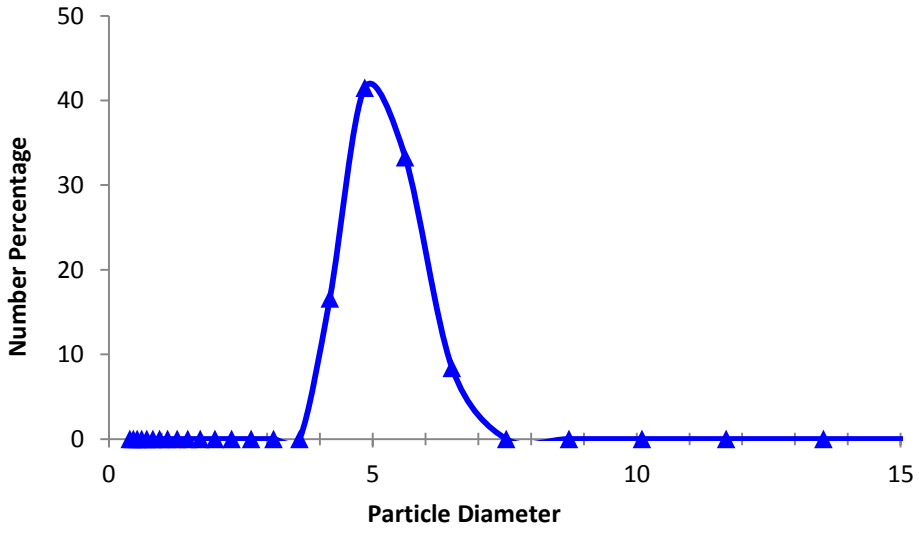

Figure 3.13 Size distribution of 11-mercaptundecanoic acid stabilised gold nanoparticles (Au_{MUA})

MUA stabilised gold nanoparticles (Au_{MUA}) were incorporated into the pre-polymerisation mixture for the PAA-IPA-MBA polymer system. Successful post-polymerisation incorporation of the nanoparticles into the polymer matrix was visually confirmed by the distinct colour change from colourless to black that accompanied the process as seen in Figure 3.14.

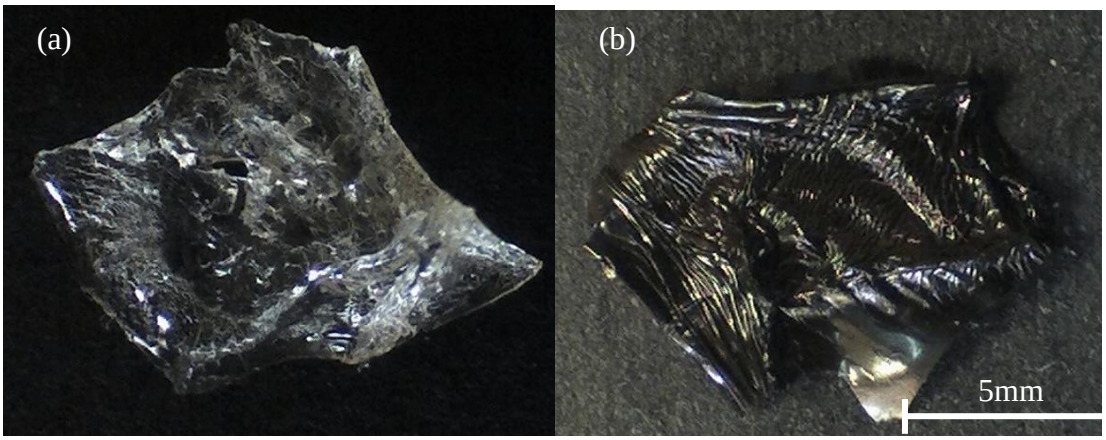

Figure 3.14 PAA-IPA-MBA MIPADR with (b) and without (a) AuMUA.

3.1.8 UV-Vis Spectroscopic Rebinding Studies

Following incorporation of Au_{MUA} into the ADR imprinted PAA-IPA-MBA system, spectroscopic studies, intended to replicate the results of Matsui et al.[68], were conducted to determine if any colourimetric shift in the plasmon absorbance of the gold nanoparticles was observed in response to template rebinding to the polymer.

Following incorporation of Au_{MUA} into the ADR imprinted PAA-IPA-MBA system, spectroscopic studies, intended to replicate the results of Matsui et al. [68], were conducted to determine if any colourimetric shift in the plasmon absorbance of the gold nanoparticles was observed in response to template rebinding to the polymer.

UV-Vis measurements were taken of Au_{MUA} dispersed in toluene to confirm absorbance in the plasmon absorption band of the nanoparticles. This was followed by measurements of the MIP_{ADR}-Au_{MUA} and NIP-$Au_{MUA,}$ which are shown in Figure 3.15. The plasmon absorbance of the embedded gold nanoparticles was not readily distinguishable from the spectrum of the polymer itself. Additional measurements were taken of the MIP_{ADR}-Au_{MUA} and NIP-Au_{MUA} following rebinding in an aqueous 1mM ADR solution, however the plasmon absorbance of the embedded gold nanoparticles remained undistinguishable.

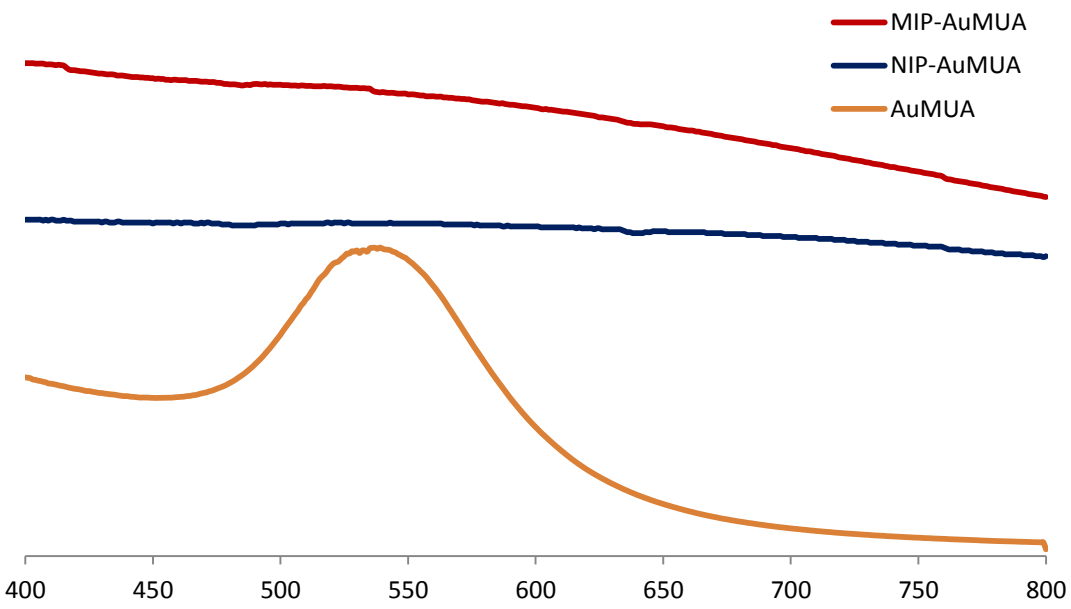

Figure 3.15 UV-Vis Spectra of (a) Au_{MUA} nanoparticles in toluene, (b) PAA-IPA-MBA-Au_{MUA} MIP_{ADR} and (c) PAA-IPA-MBA-Au_{MUA} NIP

The plasmon absorbance band of the embedded gold nanoparticles, and subsequent shift following template rebinding, observed by Matsui et al[68]., as seen in Figure 3.16, were unable to be reproduced.

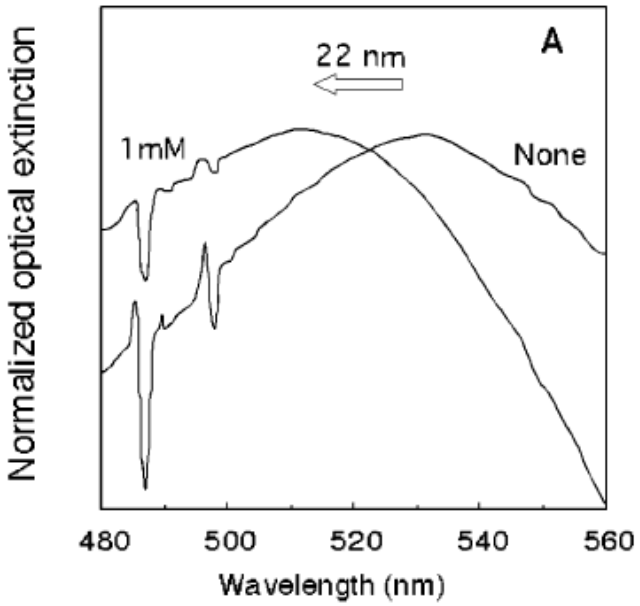

Figure 3.16 UV-Vis Spectra of PAA-IPA-MBA-Au_{MUA} MIP_{ADR} in water and ADR solution (1mM). Reproduced from Matsui (2004)[68].

3.1.9 Summary

Pre-synthetic interaction studies utilising molecular modelling and NMR titrations experiments were successfully utilised to identify AA as a suitable functional monomer for use with the ADR template. Additionally, a 1:1 template-monomer ratio was determined to produce an energetically stable cluster exhibiting as a result an acid-base interaction following protonation of the ADR template. Additional weaker interactions with additional AA were also suggested. These pre-synthetic studies also determined that template interaction with IPA and MBA is minimal making them ideal for use as a matrix monomer and cross-linker respectively.

Swelling studies identified the required time for rebinding as being greater than five hours. Rebinding studies carried out after 24 hours showed significantly higher levels of ADR rebinding to the PAA-IPA-MBA MIP compared to the NIP, with an imprinting factor of 3.37 obtained.

The work of Matsui et al. involving spectroscopic rebinding studies based on a shift on the plasmon absorbance of embedded gold nanoparticles during template rebinding was unable to be replicated. Gold nanoparticles were successfully prepared and the plasmon absorbance band was observed in the UV-Vis spectrum, however this effect was unable to be replicated once the nanoparticles were embedded in PAA-IPA-MBA system.

3.2 Model System – Poly(Acrylic Acid-*co*-N-Isopropylacrylamide-*co*-Methylenebisacrylamide) – (-)-Ephedrine Template

After assessing the work of Matsui et al.[68] using the ADR-imprinted PAA-IPA-MBA polymer, investigations were subsequently extended to include (-)-ephedrine (EPD) as a template using the same polymer system. EPD was chosen as a template as a model analyte for amphetamine-type substances, which are of increasing forensic interest as one of the fastest growing class of illicit drugs around the world.

3.2.1 (-)-Ephedrine-Functional Monomer Molecular Modelling

Molecular modelling results for AA with EPD are shown in Figure 3.17. It can be seen that the enthalpies of AA with EPD are negative for all ratios indicating energetically favourable clusters.

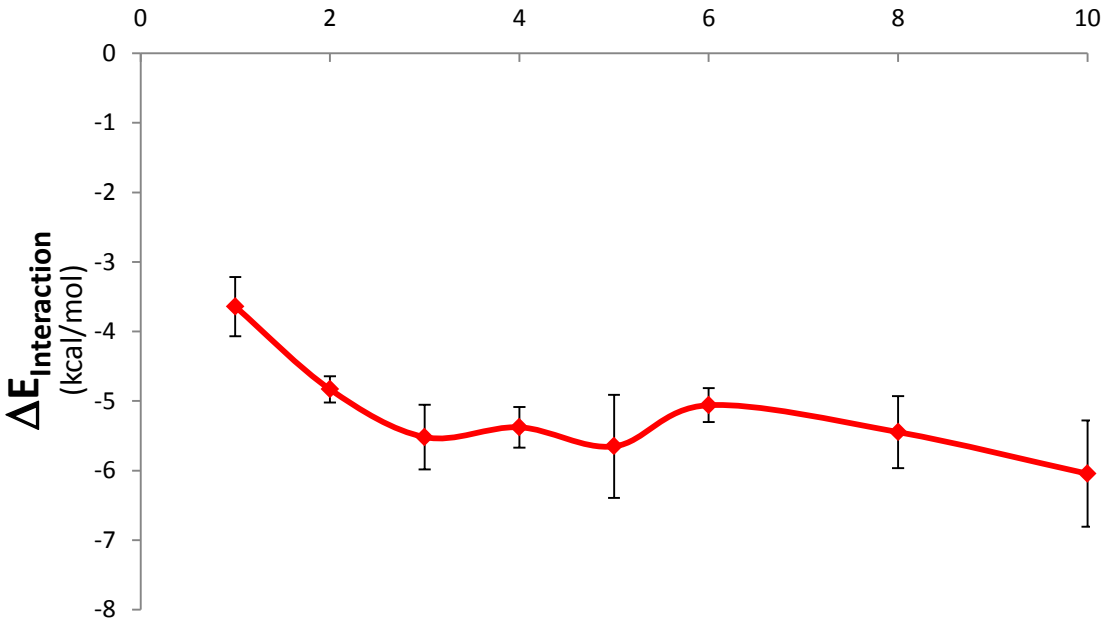

Figure 3.17 $\Delta E_{interaction}$ of EPD with AA across a range of template - monomer ratios.

AA to EPD ratios of 2:1, 3:1 and 4:1 produce $\Delta E_{Interaction}$ of -4.8kcal/mol, -5.5 kcal/mol and -5.4kcal/mol respectively, indicating increased cluster strength. As seen in Figure

3.17, the dominant interactions between the AA and EPD is hydrogen bonding between the acidic carboxyl group of the AA and the secondary amine, aliphatic hydroxyl groups of the EPD. At ratios greater than 2:1, an additional weak interaction is also observed between AA and the aromatic ring of the EPD. The 3:1 ratio is shown below in Figure 3.18.

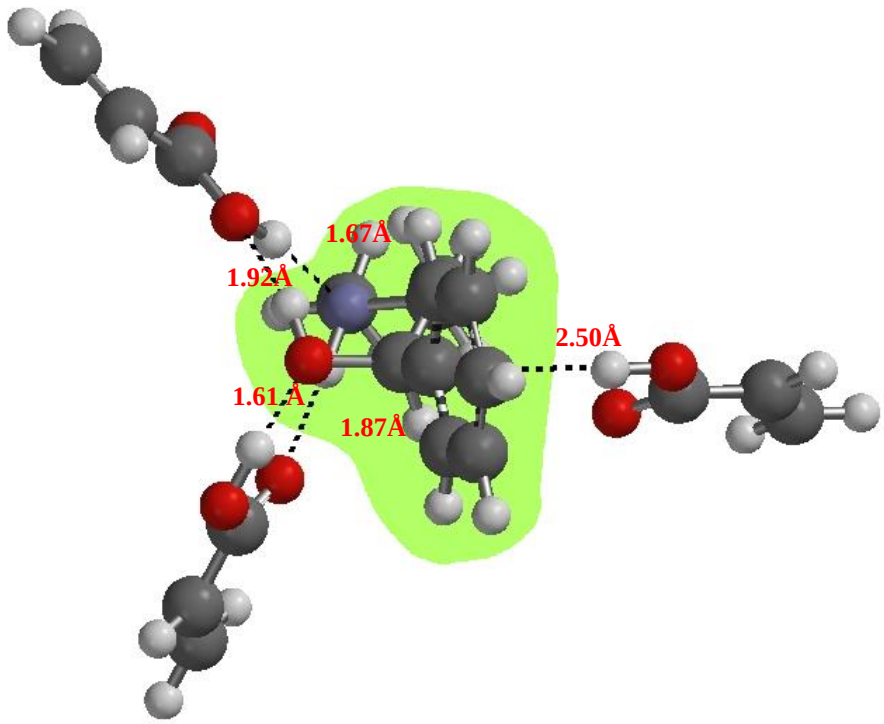

Figure 3.18 Molecular modelling of EPD with 3 AA monomer units, showing a multiple points of interaction. Template is shaded green and hydrogen bond distances are indicated in red.

AA to EPD ratios above 5:1 show high $\Delta E_{Interaction}$, (> -5.1kcal/mol), however at this stoichiometry and beyond, monomer-monomer self-association become increasingly prevalent (Figure 3.19) leading to increasingly complex clusters without additional template stabilisation.

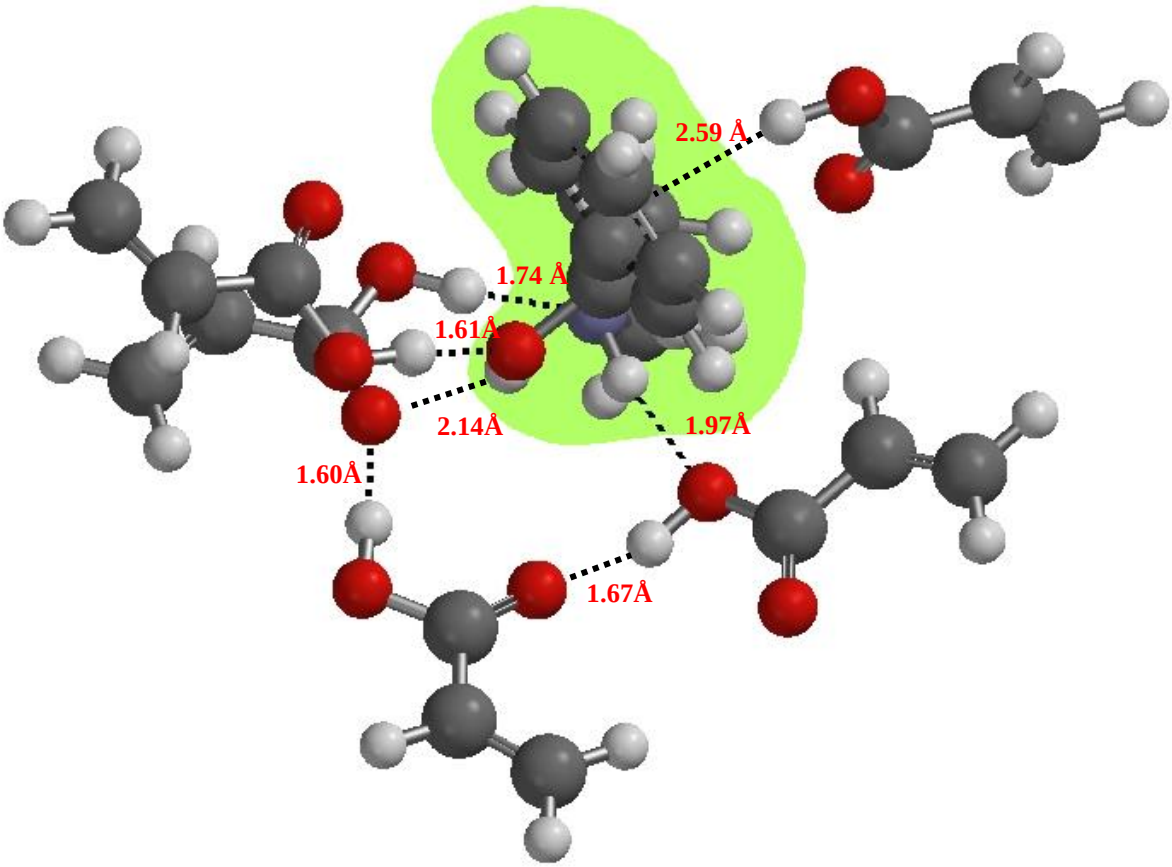

Figure 3.19 Molecular modelling of EPD with 5 AA showing a multiple points of interaction. Some monomer-monomer interaction is also observed. Template is shaded green and hydrogen bond distances are indicated in red.

The criteria of maximum $\Delta E_{Interaction}$ and minimum monomer self-association indicates a 3:1 ratio as being the preferred. The combination of multiple interaction sites and high energies of interaction have been shown to improve MIP specificity[144]. The modelling is performed *in silico* and suggests likely sites of interaction between the monomer and template. The limitations of the software prevent the modelling of the protonation of the secondary amine of the EPD template (pK_{a1} 9.6) by the acidic AA functional monomer (pK_a 4.26). This would lead to a stronger acid-base interaction which is not shown by the modelling. The site of this acid-base interaction is however still indicated in the modelling although as a weaker hydrogen bonding interaction.

3.2.2 (-)-Ephedrine – Matrix Monomer/Crosslinker Molecular Modelling

The molecular modelling results for EPD with the matrix monomers N-isopropylacrylamide (IPA) and the cross-linker N,N'-methylenebisacrylamide (MBA) are compared with those for AA in Figure 3.20.

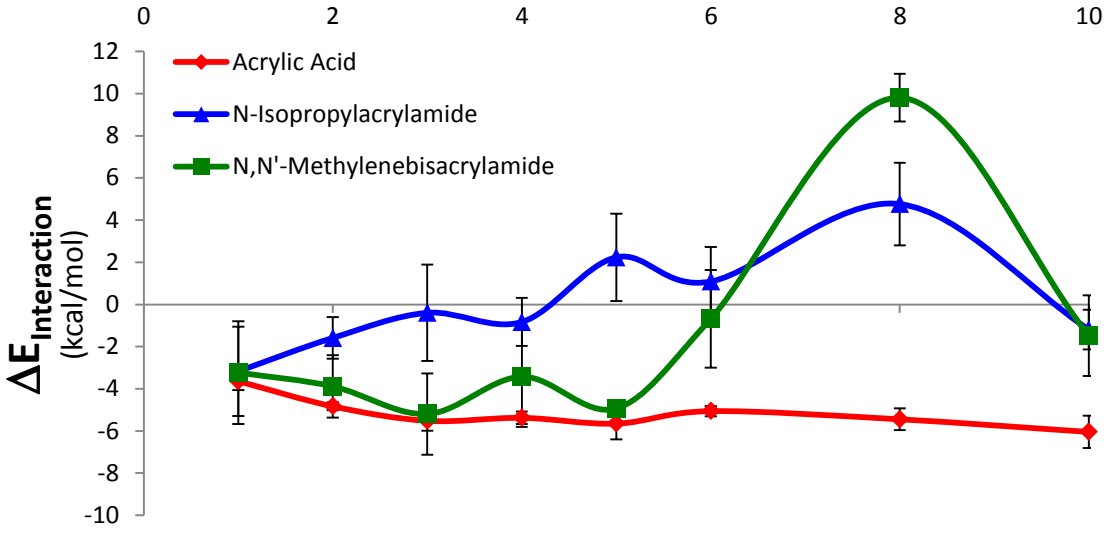

Figure 3.20 $\Delta E_{interaction}$ of EPD with AA, IPA and MBA across a range of M-T ratios.

From Figure 3.20 it can be seen that the $\Delta E_{interaction}$ for IPA with EPD are negative for M-T ratios up 4:1 signifying a favourable interaction. These energies are less negative than AA across all stoichiometries, indicating that AA interacts more favourably with EPD.

Molecular modelling indicates hydrogen bonding between the secondary amine and the hydroxyl groups of the EPD and the oxygen lone pair of the IPA amide unit. The 1:1 M-T ratio which produced the highest energy of interaction is shown in Figure 3.21.

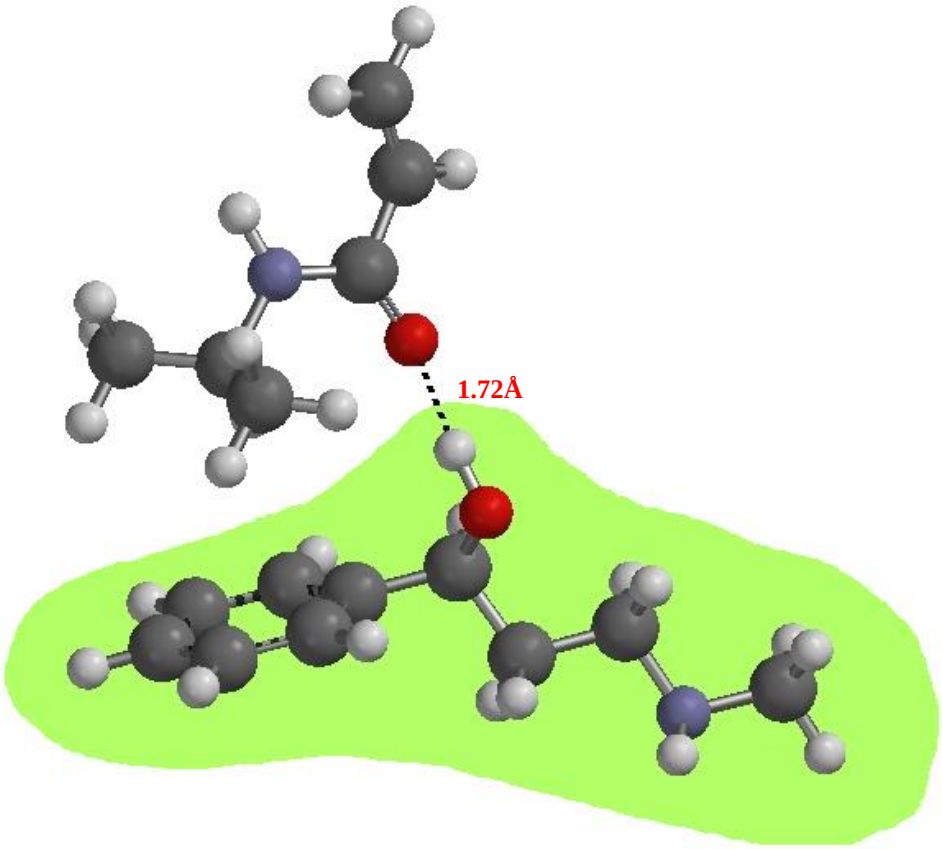

Figure 3.21 Molecular modelling of EPD with 1 IPA showing a single point of interaction. Template is shaded green and hydrogen bond distances are indicated in red.

IPA shows a modest association with EPD, indicated by an intermediate bonding distance (1.72 Å). Due the higher electronegativity of the oxygen, the primary point of interaction between IPA and EPD is between their carbonyl and hydroxyl groups respectively. Additional IPA monomers similarly interact with the secondary amine of EPD. At ratios above 4:1, modelling indicates that the additional monomer units only produce monomer-monomer interactions and do not interact with the template. These molecular modelling results indicate that IPA has only a minor association with EPD compared to the AA functional monomer.

From Figure 3.20 it can be seen that the $\Delta E_{interaction}$ for MBA with EPD are comparable to those of AA up to a 5:1 ratio signifying a favourable interaction at low cluster stoichiometry. The modelling suggests hydrogen bonding interactions between secondary amine and the hydroxyl group of the EPD and the amide units of the MBA stabilise the clusters. The 2:1 ratio, which produced the highest $\Delta E_{interaction}$ without

evidence of monomer self-association, is shown in Figure 3.22. At ratios of 4:1 and above, modelling indicates that monomer self-association dominates over monomer-template interactions.

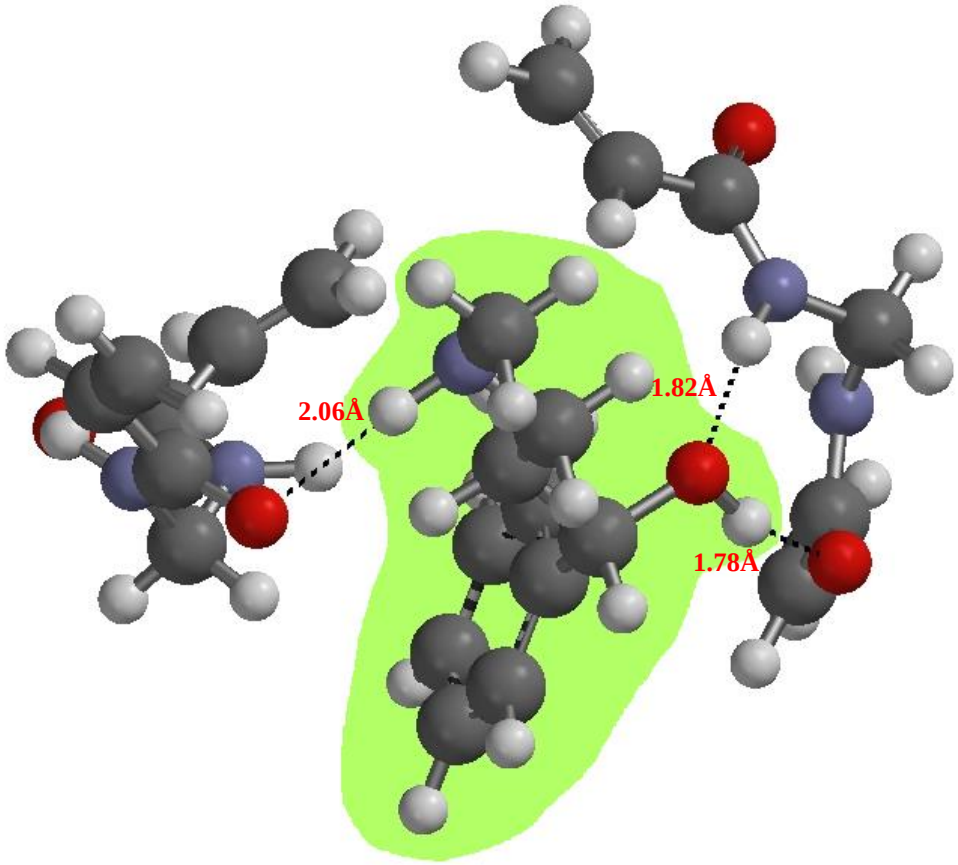

Figure 3.22 Molecular modelling of EPD with 2 MBA showing multiple points of interaction. Template is shaded green and hydrogen bond distances are indicated in red.

In the 2:1 system, the hydroxyl group of the EPD produces a two point interaction with the MBA unit, acting as both a hydrogen bond donor and acceptor (Figure 3.22 above). The electronegativity of the oxygen atoms in the template and MBA unit involved in the association leads to a relatively short bond length in the resultant hydrogen bond. By contrast, the single point interaction between the less electronegative EPD amine and MBA unit (3.21 left) results in a bond length of 2.06 Å.

The hydrogen bonds distances for EPD with MBA are on average longer than those observed for AA, indicating reduced hydrogen bond strength. These molecular modelling results indicate that MBA has some interaction with EPD, although lower than that observed for the AA functional monomer.

3.2.3 NMR Studies

^{1}H NMR titration of the AA functional monomer in the presence of the EPD template was performed to confirm the presence of the interactions identified using molecular modelling. Figure 3.23 shows the spectra of EPD with increasing molar equivalents of AA.

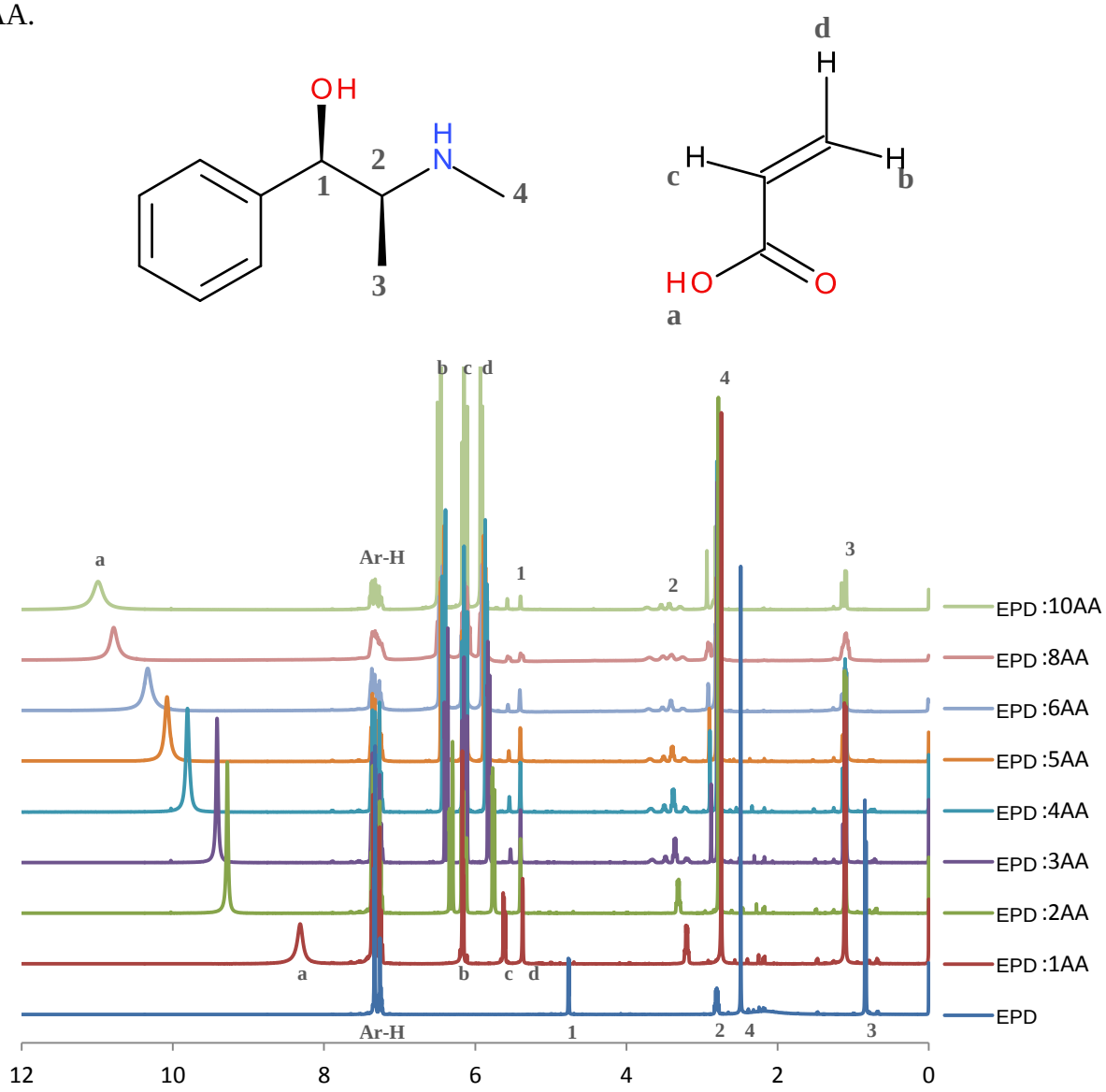

Figure 3.23 ^{1}H-NMR spectra of pure EPD and various EPD:AA ratios (as indicated on the right) in d_6-DMSO.Structures of EPD and AA are shown above, along with corresponding proton labelling.

In the presence of AA, peaks associated with EPD protons (1, 2, 3 and 4) were seen to move downfield indicating that these nuclei were experiencing a deshielding effect. This is a result of the protonation of the secondary amine in the EPD and is indicated by the peak splitting observed in protons 1 and 2 and the large changes in chemical shifts

observed for all protons. This suggests that a strong acid-base interaction will occur between the EPD and AA at this site. Figure 3.24 shows the extent of the downfield shifts as a function of the template-monomer ratio.

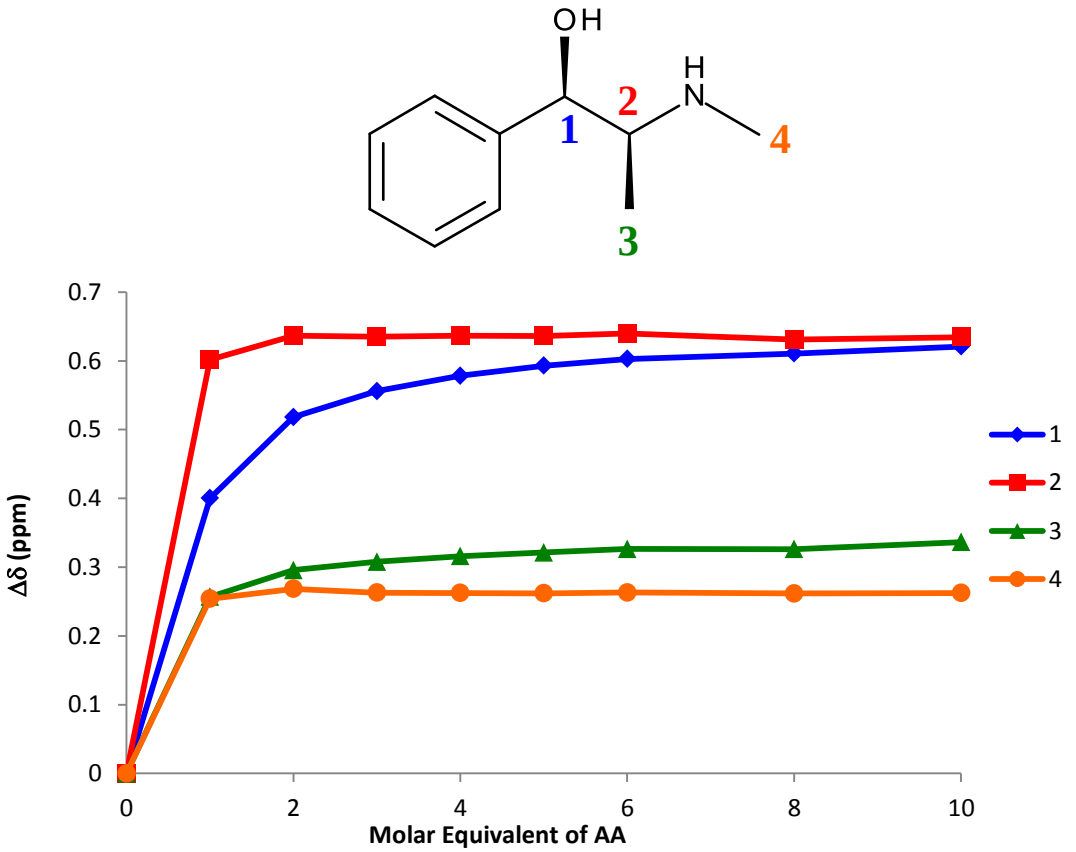

Figure 3.24 Change in chemical shift (Δδ) of different EPD protons upon titration with increasing molar equivalents of AA in $CDCl_3$. EPD structure is included above to show labelling of protons.

Figure 3.24 displays the change in chemical shift experienced by EPD protons during titration with AA. The greater shift experienced by Proton **2** suggesting an immediate (alpha) proximity to the interaction site. Methyl protons (**3** and **4**) show a significantly reduced chemical shift signifying removal from the sphere of influence of the acid-base interaction at the EPD heteroatoms[147]. The acid-base interaction determined by NMR was not observed during molecular modelling due to limitations of the modelling software in analysing this type of interaction. The modelling did however suggest this secondary amine as a likely point of interaction through weaker hydrogen bonding.

The Δδ of Proton 2 reaches a maximum after the addition of 1 molar equivalent of AA, indicating the formation of the 1:1 AA-EPD complex and is consistent with the formation of a strong acid-base interaction. The curve associated with proton 1 takes longer to plateau (>3:1) indicating that subsequent AA additions promote additional interactions with the EPD template. This suggests that although the M-T interactions will be dominated by the acid-base interaction at the site of the secondary amine which occurs at a M-T ratio of 1:1, additional weaker interaction, such as the hydrogen bonding suggested by the molecular modelling, may occur as a result of subsequent additions.

The NMR titration also showed significant changes in the chemical shift of the AA protons (**a**, **b**, **c** and **d**). Figure 3.25 shows the change in shift of AA protons as a function of AA concentration both in the presence and absence of EPD, in order to assess template – monomer and monomer-monomer interactions. EPD presence results in an upfield shift of all AA protons with increasing AA concentration, which plateaus at a 2:1 ratio in the case of protons **c** and **d** but is less defined in the case of protons **a** and **b**.

The titration also showed significant Δδ for AA proton **a**. This proton experiences a change in δ throughout the entire titration, unlike the EPD protons and the remaining AA protons which showed no significant changes beyond the 3:1 EPD-AA ratio. This is likely due to dimerisation associated with AA self-interaction, which is supported by the change in shift observed in the self-titration of AA. This confirms the presence of monomer-monomer interactions taking place in the presence of EPD.

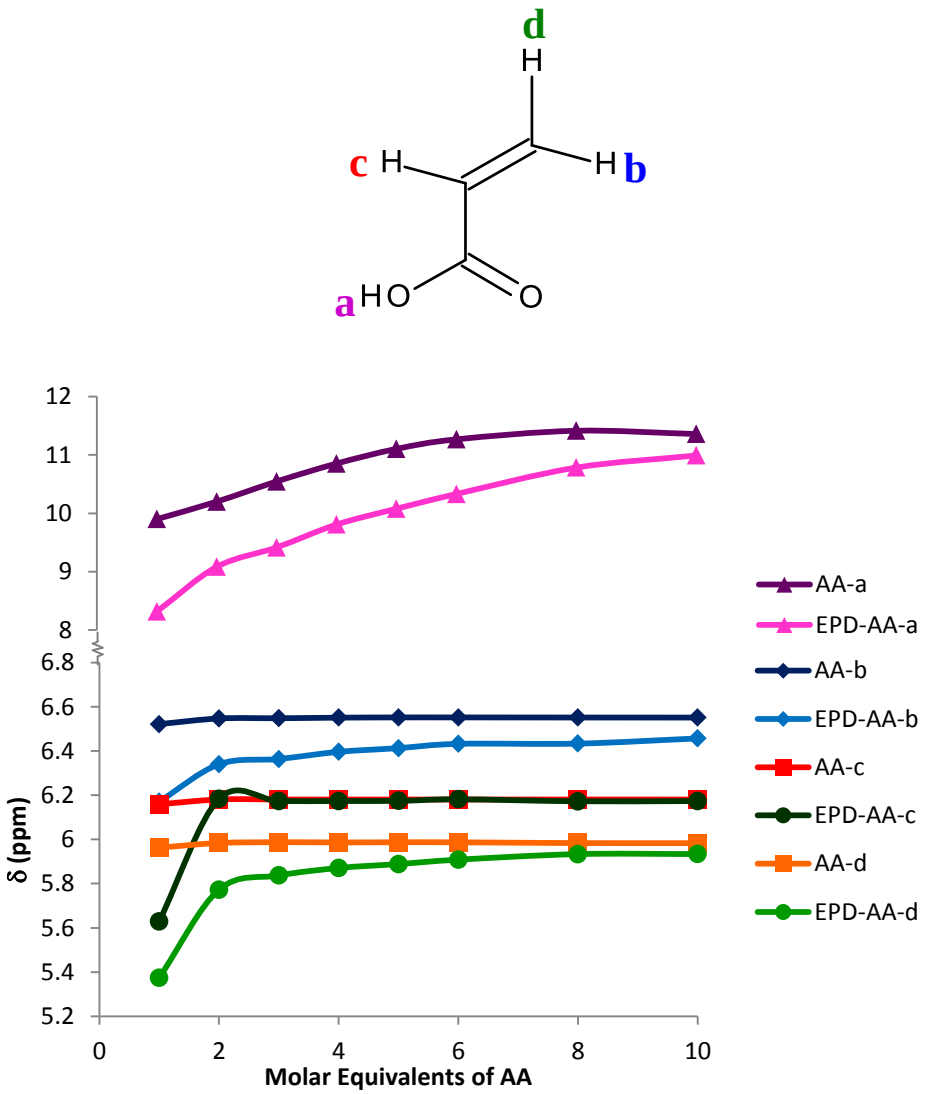

Figure 3.25 Change in chemical shift (Δδ) of different AA protons upon titration with and in the absence of EPD in $CDCl_3$. AA structure is included above to show labelling of protons.

NMR titrations of IPA and MBA with EPD were also performed to assess their interactions and validate the predictive molecular modelling studies. Figure 3.26 and 3.27 shows the extent of the downfield shifts as a function of the template-monomer ratio of the EPD protons during titrations with IPA and MBA, respectively.

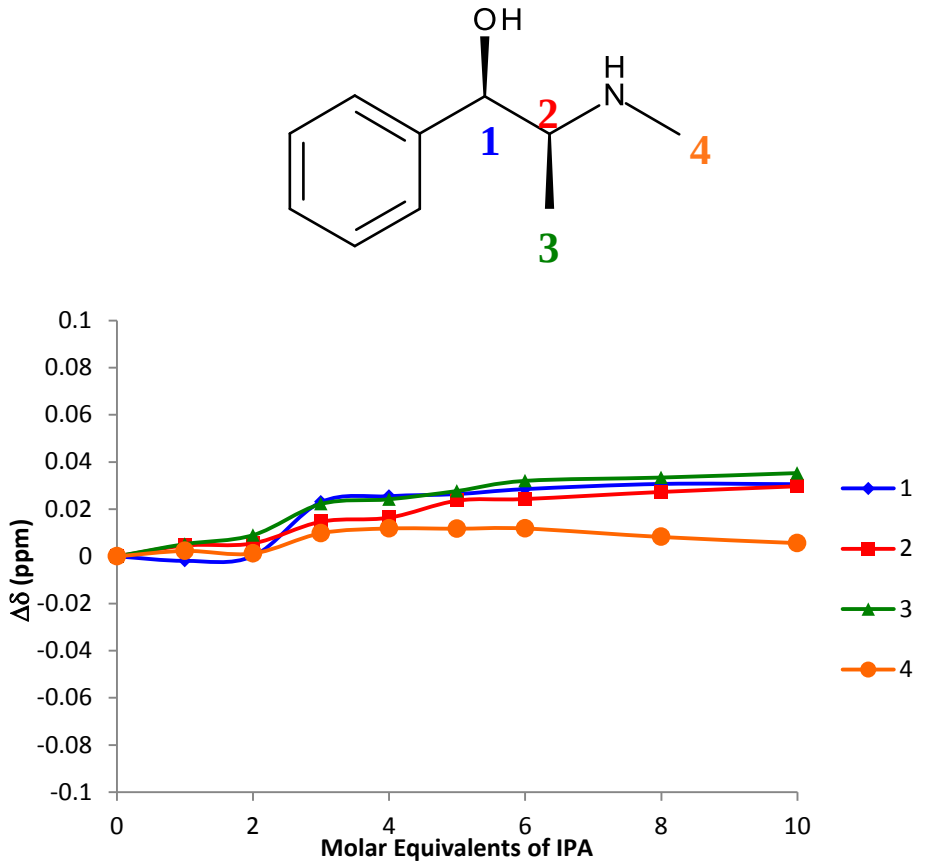

Figure 3.26 Change in chemical shift (Δδ) of different EPD proton resonances upon titration with increasing molar equivalents of IPA in $CDCl_3$. EPD structure is included above to show proton labelling.

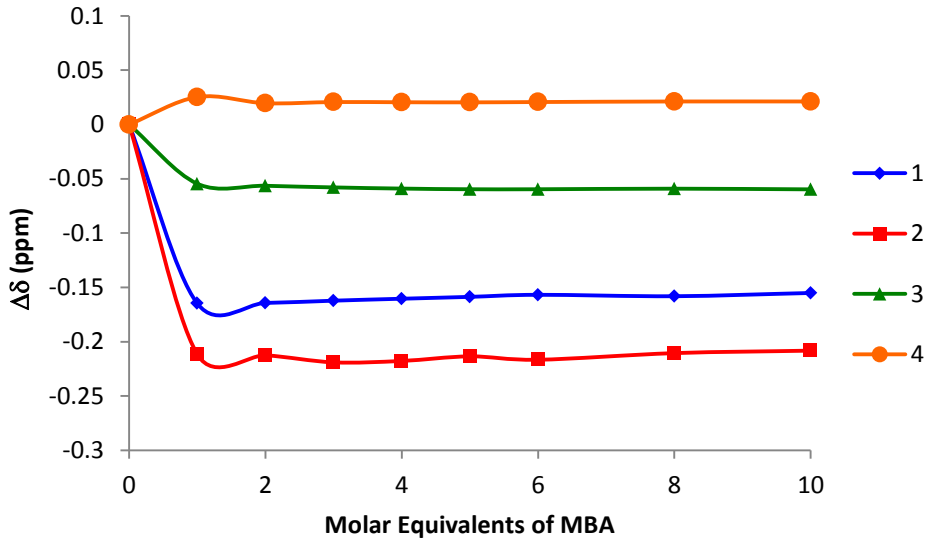

Figure 3.27 Change in chemical shift (Δδ) of different EPD proton resonances upon titration with increasing molar equivalents of MBA in d_6-DMSO. EPD structure is included above to show proton labelling.

The results show comparatively small movements in chemical shift (<0.05ppm) for all EPD proton resonances during the titration, suggesting that IPA has little interaction with the EPD template and supports the molecular modelling predictions.

Some chemical shift (up to ~0.2ppm) is observed in the EPD protons during the titration with MBA. This was similarly predicted by molecular modelling, as the presence of an additional amide group compared to IPA results in a two point interaction with the hydroxyl group of EPD. While some interaction is observed between MBA and EPD, the magnitude is again relatively small when compared to that observed with AA

The combined modelling and NMR titrations studies provided compelling evidence to warrant the use of AA as a functional monomer in the preparation of EPD imprinted polymers. A 1:1 monomer to template ratio with AA was identified as sufficient feed ratio with the monomer template interactions being dominated by the formation of an acid-base interaction following amine protonation. Additional, although weaker, interactions were observed at higher monomer template ratios up to 3:1. This was therefore selected as a preferred feed ratio as it showed a high degree of interaction, multiple points of interaction and little evidence of monomer self-association. These properties have been shown to improve the specificity and selectivity of the resulting polymer.

Low levels of interaction between the template, matrix monomer and cross-linker are desirable qualities in molecular imprinting as it improves the specificity of the resultant polymer by limiting non-specific binding interactions at the polymer surface. The results suggest that the IPA will not significantly interact with the EPD template, making it suitable for use as a matrix monomer, providing structural integrity to the polymer. Some interaction between MBA and EPD was predicted, although lower than that observed with AA.

3.2.4 Polymer Preparation

Molecular modelling and NMR studies above demonstrated that AA is a suitable functional monomer for use with an EPD imprinted polymer. A 3:1 monomer-template stoichiometry was identified to be optimal as a feed ratio because of predictive interaction energies and the presence of multi-point cluster interactions suggested in silico. The modelling results also suggested little or no monomer self-association at this ratio. Given the similarity of these findings to the Matsui formulation (3.9:1), it was decided to employ to the Matsui formulation for our MIP preparations for comparative purposes. IPA and MBA were again used as a matrix monomer and cross-linker respectively, again resulting in the formation of a hydrogel.

Success in incorporating and extracting EPD into and from the PAA-IPA-MBA membrane was initially assessed using FTIR spectroscopy. Figure 3.28 shows FTIR spectra of EPD, a non-imprinted polymer (NIP), an as synthesized or virgin EPD imprinted polymer (V-MIP_{EPD}) and an extracted EPD imprinted polymer (Ex-MIP_{ADR}) for comparative purposes. All polymers were briefly rinsed with distilled water prior to FTIR to remove any surface EPD and allowed to dry.

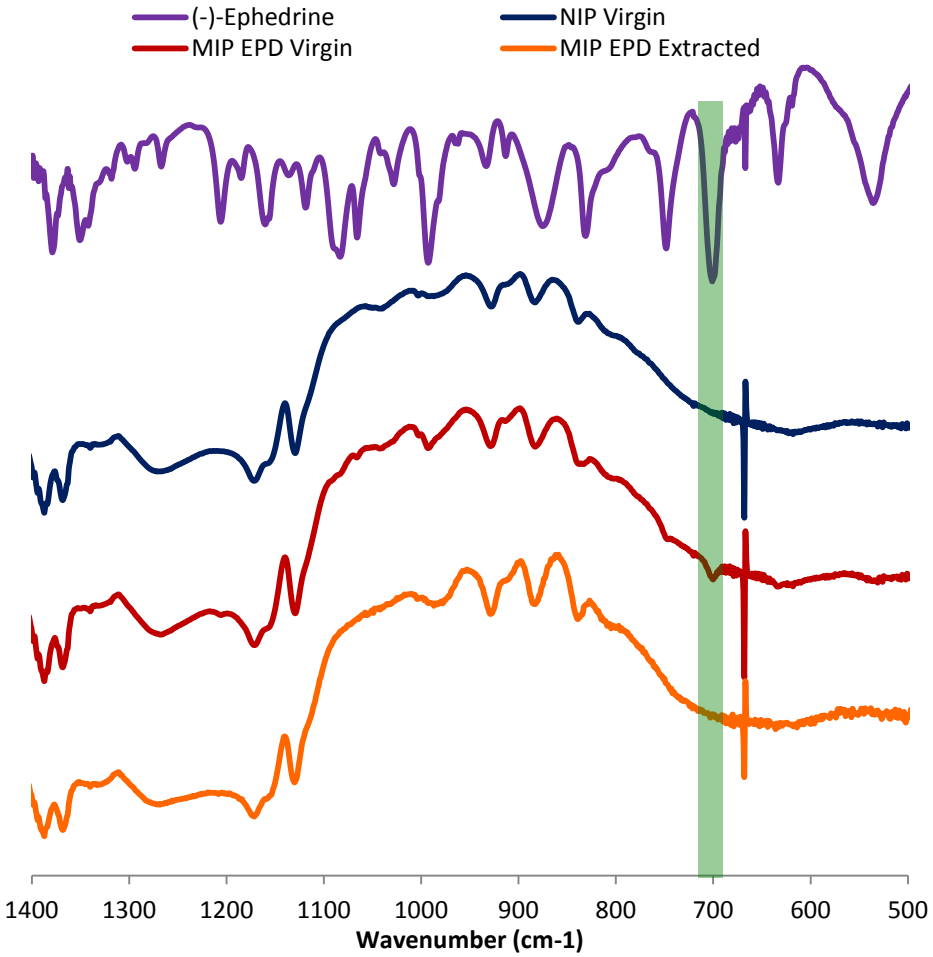

Figure 3.28 FTIR spectra of pure EPD (a) and PAA-IPA-MBA; Non-imprinted polymer (NIP) (b), Virgin EPD imprinted polymer (V-MIP_{EPD}) (c), and Extracted EPD imprinted polymer (Ex-MIP_{EPD}) (d). The diagnostic aromatic hydrogen (~700cm^{-1}) peak used to determine the presence of EPD is shaded.

A prominent peak, at approximately 700cm^{-1}, corresponding to the out of plane bending of the EPD aromatic hydrogen atoms, did not overlap with peaks present in the polymer and was therefore chosen as the diagnostic peak to assess the presence / absence of EPD. Template extraction from the polymer was also assessed qualitatively using this diagnostic peak. The presence of the EPD peak in the V-MIP_{EPD} demonstrates that EPD has been successfully incorporated into the imprinted polymer. The absence of the peak in the Ex-MIP_{EPD} spectrum indicates that the EPD template was successfully removed from the MIP by extraction.

3.2.5 Rebinding Studies

Rebinding of the template, post-extraction was qualitatively assessed using FTIR by monitoring the re-emergence of the EPD peak at 700cm^{-1} (Figure 3.29). Of note is the absence of the peak from the non-imprinted polymer (NIP) both before and after rebinding, indicating the absence of binding cavities in this film.

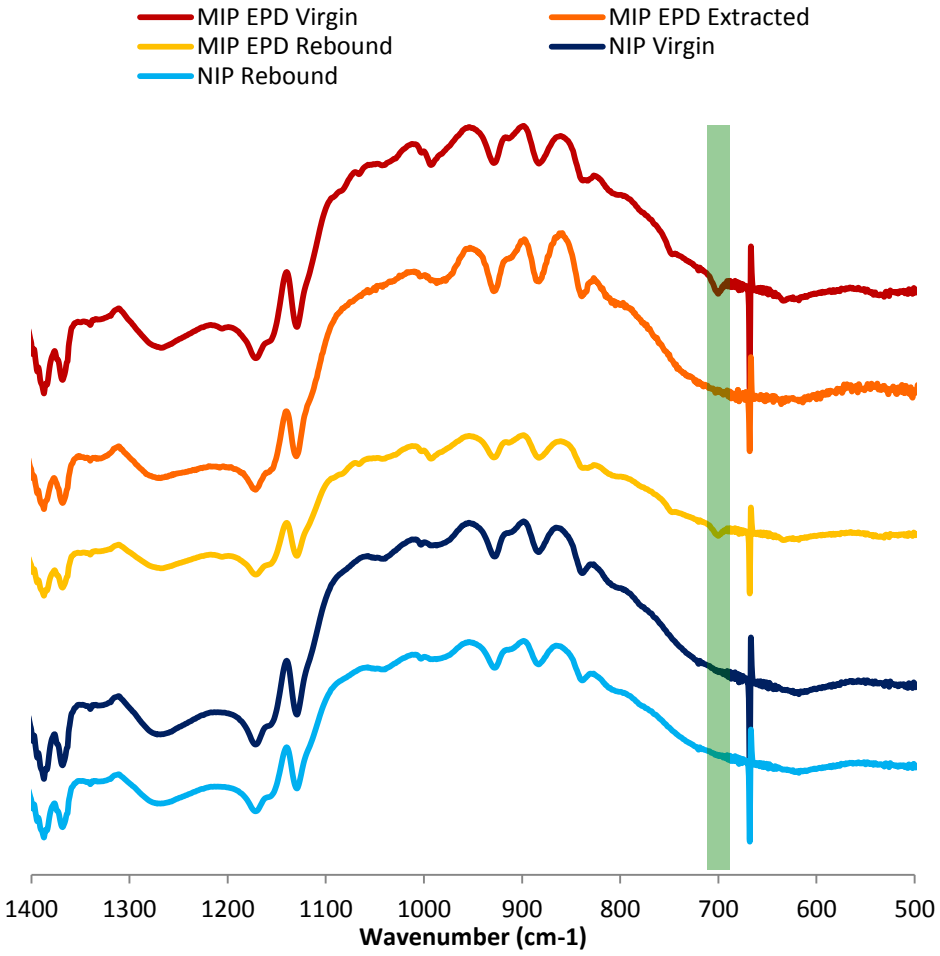

Figure 3.29 FTIR spectra of PAA-IPA-MBA; Virgin EPD imprinted polymer (V-MIP$_{EPD}$) (a), EPD imprinted polymer (Ex-MIP$_{EPD}$) (b), Rebound EPD imprinted polymer (Rb-MIP$_{EPD}$) (c), Virgin non-imprinted polymer (V-NIP) (d) and Rebound non-imprinted polymer (Rb-NIP) (e). The diagnostic peak (700cm^{-1}) used to determine the presence of EPD is shaded.

Swelling of the EPD imprinted PAA-IPA-MBA polymer was comparable to that of the ADR imprinted system as seen in Figure 2.12. As a result, rebinding studies for the EPD imprinted system were similarly carried out over 24 hours to allow for complete polymer swelling.

Quantitative rebinding results were produced using HPLC and are shown in Figure 3.30. The results show rebinding of the EPD imprinted polymers (MIP_{EPD}) in comparison to the binding of that template to the NIP. The rebinding results for the ADR imprinted polymer discussed above are also included for comparison. Imprinting factors (*I*) (Equation 3) were calculated for each polymer system.

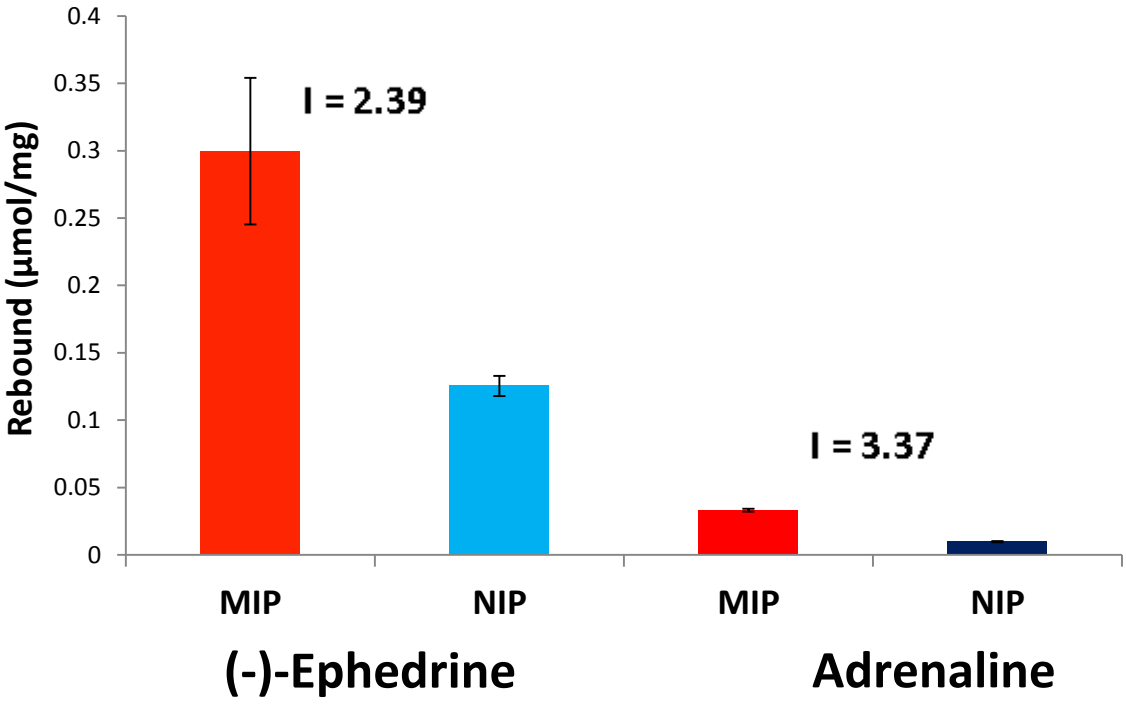

Figure 3.30 HPLC rebinding results for EPD and ADR imprinted PAA-IPA-MBA in aqueous 1mM template solutions. These studies were performed in duplicate.

The MIP_{EPD} showed high levels of rebinding with EPD, however an imprinting factor of only 2.39 was achieved due to the comparatively high levels of non-specific binding in the NIP, as shown in Table 3.2. In contrast, the MIP_{ADR} showed comparatively low levels of rebinding with ADR but achieved an imprinting factor of 3.37 due to the very low levels of non-specific binding in the NIP. The EPD imprinted polymers showed higher levels of rebinding, whilst the ADR imprinted polymers showed better selectivity for their respective templates.

Table 3.2 Template Rebinding and Imprinting Factors (I) for EPD imprinted PAA-IPA-MBA polymer

MIP Rebound (µmol/mg)	NIP Rebound (µmol/mg)	Imprinting Factor
299.2 ± 54.4	**125.4 ± 7.4**	**2.3**

NMR titrations for both templates yield comparable changes in chemical shift for similar protons in each template and molecular modelling also shows similar strengths in hydrogen bonding as indicated by bond length. Binding results however indicates that AA interacts more strongly with the EPD template resulting in higher levels of template rebinding. This also leads to an increase in non-specific binding as observed in the NIP, leading to a slight reduction in the imprinting factor.

The PAA-IPA-MBA system achieves produces excellent imprinting factors for both ADR and EPD indicating favourable binding of both templates. This shows that the PAA-IPA-MBA system used by Matsui et al.[68, 102] for the ADR template can be adapted for use with templates of forensic interest such as EPD.

3.2.6 Cross Reactivity Studies

After demonstrating the successful imprinting and subsequent rebinding of the EPD template using the PAA-IPA-MBA system, a selection of analytes were chosen to investigate the influence of structural character on the recognition qualities of MIP_{EPD}. Analytes possessing structural similarity to EPD, including: (1S,2R)-(+)-Ephedrine Hydrochloride (EPDHCL), (1S,2S)-(+)-Pseudoephedrine ((+)-PSEPD) and (1R,2R)-(-)-Pseudoephedrine ((-)-PSEPD) were selected to probe the enantiomeric and diastereomeric selectivity of the membrane; ADR to determine the effect of additional functionality on the aromatic ring; and Caffeine (CAFF) and Theophylline (THEO) to investigate the effects size, shape and electronic character on analyte binding. The structures of the chosen analytes are shown in Figure 3.31.

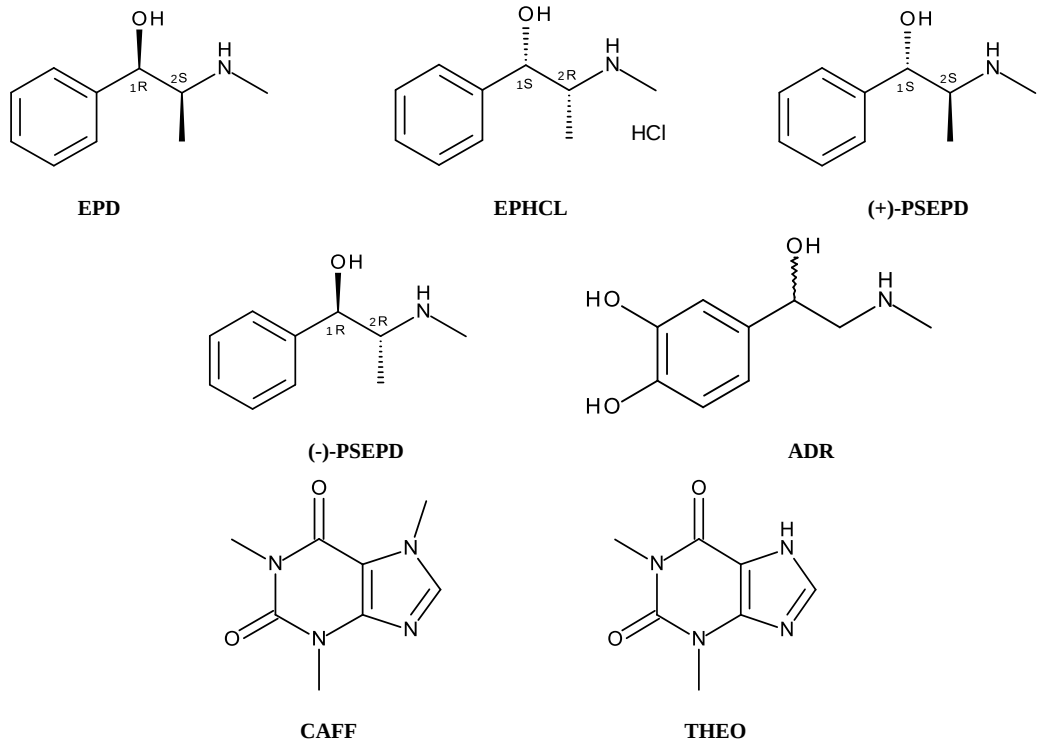

Figure 3.31 Structures of analytes selected for cross-reactivity studies

Cavity integrity within the PAA-IPA-MBA MIP_{EPD} was assessed by comparing analyte rebinding to the template. Figure 3.32 shows the cross-reactive binding of result for all the analytes.

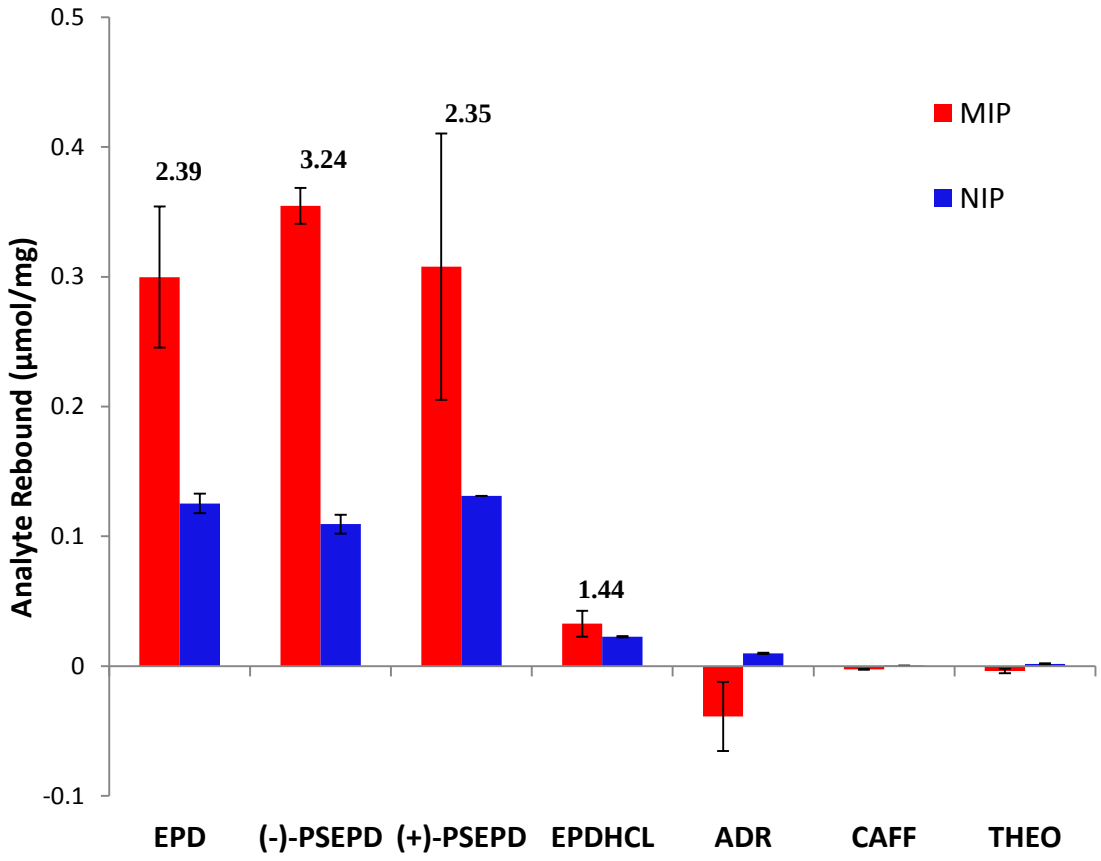

Figure 3.32 Cross reactive binding results for an EPD imprinted PAA-IPA-MBA polymer in 1mM solution of a range of analytes. Numbers above the data sets indicate corresponding imprinting factors. These studies were performed in duplicate.

The results show that the EPD imprinted polymer was incapable of discerning between stereoisomers. The polymer shows comparable selectivity towards (-)-PSEPD and (+)-PSEPD compared with that for EPDPS. The large degree of observed swelling during template rebinding is believed to result in a slight 'loosening' of the binding cavity, preventing chiral selectivity. This is due to the low cross-linked nature of the IPA-MBA hydrogel used in this polymer system compared to traditionally highly cross-linked polymers, which typically display a more rigid binding cavity[148]. Although the binding cavity is not as rigid as those formed in traditional MIP systems, sufficient size, shape and functionality is retained in the binding cavity to permit selectivity against non-structurally related analytes.

EPDHCl was shown to have a significantly reduced binding towards the MIP and NIP compared with the EPD free base form. Selectivity is also significantly reduced with an

imprinting factor of 1.44. Given that the both (-)-PSEPD and (+)-PSEPD show similar binding to EPD it is unlikely that the reduction in binding observed with EPDHCL relates to stereochemistry. As the amine is already protonated, the $EPDH^+$ is unable to form the acid-base interaction with the functional monomer (-COOH) in the binding cavity resulting in the observed decrease in selectivity. Additionally the presence of the chloride ion acts as a strong base in solution. Bulk imprinted polymers have been shown to typically possess relatively low binding kinetics which suggests the chloride ion may be outcompeting the imprinted polymer for the protonated EPD.

In the case of ADR, CAFF and THEO analytes, negligible binding was observed with the NIPs and a negative binding was observed for the MIPs. The negative binding result likely arises from preferential uptake of solvent during polymer swelling, resulting in an effective increase in analyte concentration. When rebinding with EPD, the significant amount of template rebound into the polymer results outweighs this concentration effect. However when rebinding with ADR, CAFF and THEO these analytes do not significantly rebind to the polymer. Since the amount of template rebound is calculated based on the concentration of the analyte in the remaining rebinding solution, solvent uptake due to polymer swelling combined with the lack of analyte binding results in net negative binding being observed.

ADR shows significantly reduced binding in both the MIP and NIP compared to EPD. The structures of the two compounds are very similar with the significant difference being the presence of the two ADR phenolic units. Since the size of ADR is only slightly longer than that of EPD (9.8Å compared to 9.5Å) it is unlikely that a size exclusion mechanism is solely responsible for the reduction in rebinding observed with ADR. The phenol units appear to sufficiently alter the electronic character of ADR so as to make it incompatible with the binding cavity.

The binding results of CAFF and THEO also show significantly reduced binding compared to EPD. These analytes show substantial differences in size, shape and functionality relative to the EPD template. The large difference in size and shape (6.4Å

wide x 7.4Å long for CAFF and THEO compared to 5.4Å x 9.5Å long for EPD) suggest that a size exclusion mechanism is likely responsible for to reduced binding observed with these analytes.

In summary, the cross reactivity studies have successfully shown that the EPD imprinted PAA-IPA-MBA polymer is highly specific to EPD indicating that the binding cavities in the MIP are selective to the template and will not accept analytes who size, shape or functionality differ significantly from that of the template. The PAA-IPA-MBA polymer cannot differentiate between stereoisomers of EPD suggesting some degree of 'looseness' in the binding cavity.

3.2.7 Incorporation of Gold Nanoparticles and UV-Vis Spectroscopic Rebinding Studies

MUA stabilised gold nanoparticles (Au_{MUA}) were incorporated into the pre-polymerisation mixture, which resulted in the mixture becoming distinctly coloured as seen in Figure 3.33. Following film formation, the PAA-IPA-MBA Au_{MUA} MIP, spectroscopic studies (UV-visible spectrophotometer) were performed to determine if a spectral shift in the plasmon absorbance band of the gold nanoparticles could be observed to mark template rebinding. As with the case with the ADR-imprinted MIP, no peak associated with the plasmon absorbance band was observed in the film spectrum. Measurements taken of the MIP_{EPD}-Au_{MUA} before and after template binding were comparable to those for the MIP_{ADR}-Au_{MUA} (Figure 3.15).

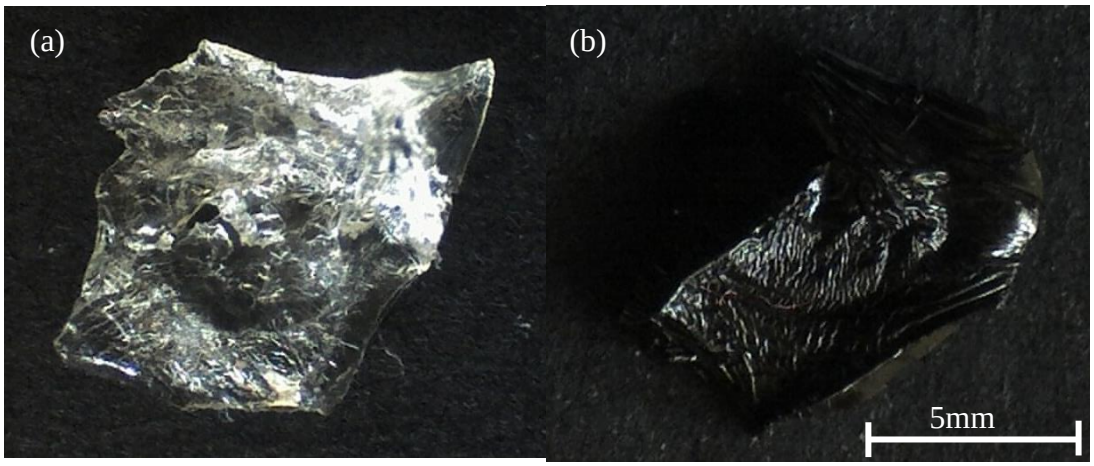

Figure 3.33 PAA-IPA-MBA MIPEPD with (b) and without (a) Au_{MUA}.

3.2.8 Summary

Pre-synthetic interactions studies utilising molecular modelling and NMR titrations were successfully used to identify AA as a suitable functional monomer for use with the EPD template. Additionally, a 1:1 template-monomer ratio was found to produce a strong acid-base interaction due to protonation of the EPD template. Further weaker interactions were also observed additional AA. These pre-synthetic studies also determined that EPD interaction with IPA and MBA is minimal making them ideal for use as a matrix monomer and crosslinker respectively.

Rebinding studies carried out after 24 hours showed significantly higher levels of EPD rebinding in the MIP compared to the NIP, with 2.39 imprinting factor obtained demonstrating that the PAA-IPA-MBA system is selective for the EPD template. This shows that the PAA-IPA-MBA system used by Matsui et al.[68, 102] for the ADR template can be adapted for use with templates of forensic interest such as EPD. In addition cross reactivity studies of EPD imprinted PAA-IPA-MBA polymers demonstrate high specificity against non-ephedrine based analytes.

Spectroscopic rebinding studies based on a shift on the plasmon absorbance of embedded gold nanoparticles during template rebinding were unsuccessful. Gold nanoparticles were successfully prepared and the plasmon absorbance band was observed in the UV-Vis spectrum, however this effect was unable to be replicated once the nanoparticles were embedded in PAA-IPA-MBA system. This in addition to the time needed for rebinding (>5 hours), makes the PAA-IPA-MBA system less than ideal for use as a forensic sensor which preferably require results as quickly as possible.

3.3 Poly(Acrylic Acid-*co*-Acrylonitrile-*co*-Methyl Methacrylate) – Ephedrine Template

Previous work within our group utilised an alternative polymer system of poly(acrylic acid-*co*-acrylonitrile-*co*-methyl methacrylate) (PAA-AN-MMA). Template rebinding in this system occurs rapidly - as little as 10 minutes after immersion in the rebinding solution, offering potentially significant improvement over the PAA-IPA-MBA film[138]. For this reason, an assessment of the poly(acrylic acid-*co*-acrylonitrile-*co*-methyl methacrylate formulation was undertaken.

3.3.1 Ephedrine-Matrix Monomer Molecular Modelling

The molecular modelling results for EPD with the matrix monomers acrylonitrile (AN) and methyl methacrylate (MMA) are compared with those for AA in Figure 3.34.

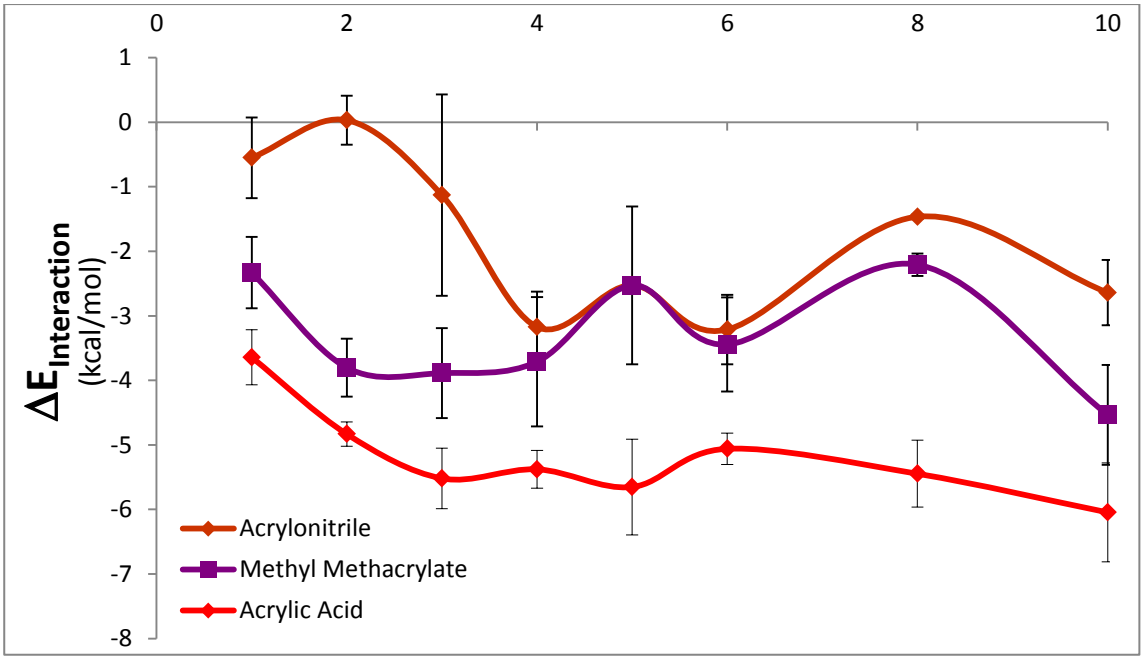

Figure 3.34 $\Delta E_{interaction}$ of EPD with AA, AN and MMA across a range of M-T ratios.

From Figure 3.34 it can be seen that the $\Delta E_{Interaction}$ for AN with EPD are all negative in value, signifying favourable interaction with the template. These interaction energies

were however significantly less favourable than the cluster energies produced by acrylic acid, indicating that AA associates more strongly with the template.

The modelling results indicate hydrogen bonding interactions involving the EPD secondary amine and hydroxyl functional groups. The 4:1 AN – EPD cluster that produced the highest $\Delta E_{Interaction}$ is also shown below in Figure 3.35. At ratios greater than 4:1, modelling indicates that the presence of additional functional monomer units does not produce additional interactions with the template.

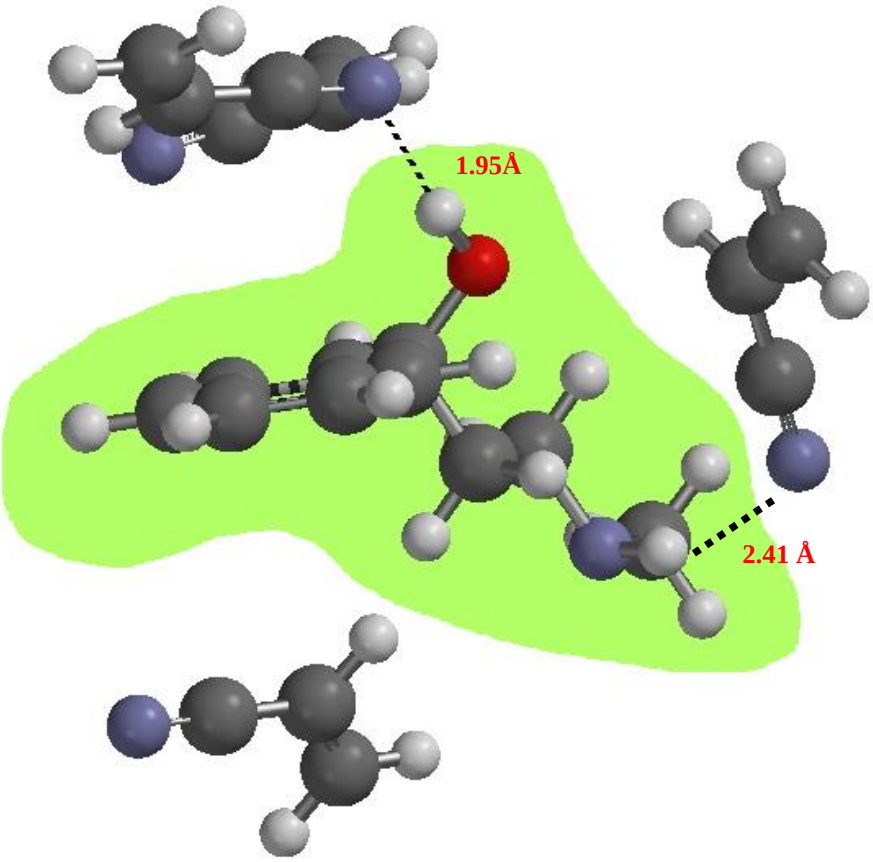

Figure 3.35 Molecular modelling of EPD with 4 AN showing a single point of interaction. Template is shaded green and hydrogen bond distances are indicated in red.

Hydrogen bond distances for AN with EPD are long (≥1.95Å) suggesting relatively weak interactions compared to those found in the AA clusters. These results suggest that AN monomers will form weaker interactions with the EPD than the AA units.

From Figure 3.34 it can be seen that the $\Delta E_{Interaction}$ for MMA with EPD are likewise all negative, signifying favourable cluster formation. While MMA interaction energies

indicate less favourable template-functional monomer associations relative to AA, the modelled system demonstrating the lowest $\Delta E_{Interaction}$ (Figure 3.34) indicates hydrogen bonds of comparable length, suggesting similar strengths. Ratios of 5:1 and greater showed no additional monomer-template interactions. These higher stoichiometries have a detrimental effect on interaction energy, presumably through increased steric factors.

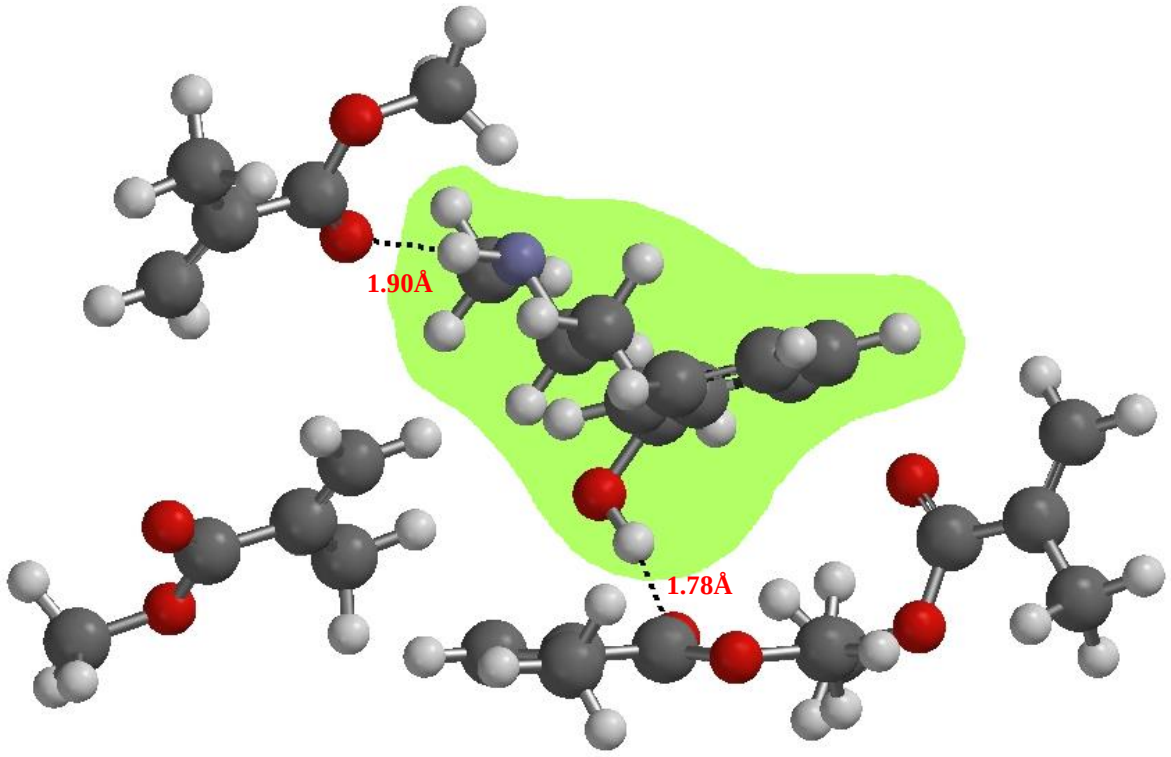

Figure 3.36 Molecular modelling of EPD with 4 MMA showing two points of interaction. Template is shaded green and hydrogen bond distances are indicated in red.

Due to the functionality of both AN and MMA, both monomers are only capable as acting as hydrogen bond donors, whereas AA possesses both donor and acceptor functional groups. As a result, AN and MMA from only single point interactions with amine and alcohol protons of EPD, whereas AA is observed to form additional hydrogen bonds with the nitrogen and oxygen atoms themselves. Simultaneous modelling of EPD with both AA and MMA has suggests that in a competitive situation AA forms stronger interactions than MMA[139].

It should be noted that at low monomer-template ratios (≤ 5:1), AN and MMA show comparable or better interaction energies than those observed for both IPA and MBA (Figure 3.3) used in the previous model system.

3.3.2 NMR Studies

NMR titration between the EPD template and the matrix monomers (AN and MMA) were performed to assess interactions previously identified through molecular modelling. Figure 3.37 and 3.38 show the extent of the downfield shifts of the EPD protons as a function of the template-monomer ratio during titration with AN and MMA respectively.

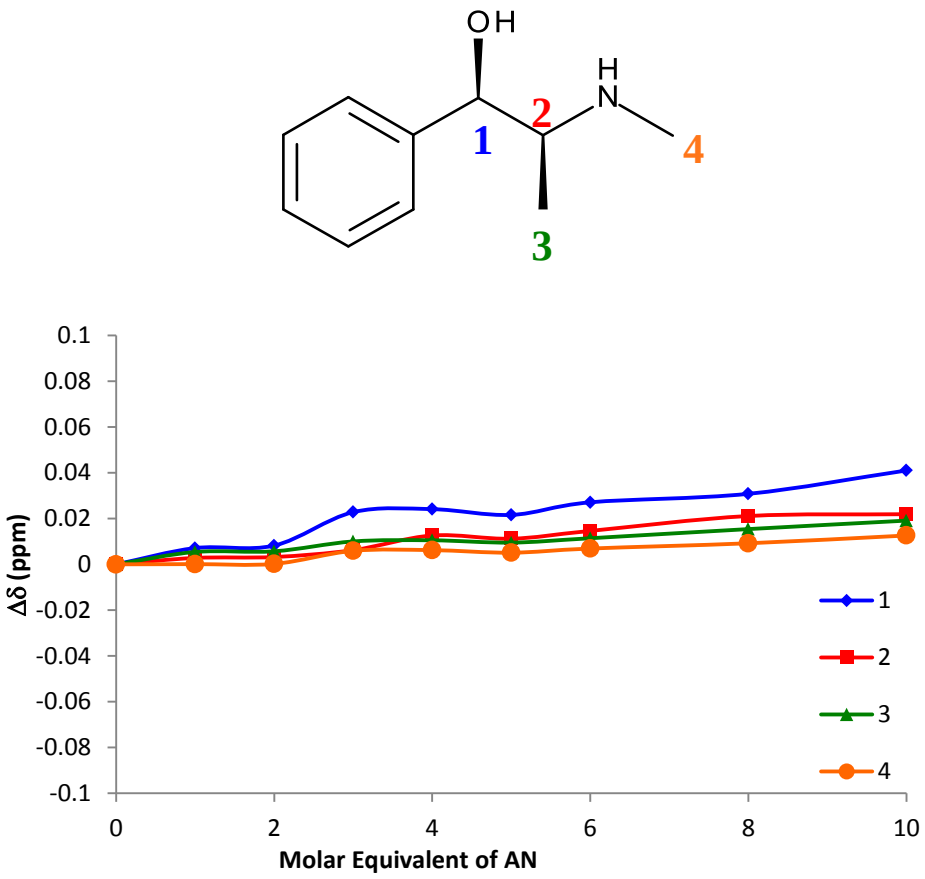

Figure 3.37 Change in chemical shift (Δδ) of different EPD protons upon titration with increasing molar equivalents of AN in $CDCl_3$. EPD structure is included above to show labelling of protons.

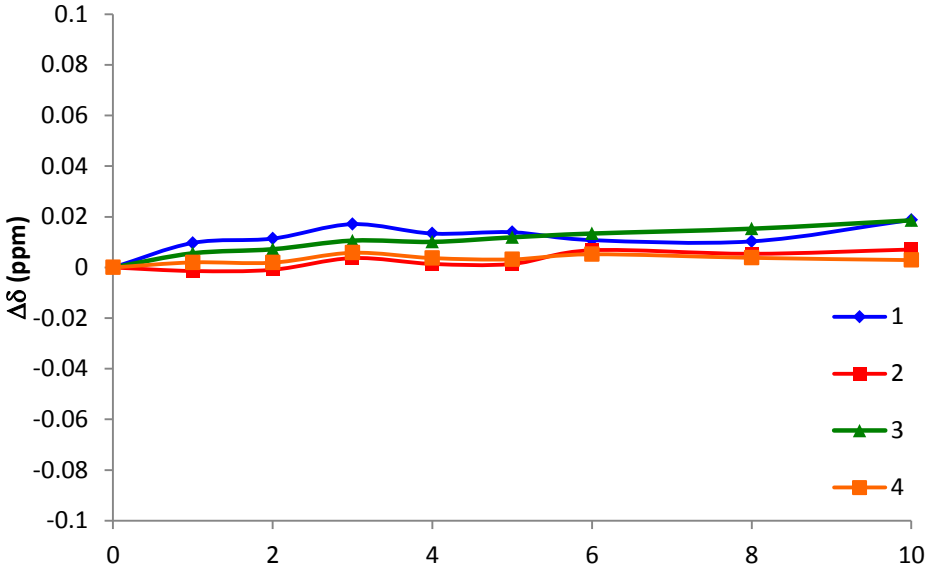

Figure 3.38 Change in chemical shift (Δδ) of different EPD protons upon titration with increasing molar equivalents of MMA in $CDCl_3$. EPD structure is included above to show labelling of protons.

These results demonstrate comparatively small (<0.05ppm) chemical shift of the EPD protons during the titration with both monomer units, suggesting that neither monomer interacts significantly with the EPD template, despite some interaction being predicted based on the molecular modelling studies.

The combination of results obtained from molecular modelling and NMR titrations indicate that the IPA and MBA will not significantly interact with the EPD template, when compared to AA functional monomer. This makes them suitable for use as matrix monomers, providing bulk and structural support to the polymer but having little affinity for the template.

3.3.3 Polymer Preparation

Molecular modelling and NMR studies above demonstrated that AA is a suitable functional monomer for use with an EPD imprinted polymer. A co-polymer of AA, AN and MMA was prepared in the absence of the template. The polymer includes AA as the functional monomer, however the bulk of the polymer is composed of AN and MMA

whose primary role, as matrix monomers, is to provide the bulk and rigidity required to support the formation of template cavities in the absence of a crosslinker species. Since the matrix monomers account for a large proportion of the polymer composition they also play a significant role in determining the physical properties of the resulting polymer.

The use of an AN-based polymer, with an AA functional monomer, was previously investigated by this author for cocaine imprinted MIPs. The resulting polymer films were of good quality and achieved imprinting factors of 4.4 after only 10 minutes of binding. AN is frequently used as a matrix monomer in film formation, as it has been shown to produce good quality films that are both flexible and porous. In addition, AN polymers are typically resistant to most solvents, making them robust and reusable.

The use of MMA as a matrix monomer has also been investigated by Brisbane et al.[138-139] and has been shown to result in films possessing uniform structure and porosity which leads to improved performance characteristics (selectivity and reproducibility). The particular polymer composition of the P(AA-AN-MMA) used herein was previously shown to produce high quality polymeric films using the phase inversion technique.

The absence of a cross-linking monomer in the PAA-AN-MMA copolymer formulation allows for dissolution in a polar aprotic solvent such dimethyl sulfoxide (DMSO). The EPD template can then be incorporated into the polymer solution in a 1:3 molar ratio (based on the quantity of AA present in the polymer) in a process known as post-polymerisation imprinting.

EPD imprinted polymers (MIP_{EPD}) were produced together with a non-imprinted control polymer (NIP). Immersion precipitation or wet phase inversion was used to produce polymeric films by coating a substrate with a thin layer of the polymer solution, followed by immersion in a coagulation (insoluble to polymer) bath. Diffusion between the solvent and non-solvent results in the precipitation of the polymer onto the substrate. If a flat substrate is used during polymer precipitation then a flat membrane or film forms. Examples of the produced films ($MIPf_{EPD}$ and NIPf) are seen in Figure 3.39.

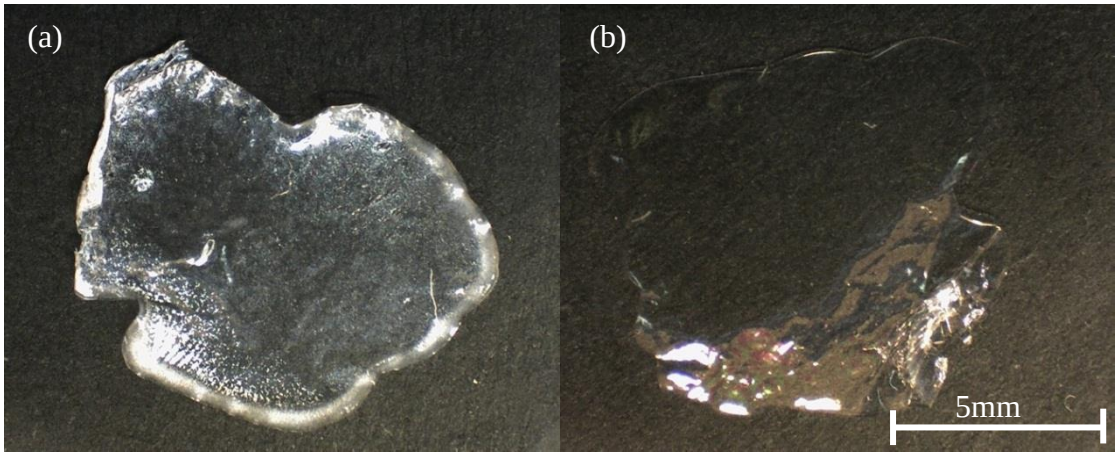

Figure 3.39 PAA-AN-MMA films; $MIPf_{EPD}$ (a) and NIPf (b)

The incorporation of EPD into the polymers was again confirmed qualitatively by FTIR spectroscopy. The prominent peak at approximately 700cm^{-1}, corresponding to the out of plane bending of the aromatic hydrogen, was again used to assess presence of EPD.

Figure 3.40 show the spectra of a non-imprinted polymer film (NIPf), an as synthesized or virgin EPD imprinted polymeric film (V-$MIPf_{EPD}$) and an extracted EPD imprinted polymeric film (Ex-$MIPf_{EPD}$). The presence of the diagnostic EPD peak in the V-$MIPf_{EPD}$ demonstrates that EPD has been successfully incorporated into the imprinted polymer. The absence of the peak in the NIP and Ex-MIP_{EPD} indicates that the EPD is not present in the NIP and can be successfully removed from the MIP through the extraction process.

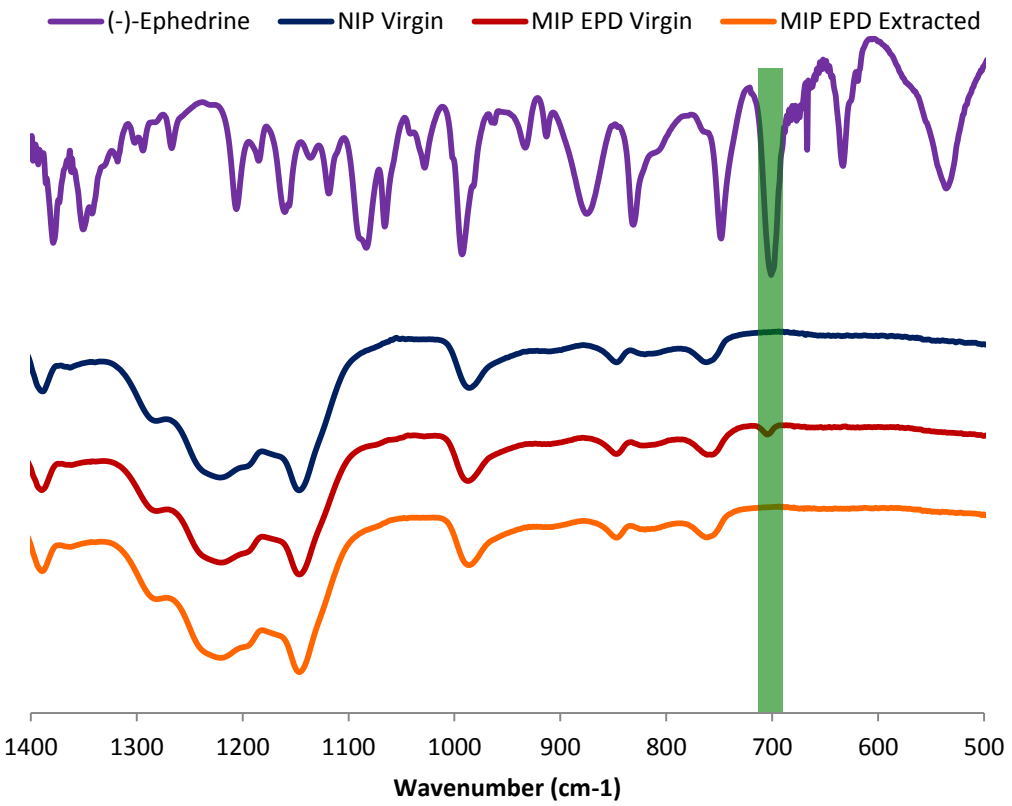

Figure 3.40 FTIR spectra of pure EPD (a), and PAA-AN-MMA; Non-imprinted polymer (NIPf) (b), Virgin EPD imprinted polymer (V-MIPf$_{EPD}$) (c), and Extracted EPD imprinted polymer (Ex-MIPf$_{EPD}$) (d). The diagnostic peak (700cm^{-1}) used to determine the presence of EPD is shaded.

3.3.4 Rebinding Studies

The success of the rebinding following template extraction was again assessed qualitatively using FTIR according to the re-emergence of the EPD peak as seen in Figure 3.41. The diagnostic EPD peak observed in the V-MIP$_{EPD}$ and absent in the Ex-MIP$_{EPD}$, is again observed in the rebound EPD imprinted films (Rb-MIP$_{EPD}$) indicating successful rebinding of the EPD into the polymer. Additionally this diagnostic peak is absent from the spectra of the non-imprinted polymer following rebinding (Rb-NIP), indicating that the EPD template does not bind to the NIP.

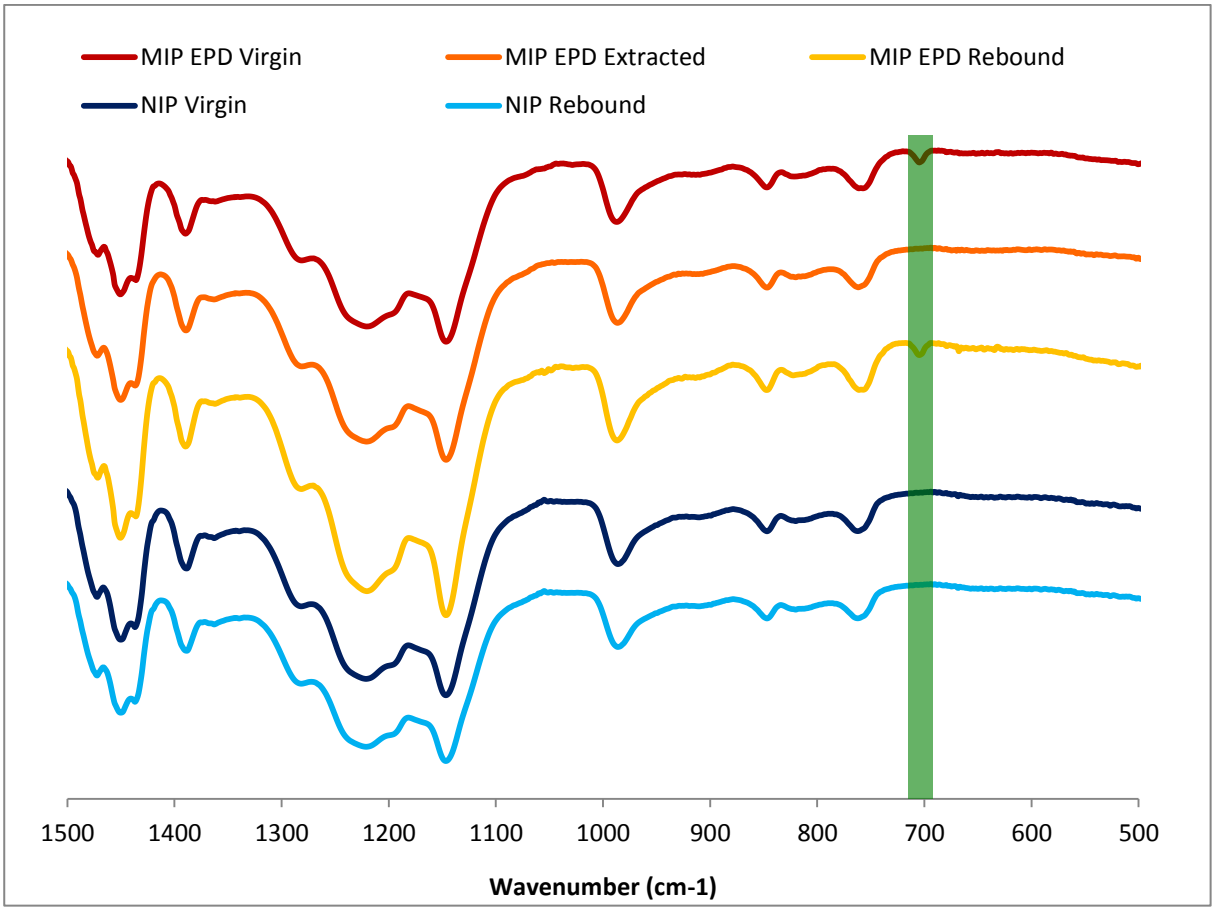

Figure 3.41 FTIR spectra of (a) Virgin EPD imprinted polymer (V-MIP_{EPD}), (b) EPD imprinted polymer (Ex-MIP_{EPD}), (c) Rebound EPD imprinted polymer (Rb-MIP_{EPD}), (d) Virgin non-imprinted polymer (V-NIP and (e) Rebound non-imprinted polymer (Rb-NIP). The diagnostic peak used to determine the presence of EPD is shaded.

Quantitative rebinding results were produced using HPLC for a number of rebinding times ranging from 10 minutes to 24 hours. Figure 3.42 show rebinding of the imprinted polymers with EPD in comparison to the binding of EPD to the NIP. Imprinting factors (*I*) (Equation 3) were calculated for each rebinding time and shown in Table 3.3.

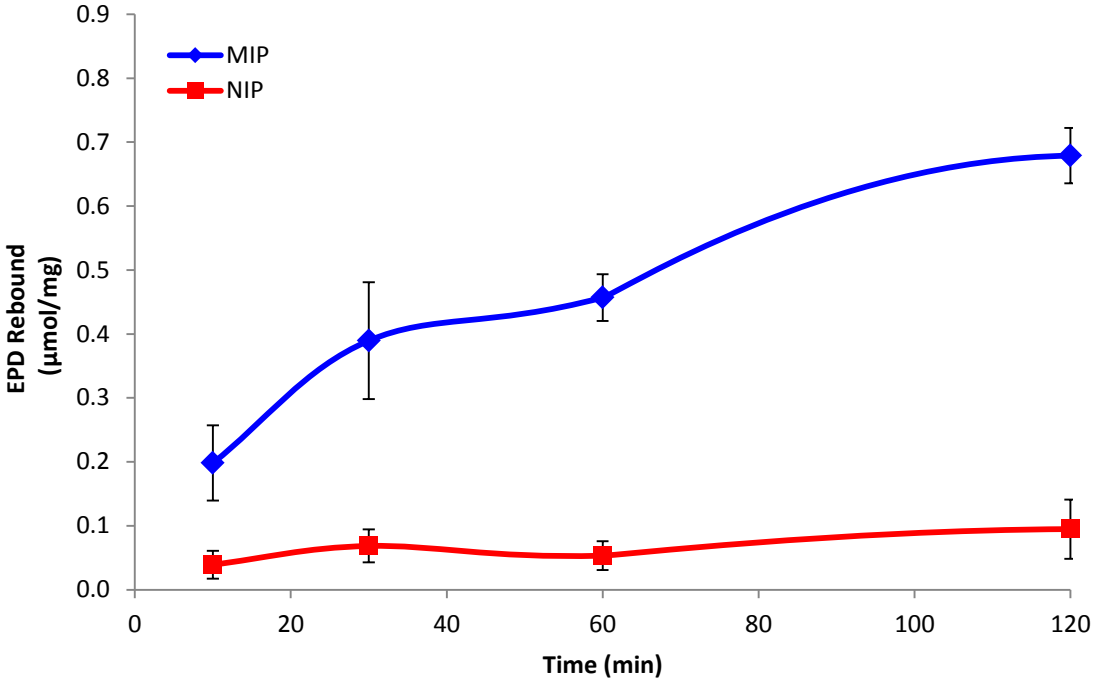

Figure 3.42 HPLC rebinding results for PAA-AN-MMA in 1mM EPD solution. Rebinding was also measured after 24 hours with no significant additional binding observed. Rebinding study was performed in triplicate.

Table 3.3 Imprinting Factors (I) for EPD imprinted PAA-AN-MMA polymer as a function of time.

Time (min)	MIP Rebound (µmol/mg)	NIP Rebound (µmol/mg)	Imprinting Factor
10	0.20 ± 0.06	0.04 ± 0.02	5.0
30	0.39 ± 0.09	0.07 ± 0.03	5.7
60	0.46 ± 0.04	0.05 ± 0.02	8.6
120	0.68 ± 0.04	0.09 ± 0.04	7.2
1440	0.70 ± 0.08	0.14 ± 0.06	5.1

The PAN-AA-MMA system shows significantly higher EPD rebinding in the MIP_{EPD} for all time periods compared to the NIP. After 10 minutes, the MIP_{EPD} shows rebinding of 0.20µmol/mg compared to 0.04µmol/mg in the corresponding NIP (imprinting factor = 5.04). Rebinding in the MIP_{EPD} increases linearly until t= 2 hours (rebinding = 0.68µmol/mg) whereupon saturation is reached allowing only an additional 0.02µmol/mg of template to be rebound at t=24 hours. Rebinding in the case of the NIP shows a less steep binding profile, suggesting low relative specificity attributable to non-specific surface binding. Plateauing also occurs after approximately 2 hours suggesting that similar mass transfer kinetics occur in both the imprinted and non-imprinted films. The

imprinting factor exceeds 5 for all time periods with maximum selectivity (I = 8.58) achieved at t = 1 hour.

The high imprinting factors achieved for the PAA-AN-MMA system combined with the short rebinding time period required makes this system far more suited to forensic sensing applications. The PAA-AN-MMA system was therefore chosen for further investigation with gold nanoparticles.

3.3.5 Gold Nanoparticle Preparation and Incorporation

11-Mercaptoundecanoic acid stabilised gold nanoparticles (Au_{MUA}) were successfully prepared and incorporated into the PAA-AN-MMA polymer during post-polymerisation imprinting. A concentration of 32.4 wt.% of gold nanoparticles in the polymeric films was used similar to the wt.% used by Matsui et al. in their polymer system. Incorporation of the nanoparticles into the polymer matrix following phase inversion was visually confirmable due to the distinct colour accompanying the inclusion of the nanoparticles (Figure 3.43 b). No visible leaching of gold nanoparticles from the polymer films was observed to occur during film formation.

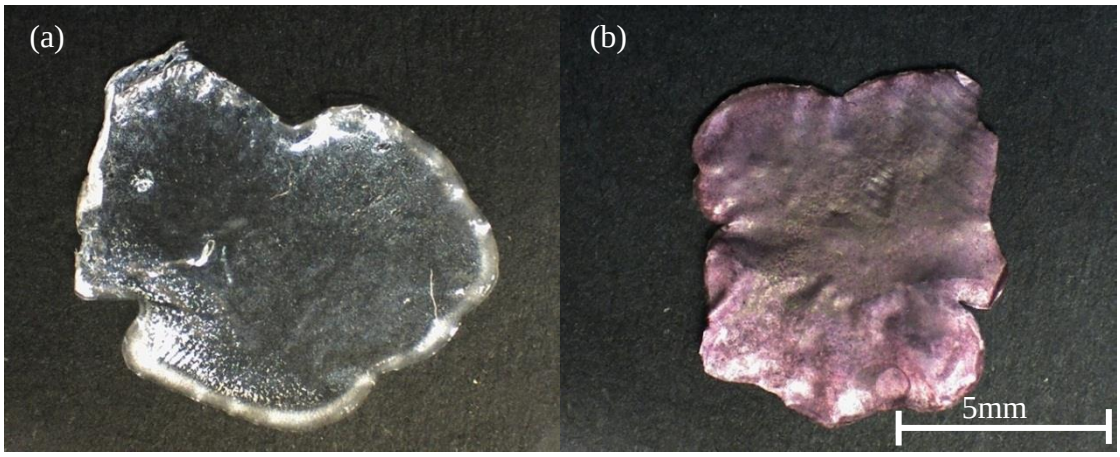

Figure 3.43 PAA-AN-MMA MIP_{EPD} films without (a) and with (b) embedded Au_{MUA}

3.3.6 Rebinding Studies

Following template extraction (confirmed by FTIR), film selectivity was quantitatively assessed using HPLC for a number of rebinding times ranging from 10 minutes to 24 hours. Figure 3.44 shows rebinding of the imprinted polymer MIP_{EPD}-Au_{MUA} with EPD in comparison to NIP-Au_{MUA}. Imprinting factors (*I*) (Equation 3) were calculated for each rebinding time and shown in Table 3.4.

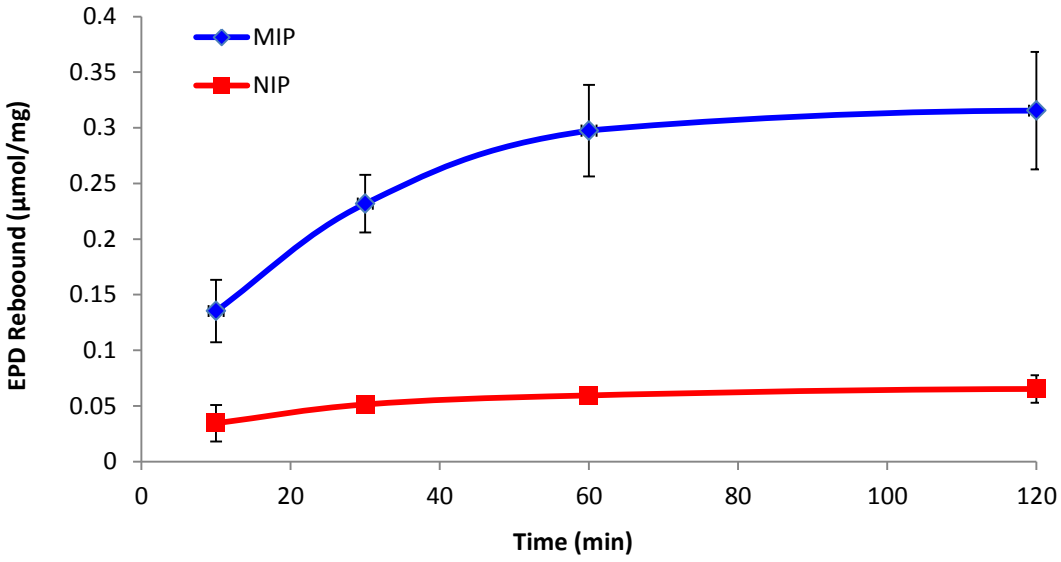

Figure 3.44 HPLC rebinding results for EPD with PAA-AN-MMA-Au_{MUA}. Rebinding was also measured after 24 hours with no significant additional binding observed.

Table 3.4 Imprinting Factors (I) for PAA-AN-MMA-Au_{MUA}.

Time (min)	MIP Rebound (µmol/mg)	NIP Rebound (µmol/mg)	Imprinting Factor
10	0.14 ± 0.02	0.03 ± 0.02	3.9
30	0.23 ± 0.03	0.05 ± 0.02	4.5
60	0.30 ± 0.04	0.05 ± 0.01	5.0
120	0.32 ± 0.06	0.07 ± 0.02	4.8
1440	0.30 ± 0.08	0.08 ± 0.01	4.0

The gold embedded PAA-AN-MMA-Au_{MUA} film shows higher rebinding across all time periods compared to the control. After 10 minutes, the MIP_{EPD} has rebound 0.13µmol/mg compared to 0.03µmol/mg in the corresponding NIP resulting in an imprinting factor of 3.93. Rebinding in the MIP_{EPD} increases steadily until plateauing at approximately 1 hour and with a maximum of 0.32µmol/mg after 2 hours. Rebinding in

the NIP increases very little with time and after 24 hours the maximum amount of template rebound to the NIP is 0.08μmol/mg.

By comparing Figure 3.44 with Figure 3.42 above, it can be seen that the inclusion of Au_{MUA} causes a significant decrease in the rebinding of the MIP. However since the rebinding of the NIP is reduced by less than of the MIP, the resulting imprinting factors are also reduced.

The relatively small difference in the rebinding of the NIP with the inclusion of the Au_{MUA} indicates that there is no significant change in non-selective binding as a result of the gold nanoparticles. This signifies that the gold nanoparticles themselves are not binding to the EPD to cause the drop in MIP binding. The reduction in MIP binding is therefore likely caused by either by the gold occupying the binding the binding cavities or by hindering template access to the cavities.

Despite this drop in binding of the MIP imprinting factors of at least 1.90 are still achieved for all time periods with the maximum of 3.72 occurring after 1 hour.

3.3.7 UV-Vis Spectroscopic Rebinding Studies

Following evaluation of the rebinding of the PAA-AN-MMA system with embedded AU_{MUA} by HPLC, spectroscopic studies of the films were carried out to determine if any colourimetric shift in the plasmon absorbance of the gold nanoparticles is observed during template rebinding.

Measurements were then taken of the MIP_{EPD}-Au_{MUA} and NIP-Au_{MUA} in 1mM EPD to determine the effect of the template on the plasmon absorbance of the embedded Au_{MUA}. An example of the shift in spectrum is shown below in Figure 3.45, with a clear hypsochromic being observed during EPD rebinding. The shift in peak wavelength is

also shown to be reversible with peak absorbance of the PAA-AN-MMA-Au_{MUA} film resembling that observed prior to EPD binding.

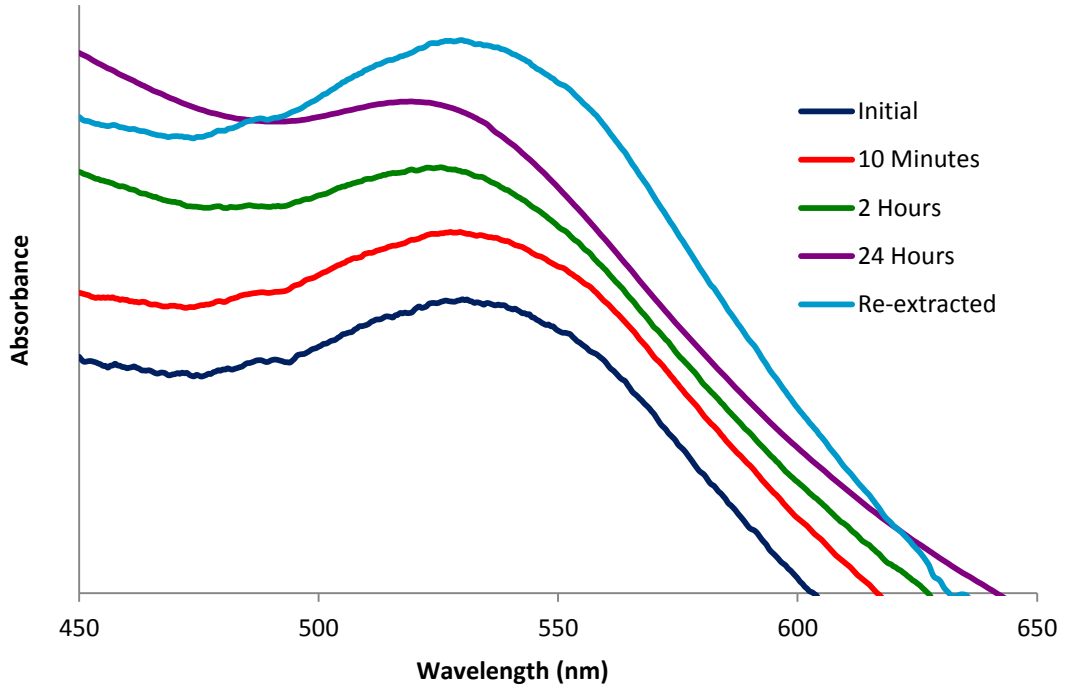

Figure 3.45 UV-Vis spectra of PAA-AN-MMA-Au_{MUA} in 1mM EPD over 24 hours and following re-extraction.

Initial measurements were also taken of the MIP_{EPD}-Au_{MUA} and NIP-Au_{MUA} in water to determine the effect of swelling from the solvent. Peak position in these polymers remains steady for both the MIP_{EPD}-Au_{MUA} and NIP-Au_{MUA} at approximately 532nm and shifting no more than 1 nm. A significant hypsochromic shift is seen in the spectra of both the MIP_{EPD}-Au_{MUA} and NIP-Au_{MUA} with the peak in the NIP-Au_{MUA} shifting 8nm to 525nm and the MIP_{EPD}-Au_{MUA} shifting 15nm to 518nm. Figure 3.46 shows the shift in peak wavelength of gold nanoparticles for MIP_{EPD}-Au_{MUA} and NIP-Au_{MUA} in both 1mM EPD and water from 10 minutes to 2 hours. A detectable shift is observed after as little as 10 minutes offering a significant improvement over the PAA-IPA-MBA system used by Matsui et al.

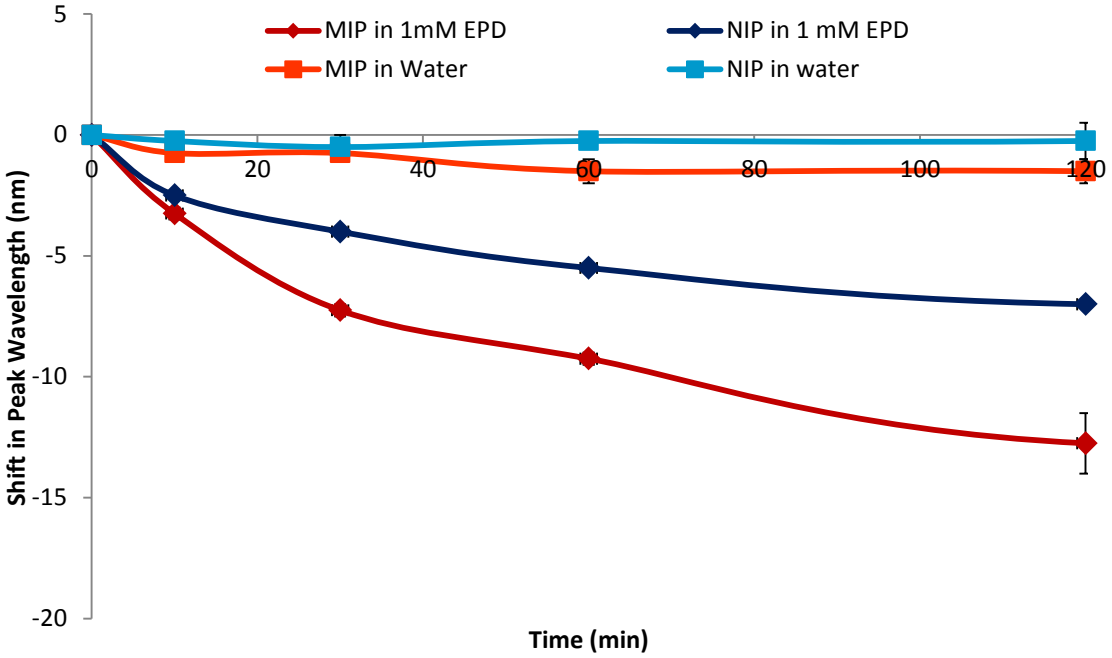

Figure 3.46 Peak shift of PAA-AN-MMA-Au_{MUA} in 1mM EPD. Peak shift was also measured after 24 hours with no significant additional shiftobserved.

This result demonstrates that gold nanoparticles can be incorporated into the PAA-AN-MMA system and used to produce a viable method of detection through a shift in the UV spectrum of the gold nanoparticles.

Figure 3.47 compares the peak shift in the UV-Vis spectrum observed during template rebinding with the quantitative rebinding results obtained via HPLC. A direct comparison of these results in Figure 3.48 shows a direct correlation (R = 0.99) between amount EPD rebound to the polymer (as determined by HPLC) and the shift in the peak absorbance of the embedded Au_{MUA}. This allows for the possibly of quantitative detection of the EPD template based on the observed shift in the UV-Vis spectrum.

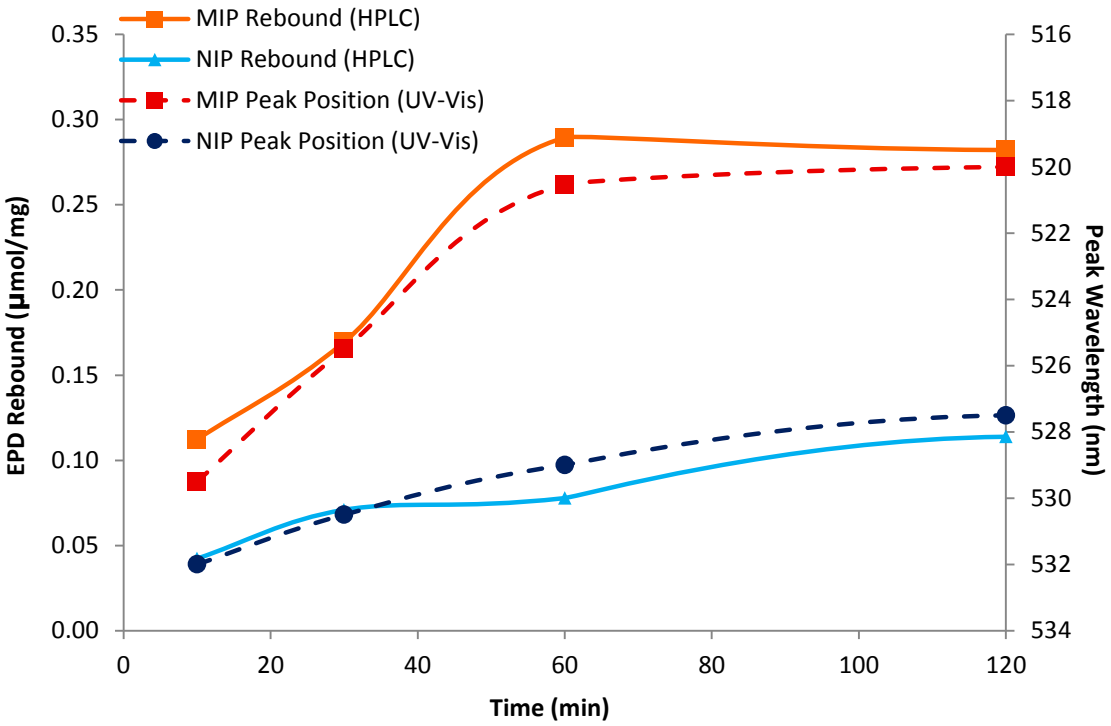

Figure 3.47 HPLC rebinding results compared with peak shift for PAA-AN-MMA-Au_{MUA} in 1mM EPD.

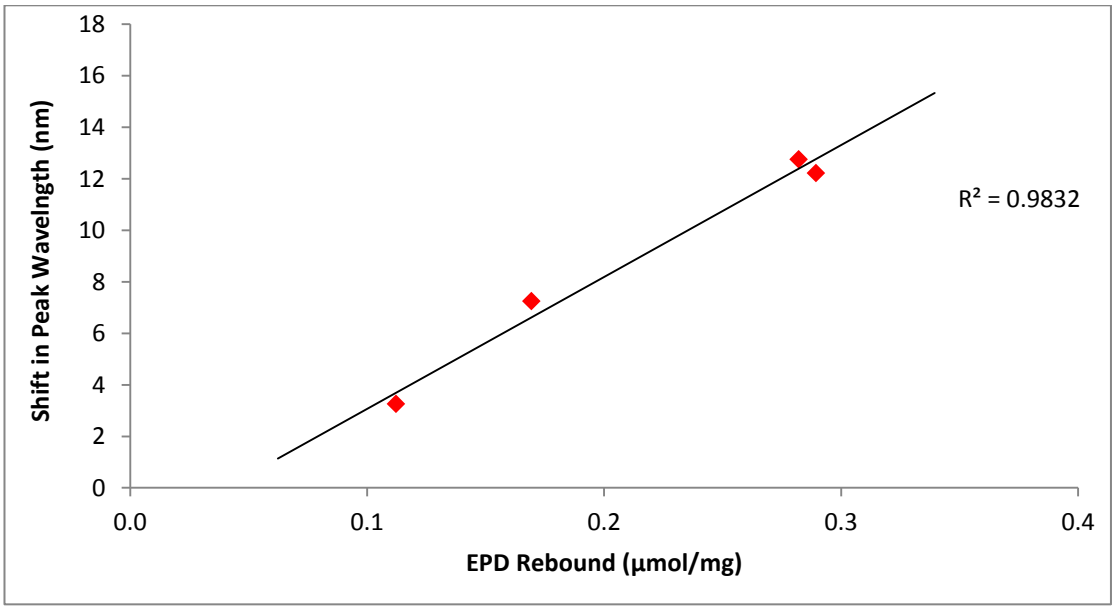

Figure 3.48 Peak shift of PAA-AN-MMA-Au_{MUA} compared to amount of EPD template rebound as determined by HPLC.

PAA-AN-MMA-Au_{MUA} polymers were rebound in increasing EPD concentration to investigate the effect of template concentration on the UV-Vis absorbance of the

embedded Au_{MUA}. Concentrations from 0.01 to 5M were used with the results shown in Figure 3.49.

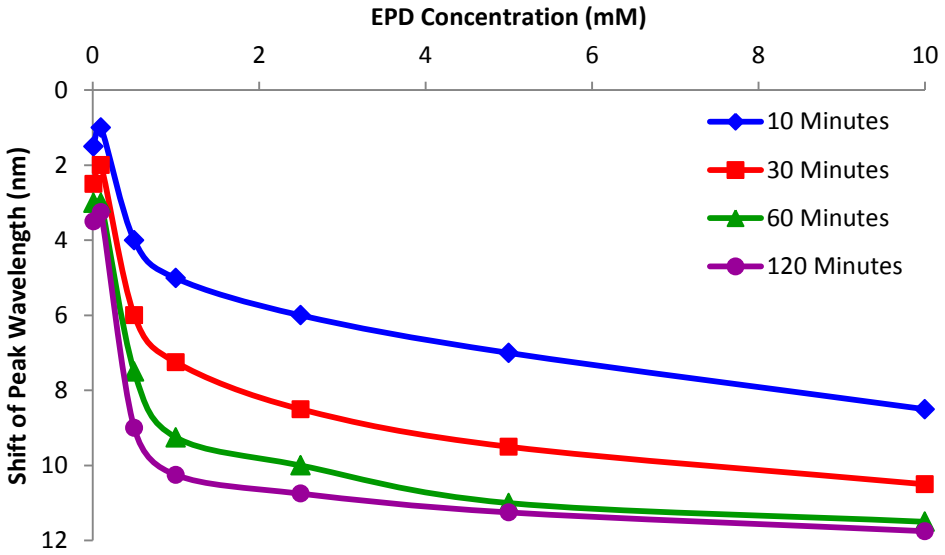

Figure 3.49 Peak shift of PAA-AN-MMA-Au_{MUA} in increasing EPD concentrations.

A concentration dependant response is observed in the shift produced in the ultraviolet spectrum of the embedded gold nanoparticles. Higher concentrations of EPD during rebinding produce a larger shift in ultraviolet spectrum.

The effect of gold nanoparticle concentration in the PAA-AN-MMA-Au_{MUA} polymers on the UV-Vis absorbance of the resulting polymer films was also investigated. PAA-AN-MMA-Au_{MUA} films were prepared with varying concentrations of gold nanoparticles as described in Table 3.5 below.

Table 3.5 PAA-AN-MMA-Au_{MUA} films prepared with varying gold nanoparticle concentrations

Polymer Code	Mass of PAA-AN-MM	Mass of Au_{MUA}	Au_{MUA} Wt.%
PAA-AN-MMA-Au_{MUA}	75 mg	36 mg	32.4
PAA-AN-MMA-0.5Au_{MUA}	75 mg	18 mg	19.4
PAA-AN-MMA-2Au_{MUA}	75 mg	72 mg	49.0

The UV-Vis spectra of these films, shown in Figure 3.50, exhibit a clear difference in the peak absorbance as a result of changes in the concentration of gold nanoparticles.

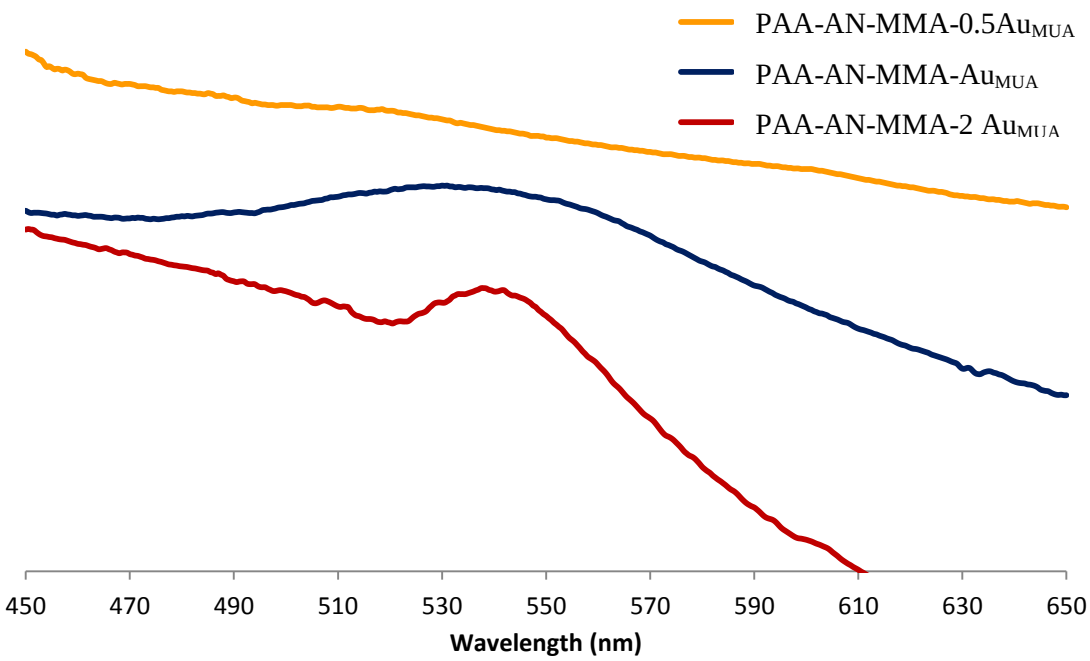

Figure 3.50 UV-Vis spectra of PAA-AN-MMA-Au$_{MUA}$, PAA-AN-MMA-2Au$_{MUA}$ and PAA-AN-MMA-0.5Au$_{MUA}$ films.

Increasing the concentration of gold nanoparticles resulted in a bathochromic, or red, shift in the wavelength of peak absorbance. The increase in concentration of the gold nanoparticles results in a decrease in their interparticle distance resulting in the observed shift in the surface plasmon resonance absorbance. The increase in concentration also allows the peak caused by the absorbance of the gold nanoparticles to be more easily distinguished from the absorbance of the polymer itself. Conversely a decrease in the concentration of gold nanoparticles results in a hypsochromic shift in the wavelength of peak absorption due to an increase in interparticle distance. Furthermore the decrease in concentration significantly decreases the absorbance due to the gold nanoparticles and is difficult to distinguish from the absorption due to the polymer itself.

The PAA-AN-MMA-2Au$_{MUA}$ films were rebound in 1mM EPD and the shift in the wavelength of peak absorbance was observed over 24 hours. These results are

compared to those for PAA-AN-MMA-Au_{MUA} in Figure 3.51. Rebinding for PAA-AN-MMA-0.5Au_{MUA} was also performed, however the wavelength of peak absorption was unable to be reliably determined and so these results are not reported.

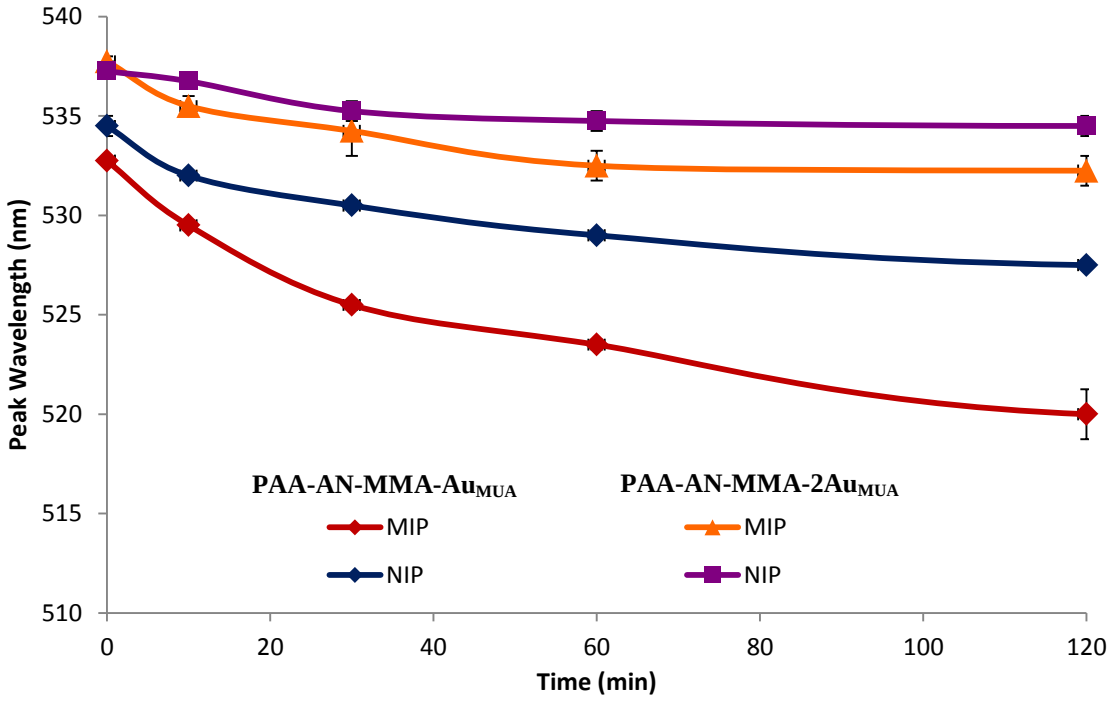

Figure 3.51 Effect of gold nanoparticle concentration on peak shift of PAA-AN- MMA-Au_{MUA} in 1mM EPD. Peak shift was also measured after 24 hours with no significant additional peak shift observed.

A hypsochromic shift is still seen in the spectra of both the MIP_{EPD}-2Au_{MUA} and NIP-2Au_{MUA} following EPD rebinding. These shifts, with the peak in the NIPf-Au_{MUA} shifting 2.5nm to 534.5nm and the $MIPf_{EPD}$-Au_{MUA} shifting 5.5nm to 532nm, are substantially lower than those observed for the for the original PAA-AN-MMA-Au_{MUA} system. This suggests that the increase in nanoparticle concentration produces a smaller relative change in interparticle distance as a result of template rebinding.

3.3.8 Cross Reactivity Studies

After demonstrating the successful rebinding of the EPD template using the PAA-AN-MMA-Au_{MUA} system, the analytes shown in Figure 3.31 were again used to investigate the effect of various factors on the ability of the analyte to rebind to the EPD imprinted polymers. A series of cross reactivity studies were undertaken by which the degree of

binding by each analyte to the MIP_{EPD} was determined. Figure 3.52 shows the cross reactive binding of result for these analytes.

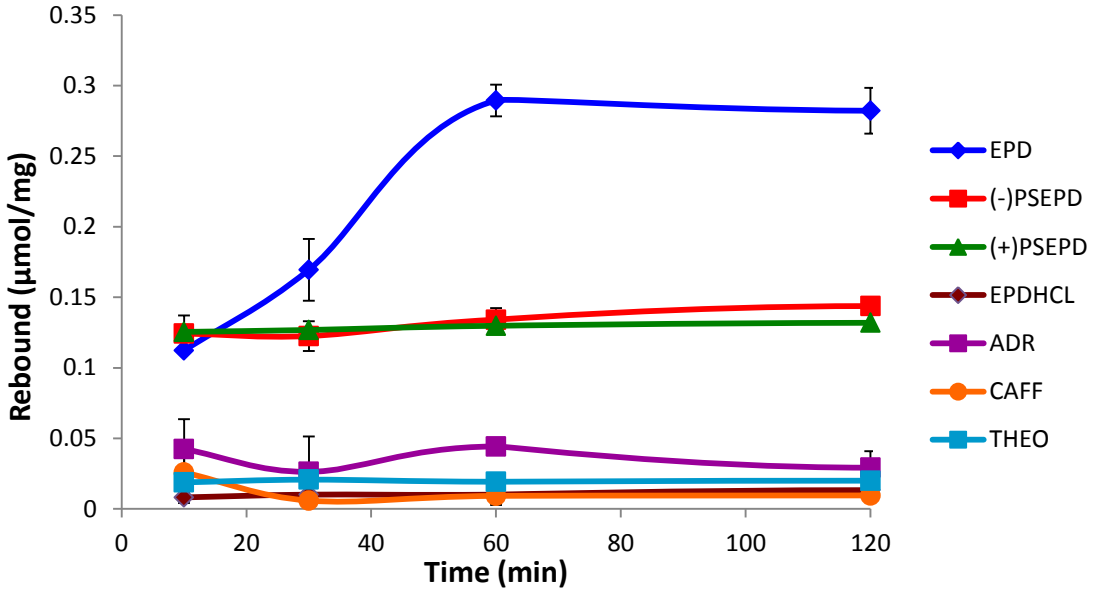

Figure 3.52 Cross reactive binding results showing the analyte binding to a PAA-AN-MMA-Au_{MUA} MIP_{EPD}. Rebinding was also measured after 24 hours with no significant additional binding observed.

Figure 3.52 demonstrates that after 10 minutes the polymer shows a similar levels of binding for EPD, (-)-PSEPD, and (+)-PSEPD of approximately 0.2µmol/mg. After 30 minutes 0.2µmol/mg of EPD is rebound however no additional (-)-PSEPD or (+)-PSEPD is observed to rebind. The binding of EPD increases to a maximum of 0.34µmol/mg after 24 hours whilst binding of (-)-PSEPD and (+)-PSEPD does not significantly increase. These results demonstrate that while significant amounts of (-)-PSEPD and (+)-PSEPD are shown to rebind to the polymer the polymer is capable of differentiating stereoisomers. This suggests a more rigid binding cavity than that observed with the PAA-IPA-MBA system, which was incapable of differentiating between EPD stereoisomers.

EPDHCL was shown to have a significantly reduced binding compared with its EPD enantiomer. This result is similar to that observed with the PAA-IPA-MBA system, and again is likely due to the competitive binding of the chloride ion in the binding solution.

ADR shows significantly reduced binding compared to EPD. The structures of the two compounds are very similar with the significant difference being addition of two phenolic groups in ADR. ADR is only slightly longer than that of EPD (9.8Å compared to 9.5Å), so it is unlikely that a size exclusion mechanism is solely responsible for the reduction in rebinding observed with ADR. The change in electronic character of the ADR due to the presence of the phenol groups appears, in addition to the slight increase in size, appears to make the ADR incompatible with the binding cavity.

The binding results of CAFF and THEO also show significant significantly reduced binding compared to EPD. Large differences in size and shape of CAFF and THEO to the EPD template as noted with the PAA-IPA-MBA system, suggest that a size exclusion mechanism, in addition to differences in functionality, is likely responsible for the reduced binding observed with these analytes.

The highest level of binding for a non-ephedrine analyte was recorded for ADR. This analyte was therefore used to for cross reactive studies on the spectroscopic shift of the embedded gold nanoparticles. Figure 3.53shows the shift in the UV spectrum associated with the gold nanoparticles whilst rebinding in water, EPD and ADR.

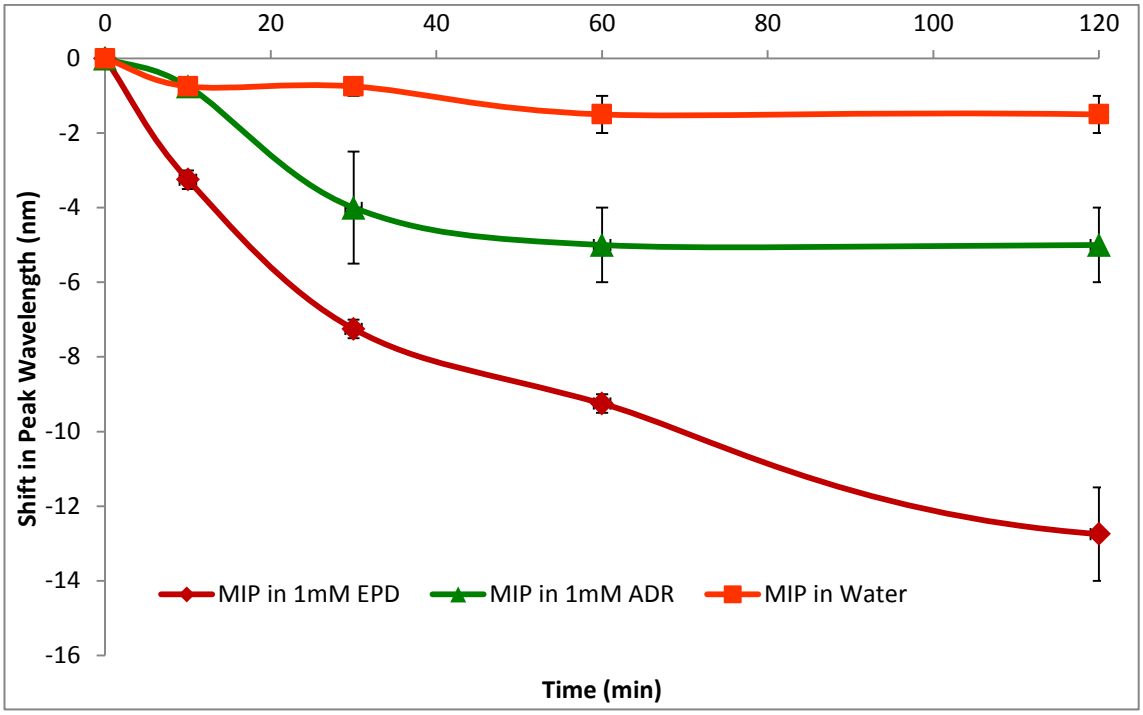

Figure 3.53 Peak shift of PAA-AN-MMA-Au_{MUA} MIP_{EPD} in water, EPD and ADR. Peak shift was also measured after 24 hours with no additional peak shift observed. Study was performed in triplicate.

The shift of up to 5nm in the spectrum of the embedded gold nanoparticles is observed when rebinding with ADR. This is slightly higher than 3.25nm shift observed when rebinding in water, which indicates some level of swelling associated with the presence of ADR in the binding cavity. The 15nm shift observed when rebinding with EPD is significantly larger than that achieved with both water and ADR indicating that rebinding EPD into the binding cavity results in the largest degree of polymer swelling, thereby producing the largest shift in the plasmon absorbance of the embedded gold nanoparticles.

In summary, the cross reactivity studies have successfully shown that the EPD imprinted PAA-IPA-MBA polymer is highly specific to EPD and for binding periods of 30 minutes or longer is capable of differentiating between its stereoisomers. In addition the polymer is capable of differentiating between very similar analytes based on a hypsochromic shift in the plasmon absorbance band of the embedded gold nanoparticles.

3.3.9 Surface Morphologies of Films

Previous work by our group investigated the surface morphology of PAA-AN-MMA $MIPf_{EPD}$ utilising scanning electron microscopy (SEM) to assess the effect of surface porosity and roughness on the resulting polymer system. . The presence of macroscopic pores (pores with a diameter >50nm) provide routes through which the template can enter and exit the bulk of the film and gain access to internal binding cavities. These pores are necessary for the formation of high performance MIPf by allowing trans-membrane transport of solvent and template through the polymer structure.

SEM images of PAA-AN-MMA $MIPf_{EPD}$ and NIPf are shown in Figure 3.54 and demonstrate clear indications of surface porosity. It should be noted that the MIPf displays far greater porosity than the corresponding NIPf, highlighting the impact the template has on the morphology of the resulting polymeric film.

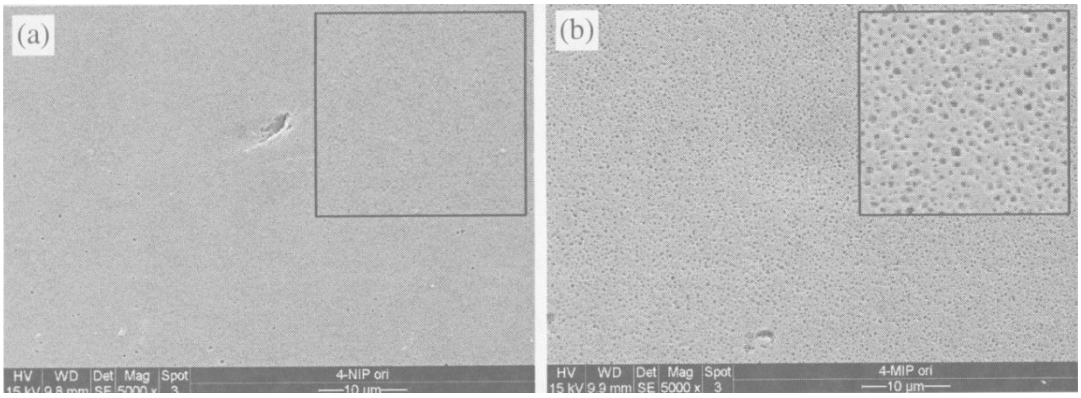

Figure 3.54 SEM images at 5000x magnification (insets are at 12500x magnification) of PAA-AN-MMA NIP films (a) and MIP films (b). Reproduced from Brisbane[139].

SEM images of PAA-AN-MMA $MIPf_{EPD}$ and NIPf with embedded Au_{MUA} were taken to investigate the effect of the embedded Au_{MUA} and are shown in Figure 3.55. It is again observed that the MIPf displays greater porosity than the NIPf.

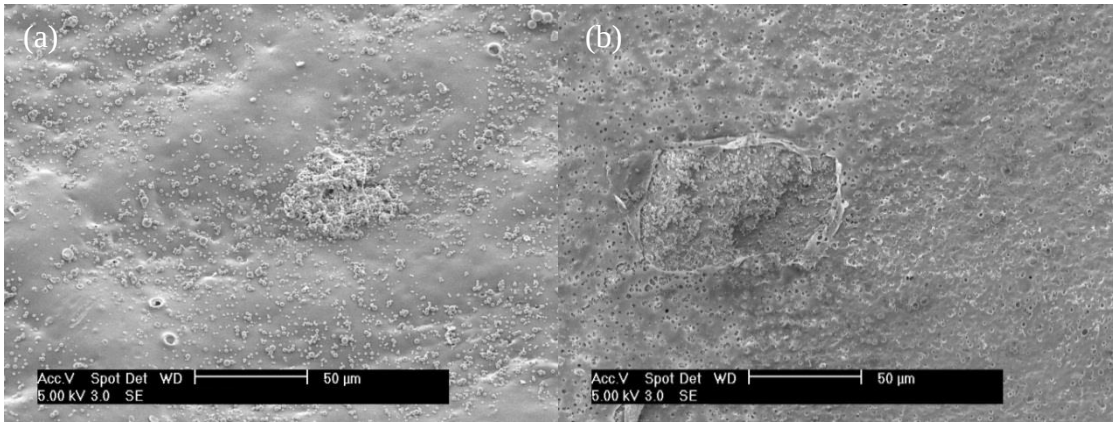

Figure 3.55 SEM images (1000x magnification) of PAA-AN-MMA-Au_{MUA}; NIP films (a) and MIP films (b).

The presence of the embedded Au_{MUA} produces an obvious morphological change in the appearance of spherical 'beads' on the films surface. It is believed that these 'beads' on the films surface are caused by the precipitation of the polymer around a gold nanoparticle core during phase inversion. While most of these nanoparticles become incorporated into the bulk film structure, some subsequently adhere to the films surface during film formation.

In addition to this 'bead' formation, the presence of the Au_{MUA} does appear to produce a slight decrease in surface porosity of both the MIPf and NIPf. This reduction in porosity may account for the reduction in template rebinding observed following incorporation of the Au_{MUA}.

3.3.10 Summary

Pre-synthetic interactions studies utilising molecular modelling and NMR titrations were used to identify AA as a suitable functional monomer for use with the EPD template. A 1:1 template-monomer ratio was determined to produce strong acid-base interaction due to protonation of the EPD amine group. Additional, weaker interactions were also identified at higher monomer template ratios up to 3:1 which are more likely to produce interactions with multiple points of hydrogen bonding which have been shown to enhance subsequent binding. These pre-synthetic studies also determined that

EPD interaction with AN and MMA is minimal making them ideal for use as a matrix monomers.

PAA-AN-MMA films were successfully using phase inversion with subsequent rebinding studies showing that the PAA-AN-MMA system is selective for the EPD template with an imprinting factor of 5.0 obtained after only 10 minutes.

Gold nanoparticles were prepared and incorporated into the polymeric films post-polymerisation. A slight reduction in template binding was observed following the incorporation of Au_{MUA}, however imprinting factors of 3.9 were still obtained after 10 minutes. Spectroscopic rebinding studies found peak shifts of the plasmon absorbance of embedded gold nanoparticles of up to 15nm for the MIPf compared to 8nm for the NIPf. The shift in plasmon absorbance of the gold nanoparticles was found to closely correlate to amount of template rebound, as well as being proportional to the concentration of the rebinding solution.

Cross-reactivity studies of the PAA-AN-MMA system demonstrated that the system is highly selective for ephedrine-based analytes and is also capable of at least partially differentiating EPD from its diastereomers. Spectroscopic rebinding studies also showed that the shift in plasmon absorbance was significantly reduced for non-ephedrine based templates.

These results show excellent promise for the use of PAA-AN-MMA polymers with embedded Au_{MUA} as a forensic sensor for the detection of EPD. The system is both selective and specific to the EPD template with detection being observed after as little as 10 minutes. The use of Au_{MUA} also allows for spectroscopic detection based on a hypsochromic shift in the UV-Vis spectrum.

3.4 Effect of Gold Nanoparticle Stabilising Agent

3.4.1 Gold Nanoparticle Preparation

The effect of the stabilising agent used in the formation of the gold nanoparticles on the resulting MIP composite was investigated by synthesising gold nanoparticles using stabilising agents other than the MUA used by Matsui et al.[68, 102]. Gold nanoparticles were successfully prepared using three additional thiol based stabilising agents; n-decanethiol (NDT), allyl mercaptan (AM) and 9-decene-1-thiol (9D1T), in addition to the MUA used previously. The comparative structures of these stabilising agents can be seen in Figure 3.56.

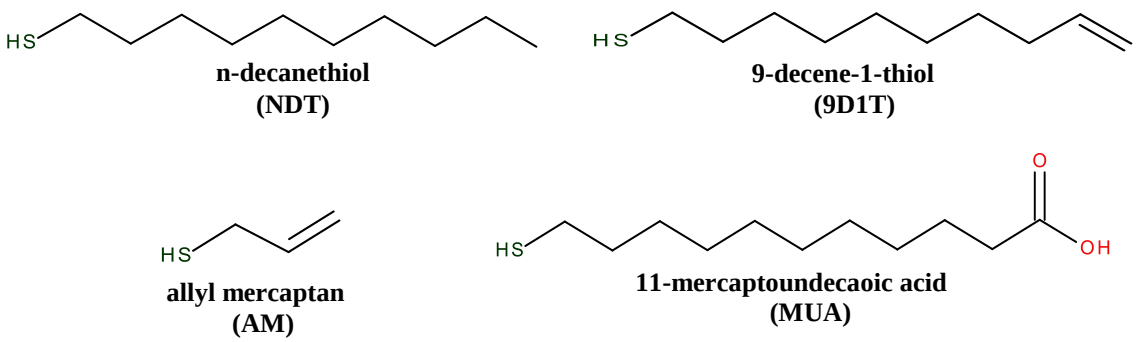

Figure 3.56 Gold nanoparticle stabilising agents

N-decanethiol was used to investigate the effect of removing the carboxylic acid functional group. Allyl mercaptan and 9-decene-1-thiol was used to determine the effect of chain length and a double bond.

Particle sizing confirmed the formation of the gold nanoparticles with mean diameters of 5.56nm (CV 11.2%), 5.50nm (CV 14.6%) and 5.88nm (CV 12.4%) for n-decanethiol, allyl mercaptan and 9-decene-1-thiol respectively. Particle size distribution as shown in Figure 5.57 indicates that the size of the gold nanoparticles were similar for all stabilising agents used and are consistent with those previously produced by Matsui et al.[68].

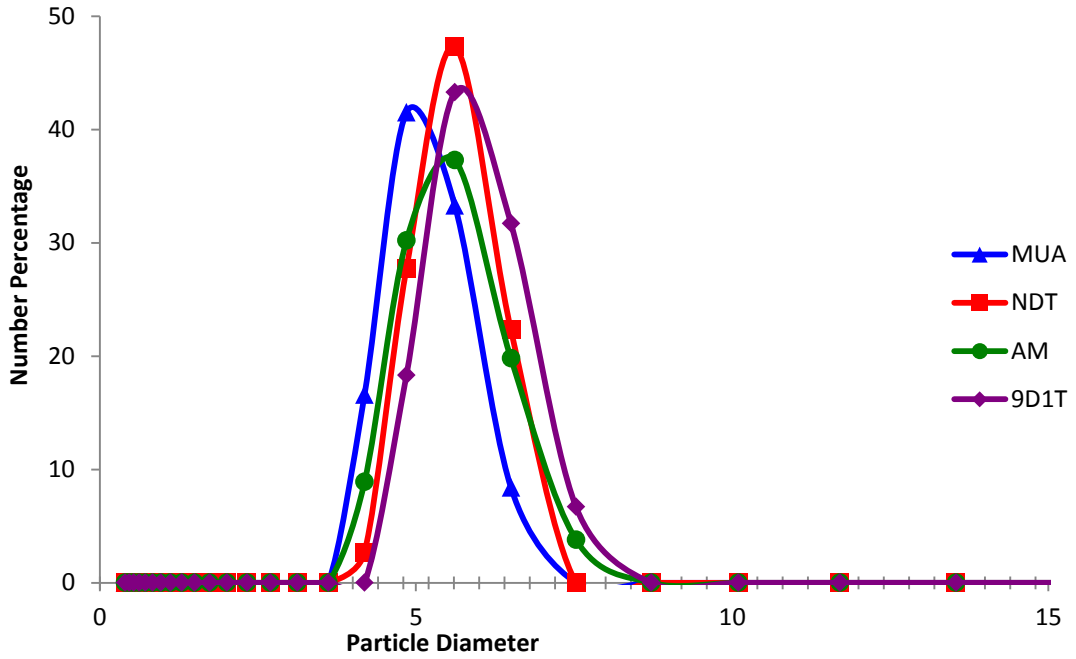

Figure 3.57 Size distribution of gold nanoparticles stabilised with 11-mercaptundecanoic acid (Au_{MUA}), n-decanethiol (Au_{NDT}), allyl mercaptan (Au_{AM}), and 9-decene-1-thiol (Au_{9D1T})

Each of the gold nanoparticles synthesised was incorporated into a PAA-AN-MMA matrix and $MIPf_{EPD}$ were produced as seen in Figure 3.58. NIP films for each stabilising agent were also produced.

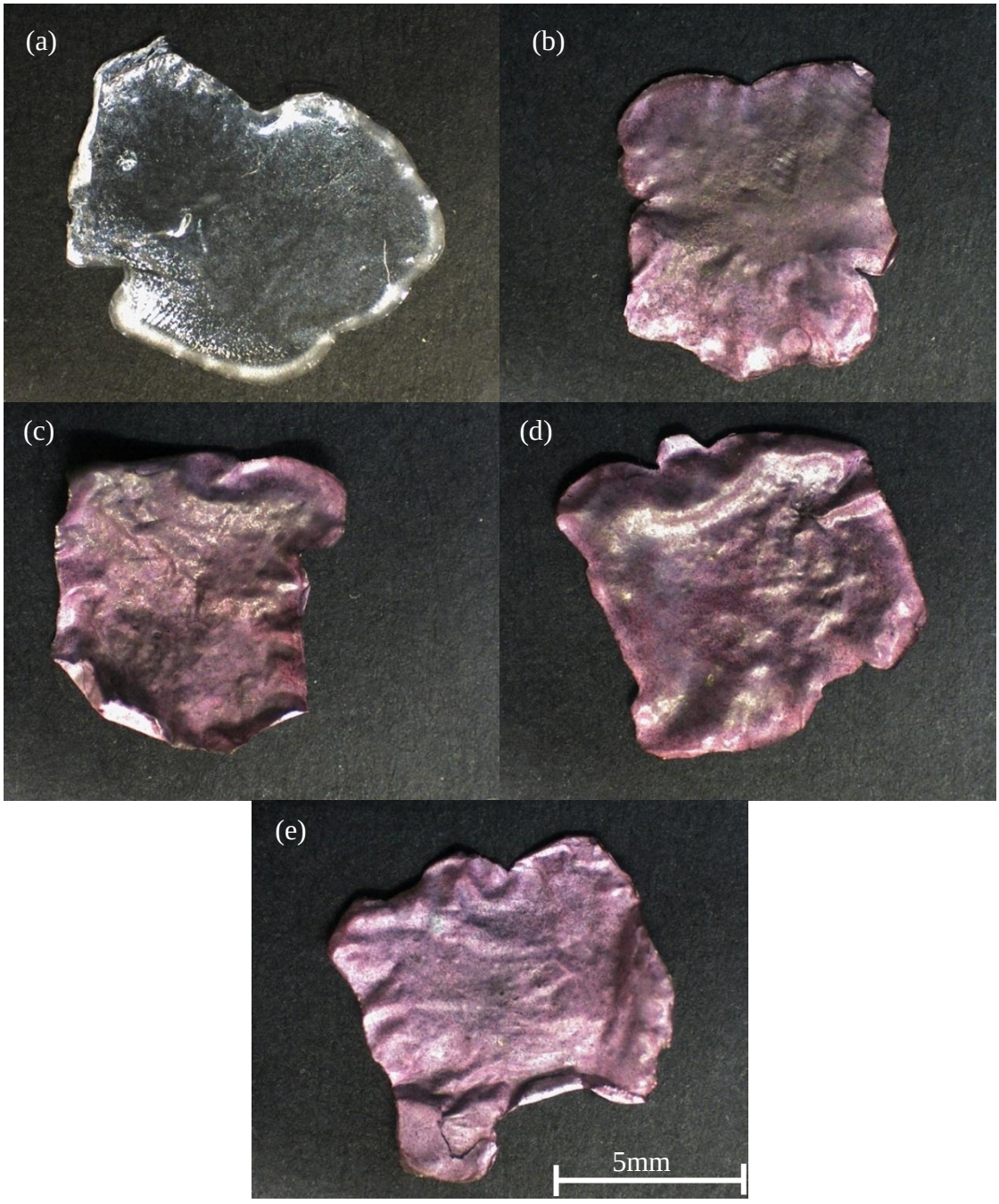

Figure 3.58 PAA-AN-MMA MIPf_{EPD} with (a) no gold nanoparticles, (b) 11-mercaptoundecanoic acid gold nanoparticles (Au_{MUA}), (c) n-decanethiol gold nanoparticles (Au_{NDT}), (d) allyl mercaptan gold nanoparticles (Au_{AM}), and (e) 9-decene-1-thiol gold nanoparticles (Au_{9D1T}).

3.4.2 Rebinding Studies

Following successful extraction quantitative rebinding results were produced using HPLC for a range of rebinding times from 10 minutes to 24 hours. Figure 3.59 shows rebinding with EPD of each of the gold nanoparticle MIPfs in comparison to their NIPfs. Imprinting factors (*I*) (Equation 3) were calculated for each rebinding time and shown in Table 3.6.

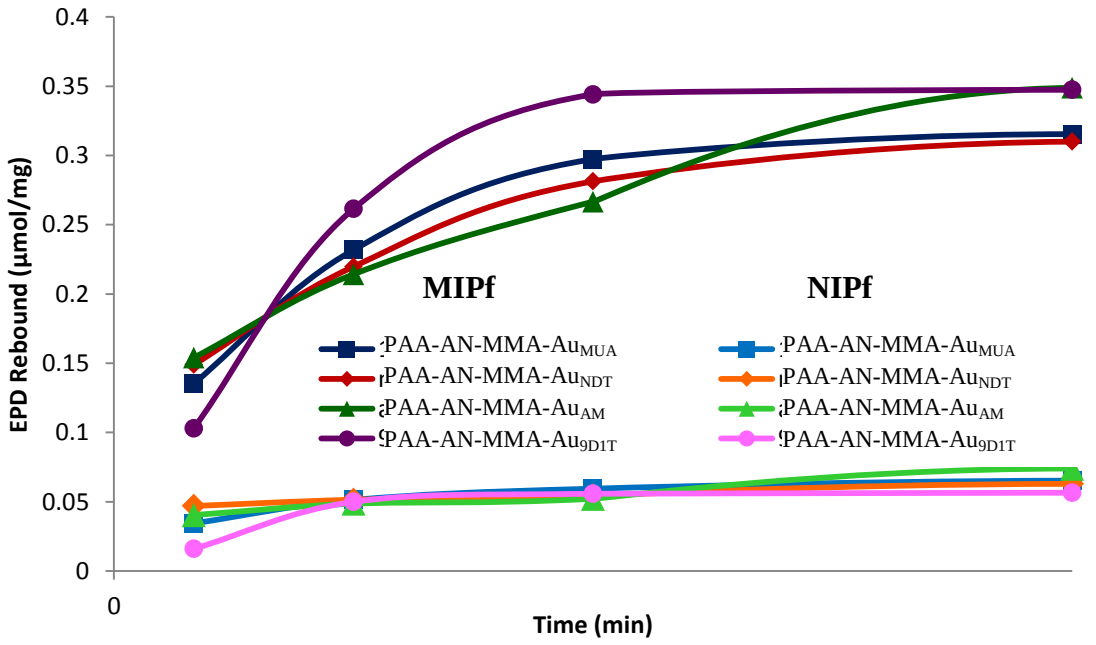

Figure 3.59 HPLC rebinding results for PAA-AN-MMA films with Au_{MUA}, Au_{DT}, Au_{AM}, and Au_{9D1T} in 1mM EPD. Rebinding was also measured after 24 hours with no significant additional binding observed.

Table 3.6 Imprinting Factors (I) for PAA-AN-MMA $MIPf_{EPD}$ with Au_{MUA}, Au_{NDT}, $Au_{AM,\ and}$ Au_{9D1T}.

Time (min)	Imprinting Factor			
	PAA-AN-MMA-Au_{MUA}	PAA-AN-MMA-Au_{NDT}	PAA-AN-MMA-Au_{AM}	PAA-ANM-MA-Au_{9D1T}
10	3.9	3.2	3.8	6.4
30	4.5	4.3	4.4	5.2
60	5.0	5.2	5.1	6.2
120	4.8	4.9	4.7	6.2
1440	4.0	5.7	6.6	5.0

Figure 3.59 demonstrates there is little effect of stabilising agent used in synthesis of the embedded gold nanoparticle on the rebinding of EPD the resulting polymer films. The rebinding of NIPs was almost identical for each of the stabilising agents, and whilst there was a slight variation in the rebinding of some of the MIPs when errors are taken into consideration these variations were insignificant.

3.4.3 UV-Vis Spectroscopic Rebinding Studies

Following evaluation of the rebinding of by HPLC, spectroscopic studies of the films were carried out to determine the effect of the stabilising agent on the colourimetric shift in the plasmon absorbance of the resulting gold nanoparticles during template rebinding. Measurements were then taken of the $MIPf_{EPD}$ and NIPf with each of the embedded gold nanoparticles in 1mM EPD. Figure 3.60 shows the shift in peak wavelength of gold nanoparticles from 10 minutes to 24hours.

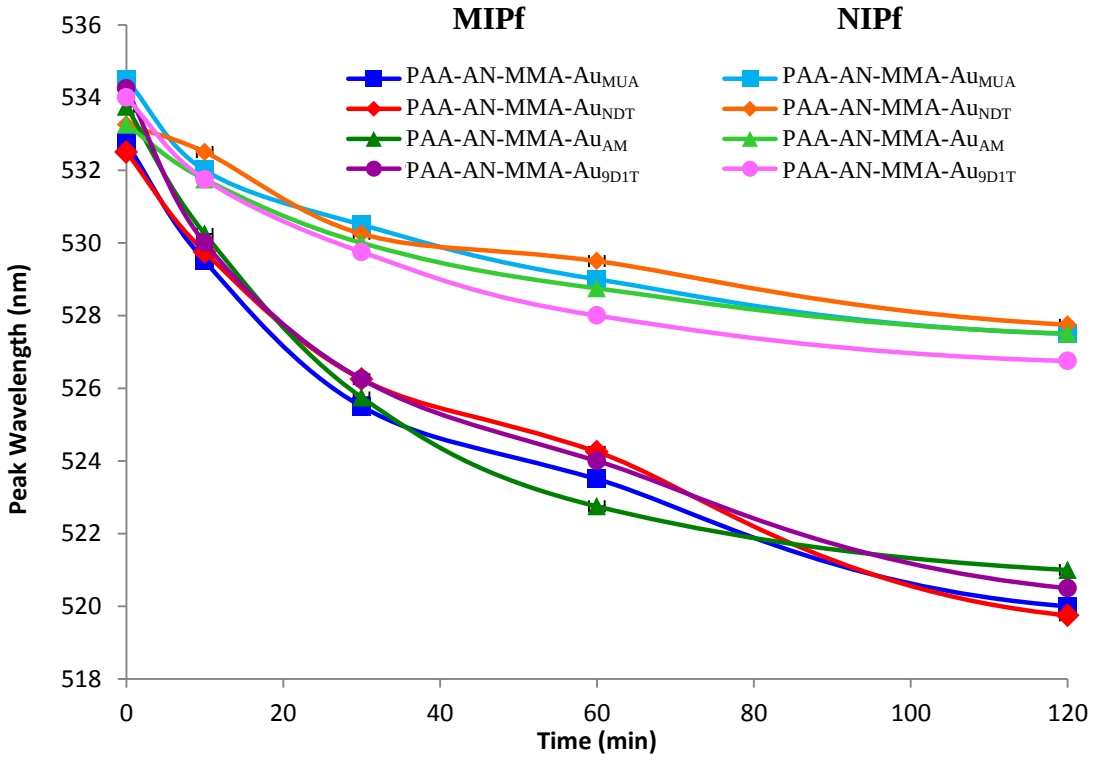

Figure 3.60 Peak shift of PAA-AN-MMA with Au_{MUA}, Au_{DT}, Au_{AM}, and Au_{9D1T} in 1mM EPD. Peak shifts were also measured after 24 hours with no additional peak shifts observed.

Similar hypsochromic shifts are seen in the spectra for each of the stabilising agents in both the MIP_{EPD} and NIP. Shifts of between 7-8.5nm were observed with the peak in the NIP and 13-15nm peak shifts were observed in the MIP_{EPD}. Differences in the peak shift between stabilising agents falls within the associated error indicating that no significant difference in peak shifting is observed as a resulting of different stabilising agents being used in the synthesis of the gold nanoparticles.

3.4.4 Summary

Gold nanoparticles were prepared using a number of thiol based stabilising agents to examine the effect of stabilising agent on the resulting MIP system. The results demonstrate that changing the stabilising agent used in the synthesis of the gold nanoparticles has a negligible result on the rebinding of the imprinted polymers into which they are embedded. In addition the shift in the wavelength of peak absorbance, caused by the SPR of the gold nanoparticles, during rebinding is similarly unaffected by the stabilising agent used during synthesis.

3.5 Conclusions and Future Work

3.5.1 Conclusions

Surface plasmon resonance of embedded gold nanoparticles was explored as a detection mechanism for EPD sorption in various MIP systems. The response is dependent on the swelling behaviour of the MIP during rebinding which increases the inter-particle distance of the immobilised gold nanoparticles producing a detectable event.

PAA-IPA-MBA (18.8%AA, 76.4%IPA and 4.8%MBA), utilised by Matsui et al.[68, 100] and phase inversed PAA-AN-MMA system (17%AA, 41%AN, and 42%MMA) MIP systems were both tested. While the PAA-IPA-MBA MIP selective to ADR and EPD showed high levels of template binding, imprinting factors 3.4 and 2.4, respectively, after 24 hours, the plasmon absorbance band of thiol-stabilised gold nanoparticles could not be detected in the UV-Vis spectrum once the nanoparticles were embedded in PAA-IPA-MBA system.

The phase inversed PAA-AN-MMA MIP film proved to be very responsive to SPR detection. This system is selective to EPD before and after the addition of gold nanoparticles displaying imprinting efficiencies of 7.2 and 4.8, respectively after 2 hours of EPD incubation. Spectroscopic rebinding studies found that wavelength of maximum plasmon absorbance of embedded gold nanoparticles shifted up to 15nm for the MIPf compared to 8nm for the NIPf. The shift in plasmon absorbance of the gold nanoparticles was found to closely correlate to amount of template rebound, as well as being affected to the concentration of the rebinding solution. The type of thiol stabilising agent used to prepare the gold nanoparticles has been shown not to affect EPD sorption and the surface plasmon resonance response of the MIPf.

Cross-reactivity studies of the PAAANMMA system with embedded Au_{MUA} demonstrated that the system is highly specific for ephedrine-based analytes and is also capable of differentiating EPD from its stereoisomers. Spectroscopic rebinding studies also showed that the shift in plasmon absorbance was significantly reduced for non-ephedrine based analytes (ADR, CAFF and THEO).

These results show excellent promise for the use of PAAANMMA polymers with embedded AuNP as a forensic sensor for spectroscopic detection of EPD. The system is both selective and specific to the EPD template with detection being observed after as little as 10 minutes.

3.5.2 Future Work

Studies that could be conducted in order to further support this work would include investigating the effect of gold nanoparticle concentration on the resulting surface plasmon response, including transmission electron microscopy to investigate gold nanoparticle sizing and distribution through the PAA-AN-MMA films. This will assist in optimising signal transduction of the EPD rebinding event.

Furthermore, the results within this chapter warrant investigation into the scope of the PAA-AN-MMA with embedded gold nanoparticles for the detection of other templates, particularly amphetamine and methamphetamine.

Finally an examination of the lack of surface plasmon absorbance of the gold nanoparticle in the PAA-IPA-MBA system will allow a greater understanding of the use of surface plasmon resonance as a signal transduction mechanism for molecularly imprinted polymers.

CHAPTER 4 - CONDUCTIVE POLYMER/ MOLECULARLY IMPRINTED POLYMER COMPOSITES

Molecularly imprinted and conductive polymers may be combined for sensing applications in several ways. Firstly, previously synthesised particulate MIPs may be incorporated into a conductive polymer matrix, which has been previously used successfully for the detection of templates including morphine[117], nicotine[129] and (-)-ephedrine[130]. Alternatively, the conductive polymer itself may imprinted with the template, which has been used for the detection of templates including morphine[124], dopamine[133], and caffeine[131a]. In these cases, the imprinted component is used as the recognition element while detection relies on an electrochemical response such as the selective electrocatalytic reduction or oxidation of the template[136].

This chapter details a preliminary investigation into the incorporation of a conductive polymer with a traditional MIP to form a combined or composite polymer (CP-MIP). By utilising an imprinted polymer with an intrinsic conductive domain, it was hoped that an improved electrochemical response could be obtained compared to traditional MIP systems merely embedded into a conductive matrix. Similarly, by utilising a conductive polymer with an intrinsic traditionally imprinted domain, it was hoped that binding site kinetics and homogeneity could be improved, as well as providing a more rational design approach to MIP synthesis[130, 136].

4.1 Molecularly Imprinted Polymeric Films Containing 3-Methylthienyl Methacrylate

In order to prepare the MIP-conductive polymer composites, a previously reported electroactive monomer, 3-methylthienyl methacrylate (MTMA, shown in Figure 4.1 below), with a vinylic functional group and a thiophene moiety was utilised[140]. This dual functionality allows MTMA to link the conductive and imprinting domains of the composite polymer; the vinylic functionality allows free radical addition polymerisation to occur while the thiophene functionality allows the inclusion of thiophene-based conductive polymers either by electro- or chemical polymerisation.

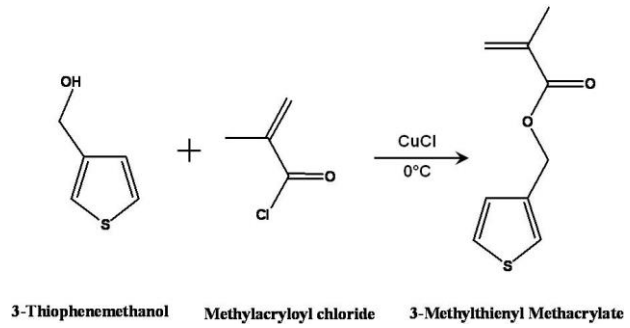

Figure 4.1 Reaction scheme for synthesis of 3-methylthienyl methacrylate

To assess the function of MTMA in an imprinting capacity for EPD, MTMA was incorporated into the PAA-AN-MMA system discussed in Chapter 3.4. This polymer showed excellent specificity and selectivity for the EPD template and so was ideal for use in assessing the effect of MTMA on a MIP system.

4.1.1 Molecular Modelling of MTMA with (-)-Ephedrine

To assess the interaction of MTMA with the EPD template, molecular modelling and NMR studies were performed. The molecular modelling results for EPD with MTMA are compared with those for AA and MMA in Figure 4.2.

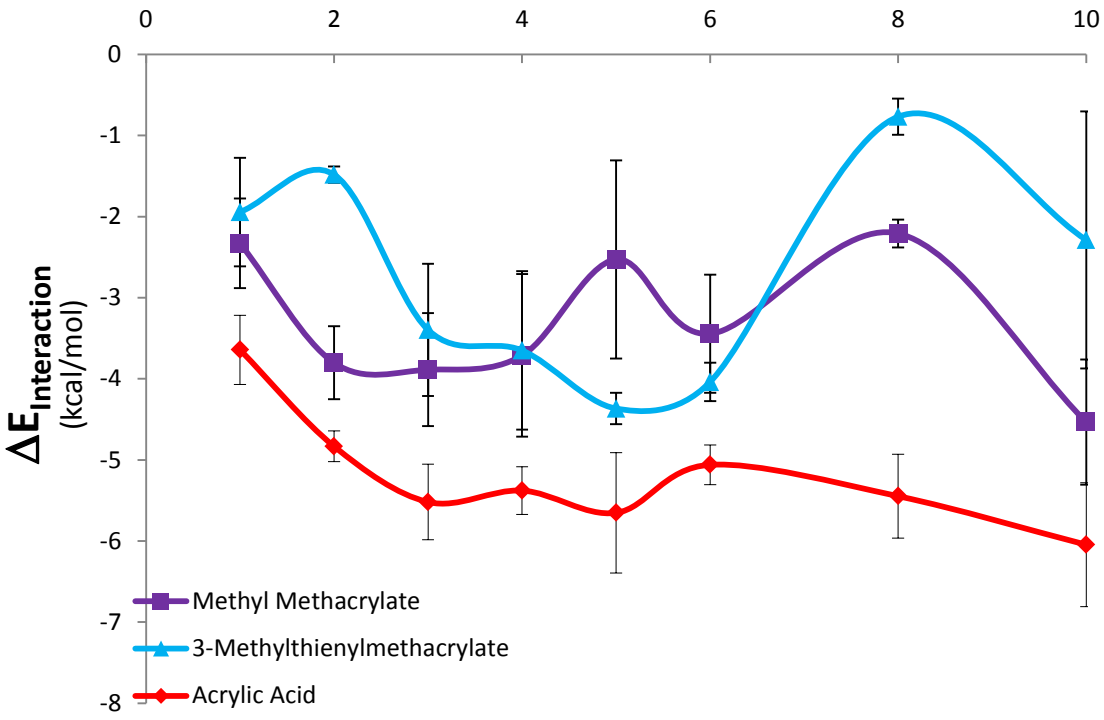

Figure 4.2 $\Delta E_{interaction}$ of EPD with AA, MMA and MTMA across a range of M-T ratios.

From Figure 4.2 it can be seen that the $\Delta E_{Interaction}$ for MTMA with EPD are negative for all ratios signifying a favourable interaction. These energies are less negative than those produced by AA indicating a less favourable interaction compared to the AA functional monomer.

Molecular modelling indicates hydrogen bonding between the secondary amine and hydroxyl group of the EPD and the carbonyl group of the MTMA. The 2:1 MTMA to EPD ratio, which produced the highest $\Delta E_{Interaction}$ without evidence of monomer self-association, is shown in Figure 4.3. At MTMA to EPD ratios $\geq$ 4:1, modelling indicates that the additional monomer units do not interact with the template.

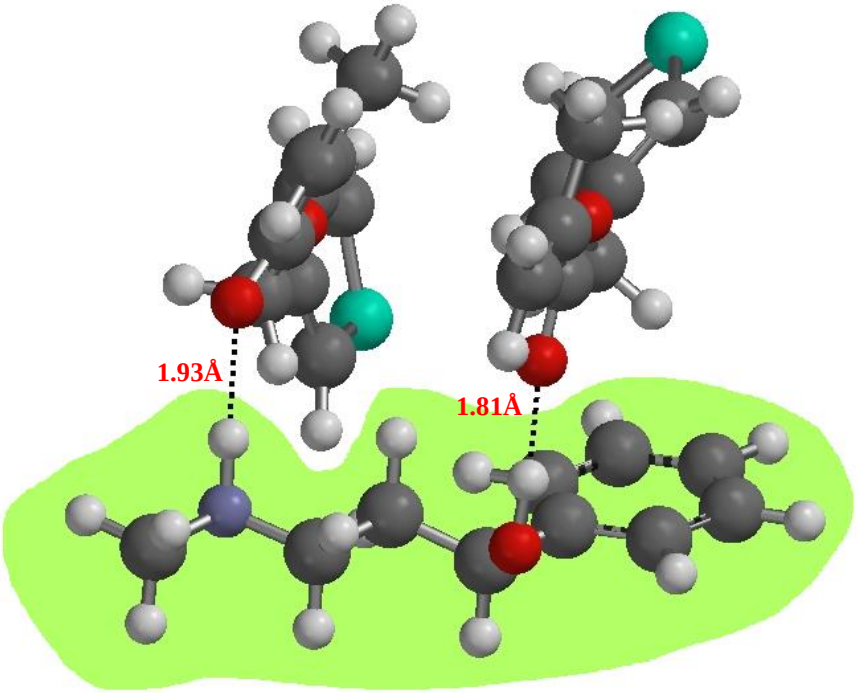

Figure 4.3 Molecular image EPD with 2 MTMA showing two points of interaction. Template is shaded green and hydrogen bond distances are indicated in red.

Hydrogen bond distances for MTMA with EPD are relatively long (≥1.81Å) suggesting relatively weak interactions compared to AA.

The functionality of MTMA makes it capable of acting only as a hydrogen bond donor, whereas AA possesses both donor and acceptor functional groups. As a result, MTMA forms only single point interactions with the amino and hydroxyl protons of EPD, whereas AA is observed to form additional hydrogen bonds with the nitrogen and oxygen atoms themselves. These modelling results are similar to those seen for MMA, which is unsurprising given the common methacrylate functionality. Since no interaction is observed between the thiophene moity of the MTMA and the EPD template, differences in $\Delta E_{Interaction}$ between MTMA and MMA are presumably caused by steric factors.

4.1.2 NMR Studies

^{1}H-NMR titration of MTMA was also performed to assess its interaction with EPD and validate the findings of the molecular modelling reported above. Figure 4.4 shows the extent of the downfield shifts as a function of the template-monomer ratio.

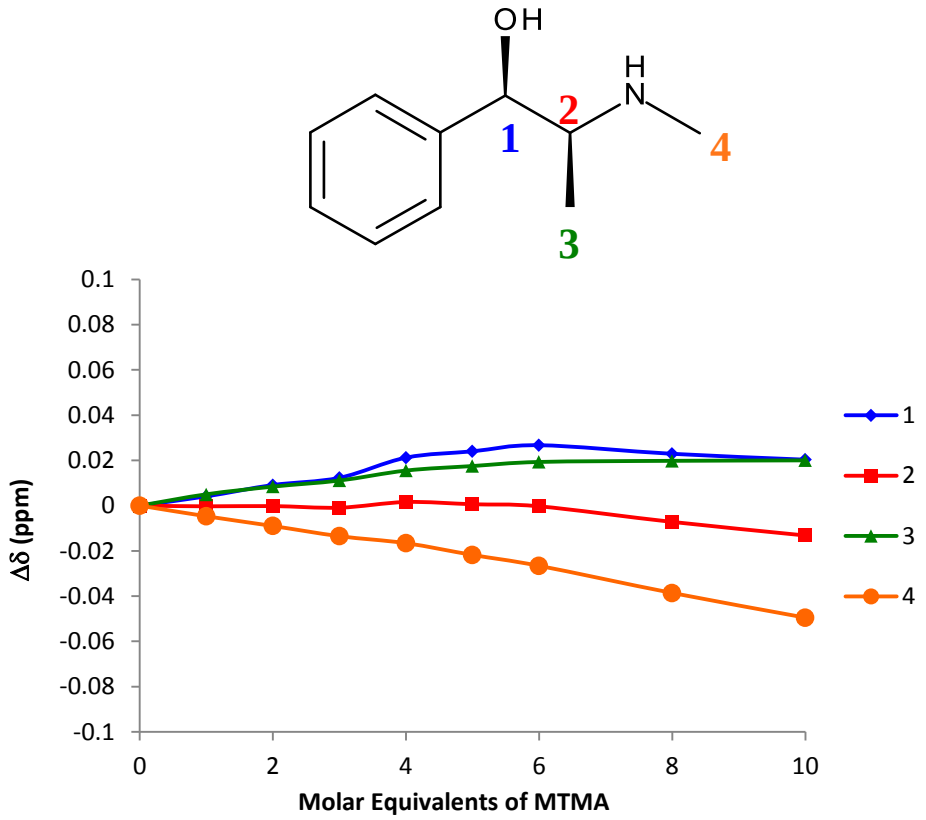

Figure 4.4 Change in chemical shift (Δδ) of different EPD protons upon titration with increasing molar equivalents of MTMA in $CDCl_3$. EPD structure is included above to show labelling of protons.

These results demonstrate comparatively small (<0.05ppm) changes in chemical shift of the EPD protons during the titration with MTMA. This is again comparable to the changes in chemical shift observed for MMA (<0.03ppm) as seen in Figure 3.37. This suggests that MTMA will have little interaction with the EPD template compared to the AA functional monomer.

The combination of results obtained from molecular modelling and NMR titrations indicate that MTMA will not significantly interact with the EPD template when

compared to AA functional monomer. The results also demonstrate similar levels of interaction between MTMA and MMA suggesting that MTMA will fulfil a similar matrix monomer function.

4.1.3 Preparation of P(AA-AN-MMA-MTMA) MIPf

Following successful synthesis, MTMA was incorporated into the PAA-AN-MMA system discussed in Chapter 3.4. The same relative ratio of AA to AN to MMA was used with increasing proportions of MTMA added. Inverse gated ^{13}CNMR spectroscopy was used for calculating the final polymer composition and results are shown in Table 4.1.

Table 4.1 Reaction ratios for synthesis of MTMA-AA-AN-MMA copolymers

Code	% MTMA		% AA		% AN		% MMA	
	Feed	Actual	Feed	Actual	Feed	Actual	Feed	Actual
PAA-AN-MMA	**0**		15	17	42.5	41	42.5	42
PAAMM5	**5.0**	**7.1**	14.3	15.1	40.4	38.6	40.4	39.1
PAAMM15	**15.0**	**18.6**	12.8	13.7	36.1	34.9	36.1	32.8
PAAMM25	**25.0**	**29.4**	11.3	13.1	31.9	28.7	31.9	28.8
PAAMM50	**50.0**	**56.0**	7.5	8.7	21.3	18.1	21.3	17.3

The final composition of all polymers differed only slightly from their respective feed ratios, with MTMA and AA both increasing and AN and MMA concomitantly decreasing in relative composition. Measurement of the reactivity ratios was not attempted for this polymer system.

Polymer solutions were prepared and post-polymerisation imprinting of EPD, in a 3:1 AA:EPD ratio, was performed. Polymeric films were prepared through spin-casting and phase inversion methods and are shown in Figure 4.5.

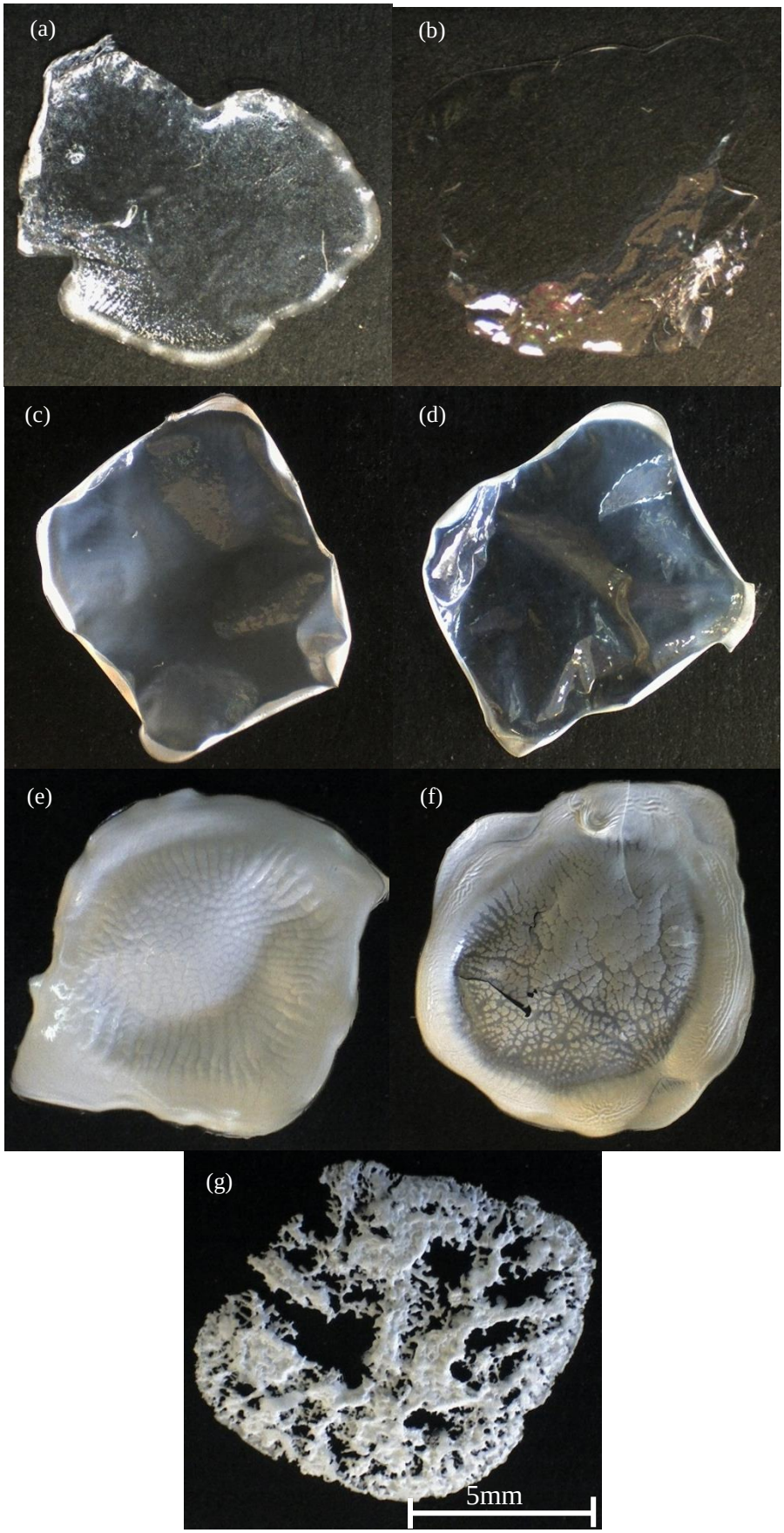

Figure 4.5 PAA-AN-MMA-MTMA films; P-AA-AN-MMA; $MIPf_{EPD}$ (a) and NIPf (b); PAAMM5; $MIPf_{EPD}$ (c) and NIPf (d); PAAMM15; $MIPf_{EPD}$ (e) and NIPf (f) and PAAMM25 - NIPf (g)

Good quality, reproducible MIP and NIP films were formed when the proportion of MTMA was 19% or less - Figure 4.5 (c-f). Poor quality NIP films were produced with the 29% MTMA - Figure 4.5(g), however MIP films were unable to be made. No films were produced for polymers with greater than 29% MTMA. As the proportion of MTMA increased in the polymer composition films, thicker and more brittle films were produced. This indicates that MTMA is not an ideal monomer for use in the preparation of MIPs in a thin film format, however in low proportions may be included in the PAA-AN-MMA system.

Figure 4.6 shows the FTIR spectrum of EPD, a virgin non-imprinted polymer film (V-NIPf), a virgin EPD imprinted polymer film (V-MIPf_{EPD}) and an extracted EPD imprinted polymer (Ex-MIPf_{EPD}). These spectra are for the polymer PAAMM15, similar spectra for PAAMM5 were also produced.

Incorporation of the EPD template and subsequent extraction was confirmed using FTIR analysis, with the prominent peak, at approximately 708cm^{-1} (Peak A), corresponding to the out of plane bending of the aromatic hydrogens, again used as the diagnostic peak. For these polymers, the presence of MTMA also results in an overlapping peaks at 708cm^{-1}(Peak A) and an adjacent peak at 697cm^{-1} (Peak B), which also correspond to out of plane bending of aromatic hydrogens. As a result, the presence of Peak A alone cannot be used to demonstrate the presence of EPD, instead the ratio of the Peak A compared to the adjacent Peak B is used, with an increase in Peak A relative to Peak B used the confirm the presence of EPD.

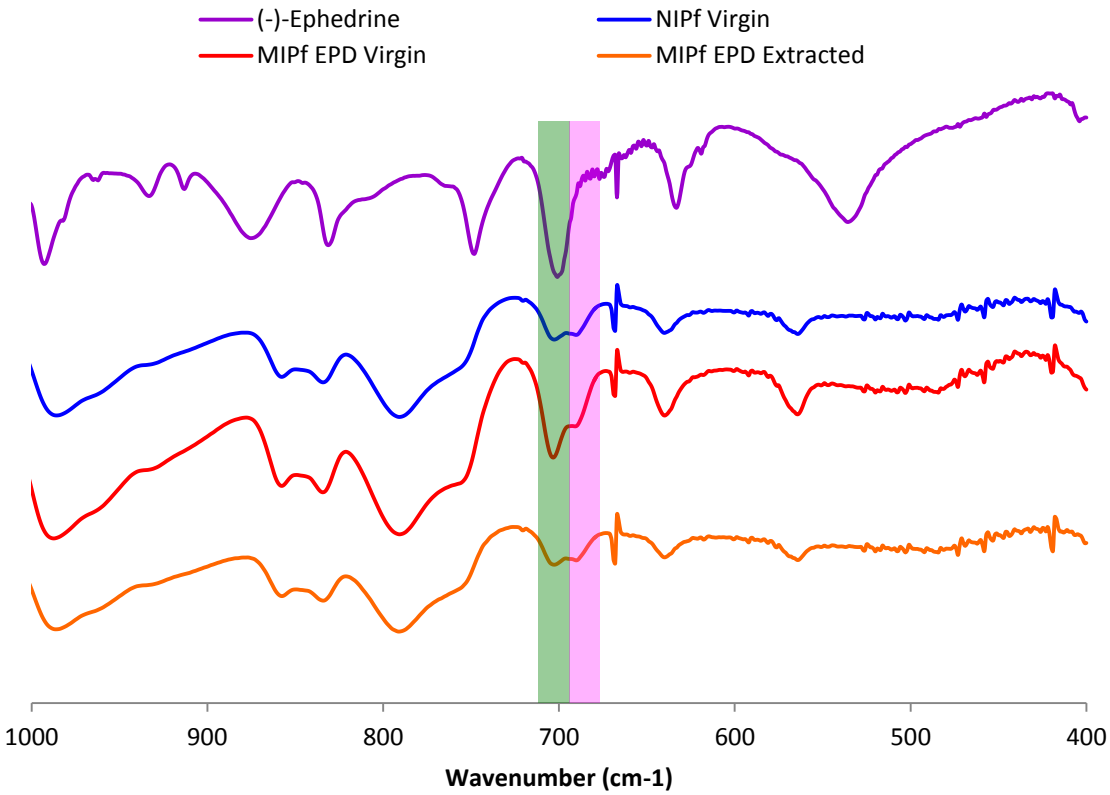

Figure 4.6 FTIR spectra of PAAMM15 films; Non-imprinted polymer (NIPf) (b), Virgin EPD imprinted polymer (V-MIPf$_{EPD}$) (c), and an extracted EPD imprinted polymer (Ex-MIP$_{EPD}$) (d). The spectrum of EPD is also included (a). Peak A (shaded green) and Peak B (shaded red) were used as the diagnostic peaks used to determine the presence of EPD.

The presence of the larger Peak A compared to Peak B in the V-MIPf$_{EPD}$ demonstrates that EPD has been successfully incorporated into the imprinted polymer. Peak A is comparable to Peak B in the NIP and Ex-MIP$_{EPD}$ indicating that the EPD is not present in the NIP and can be successfully removed from the MIP through the extraction process. Extraction of the EPD template was also confirmed through HPLC analysis of the extraction solution.

4.1.4 Rebinding Studies

The success of the rebinding following template extraction was again assessed qualitatively using FTIR according to the relative size of the diagnostic EPD peaks as seen in Figure 4.7. An increase in the relative size of the diagnostic EPD peak is observed in the rebound EPD imprinted films (Rb-MIPf$_{EPD}$) indicating successful

rebinding of the EPD into the polymer. A corresponding increase in size of the diagnostic peak is not observed for the non-imprinted polymer following rebinding (Rb-NIPf), indicating that the EPD template does not bind to the NIP.

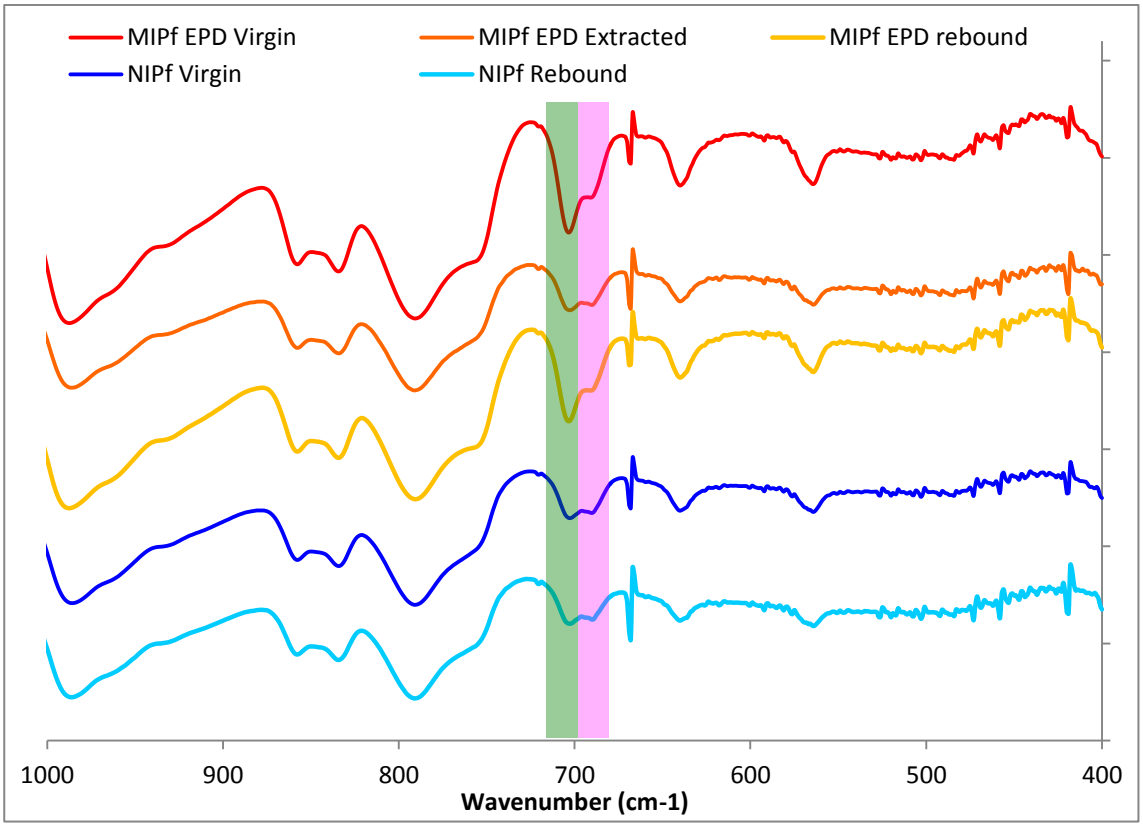

Figure 4.7 FTIR spectra PAAMM15; Virgin EPD imprinted polymer (V-MIPf$_{EPD}$) (a), EPD imprinted polymer (Ex-MIPf$_{EPD}$) (b), Rebound EPD imprinted polymer (Rb-MIPf$_{EPD}$) (c), Virgin non-imprinted polymer (V-NIP) (d) and Rebound non-imprinted polymer (Rb-NIP) (e). Peak A (shaded green) and Peak B (shaded red) were used as the diagnostic peaks used to determine the presence of EPD.

Quantitative rebinding results were produced using HPLC for a number of rebinding times ranging from 10 minutes to 24 hours. Figure 4.8 show rebinding of the imprinted polymers with EPD in comparison to the binding of EPD to the NIP.

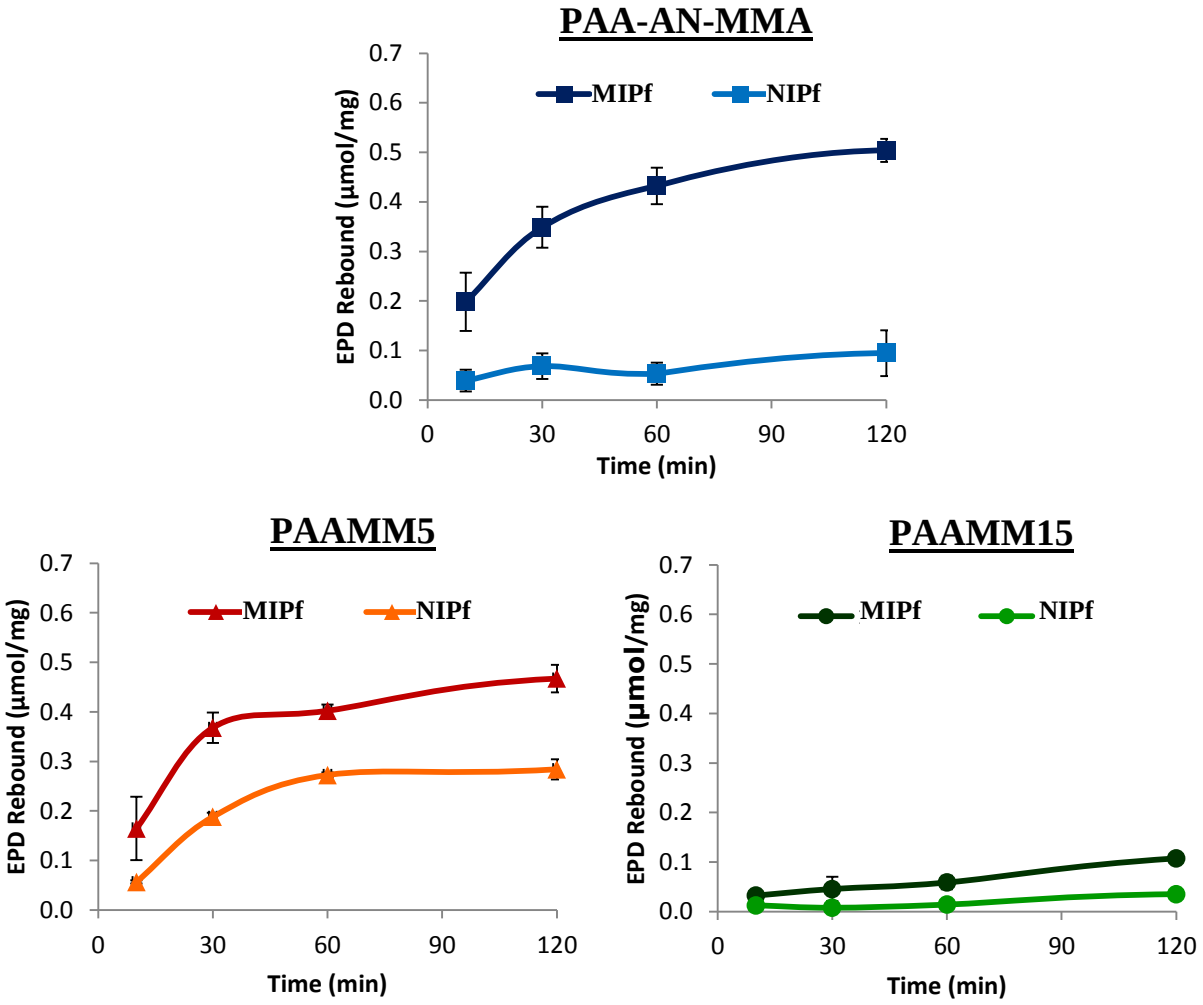

Figure 4.8 HPLC rebinding results for PAA-AN-MMA with increasing proportions of MTMA in 1mM EPD. Rebinding was also measured after 24 hours with no significant additional binding observed.

The inclusion of 7.1% MTMA into the PAA-AN-MMA polymer system does not produce a significant decrease in MIPf binding, however a significant increase in the levels of non-specific binding is observed in the NIPf. Given that interaction studies suggested a similar level of interaction between MTMA and EPD as that observed for MMA, the observed increase in NIPf binding is likely a result of changes in the chemical and physical properties of the films as a result of MTMA inclusion. Previous work suggests that small changes in the chemical composition of the polymer may result in large changes in the rebinding profiles of the resulting imprinted polymer[138-139]. This was found to be due primarily to changes in the physical properties of the films that result from changes in the composition.

Additional MTMA in the polymer system results in a marked decrease in binding to both MIPf and NIPf as seen in Figure 4.8 for the PAAMM15 system. If the increase in non-specific biding observed for PAAMM5 system was a result of EPD interaction with the MTMA, we would expect to see an even greater degree of non-specific binding for the PAAMM15 system. The lack of binding therefore further supports the notion that the observed deleterious effects of MTMA inclusion on EPD binding is due to changes to the physical and chemical properties of the polymer films.

4.1.5 Summary

MTMA, due to its dual vinylic and thiophene moieties, was identified for use as a bridge between conductive and molecularly imprinted polymers. Its efficacy in a molecularly imprinted capacity was assessed.

Pre-synthetic in silico interaction studies utilising molecular modelling as well as NMR titrations experiments were utilised to identify MTMA as having minimal interaction with the EPD template making it applicable for use as a matrix monomer.

PAA-AN-MMA was used as the model for investigating the effect of MTMA on a MIP system. Polymers containing up to 56% MTMA were synthesised. The formation of MIPf was possible for MTMA proportions up to 18.6%. The inclusion of MTMA resulted in a reduction to EPD binding, however the polymers remained selective for the EPD template. Furthermore the copolymerisation compatibility of MTMA for use with an AA functional monomer for the production of a MIP was also confirmed.

These results demonstrate that MTMA can be incorporated into a MIP system, which has demonstrated previous success, and remain selective for the EPD template. This suggests its proposed function as a bridge between the imprinted and conductive domains of the composite may be achieved while maintaining the functionality of the imprinting domain. These results indicate however that the composition of the resulting polymer will be vital to its effectiveness in rebinding the desired template. This is due in

particular to changes to the physical properties of the polymer arising from changes in chemical composition. Its utility in relation to the conductive domain will be discussed below.

4.2 Conductive Polymers Containing 3-Methylthienyl Methacrylate

The utility of MTMA in a conductive polymer capacity was then investigated. Poly(3,4-ethylenedioxythiophene):poly(styrene sulfonate) or PEDOT:PSS was used as the model for this conductive polymer investigation, due to its commercial availability and well understood chemical and physical properties. PEDOT:PSS is also easily dispersed in water making it easy to process into durable films and more versatile than other available conductive polymer systems. In this conductive polymer system, the PEDOT and PSS act as co-ionomers, with the PSS carrying the negative charge and the PEDOT carrying the positive charge, resulting in a neutral macromolecular salt[113].

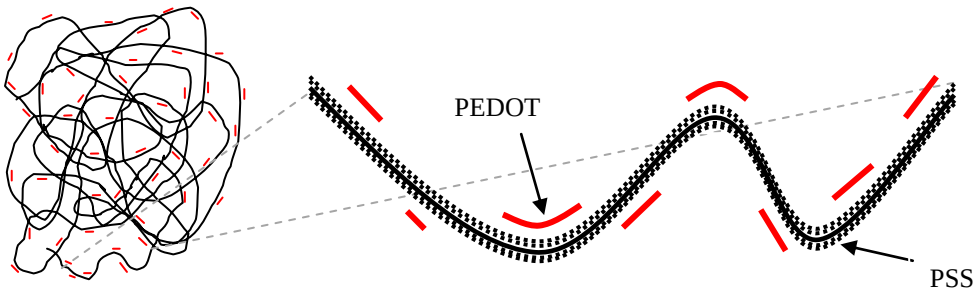

Figure 4.9 Structure of PEDOT:PSS; Segments of PEDOT adhered to part of a longer chain of PSS[149].

The mechanism of synthesis for PEDOT:PSS uses PSS as a host polyelectrolyte which is used in excess. EDOT can then be added and polymerised via oxidation which results in the removal of two electrons from the thiophene ring of the EDOT. Further oxidation results in the formation of a polycation, with the resulting PEDOT segments adhering to the longer PSS via ionic interaction, as seen in Figure 4.9[149]. These interactions also result in PEDOT chains becoming doped, increasing their conductivity. Along the whole chain the ratio of PEDOT to PSS is approximately 1:1.9.

The oxidative polymerisation of the PEDOT occurs through the thiophene moiety of the EDOT monomer. MTMA, which contains the same thiophene moiety, may therefore be similarly polymerised though oxidation into this EDOT chain. Cirpan, A. et al showed

that MTMA may be successfully incorporated into a conductive polymer chain using an oxidative process[140].

4.2.1 Preparation of Conductive Polymer Solutions

Poly(3,4-ethylenedioxthiophene):poly(styrenesulfonic acid) (PEDOT:PSS), the conductive polymer system utilised for this study, was prepared using a previously reported method[113]. Additional conductive polymers were produced as above by substituting some or all of the EDOT with MTMA and are listed in Table 4.2. The proposed chemical structure for P(EDOT-MTMA):PSS is shown in Figure 4.10.

Table 4.2 Reaction feed ratios for synthesis of conductive polymers

Polymer Code	EDOT		MTMA		PSS	Polymer Concentration (in Water) (g/L)
	%	Mass (g)	%	Mass (g)	Mass (g)	
PEDOT:PSS	**100**	10.65	**0**	-	26.30	14.9
PEMS25	**75**	7.99	**25**	3.42	26.30	15.2
PEMS50	**50**	5.33	**50**	6.83	26.30	15.5
PMTMA:PSS	**0**	-	**0**	13.67	26.30	16.2

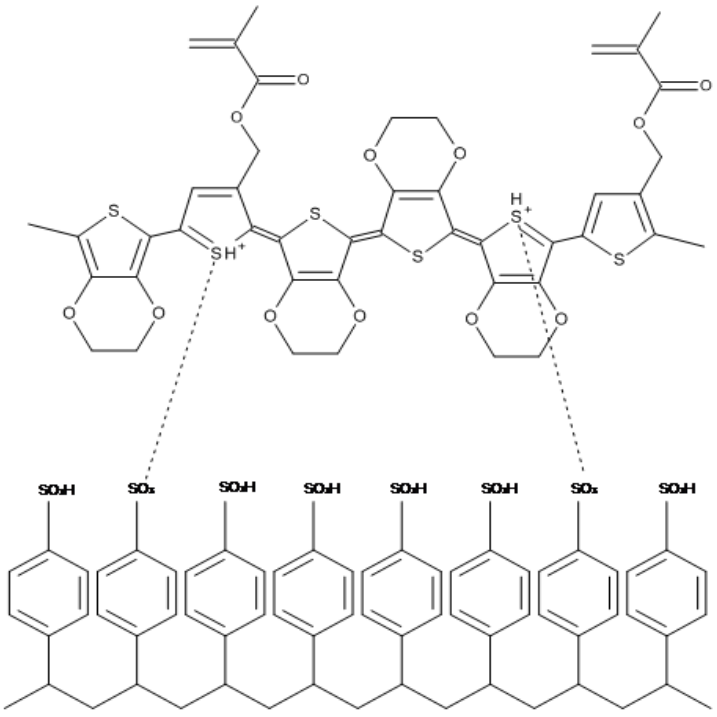

Figure 4.10 Structure of P(EDOT-MTMA):PSS[113].

The pHs of the resulting conductive polymer solution were measured and are shown in Table 4.3 below, with all polymer blends remaining acidic. This is to be expected given the use of the strongly acidic PSS (pK_a 2.1) as the co-ionomer and dopant for these conductive polymer systems. This charge is necessary for the doping process of the PEDOT chain, with one charge every 3 to 4 thiophene rings on the PEDOT chain. The acidic nature of the PSS also catalyses the reaction and reduces the formation of keto-functionalised side products on the PEDOT chain[150].

Table 4.3 pH of conductive polymer solutions.

Polymer Code	pH
PEDOT:PSS	3.2
PEMS25	3.3
PEMS50	3.2
PMTMA:PSS	3.3

The synthesis of conductive polymers was assessed using FTIR spectroscopy. Figure 4.11 shows the spectra for PEDOT:PSS, PMTMA:PSS and PEMS50.

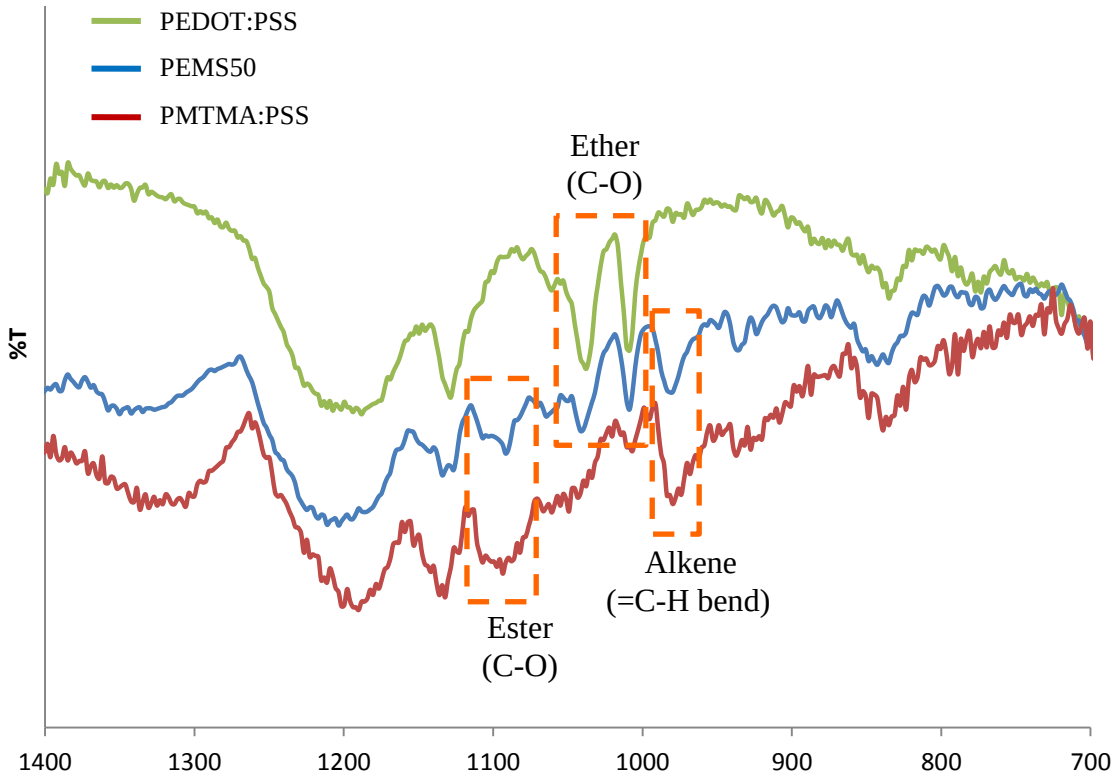

Figure 4.11 FTIR spectra of PMTMA:PSS, PEMS50 and PEDOT:PSS

The spectra of the PEMS50 shares twin peaks at 1000cm^{-1} and 1035cm^{-1} with PEDOT:PSS corresponding to the C-O stretches of an unsymmetric ether. It also shares two peaks at 975cm^{-1} and 1090cm^{-1} with PMTMA:PSS corresponding to a =C-H bend of an alkene and C-O stretch of an ester, respectively. These spectra confirm the presence of both MTMA and EDOT in the relevant polymers. Additionally the presence of the peak at 975cm^{-1} corresponding to a =C-H bend of an alkene, demonstrates that the vinylic functionality of the MTMA has been retained.

4.2.2 Conductivity Measurements

Following successful synthesis of the conductive polymer solutions, films were produced through spin-coating (1500rpm) and annealed at 110°C to assess the conductivity of the polymers. Additional films were prepared through spin-coating and

vacuum drying to remove the solvent, so as to preserve the vinylic functionality in the MTMA. Conductivity measurements using the four-point probe method were performed with results shown in Figure 4.12. A commercial PEDOT:PSS was also measured for comparison.

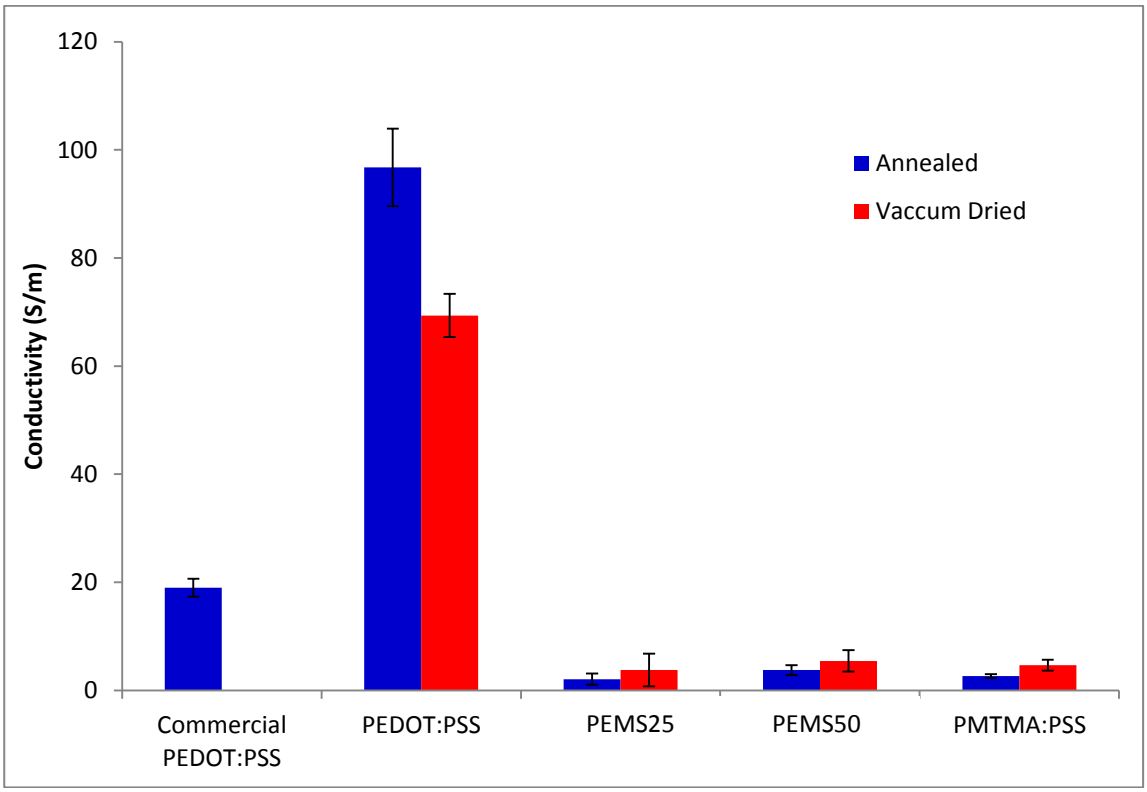

Figure 4.12 Bulk conductivity of conductive polymer films prepared via spin-coating (1500rpm) and subsequent annealing or vacuum drying. Film thicknesses were measured at 2.3±0.3mm.

These results demonstrate the inclusion of MTMA into PEDOT:PSS will result in a polymer which is still conductive however a significant decrease to the conductivity is observed. This is likely due MTMA to disrupting the stereoregularity, and therefore planarity, of the thiophene backbone. This disturbance in the chain is known to interfere with electron transport along and between the polymer chains, reducing conductivity[114, 151]. The synthesised PEDOT:PSS was five times as conductive the commercially bought PEDOT:PSS, however it should be noted that the commercial PEDOT:PSS used was a pH neutral product which has a reduced conductivity due to decreased doping in PEDOT chain.

The annealing process produced higher conductive films than vacuum drying for PEDOT:PSS due to the more uniform nature of the resulting conductive film which can be obtained using this process. Of the conductive polymers containing MTMA the PEMS50 produced the highest conductivity (5.5 S/m compared to 4.8 and 3.5 m/S for PMTMA:PSS and PEMS25, respectively.

4.2.3 Surface Morphology

Scanning electron microscopy (SEM) was used to assess the effect of inclusion of MTMA on the surface morphology of resulting conductive films. SEM images of PEDOT:PSS, PMTMA:PSS and PEMS50 are shown in Figure 4.13.

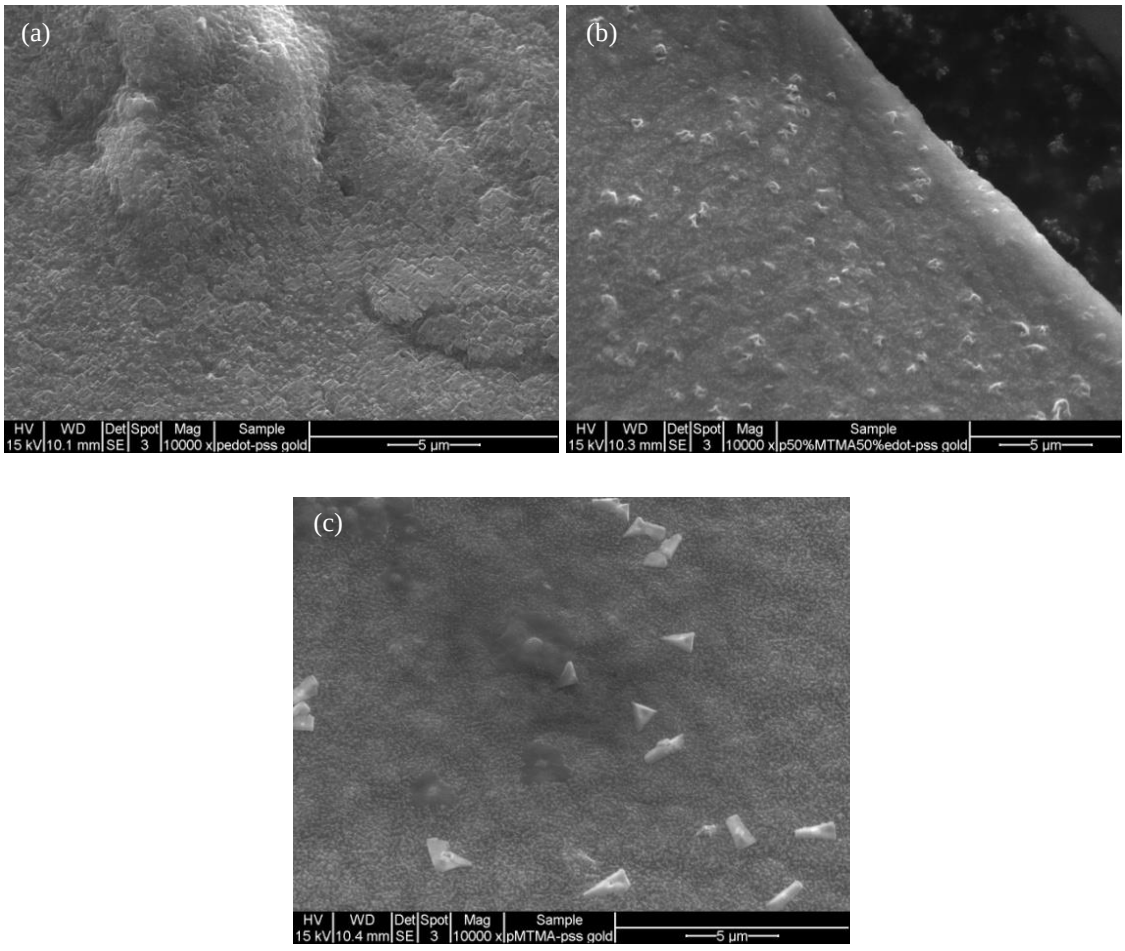

Figure 4.13 SEM images (magnification 10000x) of conductive polymer films; PEDOT:PSS (a), PEMS50 (b), and PMTMA:PSS (c).

The SEM images show relatively smooth surfaces for all conductive films; however some discrete particles appear on the surface of polymers containing MTMA. This is due to precipitation of residual salt and unreacted PSS which become embedded in the polymer surface. This reduces the homogeneity of the surface of the conductive polymer which has been shown to reduce charge flow and therefore conductivity[152].

4.2.4 Summary

MTMA, due to its dual vinylic and thiophene moieties, was identified for use as a bridge between conductive and molecularly imprinted polymers. Its efficacy in a conductive polymer capacity was assessed.

PEDOT:PSS based polymers were produced via oxidative polymerisation with increasing amounts of MTMA substituted into the polymer in place of EDOT. Characterisation of these polymers was then performed, including spectroscopic analysis, conductivity measurements and surface morphology studies. A decrease in conductivity was noted following inclusion of MTMA, likely due to a combination of steric effects and associated impact on and electron mobility. Although there is a decrease in conductivity compared to polymers prepared without MTMA, the resulting polymers still remains conductive, with conductivities of up to 5.5 S/m recorded for those polymers containing MTMA.

4.3 Molecularly Imprinted/Conductive Polymer Composite Particles

As discussed above and shown in Figure 1.12, K.C Ho et al. successfully embedded traditional MIP particles into a conductive matrix for the sensing of morphine[128]. This relied on separate binding of the morphine template by the MIP and sensing as a result of changes in measured current density due to oxidation of the morphine. Since the MIP particles themselves are not conductive, amperometric detection of morphine is limited to the surface of the particles which are in close contact to the conductive polymer. Similar methodologies have also used for both nicotine[129] and (-)-ephedrine[130] systems.

By utilising MTMA as a direct chemical bridge between the imprinted and conductive polymers it is proposed that a conductive/imprinted composite particle (CP-MIP) be produced which allows electroactive detection of the template throughout the imprinted particle. It is hoped that the creation of a polymer containing both imprinting and conductive domains, as shown in Figure 4.14, will increase the observed electroactive response. The proposed structure of this composite particle is shown in Figure 4.15.

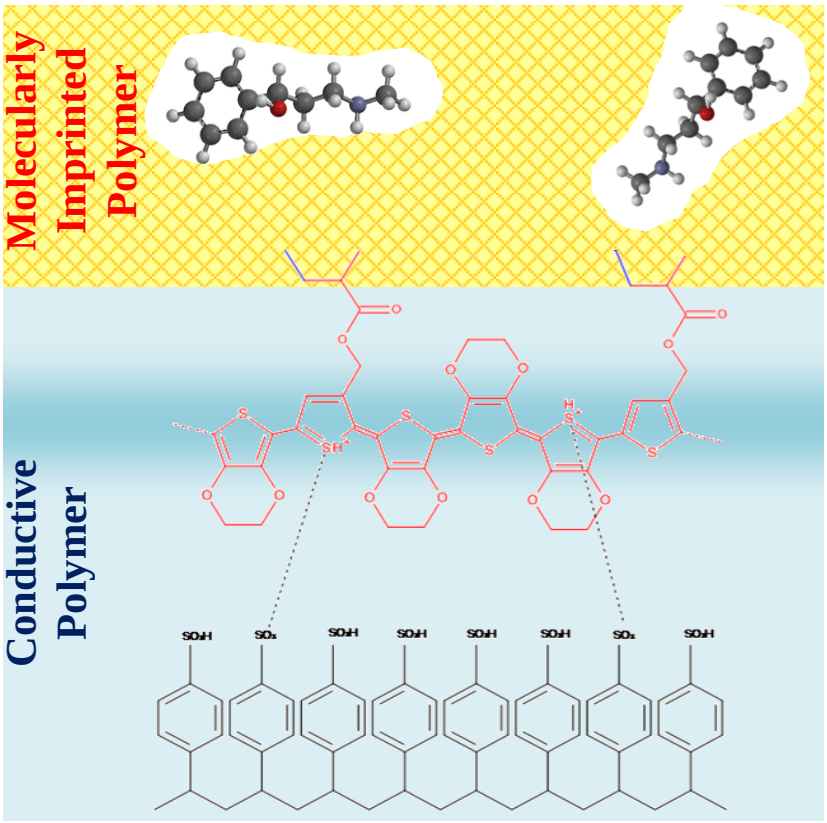

Figure 4.14 Composite polymer containing molecularly imprinted and conductive polymer domains.

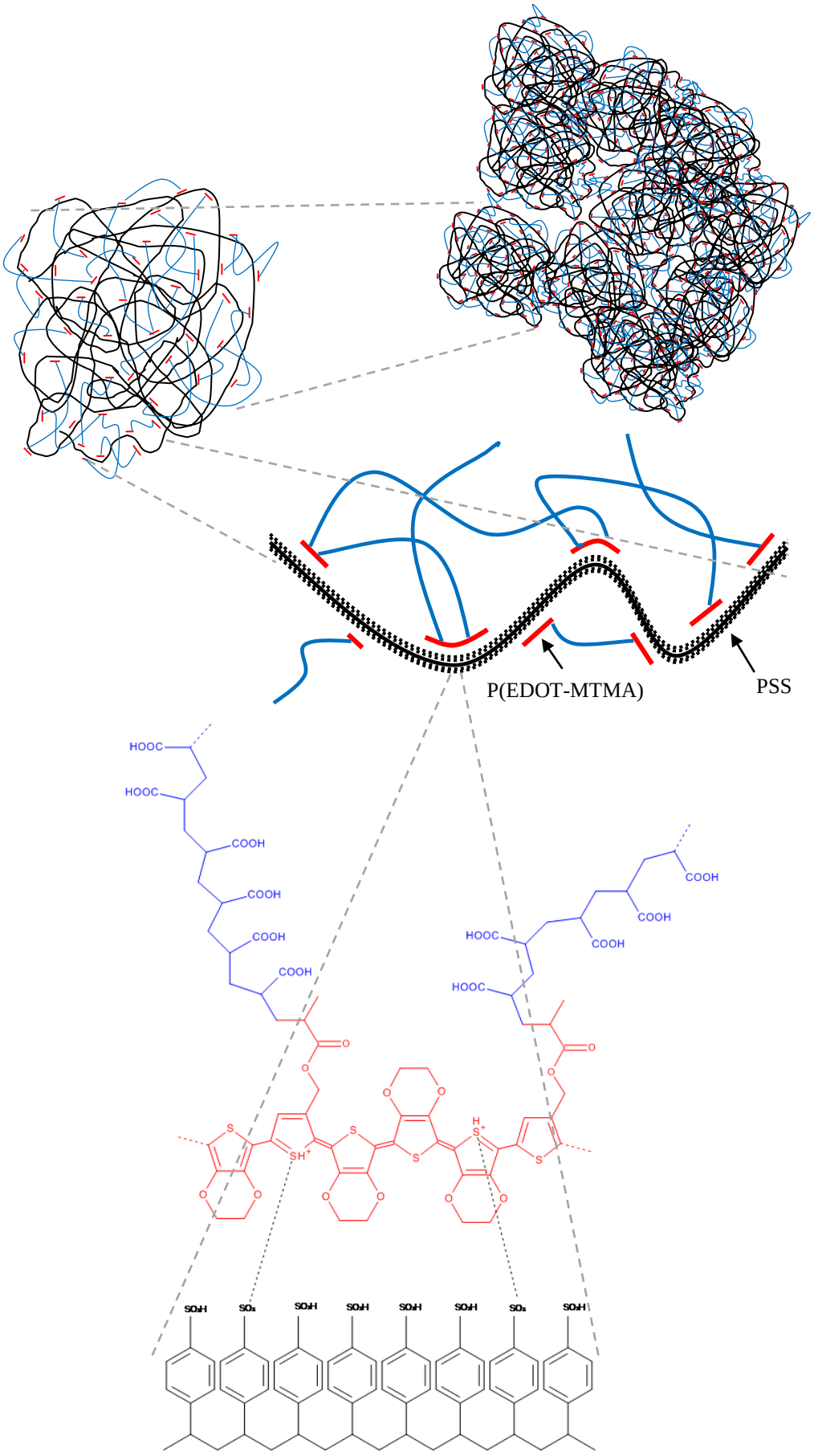

Figure 4.15 Proposed structure of molecularly imprinted polymer - conductive polymer composite[149].

4.3.1 Preparation of Molecularly Imprinted Polymer-Conductive Polymer Composite Particles

Non-imprinted composite particles (CP-NIPp) were prepared by adding 1mmol of AA to 6mL of previously synthesised aqueous solution of conductive polymer along with an initiator. For the imprinted particles (CP-MIPp_{EPD}) EPD was also added in a 3:1 M-T ratio to the AA. These polymers are listed in Table 4.4 below.

Table 4.4 Reaction ratios for synthesis of composite particles using an acrylic acid functional monomer

Polymer Code	Conductive Polymer	AA (mmol)	EPD (mmol)
PMTMA:PSS-AA1	PMTMA (97.2mg in 6mL H_20)	1	0.33
PEMS50-AA1	PEMS50 (93mg in 6mL H_20)	1	0.33
PEMS25-AA1	PEMS25 (91.2mg in 6mL H_20)	1	0.33

Following polymerisation, composite particles were isolated through filtration to remove any unreacted starting material. Since the conductive polymer solutions and AA are soluble in water, and polymerisation of the AA alone would result in water soluble polyacrylic acid, any precipitated material must therefore be a composite of the conductive polymer with AA. The insolubility of the composite is caused by the crosslinking of conductive polymer chains by the AA as shown in Figure 4.15. Subsequent template extraction from the composite particles was assessed by HPLC analysis of the extraction solution.

4.3.2 Rebinding Studies

Quantitative rebinding results were produced using HPLC following 1 hour of template rebinding, and are shown in Figure 4.16. These results show rebinding of the EPD imprinted composite polymeric particles (CP-MIPp_{EPD}) in comparison to the binding of that template to the CP-NIPp. Imprinting factors (*I*) (Equation 3) were calculated for each polymer system.

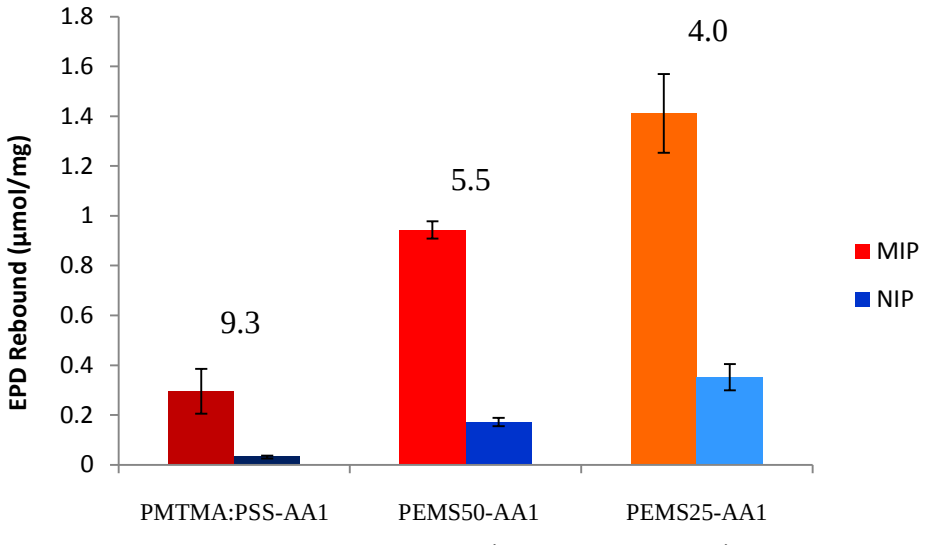

Figure 4.16 HPLC rebinding results for AA-conductive polymer composite particles (1mmolAA/6mL conductive polymer solution) with 1mM EPD after 1 hour. Imprinting factors are shown above.

These results demonstrate the successful formation of an imprinting domain in the composite particle. Additionally it can be seen that decreasing the proportion of MTMA used in the conductive polymer results in higher levels of binding in the resulting CP-MIPp$_{EPD}$. By decreasing the proportion of MTMA, the number of sites for free-radical polymerisation on the conductive polymer decreases. It is suggested that this would result in longer average chain lengths between MTMA units, allowing greater polymer chain flexibility, and a less densely cross-linked macrostructure in the composite, resulting in improved binding[84b].

Despite the increase in CP-MIPp binding there is a decrease in imprinting factor due to a corresponding increase in non-specific binding observed in the CP-NIPp. This suggests that decreasing the proportion of MTMA also increases non-specific binding. This is also likely due to reduction in cross-linking in the macrostructure of the composite, resulting in greater template access to the internal structure of the composite.

Given that rebinding is dominated by the formation of an acid-base interaction with the protonated secondary amine of the EPD template, some binding both specific and non-specific, may also be attributable to a similar interaction with the PSS component of the conductive polymer. The relative proportion of AA in these composite particles relative to the PSS in the conductive domain was calculated as approximately 2.9:1, and

suggests that the acid-base interactions of the composite polymer with the template would be dominated by those with AA. Further the suggested structure of the composite particles, with chains of AA forming between and around the already formed PEDOT-MTMA:PSS chains, would make the interaction with AA more accessible than with the more centralised PSS.

The results for PEMS50 show a good compromise between conductivity and the amount of template binding and template selectivity in the resulting composite. This conductive polymer was therefore used for all subsequent investigations.

4.3.3 Effect of Functional Monomer Concentration

The ratio of AA to conductive polymer in composite particle synthesis was investigated to determine the optimum polymer composition. CP-NIPp were prepared by separate addition of 0.5mmol, 1mmol, 2.5mmol 10mmol of AA to 93mg of PEMS50 in 6mL of water, along with an initiator. CP-MIPp_{EPD} were also produced with EPD imprinted at a constant 3:1 M-T ratio to the added AA. These polymers are listed in Table 4.5 below. The resulting composite particles were again isolated through filtration to remove any unreacted starting material or any non-composite products.

Table 4.5 Reaction ratios for synthesis of composite particles with varying amounts of the acrylic acid functional monomer

Polymer Code	Conductive Polymer	AA (mmol)	EPD (mmol)
PEMS50-AA0.5	PEMS50 (93mg in 6mL H_20)	0.5	0.17
PEMS50-AA1	PEMS50 (93mg in 6mL H_20)	1	0.33
PEMS50-AA2.5	PEMS50 (93mg in 6mL H_20)	2.5	0.83
PEMS50-AA10	PEMS50 (93mg in 6mL H_20)	10	3.33

Quantitative rebinding results for each composite formulation were produced using HPLC over 1 hour. Figure 4.17 shows rebinding of the composite particles with EPD.

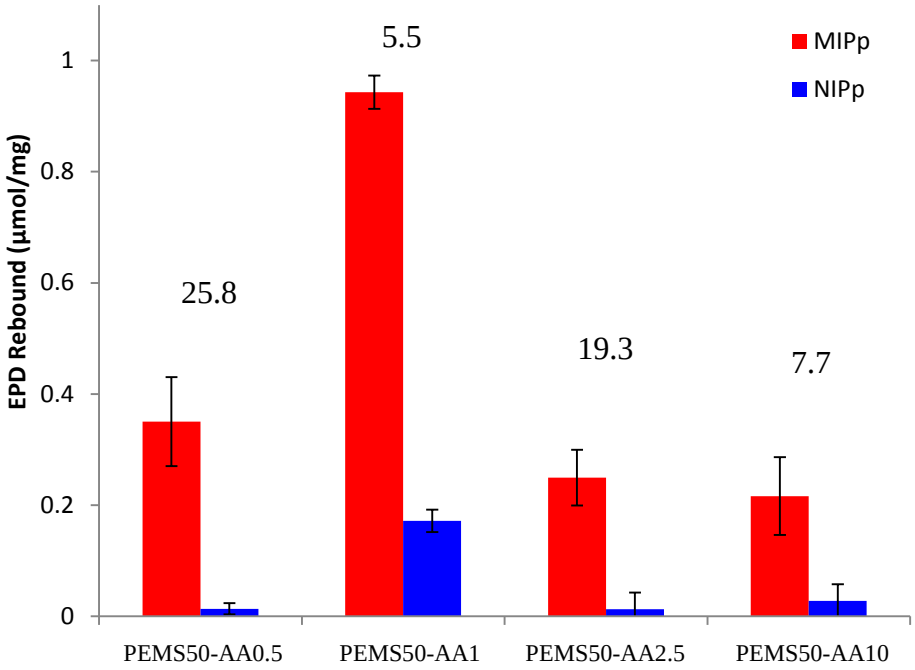

Figure 4.17 Effect of functional monomer concentration on rebinding for PEMS50-AA composite particles with 1mM EPD over 1 hour. Imprinting factors are shown above.

The PEMS50-AA1 showed the highest binding for both the CP-MIPp and CP-NIPp. Reducing the relative proportion of AA as seen in PEMS50-AA0.5 results in a decrease in binding observed in the CP-MIPp, however a significant drop in CP-NIPp binding results in a significant improvement to selectivity with an imprinting factor of 25.8 being obtained. This reduction in binding is to be expected as a reduction in AA would result in a corresponding decrease in the amount of EPD imprinted, since the 3:1 M-T ratio was kept constant, and therefore fewer binding sites will be present in the CP-MIPp.

A similar decrease in CP-MIPp binding was also observed when the relative ratio of AA in the composite particle was increased as seen in PEMS50-AA2.5 and PEMS50-AA10. Again corresponding drops in CP-NIPp binding for these composites resulted in an improvement to selectivity with imprinting factors of 19.3 and 7.7 being obtained. The reduction in binding with these composites was unexpected, as an increase to the relative amount of AA in the composite was expected to result in an increase to the number of binding cavities produced in the CP-MIPp. It is speculated the significant increases to the amount of AA in these composites results in dimerization of AA

between the polymer chains of the composite, resulting in a more densely packed internal structure to the composite, preventing access to all binding cavities.

SEM studies were also undertaken to investigate the particle size and surface morphology of these composite particles. Figure 4.18 shows SEM images of both the CP-MIPp_{EPD} and CP-NIPp for the most selective composite – PESM50-AA0.5.

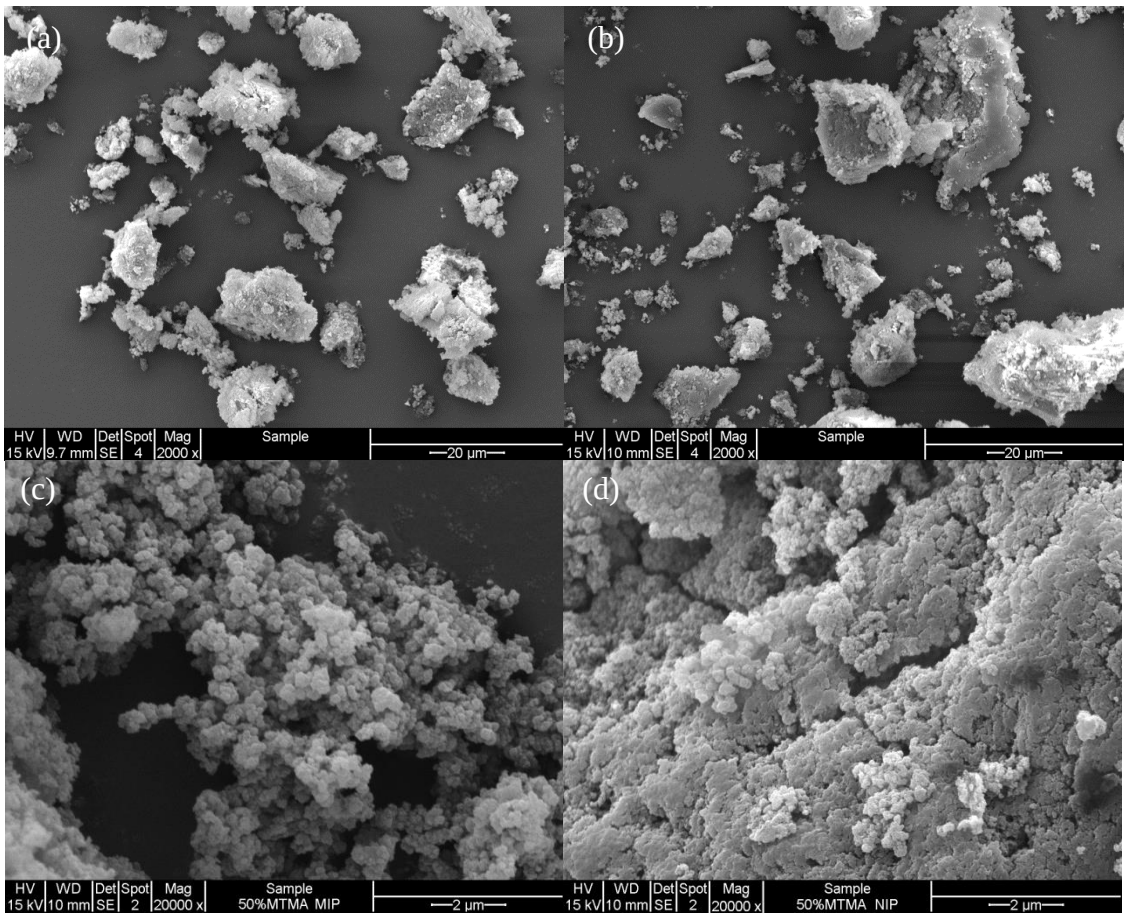

Figure 4.18 SEM images for PEMS50-AA0.5 composite particles; Magnification x2000: CP-MIPp_{EPD} (a) and CP-NIPp (b), and magnification x20000: CP-MIPp_{EPD} (c) and CP-NIPp (d) .

These images demonstrate that the CP-MIPp_{EPD} and CP-NIPp are of comparable sizes, although both are polydisperse in particles sizing. It can also be seen from these images that the MIP particles, Figure 4.18 (c), display a more irregular macroporous structure compared to the corresponding CP-NIPp, Figure 4.18 (d). Porosity within the CP-MIPp_{EPD} structure is an important aspect of the imprinting process as it is essential for template transport and access to the binding cavities[153].

4.3.4 Effect of Cross-Linker

An MBA cross-linker was included along with for AA to assess the effect of the inclusion of a cross-linker on the resulting composite particles. A total of 1mmol of MBA and AA were separately added to 6mL of PEMS50 solutions, along with an initiator, to produce CP-NIPp. CP-MIPp_{EPD} were also prepared by included EPD in the above mixtures using a 3:1 M-T ratio with AA. These polymers are listed in Table 4.6. The resulting composite particles were again isolated through filtration to remove any unreacted starting material or any non-composite products. Subsequent template extraction from the composite particles was assessed by HPLC analysis of the extraction solution.

Table 4.6 Reaction ratios for synthesis of composite particles using an acrylic acid functional monomer and a N,N'-methylenebisacrylamide crosslinker

Polymer Code	Conductive Polymer (Volume)	AA (mmol)	MBA (mmol)	EPD (mmol)
PEMS50-MBA0.2	PEMS50 (93mg in 6mL H_20)	0.8	0.2	0.27
PEMS50- MBA0.35	PEMS50 (93mg in 6mL H_20)	0.65	0.35	0.22
PEMS50-MBA0.5	PEMS50 (93mg in 6mL H_20)	0.5	0.5	0.17
PEMS50- MBA0.65	PEMS50 (93mg in 6mL H_20)	0.35	0.65	0.12
PEMS50- MBA0.8	PEMS50 (93mg in 6mL H_20)	0.2	0.8	0.07

Quantitative rebinding results were produced using HPLC across a number of rebinding times ranging from 10 minutes to 4 hours. Figure 4.19 shows EPD rebinding of the composite particles with as a function of the proportion of AA to MBA.

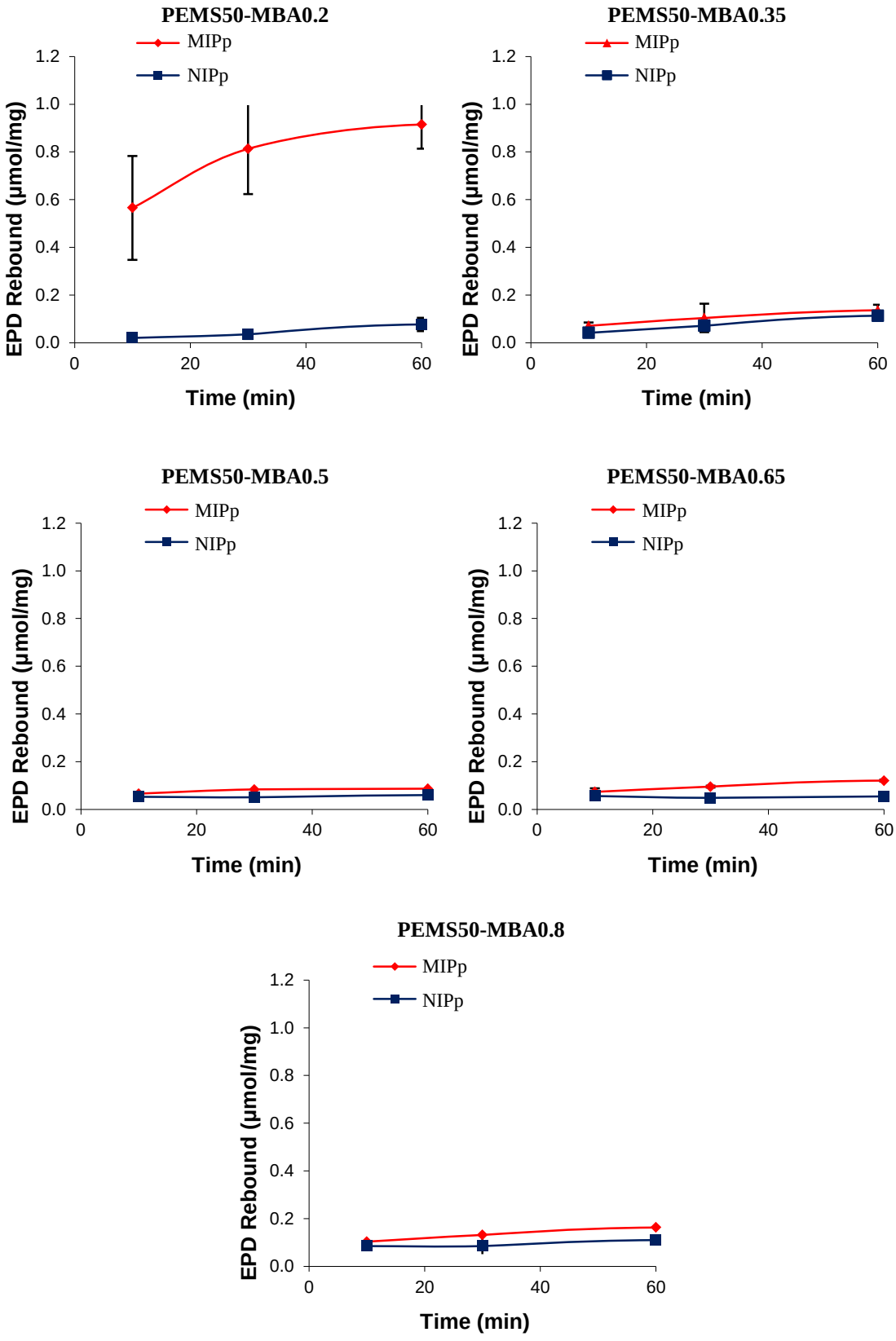

Figure 4.19 Effect of cross-linker concentration in composite particles on EPD (1mM) rebinding. PEMS50-MBA0.2 (a), PEMS50-MBA0.35 (b), PEMS50-MBA0.5 (c), PEMS50-MBA0.65 (e), and PEMS50-MBA0.8 (f). Rebinding was also measured after 24 hours with no significant additional binding observed.

An imprinting factor of 27.0 is obtained for the PEMS50-MBA0.2 composite system after 10 minutes of binding indicating it is highly selective for the EPD template. This imprinting factor reduces slightly over time due to a slight increase in CP-NIPp binding, however is greater than 11.3 for all rebinding times. The PEMS50-MBA0.2 was the most successful composite system produced, and so was used for all subsequent studies.

For compositions containing more than 20% MBA, EPD rebinding falls significantly and approximates that observed in the CP-NIPp. It is likely that significant amounts of crosslinker cause the internal structure of the composite to become densely packed, preventing access by EPD to the majority of binding cavities. The binding observed in the CP-NIPp did not change significantly as a function of both time and proportion of cross-linker indicating that the amount of cross-linker does not have a significant impact on the levels of non-specific binding.

SEM studies were also undertaken to investigate the effect of the cross-linker on the surface morphology of the resulting composite particles. Figure 4.20 shows SEM images for CP-MIPp_{EPD} particles with increasing concentrations of cross-linker.

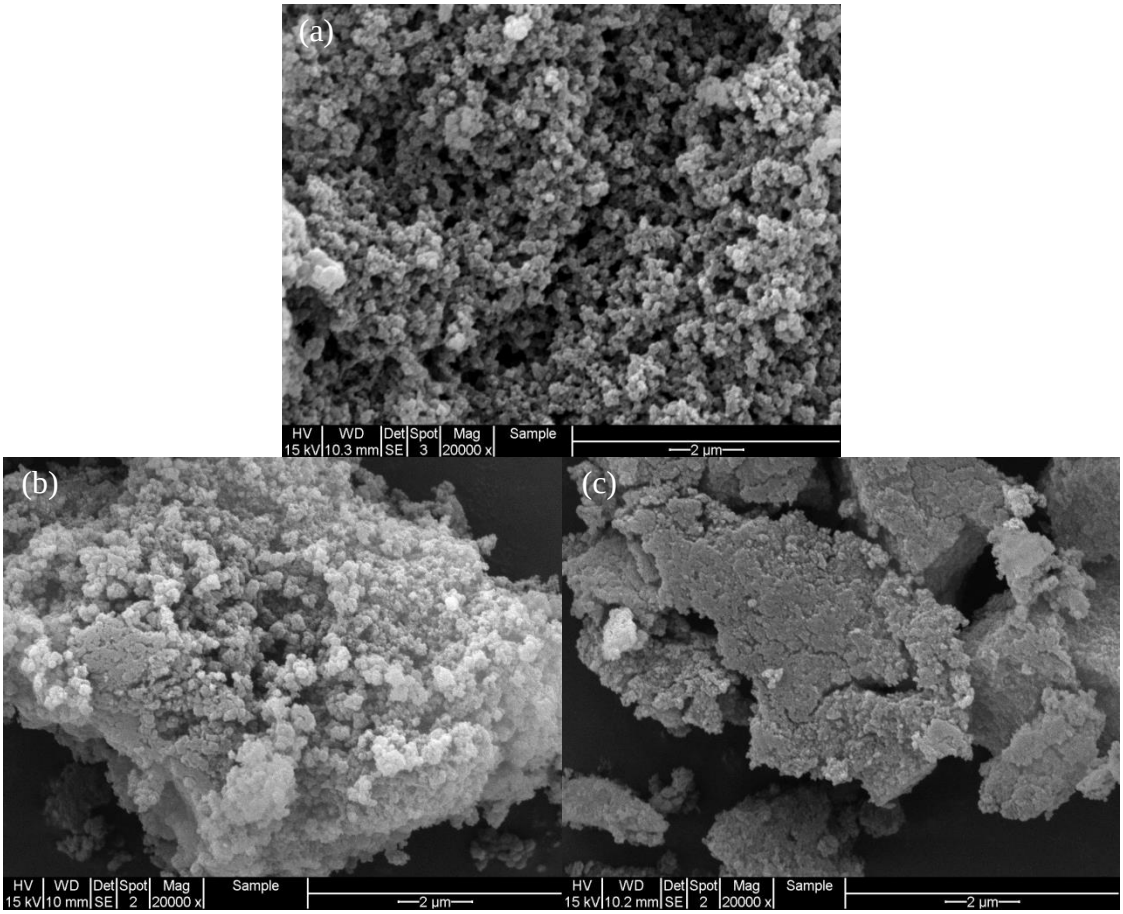

Figure 4.20 SEM images of CP-MIPp_{EPD} composite particles of PEMS50-MBA0.2 (a), PEMS50-MBA0.35 and PEMS50-MBA0.8 (c). Magnification is x2000.

It can be seen from these images that increasing proportions of cross-linker resulted in significant decreases in porosity in the resulting particles. The observed decrease in template binding is likely a direct result of the lack of porosity in these more highly cross-linked particles as the template has lower mobility though the polymer and reduced access to the binding cavities[153]. Interestingly the inclusion of a small amount of cross-linker produced a more porous surface morphology as seen in Figure 4.20 (a), compared to polymers with no included cross-linker as seen in Figure 4.18 (c). This may similarly explain the improved binding performance of the PEMS50-0.2MBA composite system.

4.3.6 Cross-Reactivity Studies

After demonstrating the successful rebinding of the EPD template with the PEMS50-0.2MBA composite, a cross reactivity study was undertaken by which the degree of binding by ADR to the CP-MIPp_{EPD} was determined as shown in Figure 4.21. ADR was used for this study as it has previously shown the highest affinity for EPD imprinted MIPs versus other non-ephedrine based analytes.

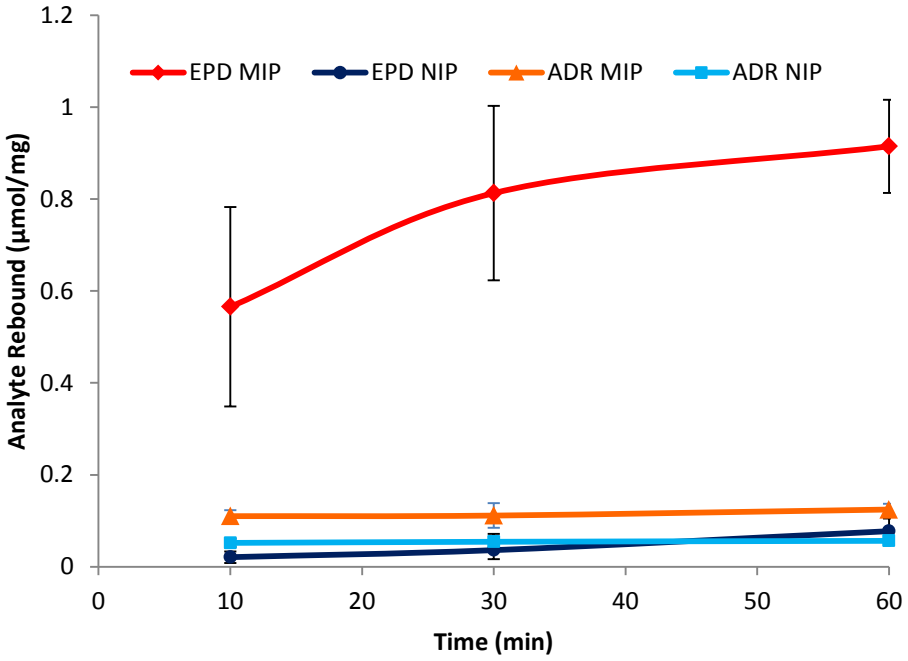

Figure 4.21 Cross reactive binding results showing PEMS50-MBA0.2 with 1mM EPD and ADR solution. Rebinding was also measured after 24 hours with no significant additional binding observed.

ADR shows significantly reduced binding in the PEMS50-MBA0.2 composite compared to EPD demonstrating that the system is specific for EPD template. Since the size of ADR is only slightly longer than that of EPD (9.8Å compared to 9.5Å) it is unlikely that a size exclusion mechanism is solely responsible for the reduction in rebinding observed with ADR. The presence of the two phenol units appear to sufficiently alter the electronic character of ADR so as to make it incompatible with the binding cavity.

4.3.7 Effect of Rebinding Solvent

Rebinding studies for the PEMS50-MBA0.2 composite particles repeated in methanol to assess the effect of the change in solvent. The effect of rebinding solvent was assessed for future studies of composite particles embedded into conductive matrices. Since matrices such as PEDOT:PSS are water soluble the ability of the composite particles to rebind in non-aqueous solvents is desirable. Quantitative rebinding results were produced using HPLC across a number of rebinding times ranging from 10 minutes to 24 hours. Figure 4.22 shows EPD rebinding of the composite particles in both water and methanol.

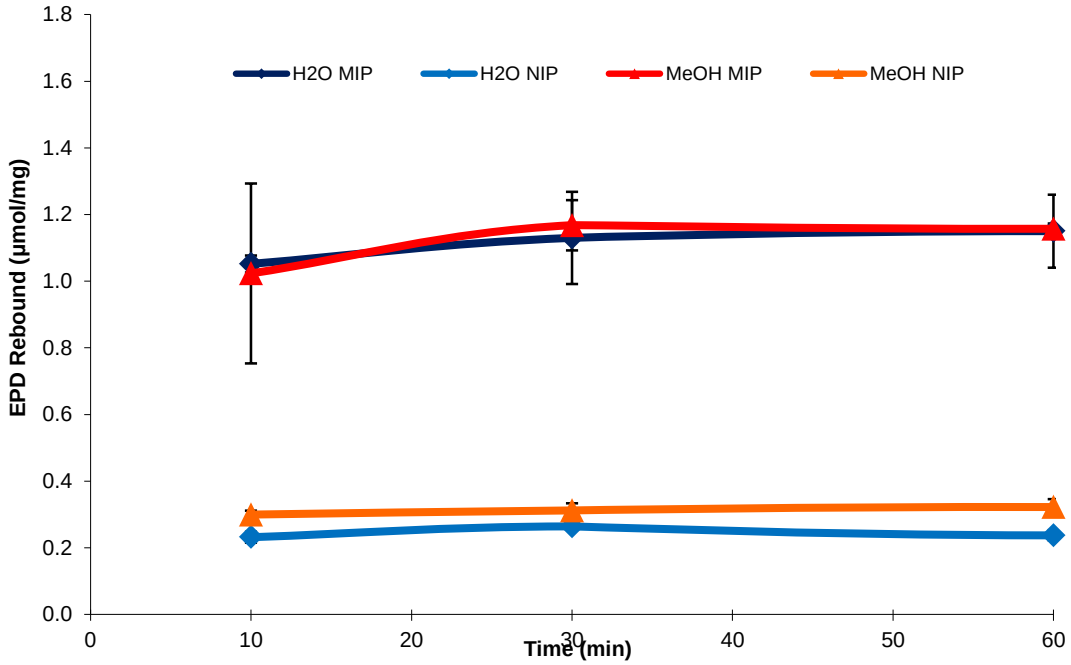

Figure 4.22 Effect of rebinding solvent on EPD (1mM) rebinding for PEMS50-MBA0.2. Rebinding was undertaken in both methanol (MeOH) and Water (H2O). Rebinding was also measured after 24 hours with no significant additional binding observed.

The rebinding for both the CP-MIPp_{EPD} and CP-NIPp in methanol is comparable to that in water for all rebinding times. This demonstrates that the PEMS50-MBA0.2 composite particles are capable of rebinding the EPD template in non-aqueous solvents. This property is an important consideration for future work embedding these particles into a conductive matrix for detection purposes.

4.3.8 Summary

Composites of a molecularly imprinted polymer and a conductive polymer were successfully prepared, demonstrating that a composite of a molecularly imprinted and conductive polymer may be created by utilising the dual functionality of MTMA. Optimisation of composite particles was achieved by investigation into the effects of MTMA proportion, the use of an AA functional monomer, and the inclusion of a MBA cross-linker.

Composites of AA and conductive polymers demonstrated that the proportion of MTMA used in the conductive polymer has a significant effect of the EPD rebinding. Decreasing the proportion of MTMA used in the conductive polymer was found to increase EPD binding, in the CP-MIPp_{EPD}, but decrease selectivity due to a corresponding binding increase in binding in the CP-NIPp.

The effect of functional monomer concentration was also investigated. A 1mmol of AA in 93mg of conductive polymer was found to produce the highest EPD binding in the resulting CP-MIPp_{EPD}. Increasing or decreasing the ratio of AA used results in a decrease in CP-MIPp_{EPD} binding, however an increase to the imprinting factor is also observed to do decreased non-specific binding in the CP-NIPp.

Composites polymers were also produced which included a MBA crosslinker in addition to the AA functional monomer. Inclusion of 0.2 mmol of MBA at results in the most successful polymer formulation (PEMS50-MBA0.2), achieving an imprinting factor of 27 after just 10 minutes of rebinding. Amounts of MBA greater than 0.2mmol resulted in a significant decrease in rebinding and a loss of selectivity.

Cross-reactivity studies using PEMS50-MBA0.2 demonstrated specificity for the EPD template versus the structurally similar ADR analyte. This polymer system was also shown to successfully rebind the EPD template in a non-aqueous solvent.

4.4 Conclusions and Future Work

4.4.1 Conclusions

A number of composite polymers containing both electroactive (PEDOT:PSS) and molecularly imprinted domains have been developed for the detection of EPD (Appendix A). The preparation of these conductive polymer CP-MIPp_{EPD} composites was made possible by the introduction of MTMA as a bridge between conductive and molecularly imprinted polymers, a synthetic method that, to the best of our knowledge, has been reported for the first time.

Phased inversed polymeric films of AA, AN, MMA, and MTMA were synthesised, however film formation was not possible for formulation with MTMA content greater than 19% and the inclusion of MTMA had a detrimental effect on film quality. The MIPfs that were successfully generated, however, were selective for the EPD template.

The inclusion of MTMA in PEDOT:PSS based polymeric films results in a marked decrease in conductivity from 98.7 to 5.5 S/m. Nevertheless, that MTMA can be incorporated into a conductive polymer, and remain conductive, validates its use in the conductive domain for a composite polymer.

Utilising the dual functionality of MTMA, CP-MIPp_{EPD} composites of various formulations using AA as functional monomer with and without the MBA cross-linker (PEMS-AA-MBA and PEMS-AA, respectively) were prepared.

The proportion of MTMA incorporated in PEDOT:PSS was found to impart a significant effect on EPD rebinding. Decreasing the proportion of MTMA used in the conductive polymer was found to increase EPD binding in the CP-MIPp_{EPD},(most likely due to less crosslinking between conductive polymer chains and the formation of a longer AA chain length) but decrease selectivity due to a corresponding binding increase in the CP-NIPp (due to a greater number of free AA).

Increasing the amount of AA (> 1mmol in 6 mL of conductive polymer solution) in the formulation resulted in a decrease in MIP binding, most likely due to an increase in cross-linking between conductive polymer chains resulting in a reduction of template access to binding cavities. Decreasing the amount of AA (< 1mmol in 6 mL of conductive polymer solution) in the formulation also resulted in a decrease in CP-MIPp_{EPD} binding, due to a decrease in the number of binding cavities. In both cases the imprinting factor also increased due to decreased non-specific binding in the CP-NIPp.

PEMS-AA-MBA proved to be the most promising among the CP-MIPp_{EPD} composite systems investigated. In particular, the CP-MIPp_{EPD} composite consisting of 93.0mg of P(50%EDOT-50%MTMA):PSS with 0.8mmol of AA and 0.2mmol of MBA was the most successful formulation achieved displaying a selectivity of 27 after 10 minutes of rebinding stabilising to 11 after 1 hour with a EPD binding of 0.91 μmol/mg, and a specificity (I_{EPD}/I_{ADR}) of 5.1 against ADR. This has demonstrated, for the first time, the potential of a CP-MIP composite for electrochemical sensing under the right conditions and matrix beyond the scope of this study.

4.4.2 Future Work

Studies that could be conducted in order to further support this work would include incorporation of CP-MIP composites into a conductive matrix to allow electrochemical detection. Some initial investigations into this process were made by this author, with attempts made to incorporate the CP-MIPp_{EPD} composites into the PEDOT:PSS matrix. PEDOT:PSS was chosen as the conductive matrix for the electrochemical detection studies due to its ease of synthesis and high processability.

PEMS50-MBA0.2 composite particles, both CP-MIPp_{EPD} and CP-NIPp, were embedded into a conductive PEDOT:PSS matrices to allow electrochemical based detection. Particle concentrations ranging from 50-500mg/mL were used, and the

resulting mixture was spun cast (1500rpm) onto a glass substrate and annealed at 110°C to form films of 3.2±0.4mm in thickness.

Quantitative rebinding results were produced using HPLC over 24 hours of template rebinding, and are shown in Figure 4.23. These studies were performed to assess the effect of the conductive matrix on template rebinding to the composite particles. These results show rebinding of the EPD to the CP-MIPp$_{EPD}$ in comparison to the binding to the CP-NIPp.

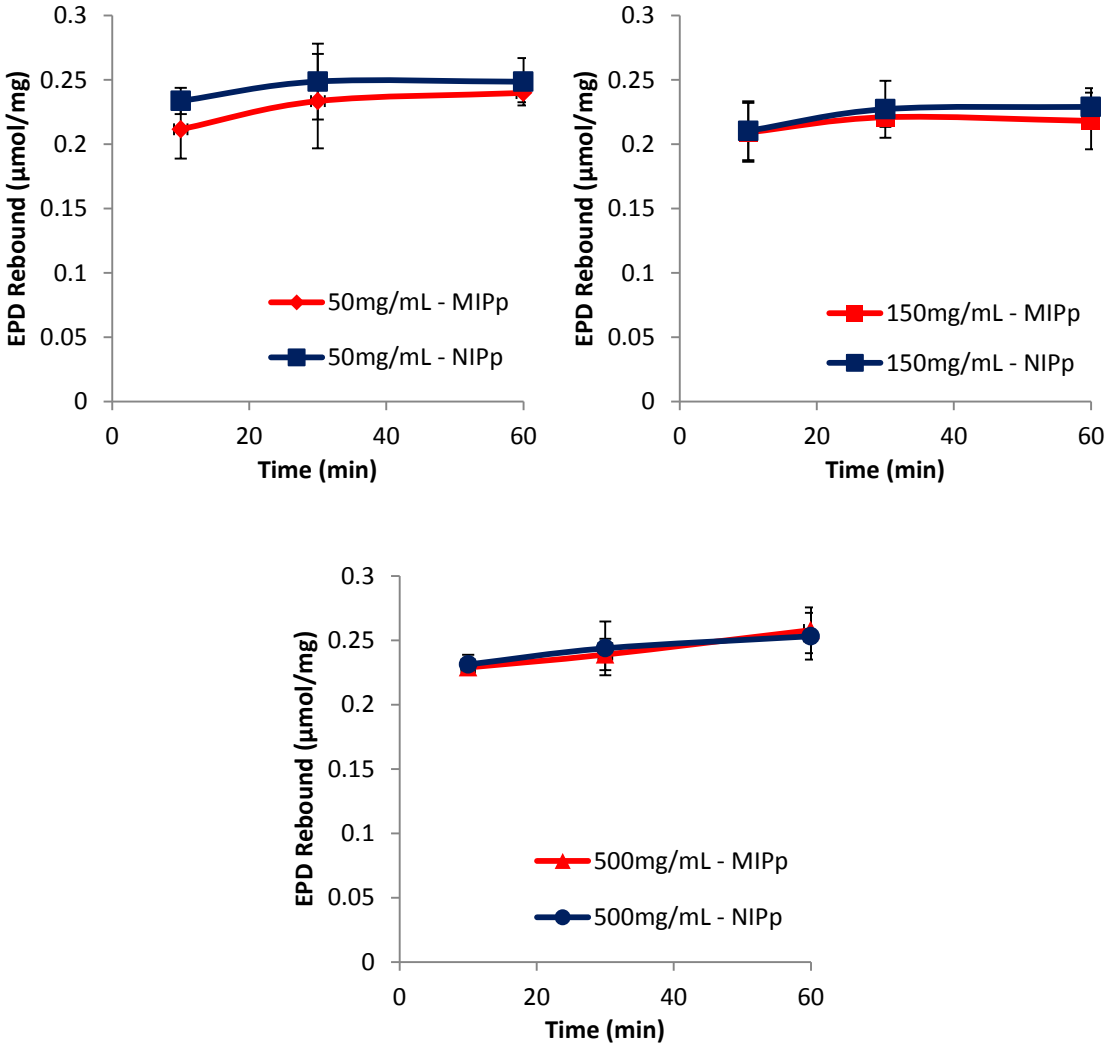

Figure 4.23 EPD rebinding results for PEMS50-MBA0.2 composite particles embedded in a PEDOT:PSS matrix; 50mg/mL (a), 150mg/ml (b), and 500mg/mL (c). Rebinding was also measured after 24 hours with no significant additional binding observed.

High levels of EPD binding were observed in both the MIPp and NIPp suggesting that non-specific binding is dominating, resulting in a lack of selectivity for the EPD template. The high levels of binding must be attributed to the PEDOT:PSS matrix, and so studies were then performed to assess the binding of EPD to PEDOT:PSS alone. Rebinding was assessed quantitatively over 24hours using HPLC and results are shown in Figure 4.24.

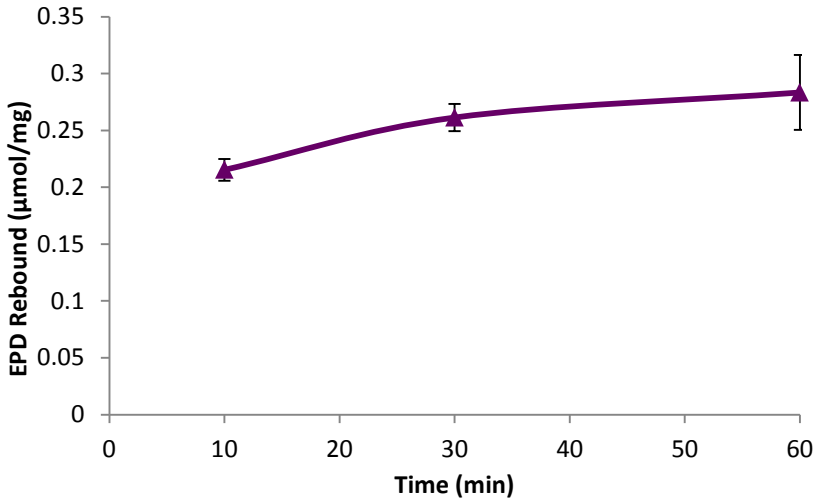

Figure 4.24 EPD rebinding results for PEDOT:PSS film. Rebinding was also measured after 24 hours with no significant additional binding observed.

PEDOT:PSS shows similar levels of binding in the absence of embedded composite particles. This confirms the notion that the observed high levels of non-specific binding for PEMS50-MBA0.2 composite particles embedded in a PEDOT:PSS matrix is due to the conductive polymer matrix itself. This can be attributed to a strong acid-base interaction of the secondary amine of the EPD template with the acidic PSS component of the conductive polymer matrix. The AA interaction with EPD was suggested as being the dominant interaction in the CP-MIPp_{EPD} composites due to the relative proportions of AA and PSS. However, once embedded the non-specific interactions with PSS in the PEDOT:PSS matrix would become far more prevalent.

SEM images of PEMS50-MBA0.2 composite particles embedded in a PEDOT:PSS matrix, as seen in Figure 4.25,were taken to investigate their surface morphology.

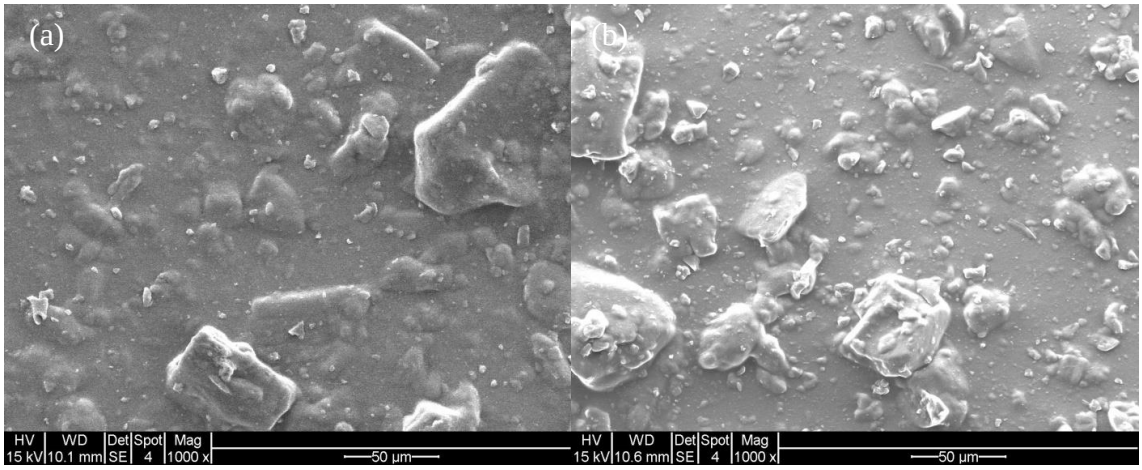

Figure 4.25 SEM images of PEMS50-MBA0.2 composite particles embedded in a PEDOT:PSS matrix; MIP (a) and NIP (b). Magnification is x1000.

The SEM images show that the composite particles are completely embedded in the PEDOT:PSS conductive matrix. Additionally the lack of porosity in the PEDOT:PSS surface means that the template cannot easily access the binding cavities of the PEMS50-MBA0.2 composite particles.

While the use of PSS in the conductive polymer makes the PEDOT:PSS both simpler to synthesis and significantly more processable. These results however suggest that the inclusion of the PSS will also prevent its use as the conductive matrix for the composite particles due the large increase in observed non-specific rebinding. The resulting lack of selectivity makes electrochemical detection using this system unfeasible was not attempted.

Future studies utilising an alternate conductive matrix, such as polypyrrole or poly(3-hexylthiophene) would make embedding the composite particles more difficult, however these conductive matrices are less likely to prevent template selectivity due to non-specific binding, making electrochemical detection possible.

Additionally an investigation of the scope of the composite particles for use with other templates is warranted. Finally the development and evaluation of a MIP based sensor utilising these composite particles for electrochemical based detection is required.

CHAPTER 5 – CONCLUSIONS

In this study, signal transduction mechanisms for molecularly imprinted polymeric systems selective to *(-)*-ephedrine have been investigated and involved the development of various MIPs, summarised in Appendix A, in film and particulate formats, both cross-linked and linear, utilising in *situ* and post-polymerisation imprinting.

In all cases, the formulation of these MIPs has been guided by interaction studies between monomers and analytes (template and competing analogues) using semi-empirical molecular modelling and NMR spectroscopy. All MIP systems employed acrylic acid as the functional monomer which strongly binds with the EPD template through the formation of an acid-base interaction, as well as additional hydrogen bonding interactions. Other monomers (IPA, MBA, AN, MMA, MTMA, EDOT) responsible for the polymer bulk generally showed minimal interaction with EPD.

MIPs developed in this study displayed imprinting efficiency, based on imprinting factors, ranging from a low of 1.3 (PEMS-AA-MBA) to a high of 27 (PAAMM). Representative systems (shaded in Appendix A) tested also showed high specificity to EPD against analogous analytes ADR, THEO, CAFF and for PAA-AN-MMA were capable of discriminating between ephedrine stereoisomers.

5.1 Gold Nanoparticles and Molecularly Imprinted Polymers

Embedded gold nanoparticles were explored as a detection mechanism for molecularly imprinted polymers. The surface plasmon resonance of the gold nanoparticles is dependent on the inter-particle distance of the immobilised gold nanoparticles, allowing the swelling behaviour of a MIP during rebinding to produce a detectable signal.

PAA-IPA-MBA (18.8%AA, 76.4%IPA and 4.8%MBA), utilised by Matsui et al.[68, 100] and phase inversed PAA-AN-MMA system (17%AA, 41%AN, and 42%MMA) MIP systems were both tested. While the PAA-IPA-MBA MIP selective to ADR and EPD showed high levels of template binding, imprinting factors 3.4 and 2.4, respectively, after 24 hours, the plasmon absorbance band of thiol-stabilised gold nanoparticles could not be detected in the UV-Vis spectrum once the nanoparticles were embedded in PAA-IPA-MBA system.

A phase inversed PAA-AN-MMA MIPf was produced which was both selective and specific to the EPD template with detection being observed after as little as 10 minutes. Gold nanoparticles were embedded into this polymer system which resulted in a decrease to selectivity with an imprinting efficiency of 4.8 after 2 hours, compared to 7.2 for MIPf without gold nanoparticles. Spectroscopic rebinding studies found that wavelength of maximum plasmon absorbance of embedded gold nanoparticles shifted up to 15nm for the MIPf compared to 8nm for the NIPf. The amount of template rebound by the polymer was found to closely correlate to the observed shift in the surface plasmon resonance spectrum of the embedded gold nanoparticles. The type of thiol stabilising agent used to prepare the gold nanoparticles was shown not to affect EPD sorption or the resulting surface plasmon resonance response in the MIPf. Cross-reactivity studies for this system showed it was highly specific for ephedrine-based analytes and is also capable of differentiating EPD from its stereoisomers. Spectroscopic rebinding studies also showed that the shift in plasmon absorbance was significantly reduced for non-ephedrine based analytes (ADR, CAFF and THEO).

These results show excellent promise for the use of PAAANMMA polymers with embedded gold nanoparticles as a forensic sensor for spectroscopic detection of EPD.

5.2 Conductive Polymers/Molecularly Imprinted Polymer Composites

Composite polymers containing both electroactive (PEDOT:PSS) and molecularly imprinted domains have been developed for the detection of EPD. MTMA was utilised as a bridge between the conductive and molecularly imprinted polymers.

Phased inversed polymeric films of AA, AN, MMA, and up to 19% MTMA were synthesised, with the inclusion of MTMA noted as having a detrimental effect on film quality. The MIPfs synthesised with MTMA found to remain selective for the EPD template.

PEDOT:PSS based conductive polymer solutions were prepared which incorporated MTMA into the conductive backbone of the polymer. Inclusion of MTMA resulted in a marked decrease in conductivity from 98.7 to 5.5 S/m. Nevertheless, that MTMA can be incorporated into a conductive polymer, and remain conductive.

Utilising the dual functionality of MTMA, CP-MIPp_{EPD} composites of various formulations using AA as functional monomer (PEMS-AA) and with an MBA cross-linker (PEMS-AA-MBA) were prepared.

The effect of changes in relative proportion of MTMA, AA and MBA on the selectivity of the resulting CP-MIPp_{EPD} was assessed, with a CP-MIPp_{EPD} composite consisting of 93.0mg P(50%EDOT-50%MTMA):PSS with 0.8mmol of AA and 0.2mmol of MBA being the most successful formulation achieved. This CP-MIPp_{EPD} displayed a selectivity of 27 after 10 minutes, and 11 after 1 hour with an EPD binding of 0.91 μmol/mg, and specificity (I_{EPD}/I_{ADR}) of 5.1 against ADR.

We have demonstrated the development of a novel composite system of conductive and molecularly imprinted polymers which is capable of the acting as a possible detection element in future electrochemical sensors.

APPENDIX

Appendix A List of EPD-imprinted polymer systems developed in this study.

Polymer Code/ Format	Polymer Formulation	MIP Binding μmol/mg	NIP Binding μmol/mg	Imprinting Factor (*I*)	Binding Time (h)	Signal Transduction Mechanism
PAA-IPA-MBA Film from bulk hydrogel (Chapter 3.2)	18.8% AA, 76.4% IPA, 4.8% MBA, + AU_{MUA}	0.30	0.13	2.4	24	SPR – No significant response
PAA-AN-MMA Phase inversed film from linear polymers (Chapter 3.3)	17% AA, 41% AN,42% MMA	0.68	0.09	7.2	2	
	17% AA, 41% AN, 42% MMA + Au_{MUA}	0.32	0.07	4.8	2	SPR – Up to 15nm shift in UV-Vis spectrum
	17% AA, 41% AN, 42% MMA, + Au_{1D9T}	0.35	0.06	6.2	2	
	17% AA, 41% AN, 42% MMA, + Au_{NDT}	0.35	0.07	4.7	2	
	17% AA, 41% AN, 42% MMA, with Au_{NDT}	0.31	0.06	4.9	2	
PAAMM Phase inversed film from linear polymers (Chapter 4.1)	15.1% AA, 38.6% AN, 39.1% MMA, 7.1% MTMA	0.47	0.28	1.6	2	
	13.7% AA, 34.9% AN, 32.8% MMA, 18.6% MTMA	0.11	0.04	3.0	2	
PMTMA:PSS-AA1 Particulate (Chapter 4.3)	6mL PMTMA:PSS, 1mmol AA	0.30	0.03	9.3	1	
PEMS25-AA1 Particulate	6mL PEMS25, 1mmol AA	1.41	0.35	4.0	1	

Appendix A Cont. List of EPD-imprinted polymer systems developed in this study.

Polymer Code/ Format	Polymer Formulation	MIP Binding µmol/mg	NIP Binding µmol/mg	Imprinting Factor (*I*)	Binding Time (h)	Signal Transduction Mechanism
PEMS50-AA Particulate (Chapter 4.3)	6mL PEMS50, 0.5mmol AA	0.35	0.01	25.8	1	
	6mL PEMS50, 1mmol AA	0.94	0.17	5.5	1	
	6mL PEMS50, 2.5mmol AA	0.25	0.01	19.3	1	
	6mL PEMS50, 10mmol AA	0.22	0.03	7.7	1	
PEMS-AA-MBA Particulate (Chapter 4.3)	6mL PEMS50, 0.2mmol AA, 0.8mmol MBA	0.16	0.11	1.5	1	
	6mL PEMS50, 0.35mmol AA, 0.65mmol MBA	0.12	0.05	2.4	1	
	6mL PEMS50, 0.5mmol AA, 0.5mmol MBA	0.09	0.06	1.5	1	
	6mL PEMS50, 0.65mmol AA, 0.35mmol MBA	0.14	0.11	1.3	1	
	6mL PEMS50, 0.8mmol AA, 0.2mmol MBA	0.91	0.08	11.3	1	
PEMS-AA-MBA in PEDOT:PSS matrix (Chapter 4.4)	6mL PEMS50, 0.8mmol AA, 0.2mmol MBA	0.24	0.25	1.0	1	Conductivity – Non-selective

Shaded MIPs have been tested for specificity through cross-reactivity studies.

REFERENCES

1. (a) *World Drug Report 2012*. United Nations Office on Drugs and Crime (UNODC): New York, 2012;

   (b) Economic and social consequences of drug abuse and illicit trafficking. UNODC.

2. *Illicit Drug Data Report 2010-11*. Australian Crime Commision: 2012.

3. Laboratory and forensic science services. http://www.unodc.org/unodc/en/scientists/laboratory-and-forensic-science-services.html (accessed 05/12/2012).

4. Klein, R. F. X.; Hays, P. A. Detection and analysis of drugs of forensic interest, 1992-2001; A Literature review. www.usdoj.gov/dea/programs/forensicsci/microgram/journal_v1/mjournal_v1_pg8.html (accessed 06/06/06).

5. Curini, R.; Zamponi, S.; D'Ascenzo, F.; Curtis, S. D. A.; Marino, A.; Dezzi, A., Thermal analytical techniques applied to the narcotic field: cocaine analysis. *Thermochimica Acta* **1989,** *153*, 11-26.

6. (a) Pirozhkov, S. V.; Watson, R. R.; Eskelson, C. D., Gas chromatographic detection of cocaine and cocaethylene in hair of mice chronically injected with cocaine or cocaethylene and fed ethanol. *Forensic Science International* **1992,** *57*, 99-107;

   (b) Valente-Campos, S.; Mauricio, Y.; Moreau, R. L. d. M.; Silva, O. A., Validation of a method to detect cocaine and its metabolites in nails by gas chromatography-mass spectrometry. *Forensic Science International* **2006,** *159*, 218-222.

7. Koulis, C. V.; Reffner, J. A.; Bibby, A. M., Comparison of transmission and internal reflectance infrared spectra of cocaine. *Journal of Forensic Science* **2001,** *46* (4), 822-829.

8. Dixon, S. J.; Brereton, R. G.; Carter, J. F.; Sleeman, R., Determination of cocaine contamination on banknotes using tandem mass spectrometry and pattern recognition. *Analytica Chimica Acta* **2006,** *559*, 54-63.

9. Yonamine, M.; Sampaio, M. C., A high-performance thin layer chromatographic technique to screen cocaine in urine samples. *Legal Medicine* **2006,** *8*, 184-187.

10. (a) Travnikoff, B., Semiquantitative screening test for cocaine. *Analytical Chemistry* **1983,** *55*, 795-796;

    (b) Tsumura, Y.; Mitome, T.; Kimoto, S., False positives and false negatives with a cocaine-specific field test and modification of test protocol to reduce false decision. *Forensic Science International* **2005,** *155*, 158-164.

11. Duncan, W. P.; Deutsch, D. G., The use of GC/IR/MS for high-confidence identification of drugs. *Clinical Chemistry* **1989,** *35* (7), 1279-1281.

12. Lorenzo, N.; Wan, T.; Harper, R. J.; Hsu, Y.-L.; Chow, M.; Rose, S.; Furton, K. G., Laboratory and field experiments used to identify *Canis lupus var. familiaris* active odor signature chemicals from drugs, explosives, and humans. *Analytical and Bioanalytical Chemistry* **2003,** *376* (8), 1212-1224.

13. Rapid testing methods for drugs of abuse. www.unodc.org/unodc/en/publications/publications_scientific_support.html (accessed 05/06/06).

14. *World Drug Report 2010*. United Nations Office on Drugs and Crime (UNODC): New York, 2010.

15. Drug Seizure Data. United Nations Office on Drugs and Crime: 2012.

16. Mizaikoff, B. MIP principle. http://asl.chemistry.gatech.edu/images/mip_principle.gif (accessed 06/06/06).

17. Sellergren, B.; Hall, A. J., Fundamental aspects on the synthesis and characterisation of imprinted network polymers. In *Moleculary Imprinted Polymers: Man-made mimics of antibodies anf their applications in analytical chemistry*, Sellergren, B., Ed. Elsevier Science: Amsterdam, 2001; Vol. 23.

18. Gao, N.; Dong, J.; Liu, M.; Ning, B.; Cheng, C.; Guo, C.; Zhou, C.; Peng, Y.; Bai, J.; Gao, Z., Development of molecularly imprinted polymer films used for detection of profenofos based on a qaurtz crystal microbalance sensor. *Analyst* **2012,** *137* (5), 1252-1258.

19. Wulff, G.; Grobe-Einsler, R.; Vesper, W.; Sarhan, A., Enzyme-analog built polymers. *Makromolekulare Chemie* **1977,** *178* (10), 2817-25.

20. Boonpangrak, S.; Prachayasittikul, V.; Bulow, L.; Ye, L., Molecularly imprinted polymer microspheres prepared by precipitation polymerization using a sacrifcial covalent bond. *Journal of Applied Polymer Science* **2006,** *99*, 1390-1398.

21. Khasawneh, M. A.; Vallano, P. T.; Remcho, V. T., Affinity screening by packed capillary high performance liquid chromatography using imprinted sorbents II. Covalent imprinted polymers. *Journal of Chromatography A* **2001,** *922*, 87-97.

22. Mukawa, T.; Goto, T.; Takeuchi, T., Post-oxidative conversion of thiol residue to sulfonic acid in the binding sites of molecularly imprinted polymers: disulfide based covalent molecular imprinting for basic compounds. *Analyst* **2002,** *127*, 1407-1409.

23. Cacho, C.; Turiel, E.; Martin-Esteban, A.; Ayala, D.; Perez-Conde, C., Semi-covalent imprinted polymer using propazine methacrylate as template molecule for the clean-up of triazines in soil and vegetable samples. *Journal of Chromatography A* **2006,** *1114*, 255-262.

24. Gallego-Gallegos, M.; Munoz-Olivase, R.; Caara, C.; Mancheno, M. J.; Sierra, M. A., Synthesis of a pH dependent covalent imprinted polymer able to recognize organotin species. *Analyst* **2006,** *131*, 98-105.

25. Arshady, R.; Mosbach, K., Synthesis of substrate selective polymers by guest host polymerisation. *Makromolekulare Chemie* **1981,** *182* (2), 687-692.

26. Reddy, P. S.; Kobayashi, T.; Abe, M.; Fujii, N., Molecular imprinted nylon-6 as a recognition material of amino acids. *European Polymer Journal* **2002,** *38*, 521-529.

27. Reddy, P. S.; Kobayashi, T.; Fujii, N., Recognition characteristics of dibenzofuran by molecularly imprinted polymers made of common polymers. *European Polymer Journal* **2002,** *38*, 779-785.

28. Kobayashi, T.; Murawaki, Y.; Reddy, P. S.; Abe, M.; Fujii, N., Molecular imprinting of caffeine and its recognition assay by quartz-crystal microbalance. *Analytica Chimica Acta* **2001,** *435*, 141-149.

29. Trotta, F.; Drioli, E.; Baggiani, C.; Lacopo, D., Molecular imprinted polymeric membrane for naringin recognition. *Journal of Membrane Science* **2002,** *201*, 77-84.

30. Kubo, H.; Yoshioka, N.; Takeuchi, T., Fluorescent imprinted polymers prepared with 2-acrylamidoquinoline as a signaling monomer. *Organic Letters* **2005,** *7* (3), 359-362.

31. (a) Wang, H. Y.; Kobayashi, T.; Fukaya, T.; Fujii, N., Molecular imprint membranes prepared by the phase inversion precipitation technique. 2. influence of coagulation temperature in the phase inversion process on the encoding in polymeric membranes. *Langmuir* **1997,** *13*, 5396-5400;

    (b) Kobayashi, T.; Wang, H. Y.; Fujii, N., Molecular imprint membranes of polyacrylonitrile copolymers with different acrylic acid segments. *Analytica Chimica Acta* **1998,** *365*, 81-88.

32. Ulbricht, M.; Malaisamy, R., Insights into the mechanism of molecular imprinting by immersion precipitation phase inversion of polymer blends via a detailed morphology analysis of porous membranes. *Journal of Materials Chemistry* **2005,** *15*, 1487-1497.

33. Park, J. K.; Khan, H.; Lee, J. W., Preparation of phenylalanine imprinted polymer by the sol-gel transition method. *Enzyme and Microbial Technology* **2004,** *35*, 688-693.

34. Hsu, H.-C.; Chen, L.-C.; Ho, K.-C., Colorimetric detection of morphine in a molecularly imprinted polymer using an aqueous mixture of Fe^{3+} and $[Fe(CN)_6]^{3-}$. *Analytica Chimica Acta* **2004,** *54*, 141-147.

35. Piletsky, S. A.; Karim, K.; Piletska, E. V.; Day, C. J.; Freebairn, K. W.; Legge, C.; Turner, A. P. F., Recognition of ephedrine enantiomers by molecularly imprinted polymers designed using a computational approach. *Analyst* **2001,** *126*, 1826-1830.

36. Zurutuza, A.; Bayoudh, S.; Cormack, P. A. G.; L. Dambies; Deere, J.; Bischoff, R.; Sherrington, D. C., Molecularly imprinted solid-phase extraction of cocaine metabolites from aqueous samples. *Analytica Chimica Acta* **2005,** *542*, 14-19.

37. Holdsworth, C. I.; Bowyer, M. C.; Lennard, C.; McCluskey, A., Formulation of cocaine-imprinted polymers utilizing molecular modelling and NMR analysis. *Australian Journal of Chemistry* **2005,** *58* (5), 315-320.

38. Piletska, E. V.; Romero-Guerra, M.; Chianella, I.; Karim, K.; Turner, A. P. F.; Piletsky, S. A., Towards the development of multisensor for drugs of abuse based on molecular imprinted polymers. *Analytica Chimica Acta* **2005,** *542*, 111-117.

39. (a) Bunte, G.; Hurttlen, J.; Pontius, H.; Hartlieb, K.; Krause, H., Gas phase detection of explosives such as 2,4,6-trinitrotoluene by molecularly imprinted polymers. *Analytica Chimica Acta* **2007,** *591* (1), 49-56;

(b) Walker, N. R.; Linman, M. J.; Timmers, M. M.; Dean, S. L.; Burkett, C. M.; Lloyd, J. A.; Keelor, J. D.; Baughman, B. M.; Edmiston, P. L., Selective detection of gas-phase TNT by integrated optical waveguide spectrometry using molecularly imprinted sol-gel sensing films. *Analytica Chimica Acta* **2007,** *593* (1), 82-91.

40. Ramstrom, O. Molecular imprinting technology. http://www.smi.tu-berlin.de/story/gloss.htm (accessed 7/4/06).

41. Harris, T. K.; Mildvan, A. S., High-precision measurement of hydrogen bond lengths in proteins by nuclear magnetic resonance methods. *Proteins: Structure, Function, and Genetics* **1999,** *35*, 275-282.

42. Idziak, I.; Benrebouh, A.; Deschamps, F., Simple NMR experiments as a means to predict the performance

of an anti-17α-ethynylestradiol molecularly imprinted polymer. *Analytica Chimica Acta* **2001,** *435*, 137-140.

43. Sellergren, B.; Lepisto, M.; Mosbach, a. K., Highly enantioselective and substrate-selective polymers obtained by molecular imprinting utilizing noncovalent interactions. NMR and chromatographic studies on the nature of recognition. *Journal of the American Chemical Society* **1988,** *10*, 5853-5860.

44. Farrington, K.; Regan, F., Investigation of the nature of MIP recognition: The development and characterization of a MIP for Ibuprofen. *Biosensors & Bioelectronics* **2007,** *22* (6), 1138-1146.

45. Dong, W.; Yan, M.; Liu, Z.; Wu, G.; Li, Y., Efffects of solvents on the adsorption selectivity of molecularly imprintined polymers: Molecular simulation and experimental validation. *Separation and Purification* **2007,** *53* (2), 183-188.

46. Dong, C.; Li, X.; Guo, Z.; Qi, J., Development of a model for the rational design of molecular imprinted polymer: Computational approach for combined molecular dynamics/quantum mechanics calculations. *Analytica Chimica Acta* **2009,** *647* (1), 117-124.

47. Boysen, R. I.; Li, S.; Chowdhury, J.; Schwarz, L. J.; Hearn, M. T. W., Selectivity optimisation of biomimetic molecularly imprinted polymer thin films. *Microelectronic Engineering* **2012,** *97*, 81-84.

48. (a) Dmitrienko, S. G.; Irkha, V. V.; Kuznetsova, A. Y.; Zolotov, Y. A., Use of molecular imprinted polymers for the separationand preconcentration of organic compounds. *Journal of Analytical Chemistry* **2004,** *59* (9), 2004;

(b) Chapuis, F.; Pichon, V.; Hennion, M.-C., Molecularly imprinted polymers: Developments and applications of new selective solid-phase extraction materials. *LC-GC Europe* **2004,** *17* (7), 408-412,414,416-417.

49. (a) Kobayashi, T.; Fukaya, T.; Abe, M.; Fujii, N., Phase inversion molecular imprinting by using template copolymers for high substrate recognition. *Langmuir* **2002,** *18*, 2866-2872;

(b) Haginaka, J.; Takehira, H.; Hosoya, K.; Tanaka, N., Uniform-sized molecularly imprinted polymer for (S)-naproxen selectively modified with hydrophilic external layer. *Journal of Chromatography A* **1999,** *849*, 331-339.

50. Byrne, M. E.; Park, K.; Peppas, N. A., Molecular imprinting within hydrogels. *Advanced Drug Delviery Reviews* **2002,** *54*, 149-161.

51. (a) Wei, S.; Molinelli, A.; Mizaikoff, B., Molecularly imprinted micro and nanospheres for the selective recognition of 17β-estradiol. *Biosensors and Bioelectronics* **2006,** *21*, 1943-1951;

(b) Ye, L.; Surugiu, I.; Haupt, K., Scintillation proximity assay using molecularly imprinted microspheres. *Analytical Chemistry* **2002,,** *74*, 959-964.

52. Vaihinger, D.; Landfester, K.; Krauter, I.; Brunner, H.; Tovar, G. E. M., Molecularly imprinted polymer nanospheres as synthetic affinity receptors obtained by miniemulsion polymerisation. *Macromolecular Chemistry and Physics* **2002,** *203*, 1965–1973.

53. Pham, H. H.; Kumacheva, E., Core-shell particles: building blocks for advanced polymer materials. *Macromolecule Symposium* **2003,** *192*, 191-205.

54. Kempe, H.; Kempe, M., Development and evaluation of spherical molecularly imprinted polymer beads. *Analytical Chemistry* **2006,,** *78*, 3659-3666.

55. Liu, Y.; Peng, H.; Nie, L.; Yao, S., Enantioseparation of L-phenylalanine, based on a continuous molecularly imprinted polymer rod, using a series quartz crystal sensor as the detector. *Instrumental Science and Technology* **2002,** *30* (4), 455-464.

56. Li, Y.; Yin, X.-F.; Chen, F.-R.; Yang, H.-H.; Zhuang, Z.-X.; Wang, X.-R., Synthesis of magnetic molecularly imprinted polymer nanowires using a nanoporous alumina template. *Macromolecules* **2006,** *39* (13), 4497-4499.

57. Blanco-Lopez, M. C.; Lobo-Castanon, M. J.; Miranda-Ordieres, A. J.; Tunon-Blanco, P., Voltammetric sensor for vanillylmandelic acid based on molecularly

imprinted polymer-modified electrodes. *Biosensors and Bioelectronics* **2003,** *18*, 353-362.

58. Kugimiya, A.; Yoneyama, H.; Takeuchi, T., Sialic acid imprinted polymer-coated quartz crystal microbalance. *Electroanalysis* **2000,** *12* (16), 1322-1326.
59. Sulitzky, C.; Ruukert, B.; Hall, A. J.; Lanza, F.; Unger, K.; Sellergren, B., Grafting of molecularly imprinted polymer films on silica supports containing surface-bound free radical initiators. *Macromolecules* **2002,** *35*, 79-91.
60. Piletsky, S. A.; Piletska, E. V.; Chen, B.; Karim, K.; Weston, D.; Barrett, G.; Lowe, P.; Turner, A. P. F., Chemical grafting of molecularly imprinted homopolymers to the surface of microplates. application of artificial adrenergic receptor in enzyme-linked assay for β−agonists determination. *Analytical Chemistry* **2000,,** *72*, 4381-4385.
61. Koster, E. H. M.; Crescenzi, C.; Hoedt, W. d.; Ensing, K.; Jong, G. J. d., Fibers coated with molecularly imprinted polymers for solid-phase microextraction. *Analytical Chemistry* **2001,** *73*, 3140-3145.
62. Lee, M.-H.; Thomas, J. L.; Tasi, S.-B.; Liu, B.-D.; Lin, H.-Y., Formation and recognition characteristics of albumin-imprinted poly(ethylene-co-vinyl-aclcohol) membranes. *Journal of Nanoscience and Nanotechnology* **2009,** *9* (6), 3469-3477.
63. (a) Brisbane, C. The formation of molecularly imprinted polymeric films for illicit drug detection. University of Newcastle, Newcastle, 2005;

    (b) Schmidt, R. H.; Mosbach, K.; Haupt, K., A simple method for spin-coating molecularly imprinted polymer films of controlled thickness and porosity. *Advanced Materials* **2004,** *16* (8), 719-722.
64. Turner, N. W.; Holmes, N.; Brisbane, C.; McGeachie, A. B.; Bowyer, M. C.; McCluskey, A.; Holdsworth, C. I., Effect of template on the formation of phase-inversed molecularly imprinted polymer thin films: an assessment. *Soft Matter* **2009,** (5), 3663-3671.
65. Ulbritch, M., Molecularly imprinted polymer films and membranes. In *Molecularly Imprinted Materials: Science and Technology*, Yan, M.; Ramstrom, O., Eds. Dekker: New York, 2005.
66. (a) Apodaca, D. C.; Pernites, R. B.; Ponnapati, R. R.; Del Mundo, F. R.; Advincula, R. C., Electropolymerised molecularly imprinted polymer films of a bis-terthiophene dendron: folic acid quartz microbalance sensing. *Applied Material Interfaces* **2011,** *3* (2), 191-203;

    (b) Blanco-López, M. C.; Gutiérrez-Fernández, S.; Lobo-Castañón, M. J.; Miranda-Ordieres, A. J.; Tuñón-Blanco, P., Electrochemical sensing with electrodes modified with molecularly imprinted polymer films. *Analytical Bioanalytical Chemistry* **2004,** *378*, 1922-1928.

67. (a) Patel, A. K.; Sharma, P. S.; Prasad, B. B., Electrochemical sensor for uric acid based on a molecularly imprinted polymer brush grafted to tetraethoxysilane derived sol-gel thin film graphite electrode. *Materials Science and Engineering C* **2009,** *29* 1545-1553;

(b) Bossi, A.; Piletsky, S. A.; Piletska, E. V.; Righetti, P. G.; Turner, A. P. F., Surface-grafted molecularly imprinted polymers for protein recognition. *Analytical Chemistry* **2001,** *73*, 5281-5286.

68. Matsui, J.; Akamatsu, K.; Nishiguchi, S.; Miyoshi, D.; Nawafune, H.; Tamaki, K.; Sugimoto, N., Composite of Au nanoparticles and molecularly imprinted polymer as a sensing material. *Analytical Chemistry* **2004,** *76*, 1310-1315.

69. Belmont, A.-S.; Jaeger, S.; Knopp, D.; Niessner, R.; Guaglitz, G.; Haupt, K., Molecularly imprinted polymer films for reflectometric interference spectroscopic studies. *Biosensors & Bioelectronics* **2007,** *22* (12), 3267-3272.

70. Schmidt, R. H.; Belmont, A.-S.; Haupt, K., Porogen formulations for obtaining molecularly imprinted polymer with optimised binding properties. *Analytica Chimica Acta* **2005,** *542* (1), 118-124.

71. Faizal, C. K. M.; Kobayashi, T., Molecularly imprinted membrane applied for selective separation. *Journal of Applied Science* **2011,** *11* (13), 2411-2415.

72. Turner, N. W.; Holdsworth, C. I.; McCluskey, A.; Bowyer, M. C., N-2-Propenyl-(5-dimethylamino)-1-naphthalene sulfonamide, a novel fluorescent monomer for the molecularly imprinted polymer-based detection fo 2,4-dinitrotoluene in the gas phase. *Australian Journal of Chemistry* **2012,** *65* (10), 1405-1412.

73. (a) Gilbert, R. G., *Emulsion Polymerization: A Mechanistic Approach.* . Academic Press: San Diego, 1995;

(b) Fitch, R. M., *Polymer Colliods: A Comprehensive Introduction.* . Academic Press: San Diego, 1997;

(c) Erbil, H. Y., *Vinyl Acetate Emulsion Polymerization and Copolymerization with Acrylic Monomers* CRC Press LLC: Boca Raton, 2000.

74. Haupt, K.; Mayes, A. G.; Mosbach, K., Herbicide assay using an imprinted polymer-based system analogous to competitive fluoroimmunoassays. *Journal of Analytical Chemistry* **1998,** *70*, 3936-3939.

75. (a) Liu, R.; Guan, G.; Wang, S.; Zhang, Z., Core-shell nanostructured fluorescent chemosensor for selective detection of atrazine herbicide. *Analyst* **2012,** *136* (1), 184-190;

(b) Nguye, T. H.; Hardwick, S. A.; Sun, T., Intrinsic fluorescence-based optical biber sensor for cocaine using a molecularly imprinted polymer as the recognition element. *Sensors Journal, IEEE* **2012,** *12* (1), 255-260;

(c) Petya K. Ivanova-Mitseva; Guerreiro, A.; Piletska, E. V.; Whitcombe, M. J.; Zhou, Z.; Mitsev, P. A.; Davis, F.; Piletsky, S. A., Cubic molecularly imprinted

polymer nanoparticles with a fluorescent core. *Angewandte Chemie International* **2012,** *51* (21), 5196-5199.

76. (a) Stephenson, C. J.; Shimzu, K. D., Colorimetric imprinted polymers as sensors. *Polymer Preprints* **2006,** *47* (1), 7;

    (b) Greene, N. T.; Shimizu, D., Colorimetric molecularly imprinted polymer sensor array using dye displacement. *Journal of the American Chemical Society* **2005,** *127*, 5695-5700.

77. Rajkumar, R.; Katterle, M.; Warsinke, A.; Mohwald, H.; Schellar, F. W., Thermometric MIP sensor for fructosyl valine. *Biosensors and Bioelectronics* **2008,** *23* (7), 1195-1199.

78. (a) Yang, Z.-p.; Zhang, C.-j., Desinging of MIP-based QCM sensor for the determination of Cu(II) ions in solution. *Sensors and Actuators* **2009,** *B142* (1), 210-215;

    (b) Percival, C. J.; Stanley, S.; Braithwaite, A.; Newton, M. I.; McHale, G., Molecular imprinted polymer coated QCM for the detection of nandrolone. *Analyst* **2002,** *127*, 1024-1026.

79. (a) Jin, W.; Lin, X.; Lv, S.; Zhang, Y.; Jin, Q.; Mu, Y., A DNA sensor based on surface plasmon resonance for apoptosis-associated genes detection. *Biosensors & Bioelectronics* **2009,** *24* (5), 1266-1269;

    (b) Iwasaka, H.; Oba, M., SPR immunosensor. *Materials Intergration* **2008,** *21* (5-6), 203-210;

    (c) Karlsson, R., SPR for molecular interation analysis: a review of emerging application areas. *Journal of Molecular Recognition* **2004,** *17*, 151-161.

80. (a) Dong, J.; Peng, Y.; Goa, N.; Bai, J.; Ning, B.; Liu, M.; Gao, Z., A novel polymerisation of ultrathin sensitive imprinted film on surface plasmon resonance sensor. *Analyst* **2012,** *137* (4571-4576);

    (b) Gupta, G.; Singh, P. K.; Boopathi, M.; Kamboj, D. V.; Singh, B.; Vijayaraghavan, R., Molecularly imprinted polymer for the recognition of biological warfare agent staphylococcal enterotoxin B based on surface plasmon resonance. *Thin Solid films* **2010,** *519* (3), 1115-1121;

    (c) Takateru, M.; Takayuki, H.; Toshifumi, T., Surface plasmon resonance sensor for lysozyme based on molecularly imprinted thin films. *Analytica Chimica Acta* **2007,** *591* (1), 63-7.

81. (a) Shoji, R.; Takeuchi, T.; Kubo, I., Atrazine sensor based on molecularly imprinted polymer-modified gold electrode. *Analytical Chemistry* **2003,** *75*, 4882-2886;

    (b) Yao, L.; Tang, Y.; Zeng, W.; Huang, Z., An electrochemical sensor for phenylephrine based on molecular imprinting. *Analytical Sciences* **2009,** *25*, 1089-93;

(c) Chen, P.-Y.; Nien, P.-C.; Wu, C.-T.; Wu, T.-H.; Lin, C.-W.; Ho, K.-C., Fabrication of a molecularly imprinted polymer sensor by self-assembling monolayer/mediator system. *Analytica Chimica Acta* **2009,** *643*, 38-44.

82. (a) Alizadeh, T.; Ganjali, M. R.; Zare, M.; Norouzi, P., Development of a voltammetric sensor based on a molecularly imprinted polymer (MIP) for caffeine measurement. *Electrochimica Acta* **2010,** *55* 1568-1574;

    (b) Lakshmi, D.; Prasad, B. B.; Sharma, P. S., Creatinine sensor based on a molecularly imprinted polymer-modified hanging mercury drop electrode. *Talanta* **2006,** *70*, 272-280.

83. Chen, P.-Y.; Nien, P.-C.; Wu, C.-T.; Wu, T.-H.; Lin, C.-W.; Ho, K.-C., Fabrication of a molecularly imprinted polymer sensor by self-assembling monolayer/mediator system. *Analytica Chimica Acta* **2009,** *643*, 38-44.

84. (a) Piletsky, S. A.; Piletskaya, E. V.; Elgersma, A. V.; Yano, K.; Karube, I.; Parhometz; Y.P. Elskaya, A. V., Atrazine sensing by molecularly imprinted membranes. *Biosensors & Bioelectronics* **1995,** *10*, 959-64;

    (b) Sergeyeva, A. V.; Piletsky, S. A.; Brovko, A. A.; Slichenko, E. A.; Sergeeva, L. M.; El'skaya, A. V., Conductometric sensor for atrazine detection based on molecularly imprinted polymer membranes. . *Analyst* **1999,** *124*, 331-334.

85. Panasyuk-Delaney, T.; Mirsky, V. M.; Ulbritch, M.; Wolfbeis, O. S., Impedometric herbicide chemosensors based on molecularly imprinted polymers. . *Analytica Chimica Acta* **2001,** *435*, , 157-62.

86. Mirsky, V. M.; Hirsch, T.; Piletsky, S. A.; Wolfbeis, O. S., A spreader-bar approach to molecular architecture: formation of stable artificial chemoreceptors. *Angewandte Chemie International* **1999**, 108-10.

87. (a) Alizadeh, T.; Zare, M.; Ganjali, M. R.; Norouzi, P.; Tavana, B., A new molecularly imprinted polymer (MIP)-based electrochemical sensor for monitoring 2,4,6-trinitrotoluene (TNT) in natural waters and soil samples. *Biosensors and Bioelectronics* **2010,** *25* 1166-1172;

    (b) Javanbakht, M.; Fard, S. E.; Mohammadi, A.; Abdouss, M.; Ganjali, M. R.; Norouzi, P.; Safaraliee, L., Molecularly imprinted polymer based potentiometric sensor for the determination of hydroxyzine in tablets and biological fluids. *analytica chimica acta* **2008,** *612*, 65-74.

88. Penn, S. G.; He, L.; Natan, M. J., Nanoparticles for bioanalysis. *Current Opinion in Chemical Biology* **2003,** *7* (5), 609-615.

89. (a) Xu, S.; Liu, Y.; Wang, T.; Li, J., Highly sensitive electrogenerated chemiluminescence biosensor in profiling protein kinase activity and inhibition using gold nanoparticle as signal transduction probes. *Analytical Chemistry* **2010,** *82* (22), 9566-9572;

(b) Tokarev, I.; Tokareva, I.; Gopishetty, V.; Katz, E.; Minko, S., Specific biochemical-to-optical signal transduction by responsive thin hydrogel films loaded with noble metal nanoparticles. *Advanced Materials* **2010,** *22* (12), 1412-1416.

90. Meixner, H.; Jones, R., *Micro- and nano-sensor technology / trends in sensor markets*. VCH publishers Inc.: Weinheim, 1995; Vol. 8.

91. Yang, M.; Yang, Y.; Liu, Y.; Shen, G.; Yu, R., Platinum nanoparticles-doped sol-gel/carbon nanotubes composite electrochemical sensors and biosensors. *Biosensors and Bioelectronics* **2006,** *21*, 1125-1131.

92. Turkevich, J.; Stevenson, P. C.; Hillier, J., A study of the nucleation and growth processes in the synthesis of colloidal gold. *Discussions of the Faraday Society* **1951,** *11*, 55-75.

93. Brust, M.; Walker, M.; Bethell, D.; Schiffrin, D. J.; Whyman, R., Synthesis of thiol derivatised gold nanoparticles in a two phase liquid/liquid system. *Journal Chemical Society, Chemical Communication* **1994**, 801.

94. Isaacs, S. R.; Choo, H.; Ho, W.-B.; Shon, Y.-S., Chemical, thermal, and ultrasonic stability of hybrid nanoparticles and nanoparticle multilayer films. *Chemical Materials* **2006,** *18*, 107-114.

95. Jin, R. C.; Wu, G. S.; Li, Z.; Mirkin, C. A.; Schatz, G. C., What controls the melting properties of DNA-linked gold nanoparticle assemblies? *Journal of the American Chemical Society* **2003,** *125*, 1643-1654.

96. Bangs, L. B., New developments in particle-based immunoassays: introduction. *Pure and Applied Chemistry* **1996,** *68* (10), 1873-1879.

97. (a) Zhong, C.-J.; Maye, M. M., Core-shell assembled nanoparticles as catalysts. *Advanced Materials* **2001,** *13* (19), 1507-1511;

    (b) Xu, S.; Han, X., A novel method to construct a third-generation biosensor: self assembling gold nanoparticles on thiol functionalised poly(styrene-*co*-acrylic acid) nanospheres. *Biosensors and Bioelectronics* **2004,** *19*, 1117-1120.

98. Liu, J.; Lu, Y., A colorimetric lead biosensor using DNAzyme-directed assembly of gold nanoparticles. *Journal of the American Chemical Society* **2003,** *125*, 6642-6643.

99. Puckett, S. D.; Heuser, J. A.; Keith, J. D.; Spendel, W. U.; Pacey, G. E., Interaction of ozone with gold nanoparticles. *Talanta* **2005,** *66*, 1242-1246.

100. Yang, W.; Bai, Y.; Li, Y.; Sun, C., Amperometric nitrite sensor based on hemoglobin/colloid gold nanoparticles immobilized on a glassy carbon electrode by a titania sol-gel film. *Analytical Bioanalytical Chemistry* **2005,** *382*, 44-50.

101. Koenig, S.; Chechik, V., Au nanoparticle-imprinted polymers. *Chemical Communication* **2005,** *32*, 4110-4112.

102. Matsui, J.; Akamatsu, K.; Hara, N.; Miyoshi, D.; Nawafune, H.; Katsuyuki, T.; Sugimoto, N., SPR sensor chip for detection of small molecules using molecularly imprinted polymer with embedded gold nanoparticles. *Analytical Chemistry* **2005,** *77* (13), 4282-4285.

103. Tokareva, I.; Tokarev, I.; Minko, S.; Hutter, E.; Fendler, J. H., Ultrathin molecularly imprinted polymer sensors employing enhanced transmission surface plasmon resonance spectroscopy. *Chemical Communications* **2006,** (31), 3343-3345.

104. (a) Bolto, B. A.; McNeill, R.; Weiss, D. E., Electronic conduction in polymers. III. Electronic properties of polypyrrole. *Australian Journal of Chemistry* **1963,** *16* (6), 1090-1103;

(b) Bolto, B. A.; Weiss, D. E., Electronic conduction in polymers. II. The electrochemical reduction of polypyrrole at controlled potential. *Australian Journal of Chemistry* **1963,** *16* (6), 1076-1089;

(c) McNeill, R.; Siudak, R.; Wardlaw, J. H.; Weiss, D. E., Electronic conduction in polymers. I. The chemical structure of polypyrrole. *Australian Journal of Chemistry* **1963,** *16* (6), 1056-1075.

105. (a) McNeill, R.; Weiss, D. E.; Willis, D., Electronic conduction in polymers. IV. Polymers from imidazole and pyridine. *Australian Journal of Chemistry* **1965,** *18* (4), 477-486;

(b) Bolto, B. A.; Weiss, D. E.; Willis, D., Electronic conduction in polymers. V. Aromatic semiconducting polymers. *Australian Journal of Chemistry* **1965,** *18* (4), 487-491.

106. Aylward, G.; Findlay, T., *SI Chemical Data*. John Wiley & Sons Australia: Milton, 2008.

107. MacDiarmid, A. G.; Heeger, A. J., Organic metals and semiconductors: The chemistry of polyacetylene, (CH)x, and its derivatives. *Synthetic Metals* **1980,** *1* (2), 101-118.

108. Heeger, A. J., Semiconducting and metallic polymers: The fourth generation of polymeric materials. In *Nobel Prize Lecture*, 2000.

109. MacDiarmid, A. G., "Synthetic Metals": A novel role for organic polymers. In *Nobel Prize Lecture*, 2000.

110. Chianella, I.; Karras, K.; Lakshmi, D.; Whitcombe, M. J.; Marson, S., Conductive polymers for plastic electronics. In *Molecularly Imprinted Sensors*, Li, S.; Ge, Y.; Piletsky, S. A.; Lunec, J., Eds. Elsevier: 2012.

111. Kumar, D.; Sharma, R. C., Advances in conductive polymers. *European Polymer Journal* **1998,** *34* (8), 1053-60.

112. (a) Hotta, S., Electrochemical synthesis and spectroscopic study of poly(3-alkylthienylenes). *Synthetic Metals* **1987,** *22* (2), 103-113;

(b) Hotta, S.; Rughooputh, S. D. D. V.; Heeger, A. J.; Wudl, F., Spectroscopic studies of soluble poly(3-alkylthienylenes). *Macromolecules* **1987,** *20* (1), 212-215.

113. Louwet, F.; Groenendaal, L.; Dhaen, J.; Manca, J.; Van Luppen, J.; Verdonck, E.; Leenders, L., PEDOT/PSS: synthesis, characterization, properties and applications. *Synthetic Metals* **2003,** *135-136*, 115-117.

114. Ogawa, K.; Stafford, J. A.; Rothstein, S. D.; Tallman, D. E.; Rasmussen, S. C., Nitrogen-functionalized polythiophenes: Potential routes to new low band gap materials. *Synthetic Metals* **2005,** *152* (1-3), 137-140.

115. Ziemelis, K., Putting it on plastic. *Nature* **1998,** *393* (6686), 619-620.

116. Angelopoulos, M., Conducting polymers in microelectronics. *IBM Journal of Research & Development* **2001,** *45* (1), 57.

117. (a) Killian, J. G.; Coffey, B. M.; Gao, F.; Poehler, T. O.; Searson, P. C., Polypyrrole composite electrodes in an all-polymer battery system. *Journal of the Electrochemical Society* **1996,** *143* (3), 936-42;

(b) Wallace, G. G.; Spinks, G. M.; Kane-Maguire, L. A. P.; Teasdale, P. R., *Conductive Electroactive Polymers*. CRC Press: Boca Raton, 2003.

118. Hashmi, S. A.; Latham, R. J.; Linford, R. G.; Schlindwein, W. S., Polymer electrolyte based solid state redox supercapacitors with poly (3-methyl thiophene) and polypyrrole conducting polymer electrodes. *Ionics* **1997,** *3* (3), 177-183.

119. Spinks, G. M.; Innis, P. C.; Lewis, T. W.; Kane-Maguire, L. A. P.; Wallace, G. G., Current state and future directions of research and development in conducting polymers. *Materials Forum* **2000,** *24*, 125-166.

120. (a) Catia Arbizzani, A. B. M. M. A. Z. G. B. M. Z., Polyalkylthiophenes as electrochromic materials: A comparative study of poly(3-methylthiophenes) and poly(3-hexylthiophenes). *Advanced Materials* **1995,** *7* (6), 571-574;

(b) Somani, P.; Mandale, A. B.; Radhakrishnan, S., Study and development of conducting polymer-based electrochromic display devices. *Acta Materialia* **2000,** *48* (11), 2859-2871.

121. Lange, U.; Roznyatovskaya, N. V.; Mirsky, V. M., Conducting polymers in chemical sensors and arrays. *Analytica Chimica Acta* **2008,** *614* (1-26).

122. Omowunmi A. Sadik, G. G. W., Effect of polymer composition on the detection of electroinactive species using conductive polymers. *Electroanalysis* **1993,** *5* (7), 555-563.

123. (a) Imisides, M. D.; Wallace, G. G., Deposition and electrochemical stripping of mercury ions on polypyrrole based modified electrodes. *Journal of Electroanalytical Chemistry* **1988,** *246* (1), 181-191;

(b) Wallace, G. G.; Lin, Y. P., Preparation and application of conducting polymers containing chemically active counterions for analytical purposes. *Journal of Electroanalytical Chemistry* **1988,** *247* (1-2), 145-156.

124. (a) Lin, Y.; Wallace, G. G., Development of a polymer-based electrode for selective detection of dichloramine. *Analytica Chimica Acta* **1992,** *263* (1-2), 71-75;

(b) Hammerle, M.; Schuhmann, W.; Schmidt, H. L., Amperometric polypyrrole enzyme electrodes: effect of permeability and enzyme location. *Sensors and Actuators B: Chemical* **1992,** *6* (1-3), 106-112.

125. Sadik, O. A.; Wallace, G. G., Corrigendum to "Pulsed amperometric detection of proteins using antibody containing conducting polymers". *Analytica Chimica Acta* **1995,** *302* (1), 131.

126. Pei, Q.; Qian, R., Protonation and deprotonation of polypyrrole chain in aqueous solutions. *Synthetic Metals* **1991** *45*, 35-48.

127. Shoji, E.; Freund, M. S., Potentiometric saccharide detection based on the pK_a changes of poly(aniline boronic acid). *Journal of the American Chemical Society* **2002,** *124* (42), 12486-93.

128. Ho, K.-C.; Yeh, W.-M.; Tung, T.-S.; Liao, J.-Y., Amperometric detection of morphine based on poly(3,4-ethylenedioxythiophene) immobilized molecularlyimprinted polymer particles prepared by precipitation polymerization. *Analytica Chimica Acta* **2005,** *54* 90-96.

129. Thoelen, R.; Vansweevelt, R.; Duchateau, J.; Horemans, F.; D'Haen, J.; Lutsen, L.; Vanderzande, D.; Ameloot, M.; vandeVen, M.; Cleij, T. J.; Wagner, P., A MIP-based impedimetric sensor for the detection of low-MW molecules. *Biosensors and Bioelectronics* **2008,** *23*, 913-918.

130. Mazzotta, E.; Picca, R. A.; Malitesta, C.; Piletsky, S. A.; Piletska, E. V., Development of a sensor prepared by entrapment of MIP particles in electrosynthesised polymer films for electrochemical detection of ephedrine. *Biosensors and Bioelectronics* **2008,** *23*, 1152-56.

131. (a) Ebarvia, B. S.; Cabanilla, S.; III, F. S., Biomimetic properties and surface studies of a piezoelectric caffeine sensor based on electrosynthesized polypyrrole. *Talanta* **2005,** *66*, 145-152;

(b) zcan, L. O.; Sahin, Y., Determination of paracetamol based on electropolymerized-molecularly imprinted polypyrrole modified pencil graphite electrode. *Sensors and Actuators B* **2007**, 362-369.

132. (a) Liu, Y.; Song, Q.-j.; Wang, L., Development and characterisation of an amperometric sensor for triclosan detection based on electropolymerised molecularly imprinted polymer. *Microchemical Journal* **2009,** *91* (2), 222-226;

(b) Kang, J.; Zhang, H.; Wang, Z.; Wu, H.; Lu, X., A novel amperometric sensor for salicylic acid based on molecularly imprinted polymer-modified electrodes. *Polymer Plastics Technology and Engineering* **2009,** *46* (6), 639-45.

133. Li, J.; Zhao, J.; Wei, X., A sensitive and selective sensor for dopamine determination based on a molecularly imprinted electropolymer of o-aminophenol. *Sensors and Actuators B* **2009,** *140*, 663-669.

134. Pernites, R. B.; Ponnapati, R. R.; Advincula, R. C., Surface plasmon resonance (SPR) detection of theophylline via electropolymerised molecularly imprinted polythiophenes. *Macromolecules* **2010,** *43*, 9724-35.

135. Yeh, W.-M.; Ho, K.-C., Amperometric morphine sensing using a molecularly imprinted polymer-modified electrode. *Analytica Chimica Acta* **2005,** *542*, 76-82.

136. Malitesta, C.; Mazzotta, E.; Picca, R. A.; Poma, A.; Chianella, I.; Piletsky, S. A., MIP sensors – the electrochemical approach. *Analytical and Bioanalytical Chemistry* **2012,** *402* (1827-46).

137. Kirpichenko, S.; Tolstikova, L.; Suslova, E.; Abanov, A.; Voronkov, M., Regioselectivity of radical cyclization of unsaturated organosilicon thiols. *Phosphorus, Sulfur, and Silicon* **1995,** *106*, 47-53.

138. Brisbane, C.; McCluskey, A.; Bowyer, M.; Holdsworth, C. I., Molecularly imprinted films of acrylonitrile/methyl methacrylate/acrylic acid terpolymers: influence of methyl methacrylate in the binding performance of l-ephedrine imprinted films. *Organic & Biomolecular Chemistry* **2013,** *11* (17), 2872-2884.

139. Brisbane, C. Optimisation of molecularly imprinted polymeric films for the detection of *L*-ephedrine. University of Newcastle, 2010.

140. Cirpan, A.; Alkan, S.; Toppare, L.; Hepuzer, Y.; Yagci, Y., Conducting graft copolymers of poly(3-methylthienyl methacrylate) with pyrrole and thiophene. *Journal of Polymer Science: Part A: Polymer Chemistry* **2002,** *40*, 4131-4140.

141. Aoki, T.; Kawashima, M.; Katono, H.; Sanui, K.; Ogata, T.; Sakurai, Y., Temperature-responsive interpenetrating polymer networks constructed with poly(acrylic acid) and poly(*N*,*N*-dimethylacrylamide). *Macromolecules* **1994,** *27*, 947-952.

142. Subrahmanyam, S.; Piletsky, S. A.; Piletska, E. V.; Chen, B.; Karim, K.; Turner, A. P. F., 'Bite-and-Switch' approach using computationally designed molecularly imprinted polymers for sensing of creatinine. *Biosensors and Bioelectronics* **2001,** *16* (9-12), 631-637.

143. Farrington, K.; Magner, E.; Regan, F., Predicting the performance of molecularly imprinted polymers: Selective extraction of caffeine by molecularly imprinted solid phase extraction. *Analytica Chimica Acta* **2006,** *566* (1), 60-68.

144. (a) Piletsky, S. A.; Karim, K.; Piletska, E. V.; Day, C. J.; Freebairn, K. W.; Legge, C.; Turner, A. P. F., Recognition of EPD enantiomers by molecularly imprinted

polymers designed using a computational approach. *Analyst* **2001,** *126* (1826-1830);

(b) Wu, L.; Li, Y., Study of the recognition of templates and their analogues on molecularly imprinted polymers using computational and conformational analysis approaches. *Journal of Molecular Recognition* **2004,** *17*, 567-74;

(c) Nicholl, I. A..; Andersson, H. S.; Charlton, C.; Henschel, H.; Karlsson, B. C. G.; Karlsson, J. G.; O'Mahony, J.; Rosengren, A. M.; Wilkman, S., Theoretical and computational strategies for rational molecularly imprinted polymer designs. *Biosensors & Bioelectronics* **2009,** *25*, 543-552.

145. Rozas, I.; Alkorta, I.; Elguero, J., Bifurcated Hydrogen Bonds: Three-Centered Interactions. *J. Phys. Chem. A* **1998,** *102* (48), 9925-32.

146. (a) Schild, H. G., Poly(N-isopropylacrylamide): experiment, theory and application. *Progress in Polymer Science* **1992,** *17* (2), 163-249;

(b) Hirokawa, Y.; Tanaka, T., Volume phase transition in a nonionic gel. *The Journal of Chemical Physics* **1984,** *81* (12), 9379-80.

147. Ansell, R. J.; Wang, D.; Kuah, J. K. L., Imprinted polymers for chiral resolution of (±)-ephedrine. Part 2: probing pre-polymerisation equilibria in different solvents by NMR. *Analyst* **2008,** *133*, 1673-83.

148. Wulff, G.; Bifis, A., *Molecularly Imprinted Polymers: Man-made Mimics of Antibodies and their Aplications in Analytical Chemistry*. Elsevier: Amsterdam, 2000; Vol. 23.

149. Lang, U.; Muller, E.; Naujoks, N.; Dual, J., Microscopical nvestigations of PEDOT:PSS thin films. *Advanced Functional Materials* **2009,** *19*, 1-6.

150. Elschner, A.; Kirchmeyer, S.; Lovenich, W.; Merker, U.; Reuter, K., *PEDOT: Principles and Applications of an Intrinsically Conductive Polymer*. CRC Press: Boca Raton, 2011.

151. (a) M.C.Gallazzi; L.Castellani; G.Zerbi, Regiospecificity and structureal properties of polyalkylthiophenes. *Synthetic Metals* **1991,** *41-43* (495-498);

(b) Maior, R. M. S.; Hinkelmann, K.; Eckert, H.; Wudl, F., Synthesis and characterization of two regiochemically defined poly(dialkylbithiophenes): a comparative study. *Macromolecules* **1990,** *23* (6), 1268-1279.

152. Diah, A. W. M. Investigation of the conductive behavior of poly(3,4-ethylenedioxythiophene)/poly(styrenesulfonic acid) for organic electronics. University of Newcastle, Newcastle, Australia, 2013.

153. (a) Ulbricht, M., Membrane separations using molecularly imprinted polymers. *Journal of Chromatography B* **2004,** *804* (1), 113-125;

(b) Sergeyeva, T. A.; Piletsky, S. A.; Piletska, E. V.; Brovko, O. O.; Karabanova, L. V.; Sergeeva, L. M.; El'skaya, A. V.; Turner, A. P. F., In Situ Formation of

Porous Molecularly Imprinted Polymer Membranes. *Macromolecules* **2003,** *36* (19), 7352-7357.